The geology and mineralogy of copper lead, Zinc sulphide veins from Bulancak, Turkey

Akinci, Omer T.

THE GEOLOGY AND MINERALOGY OF COPPER LEAD, ZINC SULPHIDE VEINS FROM BULANCAK, TURKEY

A Thesis submitted for the Degree of Doctor of Philosophy in the University of Durham

by

OMER T. AKINCI, Dipl. Geol. (Istanbul)
M.Sc. (Dunelm).

Graduate Society, June 1974.

ABSTRACT

The Bulancak Cu-Pb-Zn sulphide veins are the best representatives of their type among the varied deposits of the Eastern Pontus Ore Province. Kuroko, vein, stockwork, prophyry-type copper, skarn-type iron and manganese depesits with subduction related volcanicity have been described from this province by various authors.

Petrographic study of the Country rocks, despite their hydrothermal alteration, shows that they are mainly calc-alkaline. Volcanicity took place from Upper (possibly Lower) Cretaceous to Miocene as indicated by intrusives dated at 25 million years.

Ore microscopy studies have proved the first occurrence (in Turkey) of Betekhtinite $(Cu, Fe)_{21}Pb_2S_{15}$, and Aikinite $(PbCuBiS_3)$-Bismuthinite(Bi_2S_3) solid solution minerals. Idaite is reported for the first time from the study area. Field and Laboratory work have shown the structural control of Mn, Fe and Cd distribution in sphalerites. Mn follows a NW-SE trending zone from Kuşdere to Kaşyatak whereas Fe-Cd distribution follows a SW-NE trending zone between Kovalık Sr. and Kuloglu along Küçükgüre Dere (stream). reflecting the dependance on the two major fracture systems in the area.

Data based on a study of more than 2500 primary and secondary fluid inclusions in transparent ore and ganque minerals is given, including measurements on the temperature, pressure, density and salinity.

The inclusions were moderately saline, salinity varying within the range 13.2 equivalent wt.% NaCl to almost fresh water indicated by a density change from 0.74gm/cm^3 in the early vein stage to 0.98 at the end of the base metal sulphide stage. These variations may

reflect the mixture of deeply circulating meteoric waters with rising, saline, hydrothermal fluids.

Homogenization temperatures ranged from ca. 340°C to 80°C. Inclusions in neighbouring early formed quartz and sphalerite minerals from the same vein show a temperature rise from ca. 230 to 330°C in the early vein stage, and eventually boiling conditions were reached. At a later stage the fluids cooled from 330°C to ca. 80°C. in the base metal stage. The highest temperatures were obtained from the Tekmezar Group Veins, in comparison to the Dariköy Group Veins, indicating a horizontal temperature zoning in which the Bi-content of the aikinite-bismuthinite solid solution minerals increases from West (Saridiken Dere) to east (Kornalı Dere).

Data obtained from isotherms indicates that the ore-bearing fluids rose along NW-SE trending faults. This explains the concentration of veins around the Selmanoglu, Gonurca Dere, and Uzümlük Dere Faults.

Simple cooling of the solutions, pressure fluctuations, density and replacement processes played major roles in the formation of these veins. Fluid inclusion studies combined with geological data, are considered to be useful parameters in mineral exploration to pinpoint the richest part of an orebody.

Metal transport and the thermal history of vein mineralisation are discussed in the light of fluid inclusion data.

ACKNOWLEDGEMENTS

The writer wishes to acknowledge, with thanks, the help of all those persons and organizations that have assisted and encouraged him during this research work. I am grateful to TUBITAK, Scientific and Technical Research Council of Turkey, and MTA, Mineral Research and Exploration Institute, for financial support, also to Professors G.M. Brown and M.H.P. Bott for the use of facilities in the Department of Geological Sciences, Durham. The project would not have been possible, however, without the approval and help of Doç. Dr. S. Alpan, General Director of MTA.

I would like to express my sincere gratitude to Mr R. Phillips for acting as my supervisor, his constructive criticism, encouragement and reading sections of the manuscript of this thesis. The help of the other members of the staff and especially, Drs. G. Larwood, D.M. Hirst and G.H. Holland is much appreciated. Special thanks are due to Dr A. Peckett for demonstrating the operation of the electron probe and for allowing the use of his correction program.

Grateful thanks to J. Wilson, Chief Technician and other technical staff of the department, especially to Mr G. Randall who supported the project throughout by his skill, speed and workmanship in producing excellent polished sections and disc wafers for ore-microscopy and fluid inclusion study.

Friends and all the research students by their help, advice and criticism have been responsible for many improvements and advances in this work but non of its shortcomings. Among many I wish to thank Dr F.W. Smith, Mr R. Hardy, Mr K. Wills, Dr A. Hall and Mr T. Tansel.

The help of Mrs D. Williamson during the correction of the manuscript is gratefully acknowledged.

Finally thanks to my family, especially to my wife, without whose forebearance this thesis would not have been completed.

page

ABSTRACT ii

ACKNOWLEDGEMENTS iv

TABLE OF CONTENTS vi

LIST OF ILLUSTRATIONS

List of Figures

List of Maps and Geological Sections

List of Tables

List of Plates

CHAPTER ONE - INTRODUCTION 1

1.1 Climate and Vegetation 8

CHAPTER TWO - PREVIOUS WORK 10

2.1 History 10

2.2 Review of the tectonic units of Turkey 11

2.3 The Stratigraphy of Eastern Pontids 13

CHAPTER THREE - FIELDWORK

3A GENERAL GEOLOGY OF THE THESIS AREA 23

3.1 Introduction 23

3.2 Geological Succession 25

3.2.1 Lower Basic Series 28

3.2.2 Pelitic Limestone and tuff 31

3.2.3 Porphyritic dacite 31

3.2.4 Tuffaceous breccia and Sandstone 33

3.2.5 Rhyodacite and Rhyodacitic pyro 34

3.2.6 Biotite andesite 35

3.2.7 Agglomerate, Sandstone and Limestone 37

CHAPTER THREE - continued		page
3.2.8	Quartz-Microdiorite	41
3.2.9	Basalt Dykes	41
3.2.10	Scree	42
3B	STRUCTURAL GEOLOGY OF THE THESIS AREA	43
3.3	General Introduction	43
3.4	Detailed Structural Geology	44
3.4.1	Folds, Strike and dips	44
3.4.2	Faults	44
3.4.3	Joints	49
3.4.4	Veins	52
CHAPTER FOUR - PETROGRAPHY AND CHEMISTRY OF THE COUNTRY ROCKS		
4A	PETROGRAPHY	58
4.1	Introduction	58
4.2	Petrography of the Lower Basic Series	58
4.3	Porhyritic dacite	62
4.4	Rhycdacitic rocks	63
4.5	Biotite-Andesite	65
4.6	Quartz-microdiorite	66
4.7	Basalt dykes	67
4B	CHEMISTRY OF THE COUNTRY ROCKS	73
4.8	Introduction	73
4.9	Variation of Major oxides with SiO_2	74
4.10	Variation of trace elements	79
CHAPTER FIVE		
5A	THE MINERALOCY OF VEIN MINERALS	

CHAPTER FIVE - continued page

5.1	Introduction	85
5.2	Methods of Study	87
5.3	Oxide minerals	87
5.3.1	Quartz	87
5.3.2	Hematite	89
5.3.3	Ilmenite	92
5.3.4	Goethite	92
5.3.5	Lepidocrocite	94
5.4	Sulphates	94
5.4.1	Baryte	94
5.4.2	Anglesite	94
5.5	Carbonates	95
5.5.1	Cerussite	95
5.5.2	Calcite, Dolomite,Ankerite and Siderite	95
5.5.3	Malachite and Azurite	97
5.6	Sulphides	101
5.6.1	Pyrite	101
5.6.2	Marcasite	103
5.6.3	Sphalerite	104
5.6.4	Galena	108
5.6.5	Chalcopyrite	110
5.6.6	Bornite	113
5.6.7	Idaite	115
5.6.8	Covellite	118
5.6.9	Digenite	120
5.6.10	Betekhtinite	120

CHAPTER FIVE - continued

		page
5.7	Sulphosalts	126
5.7.1	Fahlerz	126
5.7.2	Aikinite	128
5.8	Paragenetic Sequence	133
5B	QUANTITATIVE PHYSICAL MEASUREMENTS ON VEIN MINERALS	136
5.9	X-Ray Diffraction	136
5.9.1	Pyrite	136
5.9.2	Sphalerite	136
5.9.3	Betekhtinite	139
5.9.4	Aikinite	139
5.10	Electron Microprobe Analysis	146
5.10.1	Sphalerite	146
5.10.2	Betekhtinite	151
5.10.2a	Betekhtinite Stability	152
5.10.3	Fahlerz	154
5.10.4	Aikinite	157
5.10.5	Discussion on the Aikinite-Bismuthinite Solid Solution Series	157
5C	DESCRIPTION OF INDIVIDUAL OCCURRENCES	165
5.11	Exploration activities and General Geology of Akköy Mine	165
5.12	Mineralogy of Akköy Orebody	
5.13	Darıköy, Üzümlük Occurrences	174
5.13.1	Yukari Üzümlük	175
5.13.2	Orta Üzümlük	175
5.13.3	Aşagi Üzümlük	177
5.14	Mineralogy of the Üzümlük Veins	
5.15	Kornali Dere Occurrences	

CHAPTER SIX - GEOTHERMOMETRY

		page
6A	SPHALERITE GEOTHERMOMETRY	191
6.1	Trace Element Partition Coefficients	191
6.2	FeS Content of Sphalerite	192
6B	FLUID INCLUSION GEOTHERMOMETRY	194
6.3	Introduction	
6.3.1	Previous Research	195
6.3.2	Materials studied	196
6.4	Classification and Problems of Inclusions	198
6.4.1	Primary Inclusions	198
6.4.2	Secondary Inclusions	202
6.4.3	Pseudo secondary inclusions	202
6.4.4	Types of Inclusions	206
6.4.5	Opaque Captive Minerals	209
6.4.6	Leakage Problem of the Inclusions	212
6.5	Freezing Experiments	214
6.5.1	Salinity Measurements	214
6.5.2	Freezing stage	215
6.5.3	Heat Exchange Medium	215
6.5.4	Thermocouples	216
6.5.5	Calibration	216
6.5.6	Freezing reactions and products	217
6.5.7	Fluid densities	218
6.5.8	CO_2 contents	222
6.6	Heating Experiments	222
6.6.1	Furnace	222
6.6.2	Thermocouples	223
6.6.4	Calibration	223

page

CHAPTER SIX - continued

6.6.5 Time-Temperature relations 227

6.7 Pressure Correction and interpretation of data 230

6.7.1 Pressure Correction 233

6.8 Application of the Fluid Inclusion Data to Field Problems 236

CHAPTER SEVEN - DISCUSSIONS AND CONCLUSIONS

7.1 Environment of Ore Deposition 240

7.2 Thermal History of Vein Mineralization 247

7.3 Metal Transport in the Light of Fluid Inclusion Data 252

7.4 Suggestions for possible further work 255

7.5 Conclusions 256

LIST OF REFERENCES 258-279

APPENDIX ONE - DETAILS OF SPECIMEN COLLECTION

Specimen Collection 280

Rock Type 280

Grid Reference 281

Locality Names 281

Altitudes 281

APPENDIX TWO - ROCK ANALYSIS

Specimen Preparation 284

XRF Analysis, Major elements 284

Wet Chemical Analyses, Major elements 285

XRF Trace Element Analyses 286

APPENDIX THREE - MINERAL ANALYSES 294

Electron Microprobe Analyses 295

Carbon Coating 296

page

APPENDIX THREE - continued

Analytical Conditions 296

Corrections 297

Lowest Limit of Detection and Accuracy 297

APPENDIX FOUR - X-RAY DIFFRACTION

Powder Diffraction Method 308

Measurement of Powder Photographs 308

Indexing and Calculation of Cell parameters 309

Cubic Minerals 309

Non-cubic minerals 311

FIGURES

		page
1	Part of the 1:500,000 geological map of Turkey showing study area	3
1a	Geological Map of the vicinity of Dariköy-Tekmezar sulphide veins, SW Giresun, Turkey	5
1b	Mineral Provinces and major structure unit of Turkey	6
3.2	Composite column section of the study area	26
3.2.7	A section of Senonian Sequence near Yaslıbançe	40
3.4.3a	Rose diagrams of major joint trends in the study area	50
3.4.3b	Rose diagrams measured from aerial photographs for each of the 1:25,000 scale map sheet of the Eastern Black Sea area	51
3.4.4a	Rose diagram of Cu-Pb-Zn sulphide veins in the vicinity of Dariköy-Tekmezar area	54
3.4.4b	Various example of vein exposures	55
4.7a	Distribution of feldspar analyses in the system Or-Ab-An	69
4.7b	Plot of clinopyroxene analyses from basaltic rocks of Bulancak volcanics	70
4.9.1	Variation of major oxides with silica	75
4.9.1a	Variation of major oxides with silica	76
4.9.2	Changes in SiO_2 contents with increasing FeO/MgO ratio in Bulancak volcanics	77
4.10.1	Variation of trace elements with silica	80
4.10.2	K-Rb relationships in Bulancak volcanics	82
4.10.3	The plot of titanium against zirconium	83
5.5	X-ray diffraction patterns of various ganque minerals	98
5.9.2	Frequency diagram of cell-sizes measured on sphalerite from the Bulancak area	138
5.9.4	The relationship between d_{220} and Bi-Pb contents of aikinite-bismuthinite solid solution minerals	145

page

5.10.1 Minor element proportions in sphalerite 147

5.10.5 The system PbS-Cu_2S-Bi_2S_3 showing naturally occurring compositions including minerals from the Bulancak area 163

5.11 Geological map of the vicinity of Akköy Mine, Giresun, Turkey. 166

5.13.1 State of Yukari Üzümlük prospects in 1969 176

5.13.3 State of Aşagi Üzümlük prospect in 1969 179

5.15 Underground workings and geology of Etibank Dönbül Tepe prospect 188

6.2 Composition of sphalerite in equilibrium with various other phases in the Fe-Zn-S system. Phase relations projected on the FeS-ZnS binary 193

6.4.6 A plot of homogenization temperatures from sphalerite specimen 81 showing a Gaussian distribution 213

6.5.7 Fluid inclusion homogenization temperature and salinity data for some hydrothermal deposits 221

6.6.5a Time-temperature relations of the Dariköy-Tekmezar group veins 228

6.6.5b Frequency diagram for specimen 28 229

6.7 Variation of critical temperature and pressure with salinity of NaCl solutions 231

3.7.1 Boiling conditions for some inclusions from sphalerite specimens 232

6.8 Isotherms in relation to sulphide vein mineralization near Bulancak, Eastern Black Sea, Turkey 238

7.1 Major Alpine metallogenetic belts in relation to the Pontid ore province 243

MAPS AND GEOLOGICAL SECTIONS

1. Geological map of the Tekmezar, Dariköy and Akköy area of sulphide mineralization, south of Bulancak, Eastern Black Sea, Turkey.

2. Map showing the distribution and type of mineralization in relation to Geology.

3. Map showing collected specimen localities
Cross sections from the southern Bulancak Map area.

TABLES

3.2	Geological succession and comparison with neighbouring areas	27
3.4.2	Fault measurements	48
5.1	Minerals identified in the Bulancak sulphide occurrences	86
5.8	Paragenitic sequence	134
5.9.2	Sphalerite cell-sizes calculated on the basis of Mole % metal contents	137
5.9.3	X-ray Diffraction data for Betekhtinites	141
5.9.4	X-ray Diffraction data for Aikinites	143
5.10.1	Microprobe Analysis and cell-size measurements of Sphalerites	148
5.10.2	Betekhtinite Analyses from Bulancak and Harköy in comparison with other occurrences	153
5.10.3	Fahlerz Analyses in comparison with Espiye and Inköy occurrences	156
5.10.4	Electron Microprobe Analyses of Aikinites	158
5.10.5	Composition of aikinite derivatives	160
5.13	Microprobe analyses and Homogenization Temperatures of the Üzümlük veins	181
6.5.6	Freezing data and equivalent NaCl content	219
6.5.7	Salinities and Original Densities of some Primary Fluids	220
6.6	Homogenization temperatures of fluid inclusions in transparent vein and gangue minerals	226

APPENDIX TABLES

1.	Location of rock and vein samples	282
2A	XRF Analyses of Lower Basic Series rocks	288
2B	XRF Analyses of Porphyritic dacites	291
2C	XRF Analyses of Rhyodacitic rocks	293
2D	XRF Analyses of basaltic dyke rocks	294
3.1	Optimum conditions for feldspars and pyroxenes	299
3.2	Optimum conditions for sulphide and sulphosalts	300
3A	Feldspar analysis of Bulancak volcanics	302
3B	Clinopyroxene analysis of Bulancak volcanics	305
4.1	Diffraction patterns for pyrites	313
4.2	Diffraction patterns for sphalerites	319

PLATES

		page
1a	Old slag dumps near the Körükyeri Locality old workings	2
1b	Wooden ore-carrier recovered from old workings at Körükyeri Locality, Tekmezar	2
2.3.10	River terraces of Batlama Stream below Akköy Mine	22
3.2.1	Exposure of Lower Basic Series rocks near Kovalik Sr.	30
3.2.7a	Section in Senonian Limestone sequence near Yaslibahçe	38
3.2.7b	Close up of beds to the right of the vehicle in the upper picture	38
3.4.4a	Breccia along Üzümlük veins	57
3.4.4b	Ore breccia	57
4.2.1	Ophitic texture in basalt	61
4.2.2	Vesicular texture in Lower Basic Series rocks	61
4.3.1	Pseudomorphosed feldspar phenocrysts	64
4.5.1	Hematite Lamella along cleavage planes of biotite	64
4.7.1	Euhedral, altered magnetite crystals	72
4.7.2	Skeletal growth of magnetite with feldspar laths	72
5.3.1a	Sphalerite replacing euhedral quartz	88
5.3.1b	Sphalerite replacing euhedral quartz with pyrite	88
5.3.2a	Quartz, carbonate and hematite relationship	90
5.3.2b	Bladed specular hematite crystals	90
5.3.2c	Bladed specular hematite crystals	91
5.3.2d	Bladed hematite in quartz. Colloform banding in goethite	91
5.3.4	Bladed hematite in quartz. Colloform banding in goethite	93
5.3.5	Lepidocrocite adjacent to pyrite	93
5.5.1a	Galena showing filliform texture	96

5.5.1b	Galena showing filliform texture	96
5.5.2a	Calcite showing bireflection and lamellar twinning	99
5.5.2b	Siderite replacing dolomite. Euhedral pyrite crystal	99
5.5.2c	Detail from plate 5.5.2b	100
5.5.2d	Detail from plate 5.5.2b	100
5.6.1a	Fractured euhedral pyrite with chalcopyrite veinlets	102
5.6.1b	Chalcopyrite veinlets between pyrite grains	102
5.6.3a	Lamellar twinning in sphalerite revealed by etching (HNO_3). Unetched galena and pyrite	105
5.6.3b	Late stage quartz replacing sphalerite	105
5.6.3c	Chalcopyrite exsolution in sphalerite	106
5.6.3d	Sphalerite with exsolution chalcopyrite has been replaced by fahlerz in which the chalcopyrite exsolution bodies remained unaltered	106
5.6.3e	Sphalerite-galena relationship	107
5.6.3f	Chalcopyrite replacing sphalerite along twin boundaries revealed by etching	107
5.6.4a	Galena residuals in cerussite-covellite intergrowth	109
5.6.4b	Similar to 5.6.4a	109
5.6.5a	Twinning in chalcopyrite revealed by etching Euhedral pyrite	111
5.6.5b	Chalcopyrite replacing pyrite	112
5.6.5c	More advanced stage of replacement, cf. 5.6.5b	112
5.6.6a	Mosaic texture in bornite revealed by etching	114
5.6.6b	Chalcopyrite-bornite intergrowth	114
5.6.7a	Idaite, covellite, chalcopyrite and pyrite relationship	116
5.6.7b	Idaite, chalcopyrite and sphalerite relationship	116
5.6.7c	Idaite-covellite relation	117
5.6.7d	Same as 5.6.7c, x-polars	117

5.6.8a	Lattice texture covellite with chalcopyrite and sphalerite.	119
5.6.8b	Same as 5.6.8a, x-polars.	119
5.6.9a	Galena residuals in digenite.	121
5.6.9b	Mutual boundary texture between betekhtinite and digenite with galena residuals.	121
5.6.10a	Reflection pleochroism revealed by betekhtinite grains in different orientation.	123
5.6.10b	Galena, betekhtinite, bornite, digenite and euhedral quartz relationship.	123
5.6.10c	Similar to 5.6.10b.	124
5.6.10d	Myrmekitic texture between galena-bornite and galena-digenite in betekhtinite.	124
5.7.1a	Zoning in fahlerz revealed by etching.	127
5.7.1b	Fahlerz replacing euhedral quartz in chalcopyrite.	127
5.7.2a	Reflection pleochroism in aikinite.	130
5.7.2b	Aikinite, digenite, chalcopyrite and marcasite relationship.	130
5.7.2c	Aikinite replacing pyrite.	131
5.7.2d	Aikinite replacing sphalerite.	131
5.7.2e	Unknown lamellae of bismuth sulphosalt in aikinite.	132
5.7.2f	Similar to 5.7.2e	132
5.11.1	No. 2 Adit Akköy Mine	168
5.11.2	No. 3 Adit Akköy Mine	168
5.15a	View of Etibank Waste tip below 571 Adit near Dönbül Tepe (Şişpelit Dere)	185
5.15b	The state of Demir Export Company Şişpelit Dere prospect in 1969.	185
6.4.1a	Primary fluid inclusions (in sphalerite)	199
6.4.1b	Similar to 6.4.1a	199

6.4.1c	Isolated primary inclusions with planes of secondary inclusions (in sphalerite)	200
6.4.1d	Primary fluid inclusion showing faceted negative crystal form (in sphalerite)	200
6.4.1e	Fluid inclusions showing a relationship with primary colour banding (in sphalerite)	201
6.4.1f	Isolated primary fluid inclusions in quartz	201
6.4.3a	Planar pseudosecondary inclusions showing some orientation with crystallographic directions (in sphalerite)	203
6.4.3b	Faceted pseudosecondary inclusions (in sphalerite)	203
6.4.3c	Planes of similarly orientated pseudosecondary inclusions showing stages of necking down (in sphalerite)	204
6.4.3d	Secondary (pseudosecondary?) fluid inclusions in quartz.	204
6.4.4a	Gas-rich, Liquid-rich and one phase inclusions in baryte.	205
6.4.4b	Secondary inclusions in quartz.	205
6.4.4c	Gasless inclusions with isotropic daughter minerals (in sphalerite)	207
6.4.4d	Enlargement of daughter minerals (in 6.4.4c)	207
6.4.4e	Enlargement of daughter minerals (in 6.4.4c)	208
6.4.4f	Sharply faceted three phase inclusion (in sphalerite)	208
6.4.5a	Solid inclusions and primary fluid inclusions with opaque captive minerals (in sphalerite)	210
6.4.5b	A primary fluid inclusion with a captive opaque mineral (in sphalerite)	210
6.4.5c	Primary fluid inclusion subdivided by opaque captive mineral	211

CHAPTER ONE

INTRODUCTION

This research includes the results of detailed geological mapping that was undertaken in the Bulancak area on a scale of 1 : 10 000 during the 1968-69 summer season. The mapping was carried out by MTA (the Mineral Research and Exploration Institute of Turkey) geologists with the cooperation of a group of Yugoslavian geologists as a part of a United Nations Project. The writer, in charge of this party, was responsible for writing the geological report, and also for investigating some relevant major and minor vein occurrences in the field. During this investigation over 100 veins in the area were mapped but the narrowness and pinching and swelling character of the veins coupled with the rough topography and poor exposure made the area uneconomic, and as such no further attempt was made to correlate the veins to each other.

The writer visited the area again in the summer of 1971, followed by a short visit in 1973, to collect rock and mineral samples. During the 1971 visit the 1 : 10 000 scale geological map was revised and several veins, newly exposed as a result of road construction, were mapped. Based on the field evidence and attitudes of the veins an attempt was made to correlate the veins to establish the mining map of the area. In the investigated area there are some veins which have been worked since medieval times and were possibly mined by the Genoese (Plates 1a, 1b).

This thesis discusses the geology, mode of occurrence, mineralogy, genesis of the sulphide veins and nature of the ore forming fluids of the Zn-Pb-Cu veins of the Bulancak area, west of Giresun City, a small township on the Black Sea coast. The investigated area is situated between 38°00' and 38°30' longitude and 40°30' and 41°00' latitude (Fig 1). The mineralized area, 10 Km. south of Bulancak, covers an

Plate 1a. Old slag dumps near the Körükyeri Locality old workings. The tent is located on slag dumps.

Plate 1b. Wooden ore-carrier recovered from old workings at Körükyeri Locality, Tekmezar

Fig. 1 Part of the 1:500,000 geological map of Turkey showing study area. Names of some mineralized Localities underlined.

area of about 50 $Km.^2$ around Dariköy and Tekmezar Villages (Fig. 1a).

Investigated occurrences are located in the "Dogu Karadeniz Cevher Bölgesi (Eastern Pontus Ore Province)" which covers the area between roughly Samsun and Batumi (Russia) cities on the Black Sea coast approximately 600 Km. in length, 60 Km. in width, associated with extensive volcanic rocks that are mainly calc-alkaline (Fig. 1b).

The Pontids (The Pontic Mountains), a tectonic as well as a geographical unit, form the northern rampart of Anatolia rising steeply from the Black Sea Coast, and extending westward for over 1200 Km. from the antecaucasus (Gabrelian, 1964) almost to Istanbul. They are divided into Western and Eastern major units (H.H. Schultze-Westrum, 1961) by the Kizilirmak (River Halys) to the west of Samsun City. The Pontic ranges constitute a great barrier between the Black Sea and the interior of Anatolia which is broken at only three places where the Kizilirmak, Yesilirmak and Goruh Rivers cut gorges to the sea.

Mineralization in the Eastern Pontus Ore Province can be outlined, in general, as follows: In the inland side, around the contacts of the Intrusive masses forming smoothly sloping high plateau regions, skarn type contact (Metasomatric) metamorphic deposits occur. In the coastal region,at the upper contact of volcanics and upper Cretaceous limestones, replacement deposits formed, and between Lower Basic Series dacitic lavas and overlying volcanics and pyroclastics, strata-bound, Kuroko-type massive ore bodies and veins are seen. Vein type deposits are mainly concentrated to the west of Giresun City and usually occur in the Lower Basic Series or the Dacitic Series. Stockwork type

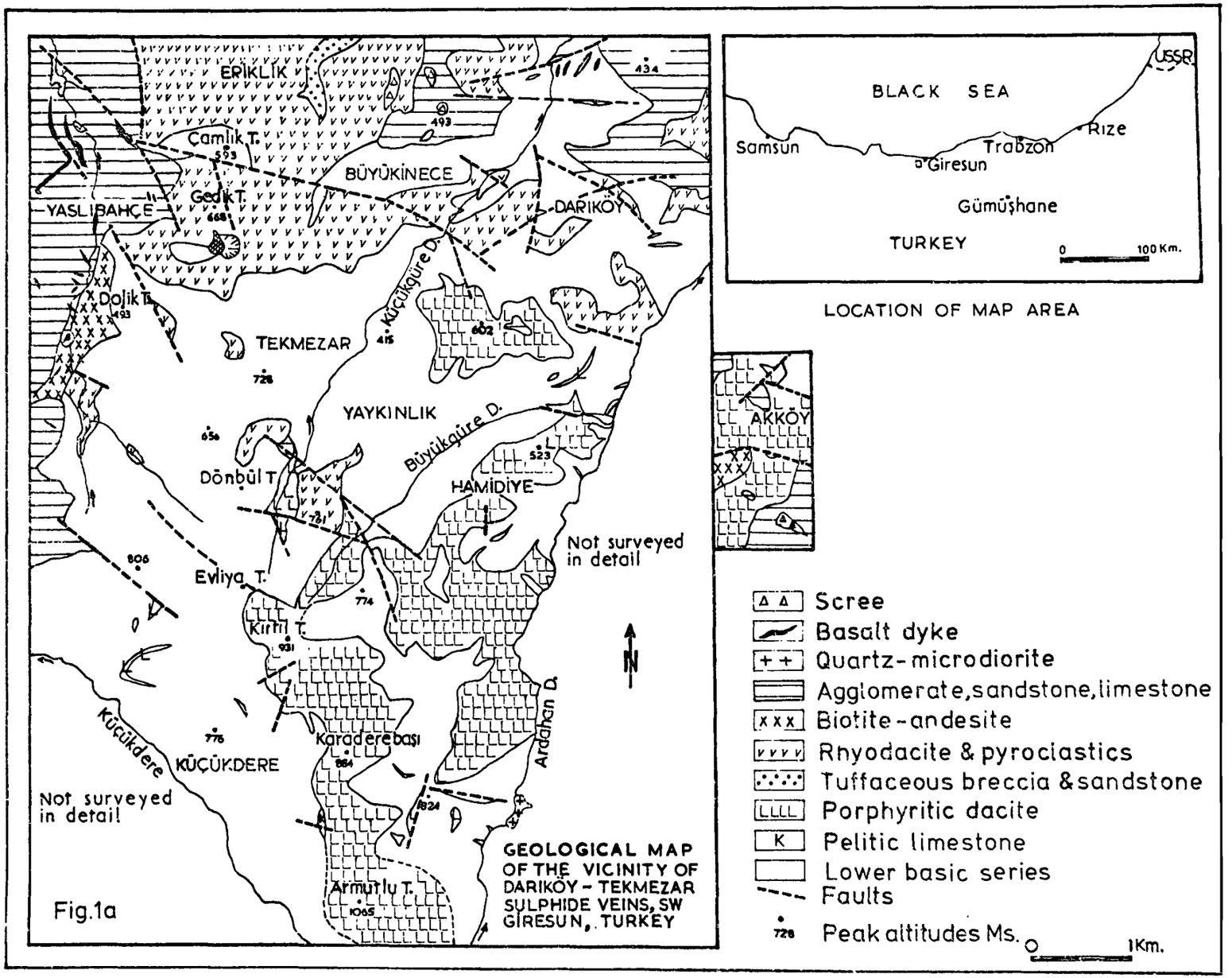
ERİKLİK
Çamlık T.
BÜYÜKİNECE
YAŞLIBAHÇE
Gedik T.
DARIKÖY
Küçükçüre D.
Dolik T.
TEKMEZAR
YAYKINLIK
Büyükçüre D.
Dönbül T.
HAMİDİYE
Not surveyed in detail
Evliya T.
Kirtil T.
Küçükdere
KÜÇÜKDERE
Karaderebaşı
Ardahan D.
Not surveyed in detail
Armutlu T.
Fig.1a
GEOLOGICAL MAP OF THE VICINITY OF DARIKÖY - TEKMEZAR SULPHIDE VEINS, SW GİRESUN, TURKEY
BLACK SEA
USSR
Samsun
Trabzon
Rize
Giresun
Gümüşhane
TURKEY
0 100 Km.
LOCATION OF MAP AREA
AKKÖY
Scree
Basalt dyke
Quartz-microdiorite
Agglomerate, sandstone, limestone
Biotite-andesite
Rhyodacite & pyroclastics
Tuffaceous breccia & sandstone
Porphyritic dacite
Pelitic limestone
Lower basic series
Faults
Peak altitudes Ms.
0 1Km.

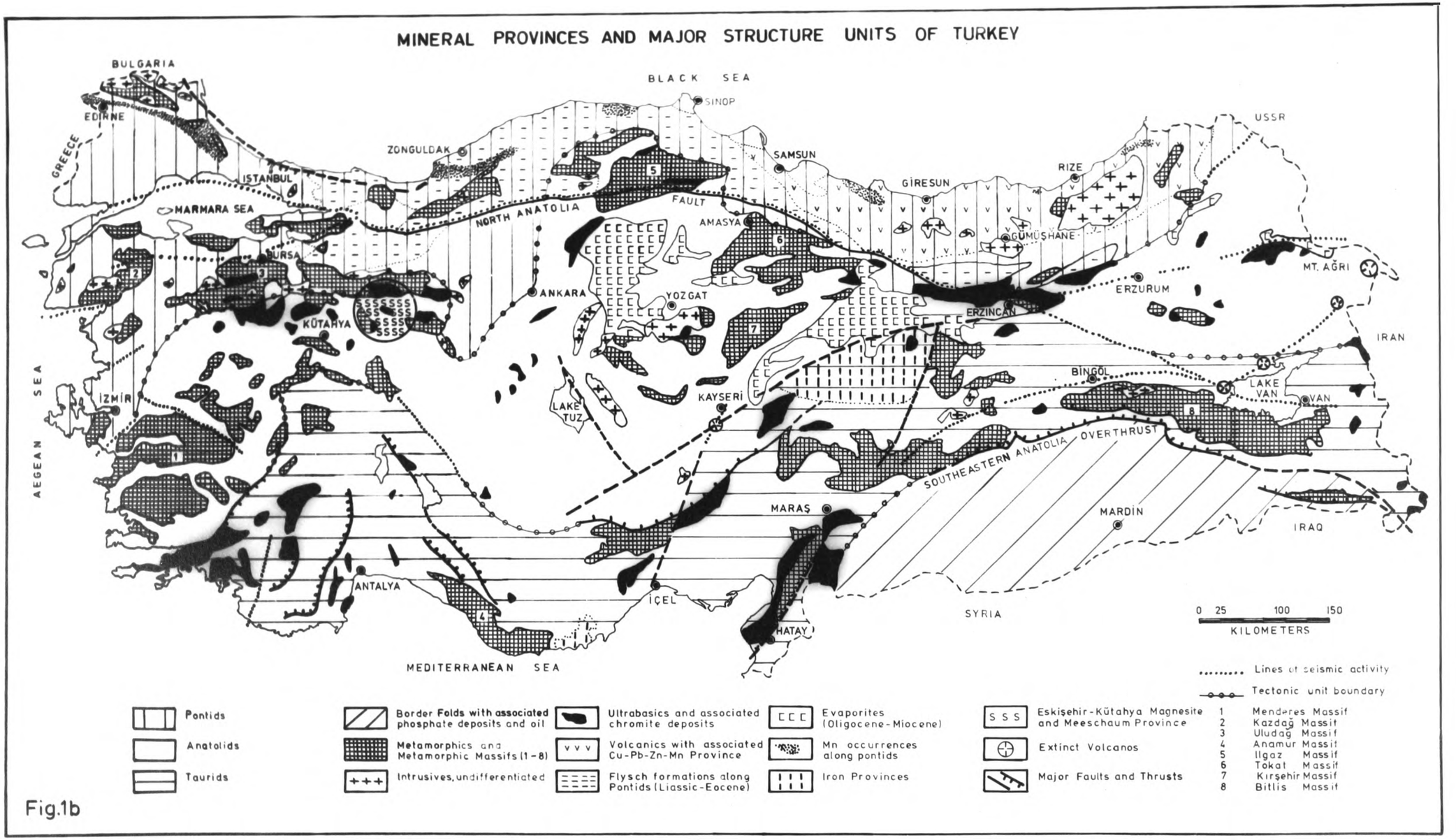
MINERAL PROVINCES AND MAJOR STRUCTURE UNITS OF TURKEY
BULGARIA
BLACK SEA
SINOP
EDIRNE
GREECE
ZONGULDAK
SAMSUN
USSR
RIZE
ISTANBUL
GİRESUN
MARMARA SEA
NORTH ANATOLIA FAULT
AMASYA
GÜMÜŞHANE
BURSA
ANKARA
YOZGAT
ERZURUM
MT. AĞRI
ERZINCAN
KÜTAHYA
IRAN
AEGEAN SEA
BİNGÖL
LAKE VAN
VAN
İZMİR
KAYSERİ
LAKE TUZ
SOUTHEASTERN ANATOLIA OVERTHRUST
MARAŞ
MARDİN
IRAQ
ANTALYA
İÇEL
SYRIA
HATAY
MEDITERRANEAN SEA
0 25 100 150
KILOMETERS
Lines of seismic activity
Tectonic unit boundary
Pontids
Anatolids
Taurids
Border Folds with associated phosphate deposits and oil
Metamorphics and Metamorphic Massifs (1-8)
Intrusives, undifferentiated
Ultrabasics and associated chromite deposits
Volcanics with associated Cu-Pb-Zn-Mn Province
Flysch formations along Pontids (Liassic-Eocene)
Evaporites (Oligocene-Miocene)
Mn occurrences along pontids
Iron Provinces
Eskişehir-Kütahya Magnesite and Meeschaum Province
Extinct Volcanos
Major Faults and Thrusts
1 Menderes Massif
2 Kazdağ Massif
3 Uludağ Massif
4 Anamur Massif
5 Ilgaz Massif
6 Tokat Massif
7 Kirşehir Massif
8 Bitlis Massif

Fig.1b

deposits are represented in the east near to the Russian border by the Murgul deposit which occurs in dacitic rock and tuffs (Hamamcıoglu and Sawa, 1971; Tugal, 1969).

In the Eastern Black Sea region, mountains form an inclined block, sloping from south to north, to the Black Sea. Major step faults run more or less parallel to the coast line and notable examples can be seen south of Trabzon City. Smaller transverse faults run perpendicular these step faults. In the south, the Pontids rest on the Anatolian Plateau and are delimited by another major fault system along the Coruh Depression and Gümüshane-Harsit Valley and continuing beyond this in a southeasterly direction (Gattinger, 1962). In the north, they form the abrupt coastal mountains of the Black Sea. The relief of the mountain chain increases eastwards and near the Russian border it reaches almost its maximum. The summit region reaches 3937m. in Kackar Dagı (Mount Kackar), a lava cone superimposed on the main eastern Tatos batholith (3500 $Km.^2$) intruded in the Upper Cretaceous volcanics of the Eastern Pontids. It broadens westwards into a smoothly sloping plateau and short, rapid streams, flowing directly to the Black Sea, cut the plateaus into narrow ridges lying perpendicular to the strike of the E - W trending mountain chain producing rugged foothill country with the land rising to over 2000 m. within 15-20 Km. of the coast.

The heights in the mapped area decrease from south to north. Armutlu Tepe (Hill) forms the highest peak (1065 m.) in the south on a ridge extending SSE-NNW. The hills such as Karaderebası (884 m.), Kırtıl Tepe (931 m.) Evliya Tepe (900 m.), Dinekkaya Tepe (728 m.), Gedik Tepe (668 m.), Çamlık Tepe (593 m.) are found along this central narrow ridge of the mineralized area (Fig. 1a). To the northeast,

triangular ridges are developed due to streams such as the Küçükküre, Büyükküre and Karadere flowing in SW-NE directions. Ardahan D., a branch of Büyükküre D., forms the eastern boundary of the map area (Fig. 1a). To the west, Küçükdere and Çamkoza D. limit the map area. Because the area is geomorphologically young, slopes are generally steep, a very young drainage pattern is developed and tributaries of these streams are usually structurally controlled and follow NW-SE trending fractures and faults (Plate 1a, Map 2). The processes of natural erosion tend to limit soil development, maintaining a close relationship between soil and parent material.

Küçükdere, Yaykınlık, Darıköy, Tekmezar, Eriklik and Yaslıbahçe, villages of the area have only small populations.

The road cuttings and stream lines are the best places to study exposures continuously, otherwise a thick cover of debris, soils, landslides and rhododendron colonies cause considerable difficulties.

1.1 Climate and Vegetation:

The narrow strip between the crest of the Eastern Pontids and the Black Sea forms a distinctive climatic region. There is a striking difference in the climates of the northern and southern regions of the coastal range, which prevents the mild maritime winds from reaching inland. Consequently a continental climate prevails in the south. The contrast between the coastal zone and the Anatolian Plateau is more marked in winter. A maritime climate is dominant. Mean annual rainfall is about 132 cm. in Giresun in comparison to Rize which is 244cm.

The Eastern Black Sea region has the most abundant, regular and evenly distributed rainfall in Turkey (Dent, 1969) while the interior of Anatolia is a region of summer drought (25 cm/m^2 rainfall). The heaviest rainfall occurs on the northern slopes of the Pontids, facing the Black Sea coast. Due to northwesterly winds the region is always humid and rainy. Snowfall is comparatively infrequent.

Hazelnuts were a minor crop until the early 19th century but now around Giresun up to 90% of the cultivated area is under hazelnuts (see Plate 5.15a). The highest hazelnut plantations in the Black Sea region are found in the Bulancak area and most plantations are grown below 700m. Besides the hazelnuts, Diospyros Lotus is cultivated as a tree crop. Beech, box and spruce, oak, chestnut and pine are the common trees. Rhododendron is common throughout the Black Sea coast area, frequently producing dense vegetation and such areas are hardly accessible. Fagus becomes the dominant tree in the foothills (Dent, 1969).

The main agricultural products are maize, beans, potatoes, tobacco and tangerines with a wide range of temperature fruits.

CHAPTER TWO

PREVIOUS WORK

2.1 History

The earliest geological investigations along the Pontids began in the middle of the 19th century and followed the general geological units and mineral deposits of the country. W. Hamilton (1849) and notably Tchihatcheff (1867) were the first investigators who travelled throughout Anatolia and made a few surveys within the area of the Samsun Sheet (1:500,000). However, Tchihatcheff identified the Cretaceous and accepted the Paleozoic as a "formation of transition" around Amasya. Their observations were published in the form of various discussions. A leucite rock from Trabzon area has been studied (A. Lacroix, 1891). G. Berg (1910) made investigations along the Samsun-Amasya-Tokat Highway and Meister (1913) described the liassic fauna in the Samsun sheet area. F. Oswald (1912) gave some details of the eastern slopes of the Black Sea mountains in his book "Eastern Anatolia". F. Frech (1914), A Phillipson (1919) and Nowack (1928, 1932) gave some information about regional-geological and tectonic studies and mining activities which as a whole completed the geological picture of the region. The earliest studies concentrated mainly on the coal basin of the Zonguldak area in the Western Pontids and Cu-Pb-Zn and iron deposits of the area.

Following the foundation of the MTA Institute in 1935 more detailed studies began in this area, as elsewhere in Turkey. V. Stchepinsky (1945) studied particularly the Miocene fauna, the mineral deposits of Erzincan and Sivas and the stratigraphy of the Kelkit-River basin.

E. Altınlı (1946) has published his surveys on the geology of the Ordu-Giresun Provinces which includes the investigated mineralized area.

E. Parejas, M. Blumenthal, C. Erentöz, T. Yücel, A.C. Okay, E. Lahn, K. Erguvanli are amongst workers who have studied different parts of the Eastern Pontids.

All the previous work until 1960 was based on the 100,000 scale topographic maps and as a result of these works the 500,000 scale geological map of Turkey was published by MTA in 21 separate sheets.

More detailed studies were carried out by Schultze-Westrum (1960-61) around Giresun, and the Espiye pyritic copper deposits by Pollak (1961). The investigated area and its surroundings was mapped by Agar and Schultze-Westrum on the 25,000 scale in 1960 but previous geological information concerning the research area is unfortunately very limited.

2.2 Review of the tectonic units of Turkey

Turkey mainly developed as a result of different stages of the Alpine Orogeny, and it has been divided into several units by previous workers (Arni, 1939; Blumenthal, 1946; Egeran, 1947; Ketin, 1959-66). There seems to be no overall agreement on the tectonic divisions, although the later authors do not differ much from the original divisions of Arni. According to Ilhan (1971) Hercynian movement in Anatolia has an E-W trend which is approximately parallel to the later and dominant Alpine trends.

More recently Brinkmann (1971) divided Turkey into six geotectonic units with a new approach:

1. The oldest structural elements (Rhodope-Istranca and Kirsehir Massifs).
2. Istanbul-Zonguldak fold zone of Variscan orogeny.
3. Lias-Dogger trough, formed along the Pontids as the nucleus of the early Alpine geosyncline.

4. Middle Alpine structures, formed from the folding of the Central Anatolian radiolarite-ophiolite facies which is described by Horstink (1971) as the Northern Anatolian Tethys ophiolite nappe.
5. Pontic and Tauric ranges which formed from the Alpine Geosynclinal on both side of the Central Anatolian axial region which for most of its geological history represented an area of shelf carbonates, clastics and evaporites sedimentation.
6. Neotectonic patterns, late Tertiary folds.

Horstink (1971) analysed the late Cretaceous and Tertiary geological evolution of Eastern Turkey, differentiating five different units from north to south namely, Pontids, Northern Tethys ophiolite nappe, Anatolids, Southern Tethys ophiolite nappe, Arabian platform. He suggests that the Pontids form the megatectonic unit of northern Turkey, and overlie the ophiolites that were generated in the Northern Tethys ocean.

Although the Pontids have been considered to be elevated large massifs of crystalline rocks by many of the authors named above, Tokel's (1973) work shows that the Pontid belt was tectonically unstable during the Mesozoic and Cenozoic. There are many breaks in the sedimentary sequence which overlies the Paleozoic granitic and metamorphic basement.

On the other hand Ketin's classification is more simple and realistic by dividing Turkey into 4 tectonic units (Fig. 1b).

1. The Pontids which form the Black Sea coastal mountains, and the Marmara and Thrace regions of Turkey (Fig. 1b).
2. Anatolids, which mainly includes the highlands of Anatolia and the Menderes, Tokat and Kirsehir Massifs.

3. Taurids mainly occupy the south and east Anatolian mountain ranges (Tauric mountains) and Bitlis Massif.
4. Border Folds covers the area of southeastern Anatolian youngest mountain ranges.

However, the theory of Ketin (1966) that the geotectonic development of Turkey started on the north and developed towards the south forming these four different units will not explain the whole geological development of Turkey satisfactorily in the view of the more recent plate tectonic studies (McKenzie, 1970; Dewey et al, 1973).

2.3 The Stratigraphy of Eastern Pontids:

The investigated area is included in the Eastern Pontid tectonic unit of Turkey which is mainly developed in volcanic facies as mountain ranges almost parallel to the Black Sea Coast. Eastern Pontid volcanicity begins with Jurassic formations of transgressive conglomerate, sandstone, shale and Ammonitico Rosso facies associated with basaltic lavas in the Gümüshane area (Yılmaz, 1973) and spilitic agglomerate series in the Giresun area (Schultze-Westrum 1961).

Extensive Cretaceous-Tertiary volcanics and associated sedimentary rocks are replaced by older rocks from the Black Sea Coast towards the southern boundary of the unit along Kelkit-Çoruh Depression which is a part of the North Anatolian Fault (Fig. 1b).

The Paleozoic metamorphism is confined to Pontids (Ketin, 1959; Kamen-Kaye, 1971) while it is mostly Alpine in the other tectonic units.

Intensely folded Paleozoic matesediments underlie the investigated area and are exposed to the south of it around the intrusive blocks or batholiths which are seen parallel to (within 20-30 Km. of) the coast line especially to the south of Ordu-Giresun Cities (Fig. 1).

No rocks older than Jurassic, except the crystalline basement, are exposed along the coastal ranges although they occur in the Western Pontids in continential and shelf facies. According to Brinkman (1968, Fig. 1) at the beginning of Tournasien a short lived geoanticline (The North Anatolian Welt) was formed covering part of the Western Pontids, the whole of the Eastern Pontids and extending into the Caucasus. This uplift is accompanied by granitic intrusion whose ages were determined by Cogullu (1970) c.a. 300 million years.

Triassic, Paleocene and Oligocene sediments are not reported from Eastern Pontids. Until the Jurassic the Eastern Pontids were a part of the Pontic Land which covered the present day Black Sea. A deep trough developed during Lias and Dogger and an extensive oceanic crust (North Anatolian Tethys) existed between the Pontic Land mass to the north and Anatolia to the south along the present day North Anatolian Fault (ophiolite-radiolarite series which is seen as "Mof" series on the geological map of Turkey). During Cretaceous-Early tertiary this boundary zone was a site of subduction which led to extensive Upper Cretaceous-Eocene volcanicity (Dewey et al,1973). According to Tokel (1973) North Anatolian Tethys closed after the Upper Cretaceous due to relative northeastward movement of African-Arabian Plate and a trench formed along the Eastern Pontids continental margin. As the oceanic crust and associated ocean-floor sediments descended beneath the trench and adjacent volcanic area, extensive calc-alkaline andesitic volcanism resulted during the Middle Eocene in the Gümüshane area.

The stratigraphic column of the Eastern Pontids was generalised after the following authors work: Schultze-Westrum (1961), Gattinger (1962), Akıncı (1969), Tugal (1969), Tokel (1973) and Yılmaz (1973), Göksu (1974).

10. Sea and River terraces, travertines.

9. Glacial Deposits.

8. The Young Basic Series and Late Dykes.

7. The Tertiary Intrusives.

6. Hypabyssal Dacite.

5. The Upper Basic Series.

4. Dacitic Series:
   c. Dacite II
   b. Dacitic tuffs or rhyodacites
   a. Porphyritic Dacite (Ore-bearing dacite)

3. Lower Basic Series and Early Dykes.

2. Paleozoic intrusives.

1. Crystalline Basement.

2.3.1 Crystalline basement of the Eastern Pontids is believed to be Paleozoic although the age of metamorphic massifs of Turkey is still controversial. The central gneissic cores of some of the massifs were interpreted as metamorphosed Cambrian sediments (Schuiling, 1962). The upper parts of the crystalline basement either grades to unmetamorphosed fossiliferous Permo-Carboniferous rocks or ophiolite-radiolarite facies of Jurassic-Cretaceous series (Ketin, 1951, 1962). They are mainly represented by Glaucophane-greenschist facies (Kaaden, 1966), gneiss, micaschists and quartzites.

2.3.2 Paleozoic intrusives of the Pontids are exposed in several places, cutting through the metamorphic schists and Permo-Carboniferous rocks of the crystalline basement. Overlying Jurassic basal conglomerates are recognised with the pebbles of these intrusives. They are varying in composition from Granite (Adamellite) to Granodiorite or Gabbro (Yılmaz, 1973) and emplaced during Hercynian Orogeny. As previously mentioned their ages were determined by Cogullu (1970) as 300 million years.

2.3.3 The lowermost sequence of the extensive Eastern Pontid volcanicity is represented in a variety of basic volcanics and pyroclastics. Due to its complex character various names have been proposed but the grouping as "The Lower Basic Series" is the most appropriate and accepted description (Tugal, 1969).

In the Gümüshane area they represent earliest Jurassic volcanism and consist of numerous basic dykes, plugs and associated basaltic lavas (Tokel, 1973) while in the Espiye investigated area they consist of a thick sequence of volcanics being interstratified with/or overlain by alternating fossiliferous pelagic limestones, marl, sandstones and pyroclastics of the Senonian age. The units forming Lower Basic Series around Giresun were described by Schultze-Westrum (1961) as spilites, keratophyres, diabases, basalts, andesites and tuffites and agglomerates. This series is the oldest stratigraphic unit in the investigated area and in Espiye (Lahanos Mine area). Although they are extensively altered around Tekmezar and Darıköy villages (Fig. 1a) to the south of the map area, partly fresh rocks were described as spilite, amygdaloidal andesite, andesitic tuff and ignimbrite and breccia (MTA Rep. No. 982) similar to the Rize-Murgul area (Kraëff, 1963a).

2.3.4a Special attention has been focused on the dacitic series from the point of view of the occurrences of sulphide deposits. Throughout the Eastern Pontus Ore Province important pyritic sulphide deposits were either located in the porphyritic dacite, which has been called by several workers as "Ore-bearing Dacite", at the contact of dacitic tuffs and porphyritic dacite, or porphyritic dacite and Senonian sediments. Amongst the known examples are Lahanos, Köprübası (Tirebolu) and Murgul Mine. In the investigated Akköy Mine, mineralisation is located at the contact of porphyritic dacite and overlying tuffs, whereas the Küçükdere village occurrence represents a lens-shaped limestone replacement orebody located at the contact between the lower basic series and overlying porphyritic dacites. Veins either occurred in lower basic series and porphyritic dacite or dacitic tuffs and rhyodacites. Due to hyrothermal alteration they are divided into 3 subdivisions by Kräeff (1963b) in the vicinity of Murgul Mine.

The overlying sedimentary sequence was described by the writer in detail in the Görele area, to the east of Giresun, and named as Akköy Formation (Akıncı, 1969a). This sequence is described by Schultze-Westrum in the Giresun area as being Red Inoceramus Limestones interbedded with dacitic series. In the investigated area, the sequence overlies the volcanics to the west and north of the map area and its age is evidenced with fossils.

2.3.4b Dacitic tuffs are not mapped as separate units in the investigated area but they immediately overlie porphyritic dacite in the Akköy Mine (Plates 5.11.1,2) and in the Lahanos Mine areas. The pyritic sulphide deposits tend to occur at or near to the contact of the porphyritic dacite with tuffs (Tugal, 1969). In places limestones and marls are intercalated with these tuff levels. Extensive fine-grained

rhyodacitic lavas and pyroclastics developed to the north of the map area but as the whole series is hydrothermally altered they are only recognized with the triangular small quartz phenocrysts and columnar joints. Since they immediately overlie/and are in contact mostly with the Lower basic series their age relations with the porphyritic dacites are not clear but several field evidences suggest a younger age than porphyritic dacites. These rhyodacitic lavas are comparable with lavas above the adit 2 of Lahanos orebody (Tugal, 1969) where orebody, as previously mentioned, occurs at the boundary between porphyritic dacites and overlying rhyodacitic lavas and tuffs.

2.3.4c. Dacite II is not developed in the map area while it is well developed and described in detail in Murgul Mine where they partly overlie porphyritic dacites and the dacitic tuffs. An unconformity has been described between porphyritic dacites and dacite II (Krüeff, 1963b). They are usually seen in varying colours in hydrothermally altered areas such as Murgul Mine but purple coloured formation was described from the Görele area by the writer (Akinci, 1969a).

2.3.5 Upper Basic Series are a very heterogenous formation reaching a thickness of up to 1000m. They are seen throughout the Eastern Pontids in the Upper Cretaceous-Eocene age. Upper Cretaceous alkaline suite comprising olivine-dolerite, hornblende-andesite, trachy-andesite and trachyte are reported from the Gümüshane area (Tokel, 1973). Along the Aksu Stream Valley in Giresun they consist of spilites and basalts, keratophyres and andesites, agglomerates and tuffs (Schultze-Westrum, 1961). To the further east in the Murgul region this series is represented by spilite, keratophyre and spilitic agglomerate and tuff. In the Görele

and Çayeli (Rize) regions they consist of basalts and basaltic volcanics together with tuff intercalations and may contain dacite II xenoliths and limestone blocks (Akıncı, 1969a; Tugal, 1969; Geoffroy, 1960). Voluminous pyroxene-andesitic volcanicity of Middle Eocene age in the Gümüshane region was attributed to the subduction along the southern boundary of the Eastern Pontids (Tokel, 1973) which finally resulted with the emplacement of Tertiary Intrusive bodies.

2.3.6 Hypabyssal dacite is described as Quartz-biotite-feldspar Porphyry by Tugal (1969) and very well known from the Lahanos Mine area where it was named as "Lahanos Tepe Dasiti" by Pollak (1961). It has an intrusive character as well as extrusive and the dykes of this NW-SE trending intrusive body in Lahanos are found cutting through the upper volcanic series and the overlying rocks suggesting a later age than the upper volcanics, possibly Early Tertiary (Tugal,op.cit). It is characterized by deep weathering, onion structure and arenaceous alteration. The equivalent of this dacite is called Dacite III in the Murgul area by Krüeff (1963b). The biotite-andesites of the investigated area are comparable with this dacite in the view of their intrusive and porphyritic character but they are overlain by Senonion limestones and cut through the Lower Basic Series therefore they must be considered in the dacitic series or the upper basic series.

2.3.7 Tertiary intrusives occupy the high plateau regions along the coastal ranges. Isolated, acid to intermediate intrusive bodies can be seen from the 50 Km. south of Ordu City to the east (Fig. 1).

A large batholith is exposed to the east of the Rize City whose age was determined by Cogullu (1970) as 25 million years (Fig. 1b). These possibly syn-orogenic intrusions contain xenoliths of volcanics and other rocks (Tugal, 1969). Tonalite, granite, and granodiorite from the Rize-Murgul region described by Krüeff (1963b) and Altınlı (1970). According to Schultze-Westrum (1961) Tertiary granitic intrusions of the Ordu-Giresun region consist of granodiorite, quartz-diorite, granodiorite porphyry, quartz-albitite, and he also includes the Lamprophyre dykes into this group. Skarn type metasomatic deposits and some pyrite impregnations are associated with these intrusives.

Although the intrusives are exposed at the south and north of the map area, only mappable intrusive body, which has been described as quartz-microdiorite is exposed in a small scale (Map 1). Similar quartz-diorite intrusions described by Tugal (1969) from the Lahanos Mine area show variations from centre to margins.

2.3.8 The youngest igneous activity is represented with the basalt dykes in the investigated areas of Espiye (Tugal, 1969), and Görele (Akıncı, 1969a)while in the Tirebolu and Murgul-Coruh areas a series of andesites and basalts developed.

In the western part of the Eastern Pontids around Giresun basaltic agglomerates, tuff, quartz-trachyte, trachy-andesite, leucitite, tephrite, olivine-leucitite, olivine-basalt and sediments of marly limestone of Oligocene-Miocene age are included in the young volcanics by Schultze-Westrum (1961). Partly albitized andesites, basalt and spilite with porphyries and diabase are described by Krüeff (1963a) in the Şirya-Ardanuç area.

Yilmaz (1973) has drawn attention to the abundance of olivine in the Upper Cretaceous volcanics and the andesitic and dacitic character of the Tertiary volcanics in the Gümüshane area which has been specified by Schultz-Westrum (1961) as basic and alkali types.

2.3.9 To the east of the Eastern Pontids glacial moraines are found on the highest peak regions of the coastal ranges. Altınli (1946) reported the cirque lakes and moraines at altitudes above 3000m. in the Giresun region. In Pleistocene times glacial valleys and boulder clays were formed.

2.3.10 During the Pleistocene travertine deposits also formed, together with sea and river terraces. Sea terraces are found at altitudes as high as 200m. above sea level around Trabzon City. In the investigated area, at Batlama D. (Stream) and Domuz D. junction where the Akköy Mine is located, river terraces are about 6 to 8 meters higher from the present day river bed (Plate 2.3.10) possibly indicating still active epeirogenetic movements.

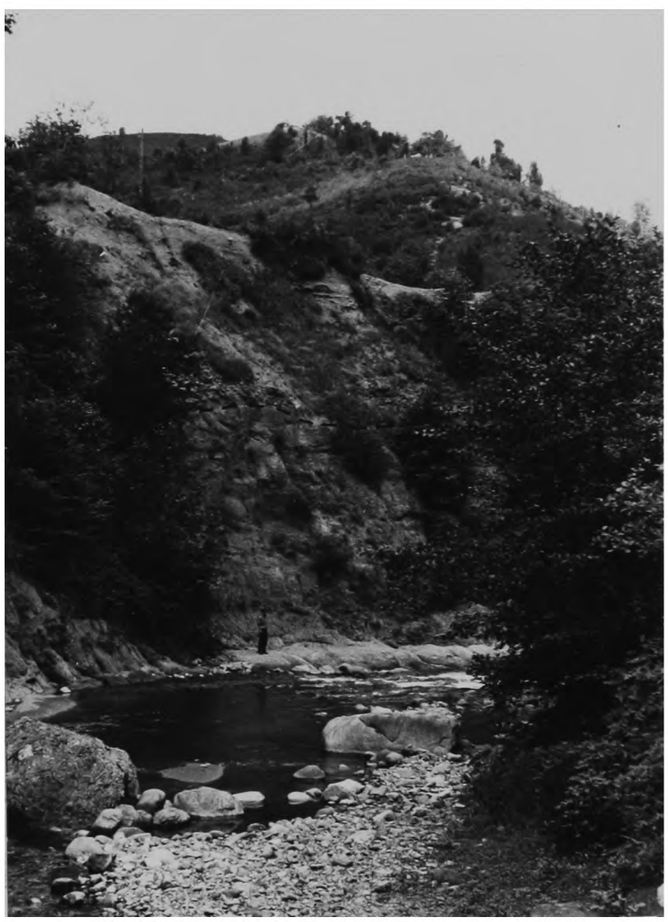

Plate 2.3.10 River terraces of Batlama Stream below Akköy Mine.

CHAPTER THREE

FIELDWORK

3A. GENERAL GEOLOGY OF THE THESIS AREA

3.1 Introduction

The investigated area is included partly in the GIRESUN G40-a2 and a3, and GIRESUN G40-b1 and b4 sheets of the 1 : 25000 scale topographic maps which are shown in Map 1 as an inset. The 10,000 scale topographic maps were obtained for geological mapping by enlargement from the above mentioned 25,000 scale sheets. The northern boundary of the area studied in detail is located about 7 Km. inland from Bulancak Town (inset of Map 1) and between Eriklik village in the north and Küçükdere villages in the south covers an area of approximately 50 Km^2.

The geological mapping work was carried out by a group of geologists under the direction of the writer. Although the areas between Bulancak and the southern intrusive block were mapped at 25,000 scale by U. Agar and H.H. Schultze-Westrum in 1959 mapping of the mineralization was not sufficiently detailed and the writer did not agree completely with the geological succession given in the Schultze-Westrum report (1960) concerning the area.

Systematic rock and vein sampling was carried out during the previous 10,000 scale geological mapping work, so the writer has given special attention to the additional sampling of the veins, microscopic study of the ore minerals and fluid inclusion study of suitable vein minerals. 75 rock samples,representing all the volcanic and some sedimentary rock units, were collected in the summer of 1971 and 300 polished specimens have been studied during the present research. Only the specimens representing dykes and the biotite-andesite specimen were found to be reasonably fresh after thin sections had been prepared and Electron

Microprobe analysis of feldspars and pyroxenes was conducted only on these specimens. The map area includes the mineralized area around the villages of Tekmezar and Dariköy. Because of the abundance of veins, most of the rocks of the area are strongly affected by hydrothermal alteration.

Due to existence of Akköy Mine, the $2Km^2$. area to the east of the main map area is included and the surface and underground mapping were carried out by the writer in addition to the Dariköy Uzümlük D., Kornalı, D., Küçükdere and Kovalık Sr. (Map 2) occurrences. Measurements and underground mapping was made with the aid of a Brunton-type compass, altimeter and tape-measure. The altimeter was found extremely useful to locate the veins due to the difficulty of finding a reference point on the map along the watercourses because of dense vegetation and abrupt morphology. Apart from the basalt dykes and sedimentary sequence, the following of formation boundaries was found to be the most difficult part of the mapping due to the intense hydrothermal alteration of volcanic rock units in addition to previously mentioned difficulties. In most cases the size and existence of quartz crystals in the dacitic rocks was used as a criterion to differentiate the formation boundaries.

Since the veins are exposed and can be studied mostly along the ridges and watercourses, prophiles along these were followed for mapping purposes during the mapping work. The following list gives the English translation of Turkish place names and topographic features on the geological and mining map.

(DARI)KÖY	(DARI) Village
MAHALLE (Mh.)	Hamlet
SIRT (Sr.)	Ridge
TEPE (T.)	Hill, peak
DERE (D.)	Stream
YAYLA	Highland, High Plateau

3.2 Geological Succession

Nine of the distinct lithological units which can be mapped throughout the Bulancak area were represented in the mainly volcanic study area. In this chapter the straigraphy of Cretaceous-Tertiary volcanic and sedimentary rocks is analysed and the composite stratigraphic section of the area studied is presented graphically in the accompanying diagram (Fig. 3.2) and compared with the Schultze-Westrum succession in Table 3.2.

The following mappable units were recognized:

9. Basalt dykes
8. Quartz-microdiorite
7. Agglomerate, sandstone and limestone
6. Biotite-andesite
5. Rhyodacitic lavas and pyroclastics
4. Tuffaceous breccia and sandstone
3. Porphyritic dacite
2. Pelitic limestone and tuff
1. Lower Basic Series

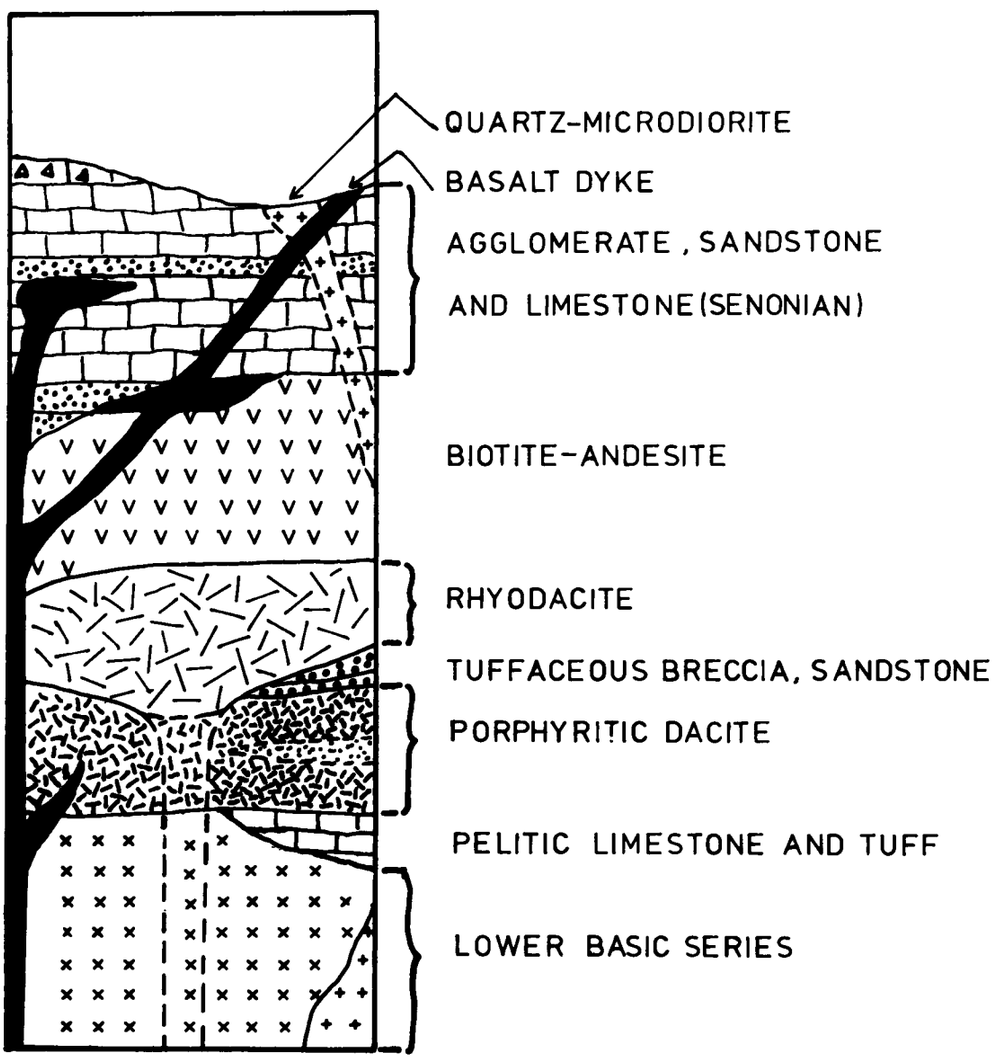

FIG 3.2 COMPOSITE COLUMN SECTION OF THE STUDY AREA

TABLE 3.2 Geological succession and comparison with neighbouring areas.

H.H. SCHULTZE-WESTRUM (1960)		PRESENT STUDY
		Scree
Sea and River Terraces		....
	Basalt dykes	Basalt dykes
Young basalts and andesites ...	Trachy-andesite	....
	Biotite-andesite	....
Granodiorite,Monzonite		Quartz-microdiorite
	Spilite-agglomerate	
Upper Basic Series	Andesitic and basaltic	....
	lavas and tuffs	
....		Agglomerate,Sandstone,Limestone(SENONIAN)
Dacite II (Rhyodacite-Hypabyssal dacite)		....
....		Biotite-andesite
Dacite-andesite mixed series		Rhyodacitic lavas and pyroclastics
Upper Inoceramus limestone and tuffite		Tuffaceous breccia and sandstone
Dacite I (Ore-bearing dacite)		Porphyritic dacite
Lower Inoceramus Limestone and tuffite		Pelitic limestone and tuff
	Agglomerate, tuff	
Lower Basic Series	Basalt, andesite,spilite	Lower Basic Series
	Massive Limestone	
	Phyllite	
Crystalline basement	Sericite-quartzite	....
	Quartzite-conglomerate	

3.2.1 Lower Basic Series: This is the oldest rock unit in the area and forms the basement of the volcanic series. About 50% of the map area is covered by these lower volcanics, which are extensively subjected to hydrothermal alteration. Due to its composite character various names have been proposed for this series but this name is the most appropriate and preferably used. Although the base is not seen there are no fossiliferous formations at the bottom of these rocks in the studied area, but Schultze-Westrum (1960) reported limestone intercalations at the bottom similar to those of the Espiye area (Tugal, 1969). These limestones reach a thickness of up to 100m. Miliolidae, Orbitolina and Textularia forms have been identified and a possible Malm-Lower Cretaceous age is suggested. A limestone-tuff intercalation has been mapped near the Küçükdere Village houses where the newly opened road ends (Map 1, 3H)* but this limestone is similar to Upper Cretaceous limestones rather than Malm-Lower Cretaceous.

The series is characterized by a thick, variety of volcanics - predominantly dark green spilite, basalt and andesite. During 1 : 10,000 scale mapping work specimens collected from this series have been determined as spilite-keratophyre, spilitic andesite, spilite, trachy-andesite, andesite, andesitic tuff, ignimbrite and breccia (MTA Rp. 982).
The writer described an interstratified tuff-agglomerate sequence at the Çimanoglu Mh. with purple coloured silicified dacite gravels and pebbles cemented and interstratified with tuffs .
Rhyodacitic lavas showing well-developed columnar jointing cover this outcrop at the rhyodacite-lower basic series contact where the watercourse shows a steep fall (Map 1, 6C). In places, at upper levels of this series, well-developed columnar joints can be seen along the Yomasapagı-Yaykınlık Road (3F) and the Hamidiye Road (4F).*

* Indicates the grid lines on the geological and mining map.

Brecciation, partly of tectonic origin and partly due to hydrothermal alteration, is widespread throughout the series. Most of the sulphide veins occur in these series. Around Tekmezar, due to mineralization, the rocks have suffered intense hydrothermal alteration and later heavy surface weathering so one can not see any fresh rock. The main alteration processes are silicification, kaolinization, carbonatization, chloritization, spilitization, albitization and also, less commonly, limonitization. They are usually dark green when they are fresh (to the west of Armutlu T.) but when altered colours vary from greyish green to white (see Plate 3.2.1).

The series extends from Küçükdere village in the southwest (2H) to Darıköy village in the northeast and is overlain by westward dipping Senonian sedimentary sequence in the west and by a eastward dipping porphyritic dacites in the east, forming possible a northeast plunging anticlinal structure whose axis is almost paralled to the Küçükgure D. watercourse.

Inliers of this series are seen along Körükyeri D. (2B), the Hamidiye village road (5F), under either porphyritic dacites or rhyodacitic rocks. The visible thickness below the porphyritic dacite lavas can reach up to 700 m. around Küçükdere village (Section V). It has been estimated as about 1000 m. in the vicinity of the Akköy Mine (METAG Rp. 1972).

The series is cut by steeply dipping porphyritic dacite (5H, 4F, 6D, 2F), rhyodacite (4H, 7B, 2C) and basalt (5H) dykes and disappears under rhyodacite lavas and a sedimentary sequence to the north. The general appearance of the lower basic series can be seen in plate 3.2.1 Specimens 8,14,23,28,72,122,128B,130,137,146 were collected from the volcanics of the lower basic series.

Plate 3.2.1 Exposure of Lower Basic Series rocks near Kovalik Sr.

3.2.2 Pelitic Limestone and Tuff: This mappable unit has two outcrops along the Lower Basic Series - Porphyritic Dacite contact. The first outcrop occurs 300 m. SW of Kirtil T. (3F), the second is located about 1 Km. southeast of Küçükdere village in the Camideresi locality.

This light pinkish-grey, in places purple coloured, massive, fine-grained rock has a porcelanite appearance. Interstratified sandy or tuff levels are clearly visible and often the rock is impregnated with sometimes more than a centimeter long pyrite cubic crystals. Due to silicification it is very hard. An approximate 25 m. thickness has been estimated for this series but it is usually tectonized and in Küçükdere village limestone levels are clearly replaced by specular he matite, pyrite and chalcopyrite along bedding planes and a thin pyrite layer has formed between limestone and interstratified spilitic tuff layers. Skarn mineralization has also been reported by Tugal (1969) in thermally metamorphosed massive limestones interbedded with the lower basic series but Schultze-Westrum (1960) has not reported the equivalent reddish Inoceramus Limestones in the Bulancak area, which he mapped at 25,000 scale including the present investigated area.

3.2.3 Porphyritic Dacite: This most important series throughout the Eastern Pontids forms the second oldest volcanic unit overlying the Lower Basic Series to the east of the Saridiken D.-Küçükgüre D. line. Apart from a few dykes there is no outcrop west of this line:

Due to hydrothermal alteration they are seen in varying white, yellowish-brown and purplish colours covering the hills such as Armutlu T. (4I), Karaderebası (4H), Kırtıl T. (3F) and ridges between Büyükgüre D.

and Ardahan D. (5I, Section V). The shape, localization and steeply dipping contacts of the Kornali D. outcrop suggest a possible vent of a dacitic volcano (Section V). In all cases it is found overlying the lower basic series and a discomformity is reported between the two series in the Akköy Mine area (METAG Rp.,1972).It has extrusive character as well as intrusive. Dykes of porphyritic dacite are found cutting through the lower basic series with steeply dipping contacts but the contacts of one dyke located about 1.5 Km. west of Kırtil T. (2G) were found to be almost parallel to the topographic contour lines gently dipping to the west. In a second dyke which is localized along a fault 200 m. east of 774 peak (4F) on the recently opened Hamidiye village road the writer collected feldspar crystals as large as 2 cm. in length (Plate 4.3.1). They are also characteristic with large quartz phenocrysts. At a location 2 Km. ENE of Karaderebası T. (5G) 1 cm. long quartz crystals were described by the writer (MTA Rp. No. 982). To the east of the Hamidiye village houses (5E), intensely silicified outcrops resemble quartzite, and only rounded quartz crystals preserve the original character of the rock.

In places at the bottom this sequence begins with a fine-grained rock but gradually upwards gains the characteristic coarse porphyritic texture with increasing size of phenocrysts. According to Schultze-Westrum (1960) in the neighbouring areas the Dacite I series begins with albite-dacite of glassy groundmass (Vitrophyric) but towards the top grades into the intensely altered ore-bearing dacite, in places showing columnar jointing. In places interstratified dacitic tuff levels were recognized but they are not found as mappable units and boundaries can not be followed due to strong alteration.

The main alteration processes are silicification, kaolinization, sericitization and carbonatization, less commonly limonitization, albitization and chloritization.

Displacements were observed along the contacts with the underlying lower basic series in areas between the villages of Küçükdere and Yaykınlık (3E, 3F, 3G, 4E).

Visible thickness of these rocks, in the studied part of the area, changes from several tens of meters to 200 meters but in the drillholes in the Akköy Mine they reach a thickness of more than 300 meters (METAG Rp., 1972) showing that the thickness increases to the east of the studied area. They are overlain only by a Senonian sedimentary sequence to the southeast and north of Akköy Mine. Some erosion relicts of this sequence on top of these lavas were mapped in Darıköy Çimanoglu Mh. (6C), along the Hamidiye road (5F) and in Yaykinlik villages (4D).

Previously all the area covered by dacitic and rhyodacitic rocks and partly by lower basic series was mapped as one lithological unit by Agar and Schultze-Westrum. Specimens 69C, 147, 166, 167 represent these rocks.

3.2.4 Tuffaceous breccia and Sandstone: The largest outcrop of this series is mapped to the east of Eriklik village along a stream valley (3A). Although it seems to be interstratified with the rhyodacitic lavas, which are here dipping 40° to the northeast (Section I), its exact relationship to the lower basic series and porphyritic dacite is uncertain. At Tekmezar, about 500 m. northeast of Dönbül T. (3D),

the outcrop of these rocks is adjacent to a NW-SE trending fault (The Kasyatak Fault). Mineralization of both the bottom and top contacts has occurred. Large scale exploration activities were carried out along the fault (see Fig. 5.15) which partly forms the Sispelit D. The well-bedded dacitic tuffs and sandstones overlying Akköy orebody can be included in this unit. One outcrop, 500m. to the east of Gedik T., has E-W strike and dips 25°N (3B).

The series consists of purple to mottled alternating breccia (agglomeratic) and tuff levels. Agglomeratic levels contain subangular dacite pebbles up to 50cm. in diameter interstratified with 0.5m. thick pelitic tuff. Feldspar, biotite and quartz crystals in these pebbles are recognized. Outcrops have suffered hydrothermal alteration.

3.2.5 Rhyodacite and Rhyodacitic pyroclastics: This unit covers large areas in the north of the map area between the villages of Eriklik and Tekmezar and extends to the east towards Darıköy. Isolated outcrops can be seen in the central parts of the map area, i.e., Sayvancilik Dere-Kusdere junction (1D), 400m. northeast of Dönbül T. (3D), 400m. northwest of Dinekkaya T. (3C). Several dykes cut through lower basic series (3A, 7B) or are exposed along fault lines, such as Gonurca Dere Fault (2C) and an E-W trending fault in Darıköy, Kuloglu Mh. (6A). In a number of places mineralization was found associated with faults cutting through the rhyodacitic rocks.

These volcanics have extrusive as well as intrusive contacts but in many places have tectonic boundaries terminated by faults. Tekmezar fault cuts across this series, causing displacements along formation boundaries in a northwest-southeast direction. To the northeast of Büyükinece village (4B) basement series rocks are exposed along Küçükgüre Dere. In three areas, at the west of Eriklik Village (3A),

around Karga T. (5A), and at the north of Dariköy this series is overlain by the Senonian sedimentary sequence. Only in one locality has a direct relationship with the porphyritic dacites been found. Along the Yomasapagi (3E) - Yaykinlik village road around 761 peak (3/4E) these rocks overlie porphyritic dacites (4E, see also section IV). The stratigraphic position and petrological and alteration characteristics of these rocks are quite similar to rhyodacitic lavas above Adit 2 at the Lahanos Mine (Tugal, 1969). Tuffaceous, intensely altered rhyodacitic rocks preserving a layered appearance were exposed in Tekmezar area around Çamlik T. (2/3A).

Due to very small and limonitized disseminations of cubic pyrite crystals the rocks have a porous, spongy or spotty appearance which sometimes helps to differentiate them from the other volcanics. In intensely altered areas these whitish-grey fine-grained rocks are hardly distinguishable from the underlying Lower basic series. One can only recognize the small, triangular quartz phenocrysts on close examination. Columnar jointing is common in these rocks as well as in the lower basic series.

It is difficult to estimate the thickness of these lavas but field evidence indicates an increase to the north of the map area. It varies between 100 to 400 meters in the map area but it can reach up to 600 meters in the north. Specimens 45, 51, 152, 150 were collected from these volcanics.

3.2.6 Biotite-andesite: These volcanics can be seen only at the western and eastern ends of the map area. At the west between Dolik T. (2C) and Yaslibahce village (1C) they are exposed on a large scale with

intrusive as well as extrusive character. The lower part in this area is brecciated and best seen along Çamkoza D. (2B)and the watercourses running due west from Doğk T. Cobbles and boulders of biotite-andesite ranging from 20 cm. to 100 cm. in diameter were described during previous work (MTA Rp. No. 982). The cementing material is also andesitic and as a whole the outcrop has the appearance of a vent breccia or agglomerate. The writers concept that this is probably a vent has been developed since writing the earlier report.

The eastern outcrop has an extrusive character and overlies porphyritic dacites (or quartz-porphyries) southwest of Akköy Mine (8E). This outcrop is terminated at the north by a fault extending along Domuzdere where Akköy Mine is located.

At Kisla Mh locality of Küçükdere village, a 2 m. wide biotite-andesite dyke (3G) extends in a northwest-southeast direction cutting through the lower basic series.

The western outcrop is overlain by a Senonian limestone sequence which starts with a thick arenaceous sandstone layer consisting of biotite-andesite (Fig. 3.2.7). Along Çamkoza D. basalt dykes were found cutting through biotite-andesites and extending into the sedimentary sequence (1C, 1D).

Contact relations of the biotite-andesites with rhyodacitic lavas are not clear although it looks as if this western outcrop is cutting across the rhyodacites exposed along Sayvancilik D. (1D). This evidence suggests an age for the biotite-andesites between that of the rhyodacites and the Senonian age sedimentary sequence.

These rocks are easily differentiated from the other volcanic units due to characteristic porphyric texture, greenish grey-pinkish purple

colours and abundant biotite crystals although limonitization and chloritization of biotites, sericitization of feldspars and silicification are common alteration processes. Alteration in the feldspars is not developed as intensely as in the other minerals so it was possible to determine them by electron microprobe analysis. Specimen 154 was collected from the western outcrop of this formation.

3.2.7 Agglomerate, Sandstone and Limestone: This sedimentary unit covers large areas extending from Yaslibahçe village towards northwestern villages (mapped by U. Agar in 1959 on the 25000 scale) covering Sümе, Ahmetli and Sasu villages. This sequence can reach more than 400 m. throughout the Eastern Pontids and Schultze-Westrum (1960) described them as "Inoceramus limestone and tuffite" being the sedimentary equivalent of the dacitic series but they must be considered in the Tuffaceous marl-Limestone series of the Upper Basic Series (Schultze-Westrum 1961). They were studied in detail by the writer in the Görele area and named as "Akköy Formation" (Akıncı, 1969a). According to Tokel (1973) limestones of this series are "Pelagic Pakcstones". Throughout the Eastern Pontids the series is characteristic with abundant Globutruncana species rather than Inoceramus, i.e., in Gümüshane (Tokel, 1973); Espiye (Tugal, 1969) and Görele areas (Akıncı, 1969a).

The northern part of the volcanics in the studied area is covered by the sedimentary sequence as isolated patches around Karga T. (5A), along the Dariköy-Giresun road north of Darikoy (7A) and south of the Akköy Mine (8E). Alternating limestone, marl, and sandstone facies are dominant around Yaslıbahce village (Plates 3.2.7a,b) while volcanic breccia,

Plate 3.2.7a Section in Senonian Limestone sequence near Yaslibahçe

Plate 3.2.7b Close up of beds to the right of the vehicle in the upper picture.

agglomerate and tuffaceous sandstone almost replace the limestone facies in the other areas east of Yaslibahçe.

Fig. 3.2.7 shows a section, about four meters thick, west of Yaslıbahçe village (1C) where sedimentary rocks begin with a loosely cemented, poorly sorted, arenaceous sandstone layer which consists of biotite-andesite sands and pebbles. Fine-grained, massive-bedded, sandy and argillaceous limestone beds alternate with marl, sandstone and purple siltstone. Limestone layers in the middle of this 4 meters thick section contain:

Globutruncana Lapp. Tricarinata (Querreau)

Globutruncana Lapp. Bolli

Globigerina Sp.

Radiolaria Sp. and in addition to these microfossils

Globutruncana Stuarti (de Lappar) from Karakoç Mh. locality suggest a Senonian* (possibly Santonian-Campanian) age for this fauna. In the western extension of this series Shultze-Westrum (1960) reported, in addition to this fauna, Inoceramus Balticus as a macrofossil. This fauna is identical to that reported in Espiye (Tugal, 1969 p.33) and the Görele area (Akıncı, 1969a p.27).

The volcanic facies of this unit along the Darikoy-Giresun road consists of coarse-grained agglomerate cemented with altered tuffs. Gravels are predominantly dacitic ranging from pebble to cobble sizes. At the upper levels of these agglomerates, graded-bedded, purple coloured sandstones (or tuffs) showing loadcasts are interbedded with violet

* Fossils determined in the MTA Paleontology Laboratories by Zeki Dager.

FIG 3.2.7 A SECTION OF SENONIAN SEQUENCE NEAR YASLIBAHCE

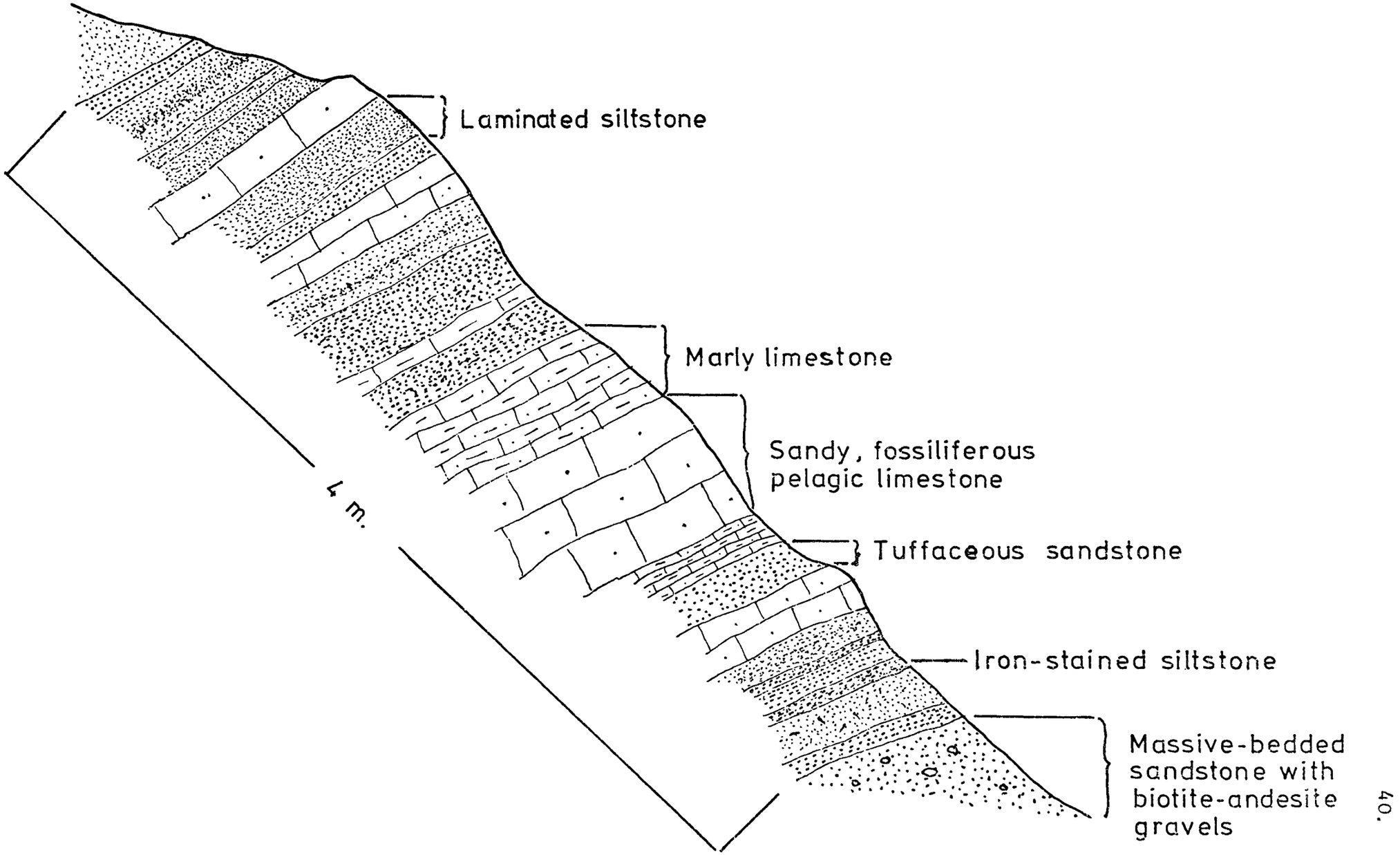

coloured opal-like layers which contain Radiolaria Sp. with no definite age. Dacitic tuffs with similar characteristics can be seen at the entrance of Adit 2 of Akköy Mine immediately overlying brecciated orebody but these are believed to be at the bottom of the stratigraphic column.

3.2.8 Quartz-Microdiorite: Although granodioritic and monzonitic intrusives are exposed extensively, and mapped approximately 10 Km. south of the map area around Kümbet Yaylasi (Highland) and 4 Km. north of Dariköy village along Küçükgüre D., they are represented only on a small scale in the southeast corner of the map area along Ardahan D. (5H).

Dark green coloured, choritized and sericitized rock is hardly distinguishable from the dark green coloured rocks of the Lower basic series. Quartz-diorites (Tonalites) with 10 mm. long quartz crystals have been reported in the neighbouring areas to the east with similar alteration processes but the intrusion age is not the same as the Tertiary intrusion reported so far (METAG Rp. 1972). Specimen 138 collected from this unit.

3.2.9 Basalt Dykes: These dykes represent the youngest volcanism in the investigated areas as is the case in the Görele (Akinci, 1969a) and Espiye areas (Tugal, 1969). If the two dykes cutting through lower basic series at the southeast of the map (5H) are excluded, all the dykes are concentrated in the Senonian sedimentary sequence at the northwest of the map area (Plate 3.2. 7a) and in places show a sill-like appearance. The general trend is parallel to the major fracture patterns of the map area, i.e., northwest-southeast, and some of the dykes are exposed along fault lines (1A). Surface outcrops are 2 to 5 meters wide and can be followed in places several tens of meters along the strike (1A).

Along Camkoza D. at the boundary of the Senonian sedimentary sequence and brecciated biotite-andesite a basalt outcrop (1C) was thought to be lava flow older than the dykes during previous mapping work in 1968, but if the circular shape of the outcrop and its similar mineralogy to the dykes is taken into consideration, the existence of a basalt plug in the biotite-andesite rocks can be suggested. To the south and north of this outcrop basalt dykes are found along Camkoza D. cutting through biotite-andesites.

These massive, dark-green-black coloured dykes suffered from propylitization and uralitization.

During previous 10,000 scale mapping work these dykes were accepted as younger than the intrusives, but due to similar characteristics to the dykes of the Görele, and Espiye areas and with special reference to Schultze-Westrum's (1961) work in the Giresun Aksu Valley, the writer is now inclined to believe that they represent the youngest volcanism in the area. Specimens 52, 128A, 155 to 159 represent these dykes.

3.2.10 Scree: Loosely cemented volcanic breccia and limestone blocks of different size possibly related to recent landslide activities around Karga T. (5A) and Kısla Mh. (3G), have been mapped as scree.

3B STRUCTURAL GEOLOGY OF THE THESIS AREA

3.3 General Introduction

In accordance with the changing stratigraphy from the coastal ranges of the Eastern Pontids to the highlands of Anatolia, striking variations occur in the tectonic style. This eventually led to two divergent and contradictory views on the tectonic style of the Eastern Pontids:

1. According to Staub (1924), Blumenthal (1946), Pınar and Lahn (1954) and Ketin (1959, 1966) the Pontids owe their tectonic development to the Alpine orogeny in the form of a folded mountain chain.

2. Following Oswald's (1912) definition of the Pontids as the "Northern Broken Mass" Schultze-Westrum (1961) and Zankl (1961) Tugal (1969), Akıncı (1969a) and Kronberg (1970) demonstrated the similarity of tectonic style between the Eastern Pontids and the Hartz Mountain ranges which represent Germano-type faulted blocks due to the absence of typical Alpine structure such as overthrusts, nappes, etc. In general, fault tectonics are predominant along the coastal ranges while typical Alpine structures dominate in the boundary zones of the Pontids and Anatolids marked by ophiolite-radiolarite and Mesozoic limestone-flysch series.

Amongst the workers in the Pontids, Kronberg (1970) in particular studied the fracture pattern of the area between the Ordu and Trabzon cities along the coastal ranges from aerial photographs and found that it accords well with the trends obtained by other workers including the present author, i.e. throughout the Eastern Pontids N(30-70)W and N(50-60)E trending fracture patterns are dominant. According to Tokel (1973) deformation which formed NW-SE trending faults started in the Liassic and continued up to present; Schultze-Westrum (1961) reported present day activity in the Tirebolu area. As a result of repeated activity a complex development

of Horst and Graben structures has been formed. This type of structure can be seen in the south of the map area on a small scale, especially in the porphyritic dacite areas in the south.

Northwest-southeast trending veins in Paleozoic formations, basalt and dacite dykes of Jurassic-Cretaceous ages and Tertiary age northeast-southwest trending dykes were thought to indicate the same age for both fracture systems by Kronberg (1970). Pyrite mineralization prefers NE-SW trending fractures while copper deposits are associated with NW-SE trending fractures (Gümüs, 1970). At the intersection points of these systems copper enrichment can be expected (Pollak, 1961). In the following paragraphs strike and dips, faults, joints and relations with the veins will be analysed.

3.4 Detailed Structural Geology

3.4.1 Folds, Strike and Dips: The Tekmezar-Dariköy mineralization area is essentially unfolded in a small scale. The changes in dip of the sediments are largely due to faults, and dykes, but are also believed to be related to the irregular topography of the surface on which the sediments were deposited.

Dips measured in the sedimentary sequence vary between 10^{o} and 40^{o}. Most of the measured dips over 15^{o} are found very close to basalt dykes or faults (see plate 3.2.7a,b).

3.4.2 Faults: A series of NW-SE trending faults arranged en echelon is found cutting through almost every lithological unit of the map area. Since the most common feature along the fault line is displacement of the formation boundaries and observed slickensides on the fault planes

are horizontal, these faults represent strike-slip (wrench) types. When the broad structure of adjacent areas is considered, it seems that a large scale gentle NE-SW trending anticline with flanking synclines may be present. These cross faults (de Sitter, 1964) occur perpendicular to the anticline axis and may be due to stretching of the longitudinal arch of a culmination in the anticline axis and uplift which are the most common events in the Pontids. Step faults with associated graben and horst structures can be seen in various scales, e.g. Gedik T. (2B) and the Evliya T.-Kırtıl T. (3F) horst block, terminated on both sides by NW-SE trending faults.

The following NW-SE trending major faults were studied and named during visits to the area for sampling in 1971.

Selmanoglu Fault: This fault extends about 2 Km. from Selmanoglu Mh. (Map 2, 1E) in a SE direction towards Kovalik Sr. (2F) causing displacement along the Senonian sedimentary sequence and Lower basic series contact. It dies out between Saridiken Dere and Kovalık Sr. terminating a series of an echelon porphyritic dacite dykes (2F). Veins are mapped parallel to this fault across Saridiken Dere. The strike and dip of the fault were measured as N50W75SW. The northwestern part of the fault was inferred by the writer, after 1971 field work, due to a steeply dipping limestone sequence in Selmanoglu Mh. (1E) and fluid inclusion study of the veins around Kovalik Sr. Isotherms supported the NW-SE extension of the fault (see Fig. 6.8).

Evliya Tepe Fault: This NW-SE trending, steeply NE dipping, 2 Km. long, slightly curved fault is arranged en echelon with the Dönbül Dere watercourse in the north (2E) and is marked by a N40W trending barren quartz vein of about 1.5-2 m. thick. It ends with a net-work of

milky quartz veinlets in the porphyritic dacite 350m. to the northeast of Kirtil Tepe (3F) and this rock's contact with the lower basic series to the east of Evliya Tepe is displaced by the fault. Veins were mapped very close to the southern end of the fault at the head of Büyükgüre Dere. This fault was not mapped during the 1968 field work.

Kaşyatak Fault: The veins 500 m. to the northeast of Dönbül Tepe, mined on a small scale by Etibank and the Demir Export Company, occur along the northern end (3D) of this 2 Km. long fault. It extends to the southeast cutting across a rhyodacite outcrop in Kasyatak Mh. (4E) of Yaykinlik Village and ends with the displacement along the porphyritic dacite (4E) - Lower basic series contact. Veins parallel to this fault across the Büyükgüre Dere were also mapped. The southern half of the fault between the villages of Yaykinlik and Hamidiye recognised by the writer has not been previously mapped.

Tekmezar Fault: This 4 Km. long fault extends from Kurukõseoglu Mh. (2A) passing between Gedik Tepe and Çamlik Tepe and across the Tekmezar-Büyükinece car road and ends to the west of Elevlioglu Mh. (5B) of Darıköy. Its surface trace is marked by intense kaolinization and silicification. The southern end of the fault (5B), where it is cut by other faults, is richer in terms of vein mineralization than the other parts. The fault trends approximately N75W, dipping 55°NE.

Micro scale displacements along the several fractures were measured during field work by the writer. At the 215m. altitude along the Küçükgüre Dere (4B) and at the 700m. altitude along the Büyükgüre Dere (3F) watercourses N15W trending quartz veins were found to be rich in chalcopyrite, displacing a N75W trending vein rich in pyrite in the first case

and displaced by a N50W trending quartz vein in the second case. A third N15W trending quartz vein in the Kuzgunkayasi locality (7B) of Dariköy is displaced 10cm by a N63E trending fracture which is parallel to a mineralized fracture nearby. On the other hand at 550m. altitude along the Büyükgüre Dere watercourse (4F) a N50E trending vein is displaced by a N40W trending fracture.

This evidence suggests the conjugate nature of the NW-SE and NE-SW trending fractures although there are several cases where cross joints and faults tend to develop first in an anticline structure or in a cooling igneous mass (de Sitter, 1964, p.192; Price, 1966, p.157). It is difficult to establish evidence of earlier formation of the predominantly mineralized NW-SE trending cross fractures.

In the accompanying table 3.4.2, measured faults of the area are listed to show major trends and examples of strike-slip movement. In most cases brecciation, silicification and limonitization due to pyrite alteration are common along the fault lines.

Finally another 2 Km. long fault, inferred by the writer extends from Karga Tepe (5A) to Kuloglu Mh. (6A) of Dariköy in an E-W direction cutting across Küçükgüre Dere. To the east of Karga Tepe, this fault brings into contact the Senonian sedimentary sequence, rhyodacitic rocks and Lower basic series. The eastern end of the fault is followed by a rhyodacite dyke cutting through Lower basic series. Two veins subjected to some exploration activities were found extending NW-SE in the Karayalak locality where this fault ends (6A). Two faults are also inferred along the Körükyeri Dere watercourse (2B) where several old workings and the largest area covered by slags were found (Plate 1a) and to the east of Gedik Tepe (2B) respectively.

TABLE 3.4.2 Fault Measurements

Nature of the Fault	Strike and Dip	Remarks
Strike Slip	N17W70SW	Horizontal slickensides on fault plane
"	N25E90	Silicification along the fault
	N70E60SE	
	N60W90	
	N20E90	Silicification along the fault
	N5E90	Brecciation and Limonitization
	N70W90	
	N30E90	
	N65W85SW	Quartz vein along the fault
	N10E75NW	
	N30E70NW	
	N35E	
	N20W68SW	
	N25W65SW	
	N40W70SW	
	N10W65NE	
"	N45W53NE	Horizontal slickensides on fault plane
	N40E45NW	
	N65E90	
	E-W90	

3.4.3 Joints: During the 1971 field work in addition to vein measurements, systematic joint measurements, mainly in the Lower basic series and porphyritic dacite rocks, were conducted along the main streams of the area such as the Ardahan, Büyükgüre, and Küçükgüre Dere watercourses, to analyse the fracture patterns and structural control of the veins. As a result of this survey numerous joints systematic as well as non-systematic (Price, 1966), have been recognised. 262 joints and 131 vein measurements were made and rose diagrams were prepared for the measured joints along each individual watercourse (Figs 3.4.3a), and for veins to compare with the results of the structural analysis carried out by Maucher, et al (1962) and Kronberg (1970) on a regional scale which is seen in Fig. 3.4.3b. Qualitatively, as far as dominant trends are concerned, the results are similar and comparable with the regional as well as areal fracture patterns obtained by the above mentioned authors and Tugal (1969, fig. 2B).

Due to the absence of well-defined primary tectonic structures, i.e. fold axis, lineations in igneous rocks, and hydrothermal alterations it is difficult to give a genetic classification of joint systems. But the planar nature of the joint planes and some observed slickensides may indicate the shear nature of the joints. It has been found that the dominant joint set, essentially vertical to subvertical, is approximately parallel to the NW-SE trending major faults and veins (Fig. 3.4.4a) and gradual changes in the major trends were observed from Ardahan Dere towards Küçükgüre Dere (Fig. 3.4.3a). For example, along Ardahan Dere northeasterly joints dominate while in Büyükgüre Dere and Küçükgüre Dere northwesterly major joints are predominant. There is a tendency for a WNW-ESE orientation rather than NW-SE in Küçükgüre.

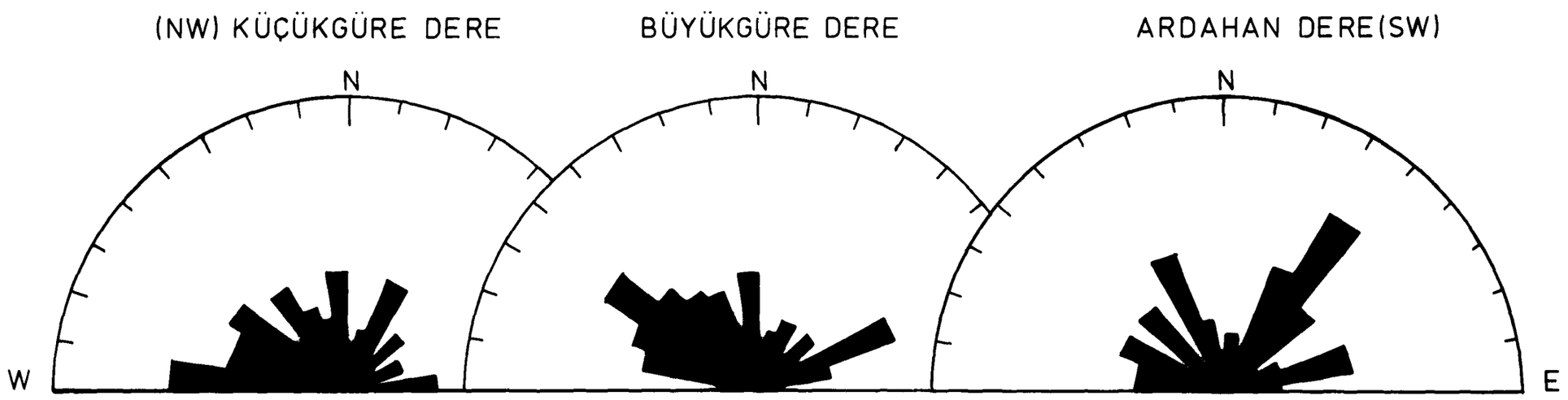

FIG 3.43a ROSE DIAGRAMS OF MAJOR JOINT TRENDS IN THE STUDY AREA

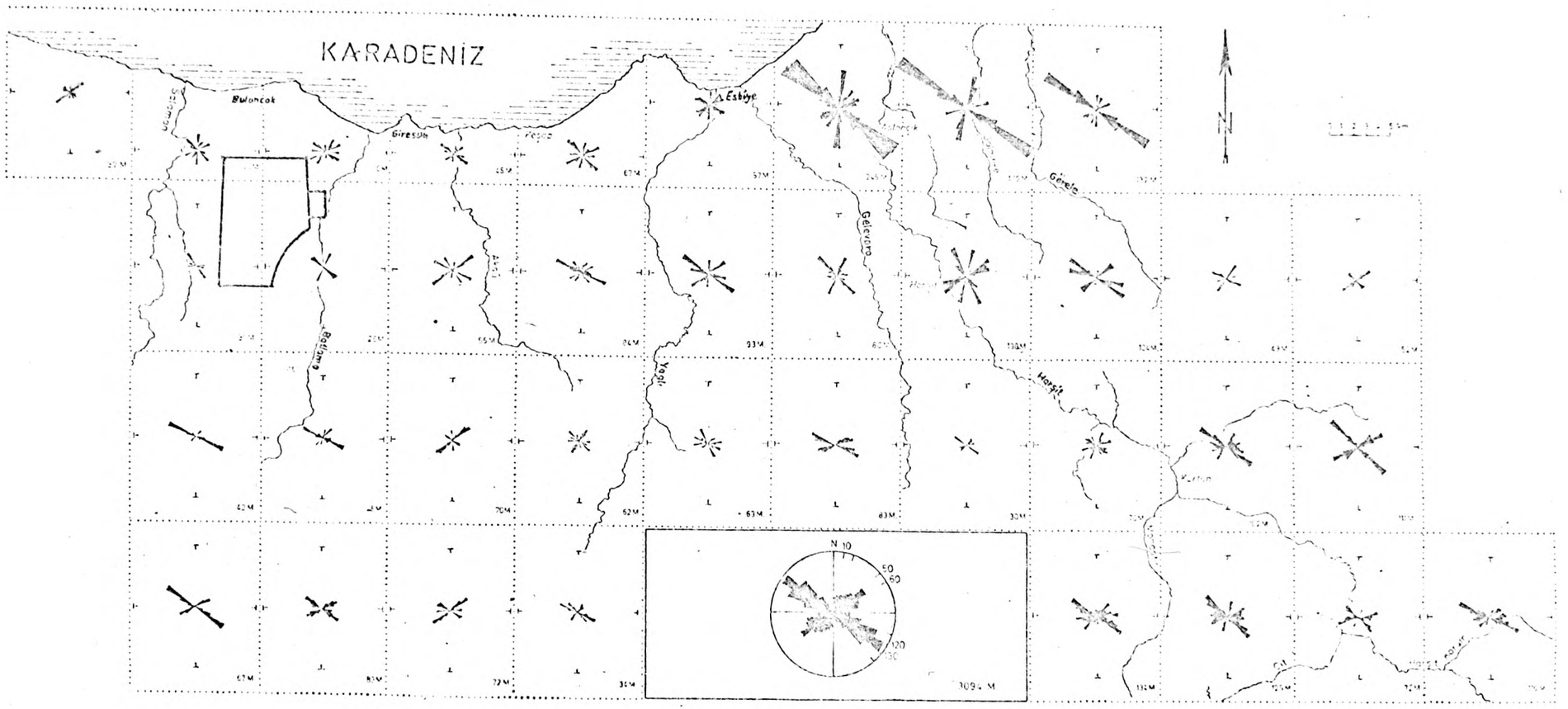

Şek. 5 - Her pafta kesimi ve bütün sahadaki (altta ve ortada) haritalanan foto lineasyonların doğrultu gülleri. M. = ölçüm sayısı.

Fig. 3.4.3b Rose diagrams measured from aerial photographs for each of the 1:25000 scale map sheet of the Eastern Black Sea area, from P. Kronberg, MTA Bulletin No. 74, 1970 p.63. ⌐¬ Thesis area.

This may be the result of the very well known dependence of the joint systems on the lithological character of the rocks (de Sitter, 1964) as well as a shift in the directions of maximum stress (Yılmaz, 1973).

In addition to systematic regional joints well-developed columnar joints were found in places in every volcanic unit, perpendicular to the cooling surface of the lavas.

Parallelism between major NW-SE basalt dyke trends and the fracture patterns of the area suggests that these dykes were emplaced along pre-existing joints in the rocks. Similar examples are given and illustrated by Yılmaz (1973) in the Gümüşhane area.

3.4.4 Veins: In the study area several surface maps from 1 : 100,000 to 1 : 100 scale were prepared over the years and various exploration activities were carried out, e.g. geophysical survey (IP and PS), drilling, underground and small scale pit-mining but there is no record of the vein analyses, detailed plans and sections to see the vein pattern in three dimensions because as expected, these mining activities were not very successful nor long-lasting.

Recent mining activities carried out by Etibank (The Government owned mining company) around Dönbül T. (3E) and the Kovalik Sr. area (Map 2G) has given the writer the chance to study several veins in underground workings and trenches opened across the veins using explosives. Several veins exposed along newly opened village roads were studied and added to the geologic map prepared in 1968.

After all the veins and structural units had been transferred to another map showing the type of mineralization in relation to geology,

an attempt was made by the writer to correlate the veins to each other taking into consideration the attitude, mineral associations and the thickness of the fractures under consideration. Such a correlation has not previously been attempted.

Since the great majority of the veins are exposed mainly along the watercourses, the vein pattern and extension of the veins must be checked. If the accuracy and the existence of the inferred vein pattern established by the writer is proven the area could be more economic than has so far been considered. The characteristics and pattern of the veins studied in the area can be seen on map 2 and outlined as follows:

1. Veins are found in an approximately 3 Km. wide 7 to 8 Km. long mineralization zone (in a broad sense) extending from the Saridiken D.-Küçükdere junction to the Kuloglu Mh. of Darıköy village along an axis marked by the Saridiken D.-Küçükdere watercourses (Map 2).

2. Along this NE-SW trending zone the dominant direction of the approximately parallel veins is NW-SE (Fig. 3.4.4a). The general arrangement of the veins suggest a conjugate vein system. In places en echelon veins occur parallel to the dominant trend possibly mineralized tension fractures. In the area en echelon faults on varying scales can also be seen (4D, 5B).

3. Although the veins are arranged en echelon, the mineralization along the entire length of the vein is not regular in terms of attitude, thickness and mineral associations. Lens-shaped pockets of pinching and swelling character, are linked to each other with fine veinlets or barren fractures. At the intersection points of the cracks enrichments (or ore-localization) were observed on a small scale (Fig. 3.4.4b) and this may reflect the major character of the veins on a broad scale.

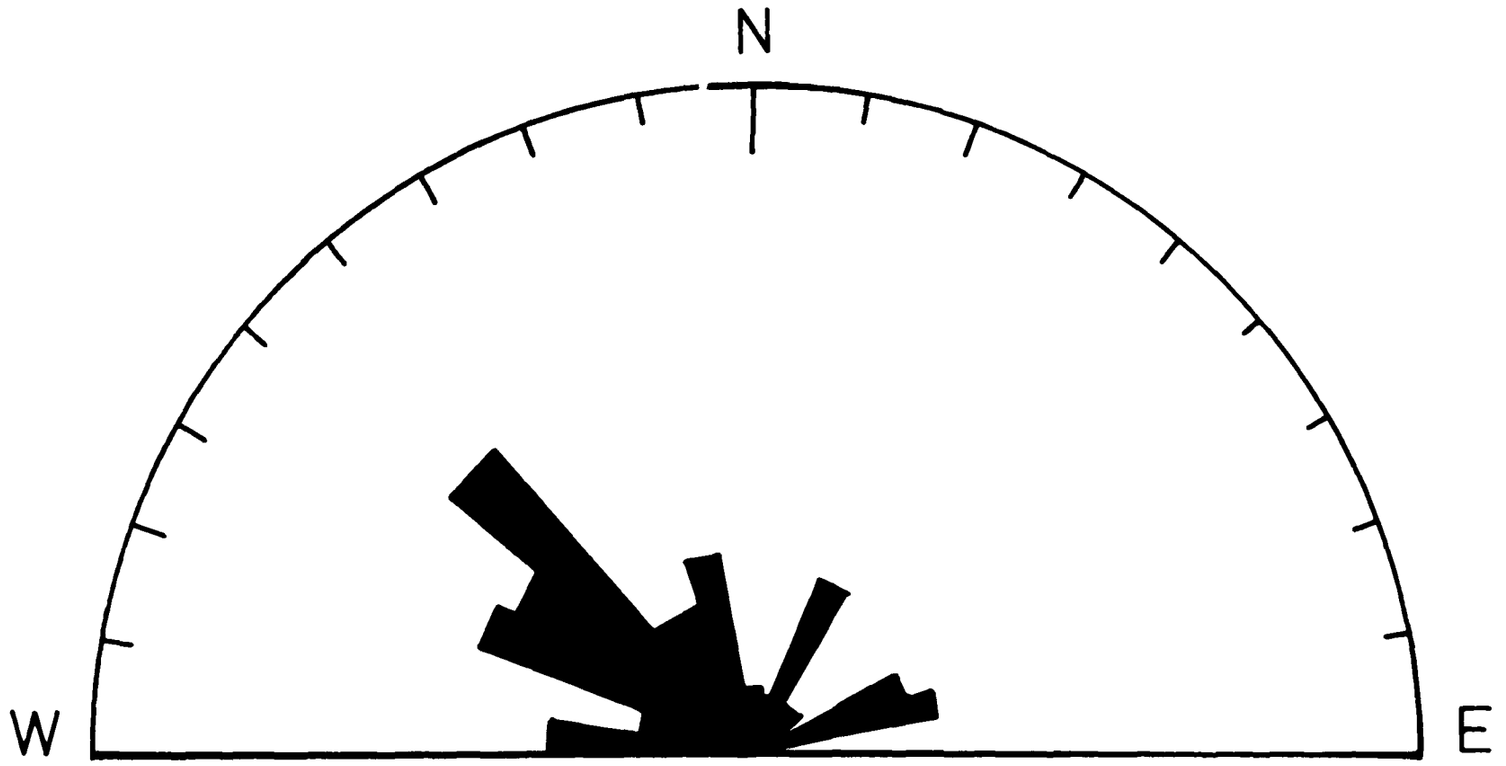

Fig 3.4.4a Rose diagram of Cu-Pb-Zn Sulphide veins in the vicinity of Darı-köy-Tekmezar area, Bulancak, Turkey.

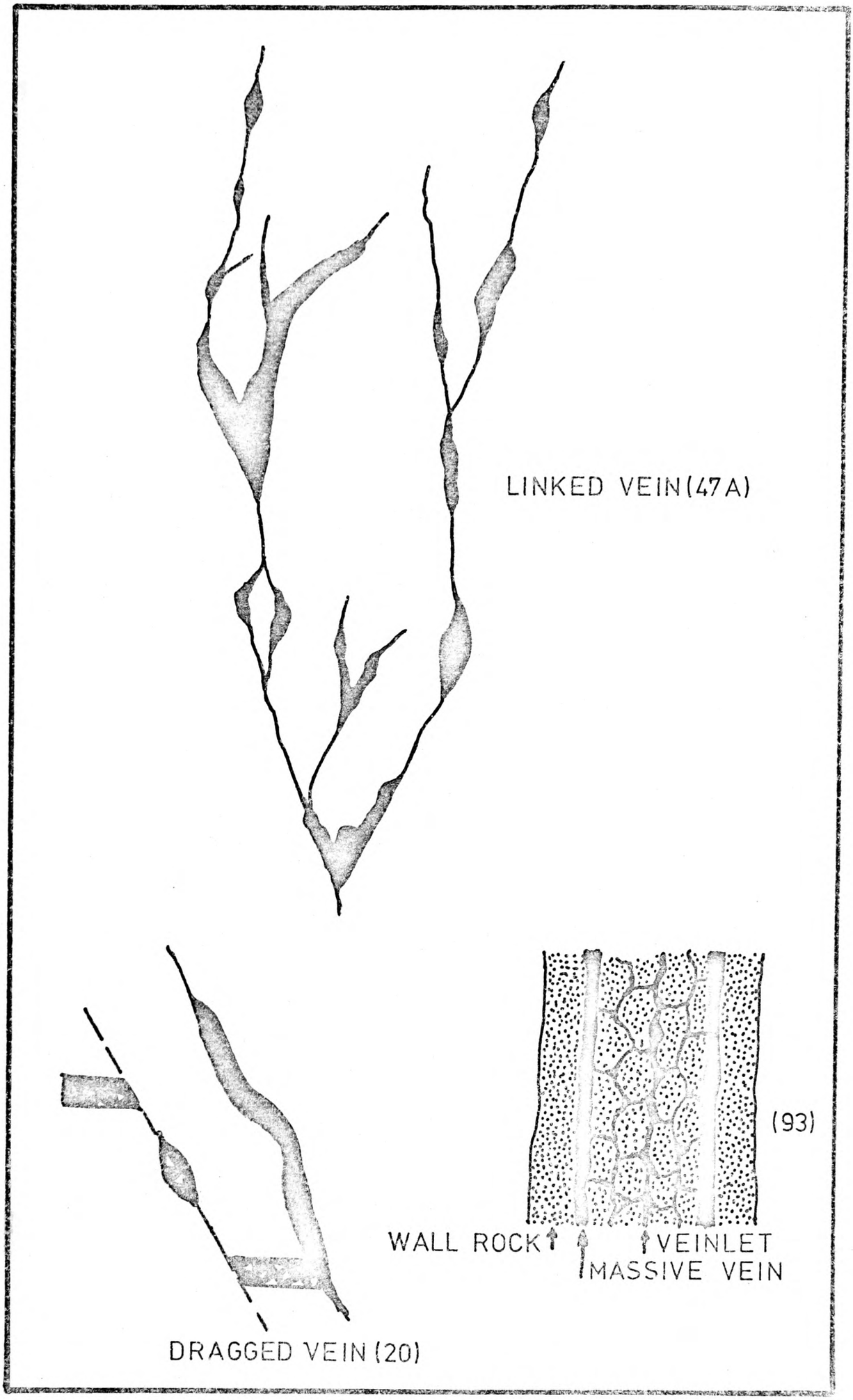

FIG 3.4.4b VARIOUS EXAMPLES OF VEIN EXPOSURES

Sets of parallel veins or veinlets are joined by diagonal branches similar to braided systems (McKinstery, 1949) in which two veins run parallel then join, then separate and become parallel again. The visible thicknesses of the veins vary between one and 50cm. Braided or linked veins can form a vein zone up to 5m. thick along brecciated fractures.

4. Tectonic, as well as hydrothermal brecciation along the vein zones are the most common features (Plates 3 4.4 a,b) with brecciated rock fragments cemented by ore and crustification is not uncommon . Most of the narrow veins are associated with vuggy quartz veins. Quartz was found as ganque in almost every polished specimen studied.

5. The strike and dip of the veins change along the length and there are some indications of variation in width of vein with changes in strike.

6. The great majority of the veins exposed along Büyükgüre D. and Ardahan D. are chalcopyrite-rich (Map 2). This chalcopyrite-rich zone generally is limited to the area between the Armutlu T. (4I)-Yomasapagı (3E)-Dariköy (7B) car road and the Ardahan D. watercourse. This is the area where Lower Basic Series is largely covered with porphyritic dacite formations. Outside this zone the veins are polymetallic.

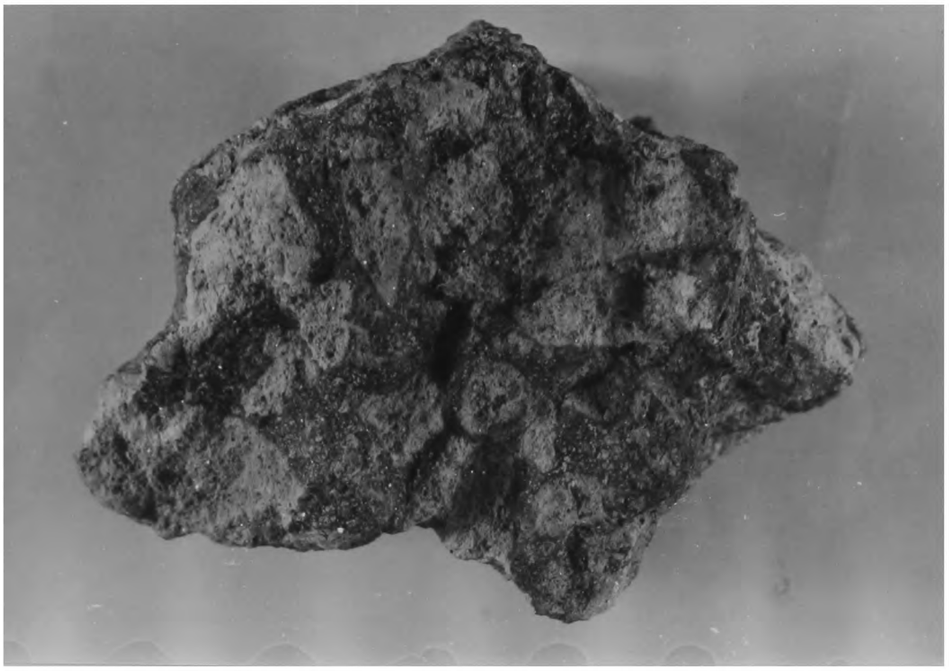

Plate 3.4.4a Breccia along Üzümlük veins

Plate 3.4.4b Ore breccia.

CHAPTER FOUR

PETROGRAPHY AND CHEMISTRY OF THE COUNTRY ROCKS

4A. PETROGRAPHY

4.1 Introduction.

As described in chapter 3 widespread severe hydrothermal alteration made it difficult to obtain any fresh rock, apart from dykes representing the youngest volcanism in the area and fresh outcrops of Lower Basic Series to the south of the map area. Furthermore the fine-grained character of the rocks made identification difficult therefore most of the mineralogical study of the thin sections was carried out on dyke rocks.

No attempt was made to put a strict boundary between different rock types for classification purpose because of the high degree of alteration in most specimens. This account of petrography is not intended to be an exhaustive one since this is not the primary aim of this thesis.

4.2 Petrography of the Lower Basic Series

Reasonably fresh rocks of this series are found to the south of Kügükdere Village. In this part of the area, rocks in hand specimens are massive, light to dark green or greyish and vesicular or amygdaloidal.

Specimen 23 is one of the few relatively unaltered rocks available. Plagioclase and clinopyroxenes are its major minerals. Oligoclase, andesine, hornblende and biotite have also been found in the rocks of this group to the east of the map area in the vicinity of Akköy

Mine (METAG Rp., 1972).

The Plagioclase is mainly oligoclase. There is almost no compositional difference between the matrix plagioclase and the phenocrysts. Matrix plagioclase is optically positive with a maximum extinction angle of 8-12 degrees, whereas this value is 10-12 degrees for the phenocrysts with n_β = 1.543-1.548. Plagioclase phenocrysts are also optically positive.

Feldspars appear to be somewhat less affected by the alteration. A limited degree of albitization (sausiritization) and chloritization with small chlorite veinlets, generally following the original cleavage directions of the individual felspar phenocrystals can easily be observed. Albitization preceeds prior to chloritization. Phenocrysts or lath shaped crystals may be seen as ghost pseudomorphs due to alteration to calcite and sericite. Complete alteration to Albite has been described previously (MTA Rp. No. 982). Albite and Carlsbad twins are very common.

The pyroxene is colourless or pale green in thin sections and appears in the usual short prismatic crystals or four to eight-sided sections (Plate 4.2.1). The maximum extinction angle varies between 29 and 45 degrees, with occasional polysynthetic twinning which suggests compositions varying from augite to augite. However microprobe analysis of several crystals has given compositions varying into the Diopside field (Fig. 4.7.b).

Pyroxenes show various stages of alteration to fibrous amphibole (uralitization) and chlorite. Uralite hornblende is probably actinolite, which is greenish in colour and slightly pleochroic

with a maximum extinction angle of 17 to 20 degrees. It usually replaces the pyroxene along its cracks and cleavage directions but occasional rims of hornblende to pyroxene can also be observed. In the later stages of alteration this amphibole gives way to chlorite.

The most advanced stage of alteration is represented by the total replacement of pyroxenes by epidote and chlorite pseudomorphs, lined by an aggregate of quartz. Chlorite is virtually the ultimate alteration product, impregnating virtually all of the previous silicate minerals.

Biotite is rare, usually leached and altered, and sometimes with opaque rims.

The vesicular texture seen on plate 4.2.2 is characteristic of most of the green coloured Lower Basic Series rocks in which vesicles are seen infilled with chlorite in the core with wedge-shaped aggregates of quartz lined along the margins. Some amygdales may be seen infilled with chalcedony.

As a general feature, a greenish colour, due to extensive chloritization, is very common away from the SW-NE trending mineralization zone. These basic, green coloured lavas, exposed to the south of the map area and in lower levels of the main water courses, were described earlier as a Spilite-keratophyre association due to their highly sodic plagioclase content, pyroxenes or alteration products such as chlorite-epidote and chlorite-limonite as suggested by Turner and Verhougen (1960). Large altered felspar phenocrysts with relict patches of Labradorite-Andesite composition suggest their calcic-origin.

The albite-epidote-chlorite-calcite assemblage is conspicuous. Whether it is an assemblage of low-grade metamorphism or a direct

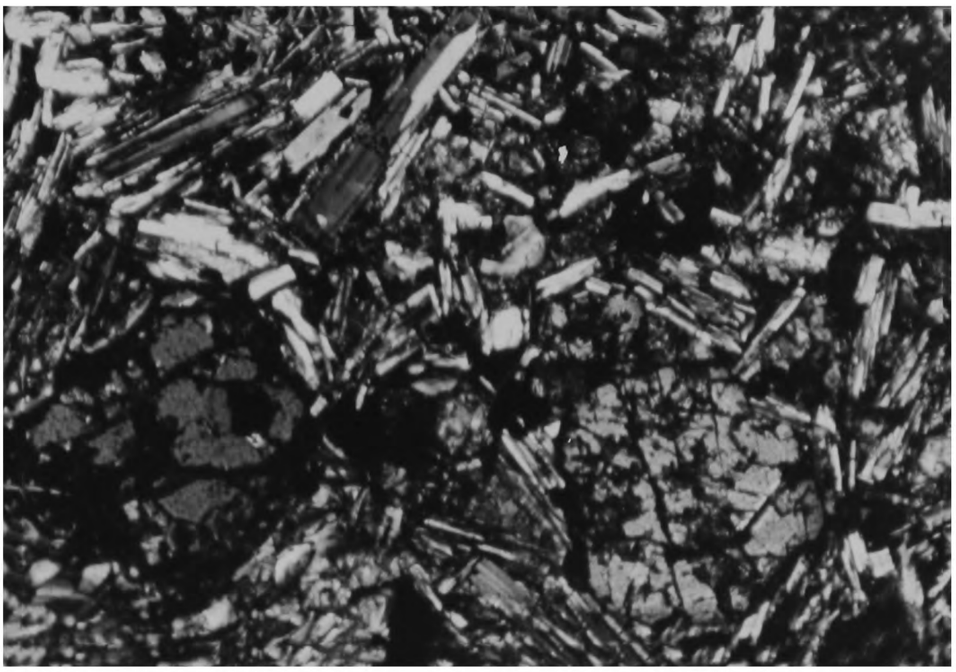

Plate 4.2.1 Ophitic texture in basalt. x 50

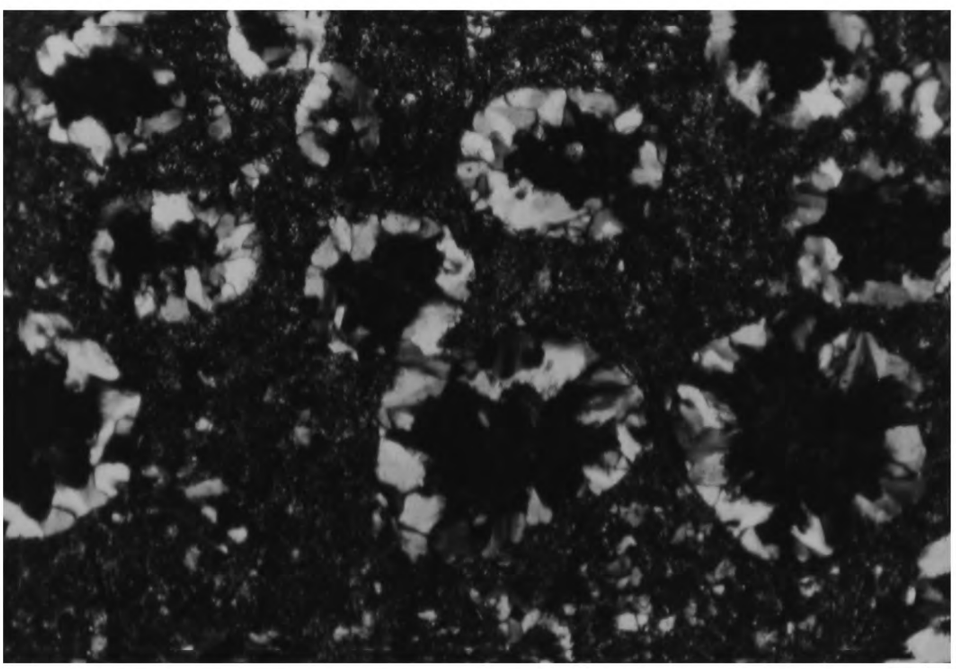

Plate 4.2.2 Vesicular texture in Lower Basic Series rocks. x 50.

result of hydrothermal alteration needs further detailed study. Also the K_2O content is not as low as it ought to be.

The use of keratophyre as a rock name is beset by confusion and ambiguity, partly due to albitization of potassic rocks (trachyte and rhyolite). The nomenclature of keratophyre rocks was recently discussed in detail, by Schermerhorn (1973). According to this author "Keratophyres are not albitized trachyte or rhyolite, they are sodic-plagioclase counterparts of those rocks".

4.3 Porphyritic Dacite.

These rocks are characterised by large quartz phenocrysts and coarse prophyritic textures throughout the eastern Pontids. The intensity of alteration in this series varies throughout the area. In places, to the north of Hamidiye Village intense silicification produces quartzite-like rocks in which the only remnants of the original character of the rock are rounded, large, quartz phenocysts.

In general, corroded, idiomorphic to hypidiomorphic, 1 to 7mm long quartz crystals and feldspars are set in a light coloured mosaic of xenomorphic groundmass containing quartz, albite microlites and possibly potash-feldspar). Calcite, sericite, chlorite kaolinite and limonite are major alteration products.

In a dyke specimen (4F) altered amphibole sections normal to the c-axis and also parallel to 010 were identified together with chloritized and limonitized biotite crystals. Feldspar phenocrysts up to 2cm long were collected from the weathered exposure surface (Plate 4.3.1). Almost all of these crystals show carlsbad interpenetrant twins. Microscopic study of these

crystals has shown complete alteration to calcite and cryptocrystalline quartz.

Biotite is present only as phenocrysts. It is intensely altered to secondary sericite and muscovite leading sometimes to complete pseudomorphs of sericite after biotite. The removal of iron during this process results in the formation of granular magnetite and hematite aggregating along the borders and cleavage planes of the former biotite. Superimposed weathering produces the iron hyroxides (Goethite).

Hornblende is also altered and corroded in a way very similar to that of biotite and its characteristic outlines have been pseudomorphed by the later calcitic material.

Phenocrysts of quartz are markedly rounded and corroded. They are usually surrounded by a rim of silica which may suggest the possible existence of some disequilibrium conditions between the groundmass and the quartz phenocrysts.

In transition zones to underlying Lower Basic Series rocks, the coarse porphyritic appearance grades down into fine or medium grained rocks.

Zircon, apatite and pyrite are the main accessory minerals. According to the mineralogy and chemistry the rock may be called biotite-hornblende dacite porphyry.

4.4 Rhyodacitic Rocks.

These rocks are found totally altered in the map area. They are differentiated from the other units by small triangular quartz crystals.

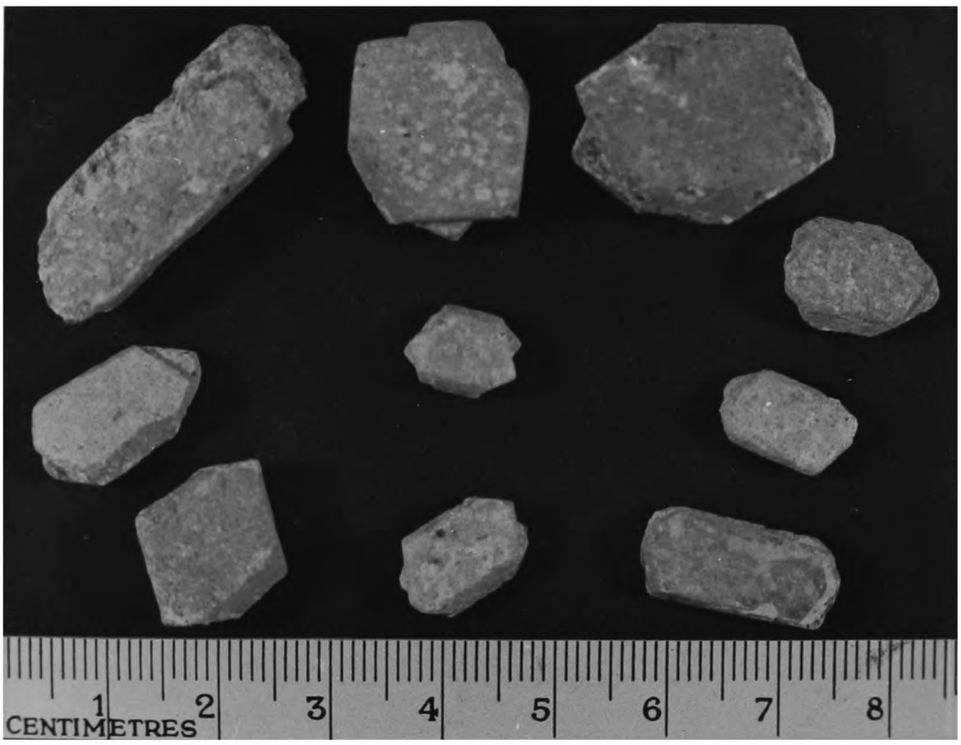

Plate 4.3.1 Pseudomorphosed feldspar phenocrysts.

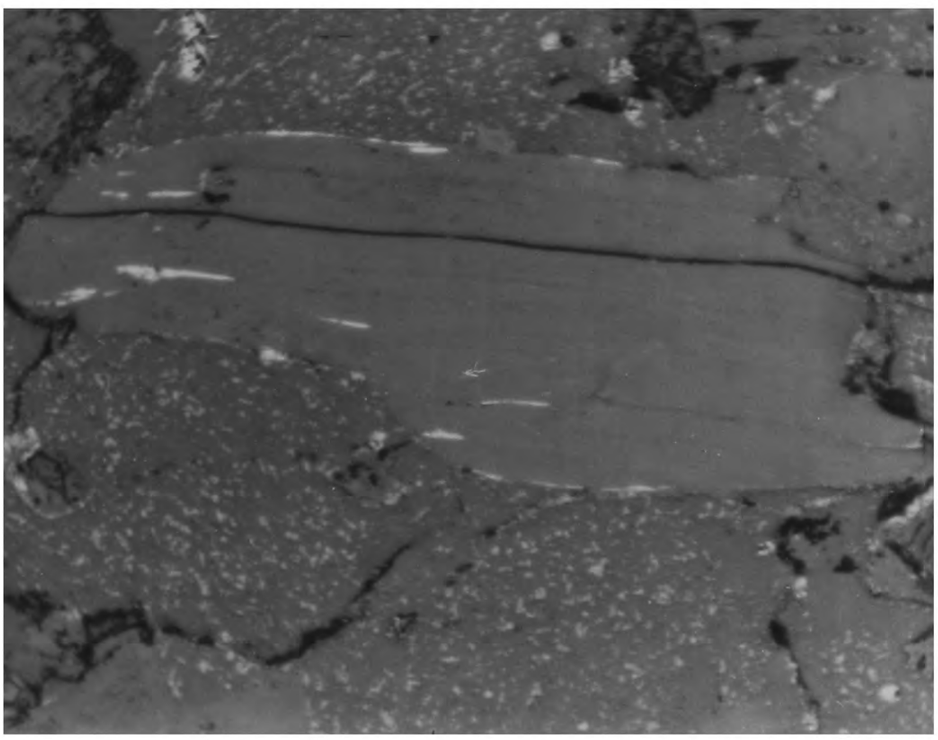

Plate 4.5.1 Hematite Lamella along cleavage planes of biotite.x 150.

They are usually seen to be white to purplish-grey coloured, and fine to medium-grained. Idiomorphic to xenomorphic, corroded quartz crystals are set in a devitrified felsitic groundmass together with pseudomorphs of feldspar phenocrysts which are sericitized and carbonitized. The groundmass consists of cryptocrystalline quartz and altered feldspar microlites. Occasionally altered mica and hornblende(?) crystals may be seen.

The texture is usually porphyritic. Zircon, apatite, pyrite and baryte have been described as accessory minerals (MTA Rp. No. 982).

4.5 Biotite-Andesite.

These porphyritic rocks are characterised by abundant biotite crystals. Although various degrees of alteration are seen, the feldspar and biotite phenocrysts are fresher than in the dacitic and Lower Basic Series rocks. Phenocrysts of plagioclase, biotite and completely calcitized and chloritized clinopyroxene appear in a brownish, partly devitrified glassy material full of feldspar microliths. The altered brownish glass may be palagonite. Quartz is virtually absent.

Plagioclase is in the Labradorite range from measurements of refractive indices but probe analysis proved it to have Andesine compositions (Fig. 4.7.a, Appendix 3A). Fresh albite or possibly sanidine was described in the previous field report (MTA Rp. No. 982, Dtm. No. II/722,781). The plagioclase is usually zoned, the type of zoning being oscillatory. Albite-Carlsbad and Pericline twins were recognised. Core or rims may be as calcic as anorthite as is indicated by the difference in their refractive indices. More calcic zones are more readily replaced

by calcite forming calcite cores or rings. Alternatively, some rounded minute inclusions of brown glass can also occur here and there in plagioclases. In places feldspar laths may be seen intruding into the biotite sections parallel to 010.

Some limonitized ghost pseudomorphs suggest amphibole sections normal to the c-axis.

Biotite occurs as lath shaped sections parallel to 010 with occasional six-sided 001 sections and is never observed in the matrix. It is strongly pleochroic in light to dark brown colours. Formation of hematite (magnetite) as lamellae oriented along cleavage planes and crystal outlines is very common (Plate 4.5.1). Bent crystals of biotite are found with curved cleavage planes. No alteration of the biotite was observed.

Magnetite was found as large, anhedral crystals in major amounts (Plate 4.7.1).

Pyroxene is completely replaced by calcite and chlorite and its former place is indicated only by the outlines of the pseudomorphs. In some instances, these four to eight-sided outlines still preserve the characteristic perpendicular pyroxene cleavage.

Zircon and pyrite may be seen as accessory minerals. This rock may be named basaltic biotite-andesite (see analysis 154, Appendix p.294).

4.6 Quartz-Microdiorite.

As a result of chloritization, outcrops of these rocks are almost indistinguishable from the greenish lower basic series rocks. In addition to this difficulty, the topographic position of the

formation does not allow for good sampling. Only one specimen (138) was collected.

In the thin sections (studied) saussiritized feldspars are found completely altered to calcite, chlorite and epidote although its zoned character is seen in some fresher relict patches.

A few chloritized biotite crystals may also be seen. Chloritization has extensively affected the rock, and alteration also produces goethite from accessory magnetite and pyrite. The texture is porphyritic and granular.

4.7 Basalt Dykes.

These, previously described as Pyroxene-basalt dykes, are massive, medium to fine-grained, light to dark green or black coloured rocks. In some cases they may be seen as vesicular and cut by calcite (dolomite?) veinlets.

Major phenocrystals are feldspars, clinopyroxenes, biotites and altered amphiboles. Feldspars are mainly euhedral to subhedral slender laths of well-twinned labradorite and bytownite. In most cases they look remarkably fresh. Bytownite, Labradorite and sanidine compositions were established by probe analysis (Fig. 4.7a). Maximum extinction angles were measured as 34 to 40 degrees for Labradorite (see analysis 159/2) and 41 to 46 degrees for bytownite. Zoning is common. Occasional undulose extinction may be seen. Mainly albite and carlsbad twins were observed.

In specimen 156, two of the feldspar crystals analysed proved to have sanidine composition whereas the others proved to have bytownite

compositions.

In specimen 128A feldspar crystals are almost totally replaced by a mixture of microcrystalline quartz and chalcedony. The previously zoned nature of the individual phenocrysts is still recognizable due to the stronger resistance of the more sodic zones to the alteration. Skeletal groundmass feldspar may be seen extensively chloritized.

Pyroxene usually occurs either as large euhedral to subhedral grains, or forms rather irregular clusters of smaller individuals. Phenocrysts have a short, prismatic habit with four to eight-sided sections, pale greenish colours and slight pleochroism. They are usually zoned, structures similar to hour-glass zoning are rarely seen, and the outer shells are commonly replaced by greenish amphibole (uralitic hornblende). More tentative uralitization takes place in the form of small veinlets following the cleavage directions of the host. Alteration of pyroxene is by complete calcitization accompanied extensively by chloritization. During the course of alteration, a small amount of silica is also released in the form of tiny quartz aggregates which are always associated with the heavily altered mineral.

Diopside, endiopside, augite and salite compositions were established by microprobe analyses of several grains in the same section. These composition plots are seen in Fig. 4.7b.

Amphibole is totally chloritized and only the outlines of it remain. In most cases the alteration of amphibole resulted in the formation of granular iron oxides.

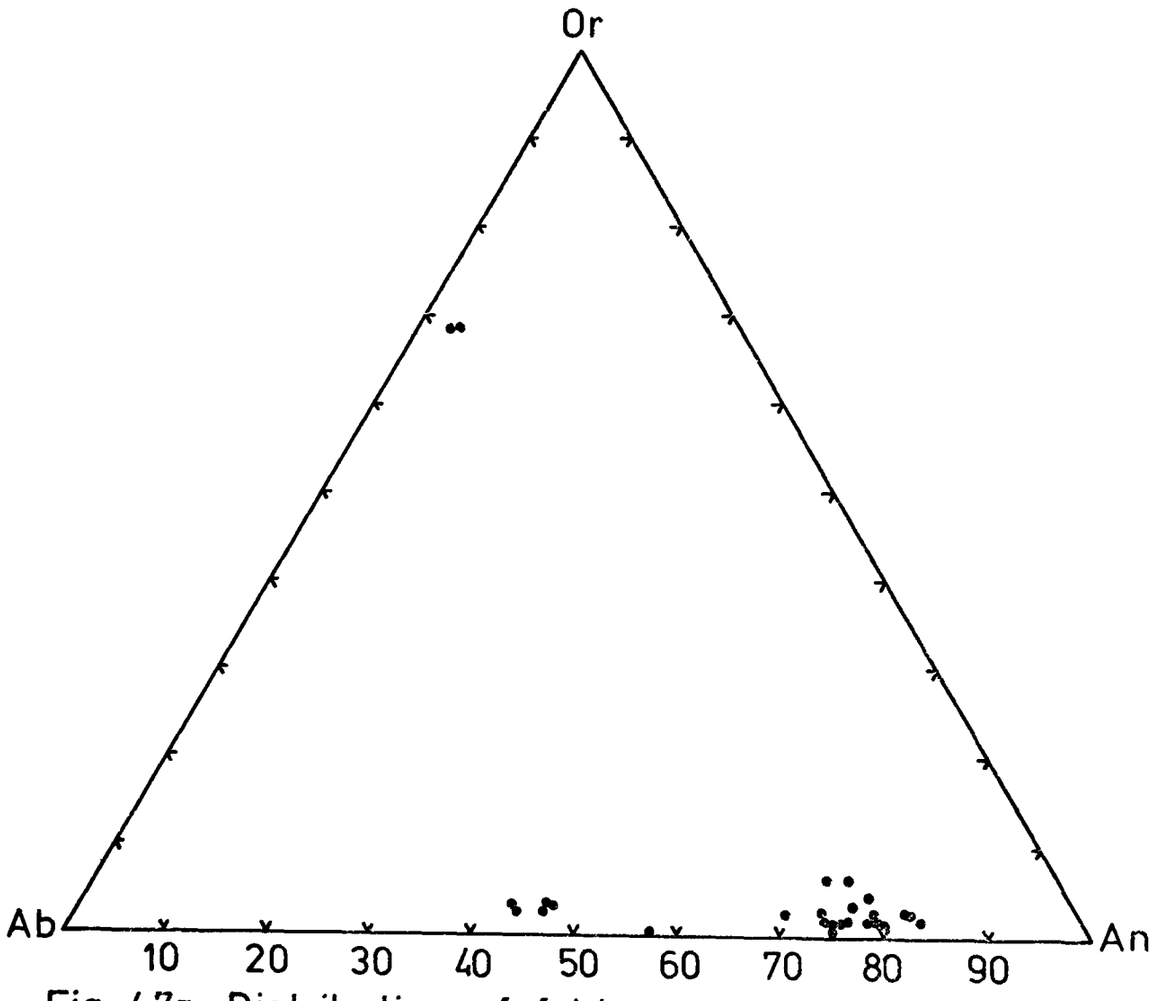

Fig 4.7a Distribution of feldspar analyses in the system Or - Ab - An.

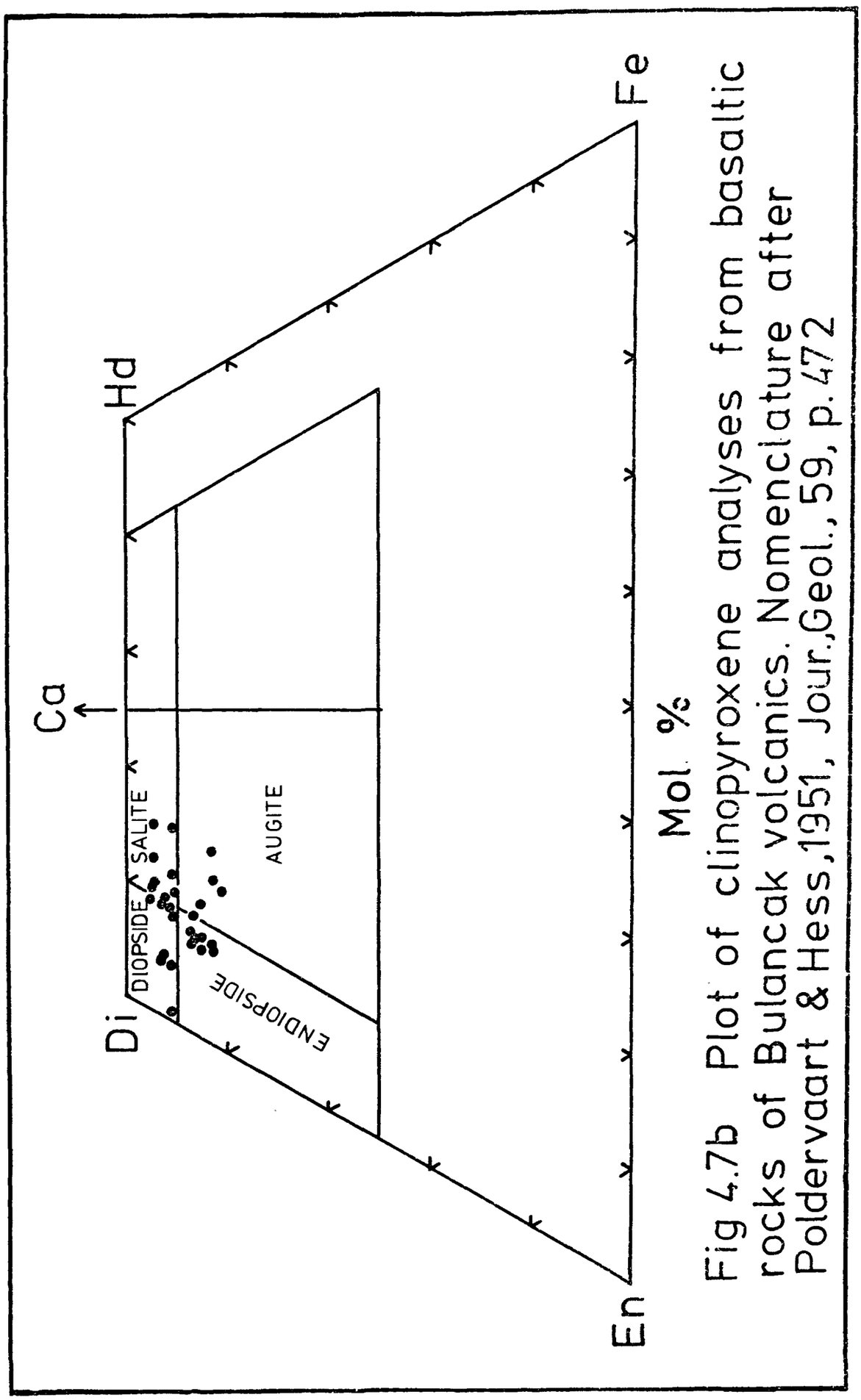

Fig 4.7b Plot of clinopyroxene analyses from basaltic rocks of Bulancak volcanics. Nomenclature after Poldervaart & Hess, 1951, Jour. Geol., 59, p. 472

Biotite appears as basal sections and sections parallel to 010 with brown colours. It may also occur as tiny little acicular crystallites in the groundmass.

Magnetites in specimen 52, 157 and 159 were found in major amounts as large, skeletal and subhedral to anhedral forms (plate 4.7.1) with rare ilmenite exsolution lamellae in specimen 159. They are seen in various sizes, in some cases with the development of goethite along a fine network in euhedral crystals. Occasionally a tiny pyrite grain may be enclosed in anhedral crystals. It may show characteristic skeletal growth with feldspar Laths (Plate 4.7.2). Lamellae of magnetite or hematite may be seen oriented along the cleavage planes of biotite similar to those in specimen 154.

Isolated and much rounded, corroded grains of xenolithic quartz are common in specimen 128A and 157. These crystals are believed to be xenocrysts caught up during the uprise of the magma (Hatch, Wells and Wells, 1972 p.359).

The groundmass is heavily carbonatized and largely devitrified glassy material full of tiny skeletal feldspars, poorly crystalline quartz and acicular biotite microlites. The rock may contain vesicles infilled with calcite, chalcedony and spherulitic glass, and surrounded by a reaction rim of brownish glassy material. This glassy material is partly devitrified and contains abundant acicular feldspar microliths. The texture is commonly ophitic to sub-ophitic with extensive grains of clinopyroxene in the interstices of lath shaped plagioclase masses. It may be porphyritic to largely vitrophyric in texture (e.g. Specimen 128A). Totally silicified phenocrysts of former feldspars tend to show highly perfect outlines in a dominantly devitrified glassy groundmass.

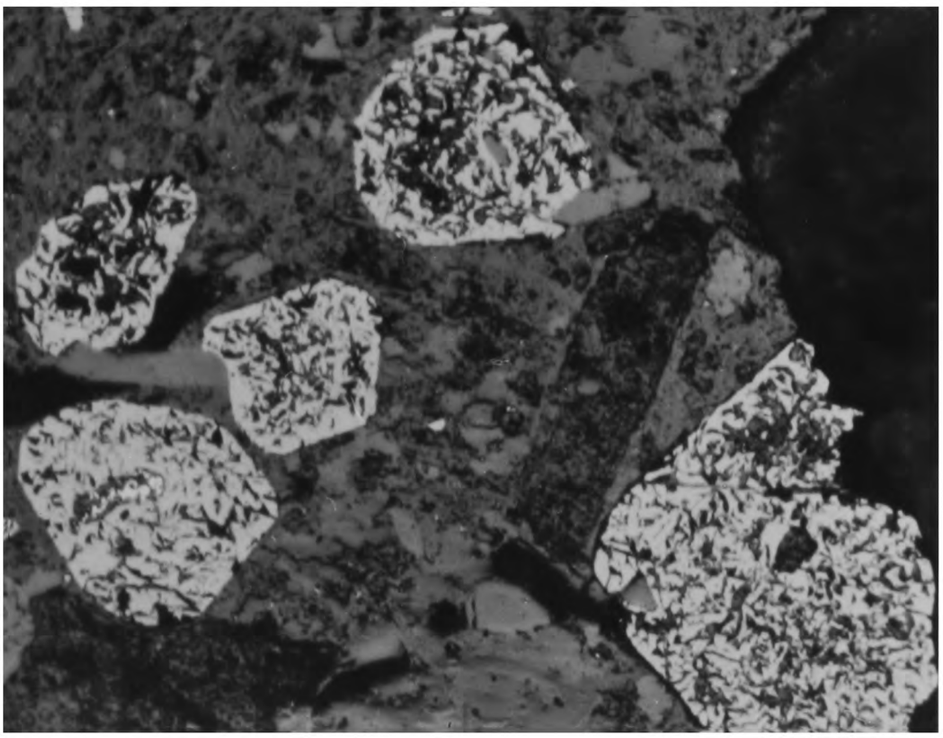

Plate 4.7.1 Euhedral, altered magnetite crystals. x 150

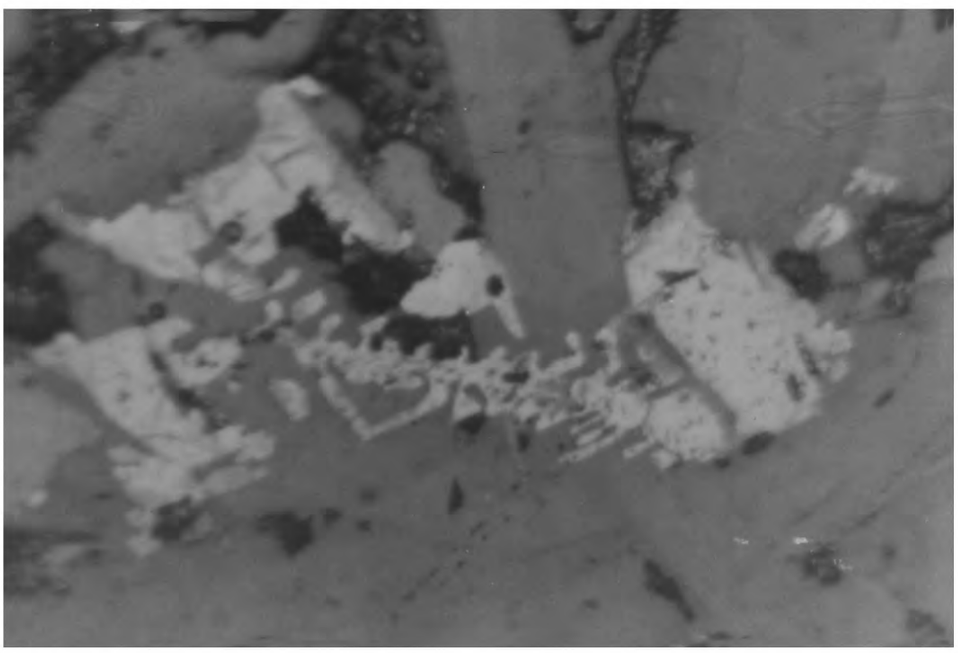

Plate 4.7.2 Skeletel growth of magnetite with feldspar laths. x 300

4B. CHEMISTRY OF THE COUNTRY ROCKS

4.8 Introduction.

In the course of the Laboratory work, collected rock samples representing country rocks were analysed by XRF. Sample preparation, analysis techniques and correction procedures are described in Appendix 2. Major and trace element analyses are presented in Appendix Tables 2A-2D.

All samples were analysed for Si, Al, Fe, Mg, Ca, Na, K, Ti, Mn, S, P, CO_2 and H_2O. FeO determinations of mainly basaltic dyke rocks, together with CO_2 were done by wet chemical methods. Undetermined FeO's are indicated by 'N.D.' in the Appendix 2 tables, which lists the major and trace element analyses.

As previously explained, due to the extensively altered nature of the rocks in the map area, a classification based on the normative mineralogy was not possible. A simple case was seen when allocating CO_2 to calculate normative calcite, where it was found necessary to use almost all the CaO content. An attempt to plot an AFM diagram also failed because there was no distinct trend.

The calc-alkaline affinities of the volcanic rocks along the Eastern Pontids have been demonstrated by Tugal (1969) and Tokel (1973) to the east of the map area. Therefore these rocks will be compared with those from similar environments and possible parental magma types will be discussed.

4.9 Variation of Major Oxides with SiO_2

For the present purpose, the SiO_2 contents of the rocks are taken as basis for a simple classification (Middlemost, 1973; Fitton, 1971). The volcanic rocks of the area show a trend of SiO_2 enrichment with the resultant formation of the basalt-andesite-dacite-rhyodacite (possibly rhyolite) association as commonly observed in volcanic fields of orogenic belts. Since the SiO_2 content increases regularly with little gap, Harker-type variation diagrams can be used to represent the compositional variations. The variation of the major oxides with wt. SiO_2% in the rocks of the map area have been plotted in Figs. 4.9.1 and 4.9.1a.

Initially Al_2O_3 shows an increase but with increasing silica content decreases. Within the general trend, pairs of specimens from the same rock unit show the effect of alteration. Maximum Al_2O_3 is 25.47%, but generally ranges from 12% to 21%. A tendency for Al_2O_3 to decrease with increasing SiO_2 content may partially be related to silicification. Brown and Schairer (1971) consider that high alumina content characterizes the calc-alkaline parental basalts and that a high alumina content is characteristic also for the whole volcanic suite.

ΣFe_2O_3 (total Fe as Fe_2O_3) decreases with increasing silica content for all rock units. However, it should be noted that the Σ FeO/MgO ratio increases from the basic to acidic varieties, probably indicating the influence of silicates rather than Fe-Ti oxides (Fig. 4.9.2). It has been noted that ilmenite was not seen as discrete grains in any of the rocks studied although it

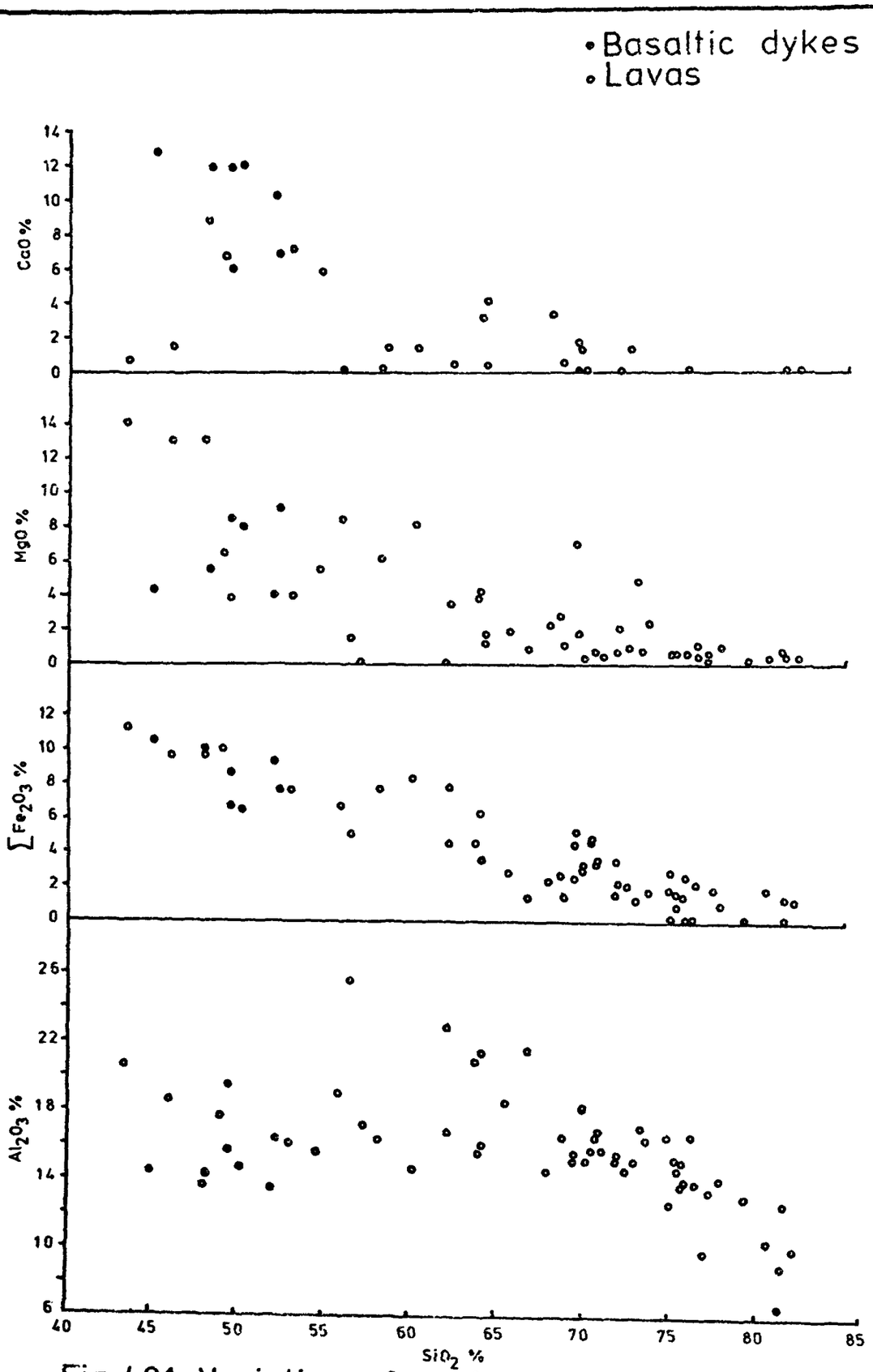

Fig 4.9.1 Variation of major oxides with silica

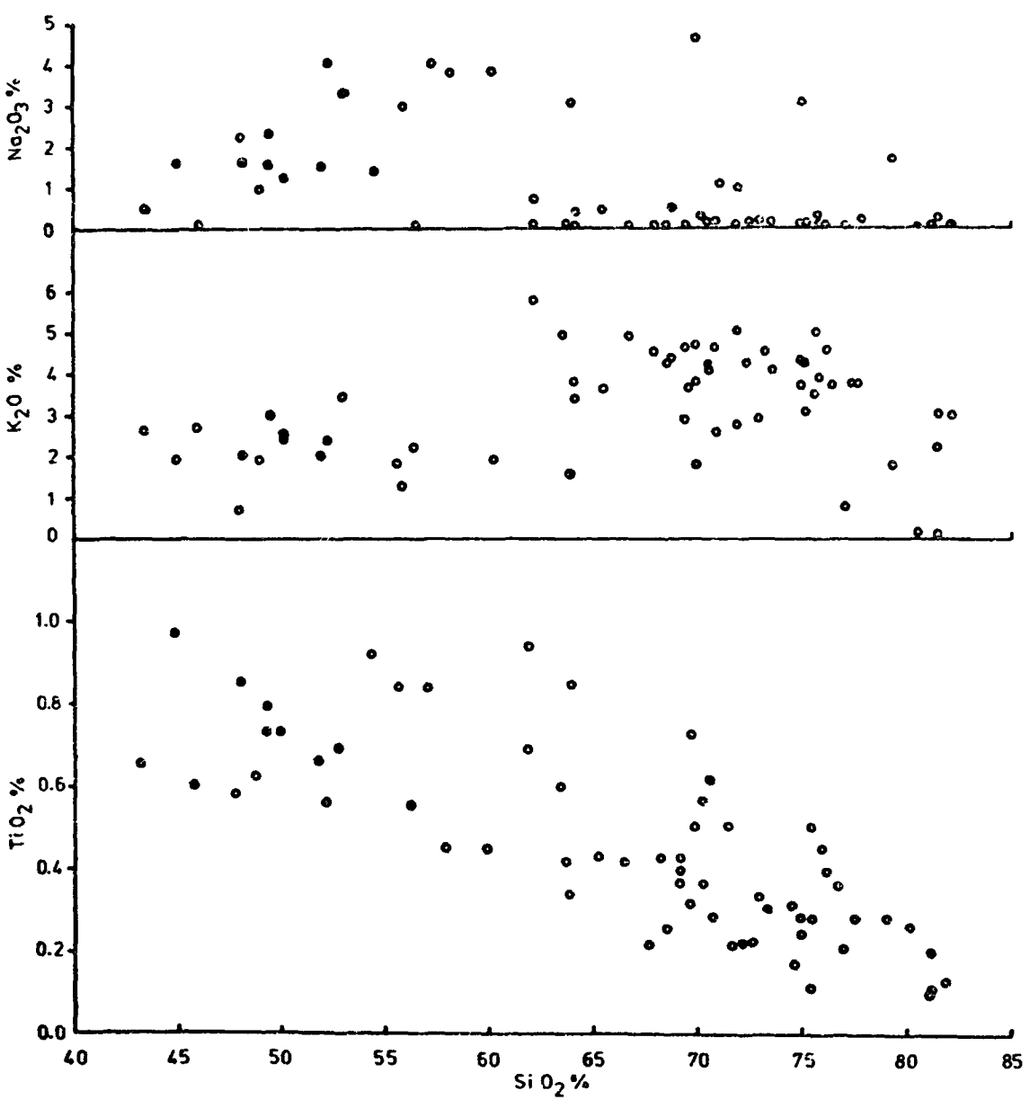

Fig 4.9.1a Variation of major oxides with silica

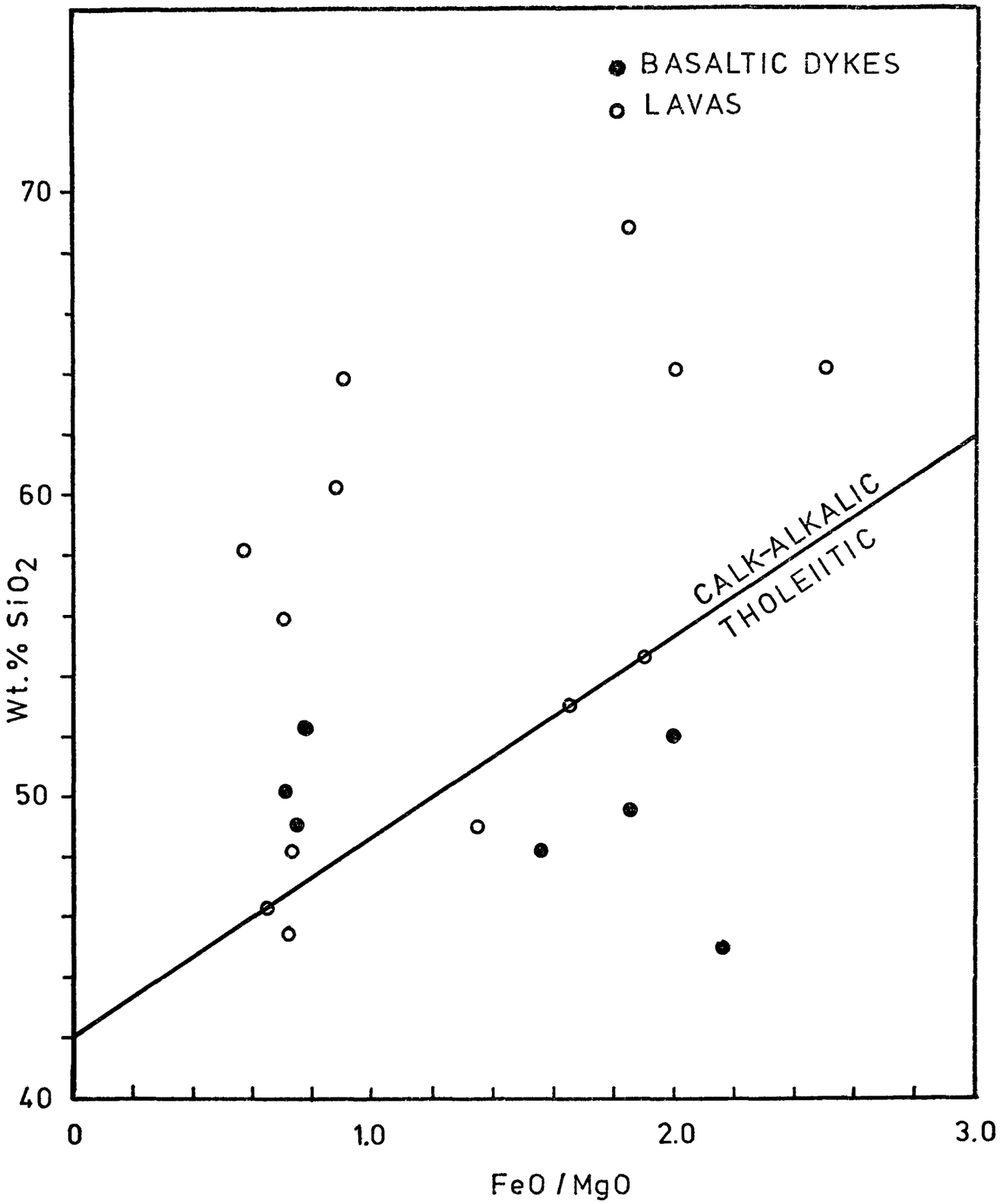

Fig 4.9.2 Changes in SiO_2 contents with increasing FeO/MgO ratio in Bulancak volcanics. FeO represents total Fe as FeO. Boundary line after Miyashiro (1974).

occurs only in one specimen as exsolution lamellae in magnetite. The absence of ilmenite was noted by Lowder (1970) as a widespread feature of calc-alkaline rocks. The majority of the calculated Σ FeO/MgO ratios, when plotted against SiO_2, fall in the calc-alkaline field defined by Miyashiro (1974). Lower Basic Series rocks fall in both fields. It must be remembered that the dyke basalts falling in the tholeiitic field represent the youngest volcanism in the map area.

The MgO content ranges from 0.0 to 8.47% and decreases from basic to acid rocks are possibly due to the widespread secondary dolomitization.

The CaO content shows a more erratic scattering in the basaltic end although the general outline suggests a fall towards the acidic end. The maximum effect may be seen in the Lower Basic rocks in the direction of Küçükdere - Kovalık Sr., where lime content suddenly drops from 8.76% to 0.71% with increasing hydrothermal alteration from south to north.

Plots involving alkalis show a wide scatter of points, probably resulting from the mobility of these elements during alteration of the rocks. K_2O increases in general with increasing SiO_2. However, it decreases in the basic rocks, while Na_2O is increasing, possibly due to Na-enrichment as a result of albitization. On the other hand K_2O content is remarkably high for both basic and acidic rocks in the range 0.0 to 4.94%. These high K_2O contents have been suggested by several authors to characterize Calc-alkaline suites of continental margins, as in the case of Cascades (Dickinson, 1968) and in the

islands of the northeastern Aegean Sea (Nicholls, 1971). In particular, Kuno (1966) has drawn attention to the regular increase in alkali contents of island arc lavas, with increasing distance from the trench. This feature has been ascribed to variation in the nature and the thickness of the underlying crust (Moore, 1962), to an increasing depth of formation of magma (Kuno, op. cit.) or to an increasing depth to the Benioff zone (Dickinson and Hatherton, 1967).

TiO_2 has given a better, less-scattered trend in the range 0.97% to 0.11%. It steadily decreases from the basic to acidic varieties. The trend is similar to that of the Borrowdale volcanics southern outcrop rocks (Fitton, 1971), and islands of northeastern Aegean (Paraskevopoules, 1956; Nickolls, 1971). However, the TiO_2 contents are lower than those of the Borrowdale volcanics.

4.10 Variation of Trace Elements:

In Fig. 4.10.1 Zr, Ba and Sr were plotted to show variations with increasing SiO_2. Other elements were not included because of their very low contents near to the Lower Limit of detection. Cu and Zn were also avoided as the rocks come from a Cu-Pb-Zn mineralization area. Ti-Zr and K-Rb relations were considered together.

The general distribution of Barium in the rocks of the study area shows a very erratic scattering. This can be explained by the mobilization of Ba to form baryte, which was found as an accessory mineral in the rocks and as a ganque in the ore specimens. The abnormal increase of Ba with hydrothermal alteration from 311 ppm

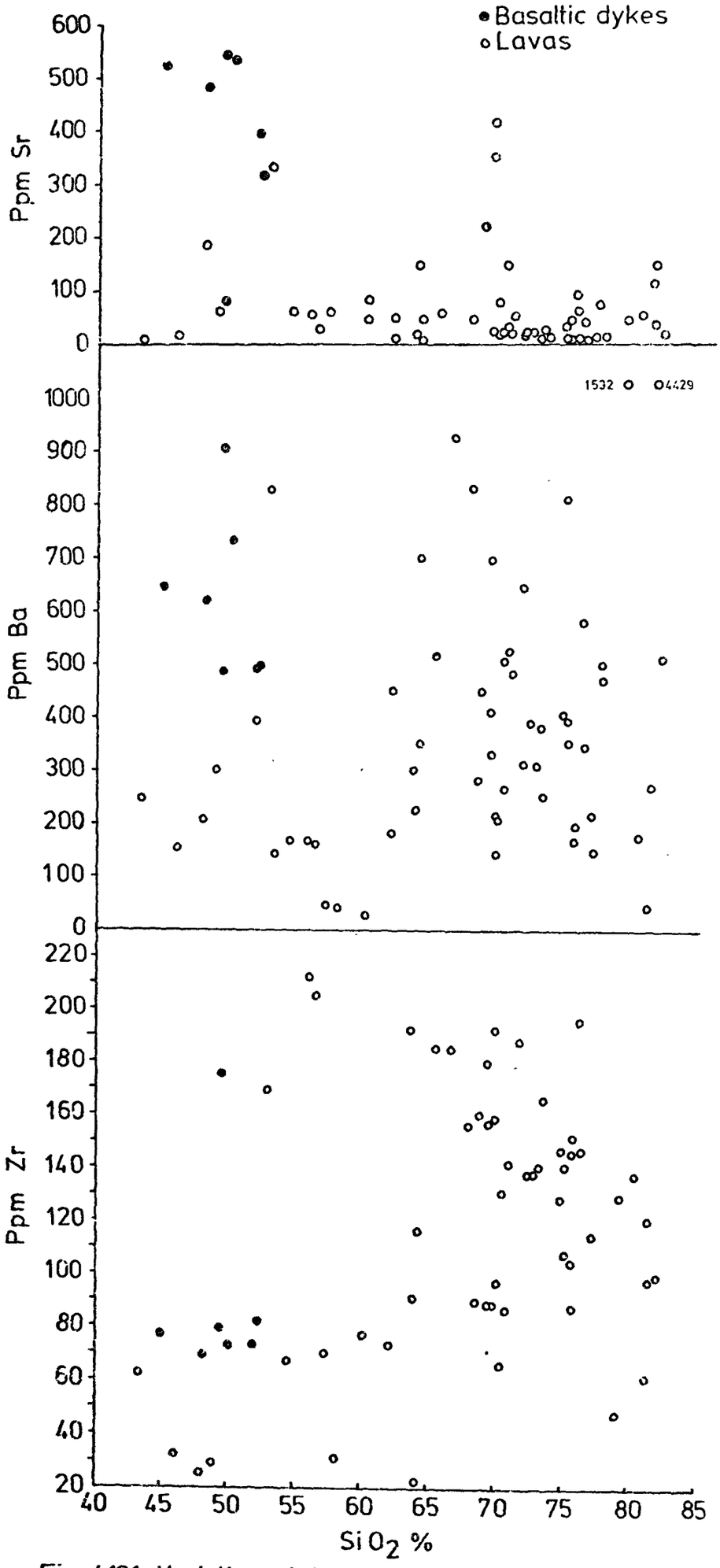

Fig 4.10.1 Variation of trace elements with silica

to 4429 ppm can be seen in porphyritic dacite specimens 165 and 166, the latter being closer to the Akköy orebody.

Sr varies from 542 ppm to 6 ppm. It has a general decreasing trend in basaltic dyke rocks in the range 542 to 513 ppm, but in the other rock units it is fairly constant in the 75 to 6 ppm range. Some high Sr values in the acidic range are possibly related to the formation of secondary baryte, since $BaSO_4$ is known to show complete solid solution with $SrSO_4$ (Deer, Howie and Zussman, p.465).

Rb contents vary from 49 to 107 ppm in basaltic dykes, 1 to 165 ppm in Lavas. The general study of rubidium is to increase with acidity. The K/Rb ratios of the volcanic rocks of the map area are shown in Fig. 4.10.2. Both basic and acidic rocks give K/Rb ratios of around 150, falling slightly with increasing potassium. This ratio was found to be lower than all described trends in the literature (Shaw, 1968; Jakes and White, 1970). The latter authors have shown that the increase in the potassium content of Lavas across island arcs is accompanied by a decrease in the K/Rb ratios.

Zr, Y, and Ti (as earlier described) are amongst the elements less affected by hydrothermal alteration. As recently suggested by Cann (1970), the abundances of these elements in ocean floor basalts are little affected by secondary processes. It has also been shown that their distribution can be related to various magma types (Pearce and Cann, 1971). In Fig. 4.10.3 plots of Ti-Zr are shown. As seen from the Figure the majority of the points fall in the island arc Andesite type magma field (Pearce and Cann, 1971 Fig. 2). As suggested by the authors, rocks of the area probably indicate formation near a destructive plate margin at some distance from the plate boundary.

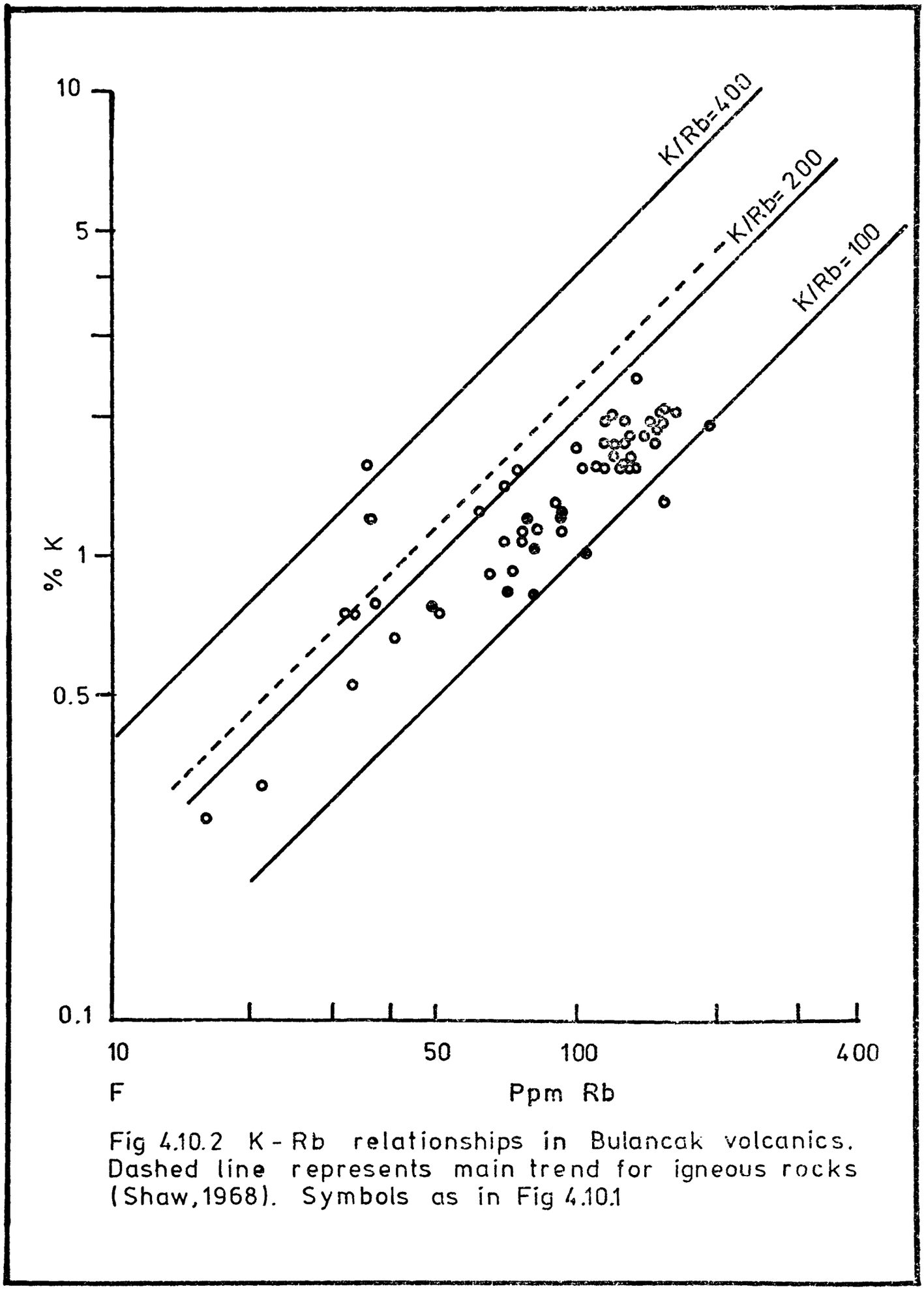

Fig 4.10.2 K - Rb relationships in Bulancak volcanics. Dashed line represents main trend for igneous rocks (Shaw, 1968). Symbols as in Fig 4.10.1

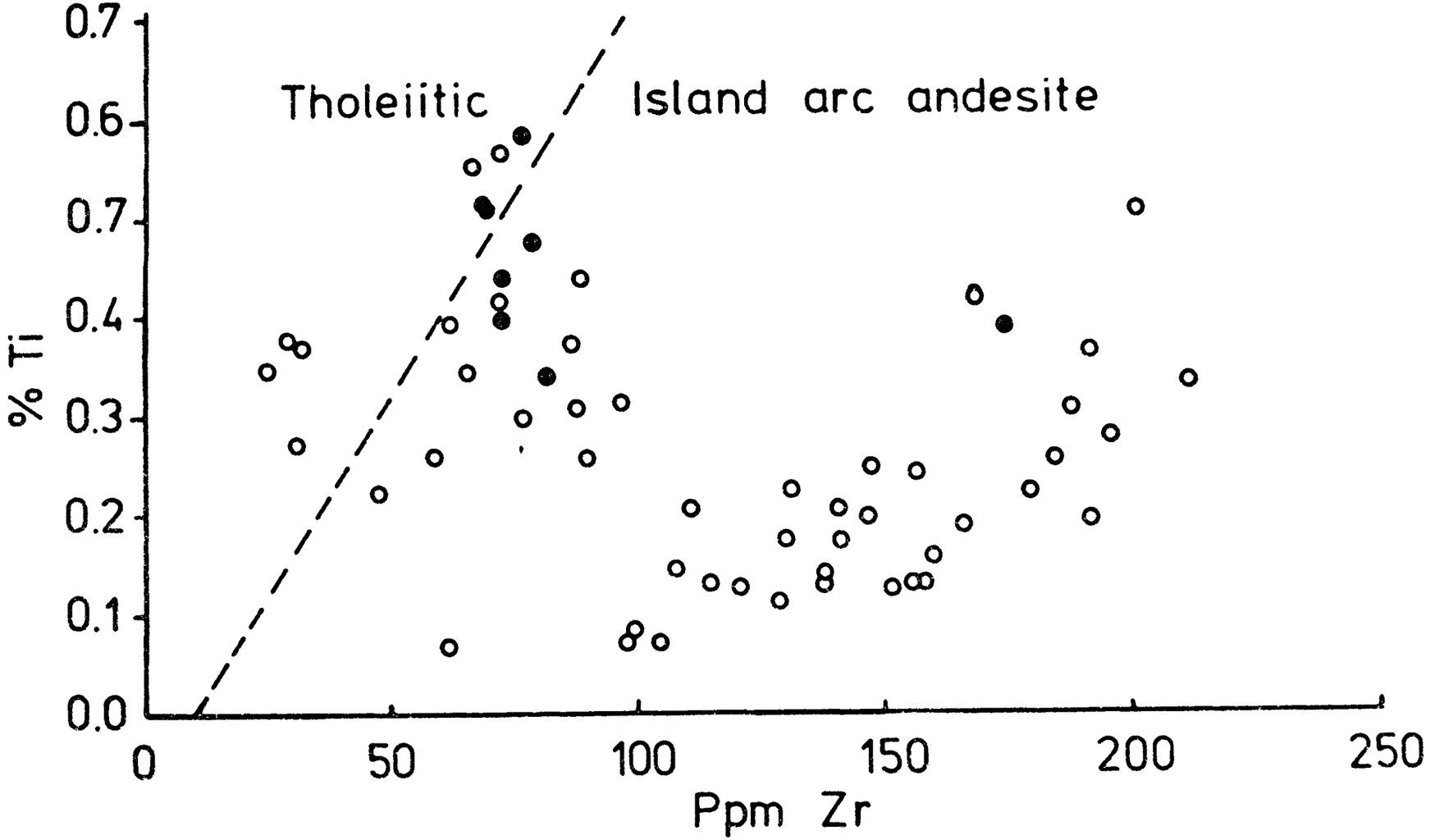

Fig 4.10.3 Plot of titanium against zirconium. The relative boundary between two magma types from Pearce and Cann (1971).

It has been demonstrated in the Gümüşhane region by Tokel (1973) that subduction is related to volcanic activity. However, the rocks studied are collected from a limited area around the mineralization zone, and the sampling is insufficient. The possibility that the present area may represent a transverse section in an island arc or continental plate margin environment is therefore a subject for further study.

CHAPTER FIVE

MINERALOGY

5A. THE MINERALOGY OF VEIN MINERALS

5.1 Introduction

The sulphide occurrences, starting almost from the coast line between Bulancak and Giresun, to the southeast of Bulancak spread over an area of 60 Km^2 between Boztekke Village in the north and Küçükdere Village in the south including occurrences in Inece, Eriklik, Tekmezar, Yaykinlik, Hamidiye, and Dariköy villages. Individual occurrences such as Körüktepe in Tekmezar have long been known and according to Ayışkan (1959) were mined along 9 adits opened during the 1870-1880 Russian war. Veins at the Karayalak locality near Dariköy, and at the Yaykinlik and Inece occurrences are described briefly in the literature (Akol and Alpay, 1955; Ayıskan, 1959; Ryan, 1960). Ayışkan has given a list of about 50 vein occurrences and the minerals determined in polished specimens around the Tekmezar area. Apart from locations of the veins, lists of the minerals determined and some random analysis, there is no detailed information about the textural relationships of the minerals and paragenesis. Hematite, pyrite, marcasite, sphalerite, chalcopyrite, galena, bornite, tetrahedrite, covellite, chalcocite, malachite, azurite, cerussite, anglesite, ankerite, dolomite, calcite, baryte and quartz are reported from these occurrences. In addition to these minerals, the writer was able to identify and confirm the existence of Betekhtinite, Bismuthinite-Aikinite solid solution minerals, Idaite, Tennantite and Digenite by X-Ray Diffraction and Electron-Microprobe analysis. The identified minerals are listed in table 5.1.

TABLE 5.1 Minerals identified in the Bulancak sulphide occurrences

OXIDE	SULPHATE	CARBONATE	SULPHIDE	SULPHOSALT
Hematite	Baryte	Cerussite	Pyrite	Tetrahedrite
Idmenite	Anglesite	Calcite	Marcasite	Tennantite
Quartz		Dolomite	Sphalerite	Aikinite
Goethite		Ankerite	Galena	
Lepidocrocite		Siderite	Chalcopyrite	
		Malachite	Bornite	
		Azurite	Idaite	
			Covellite	
			Digenite	
			Betekhtinite	

5.2 Methods of Study

The samples studied came from approximately 145 individual sulphide vein exposures within mainly the Dariköy - Tekmezar area and neighbouring villages. Specimens were collected from veins, dumps or, in some cases, accessible underground workings.

Polished specimens and several polished thin sections were prepared for initial examination. X-Ray diffraction methods were mostly employed for the identification of carbonate gangue and barytes as well as for betekhtinite, aikinite, and especially for cell-size determinations of sphalerites. Disc wafers prepared for fluid inclusion study also helped to some extent in observing the transparency and colour of sphalerites.

Several different sulphide minerals were also etched to see the orientation of chalcopyrite exsolution blebs and inclusions in sphalerites and to bring out cleavage, twinning and zoning of sulphides. Nitric acid, hydrochloric acid, chromic acid, and $KMnO_3$ + HCl solution were used for etching.

5.3 Oxide Minerals

5.3.1 Quartz Is the principal gangue mineral and is present in almost every specimen studied. Commonly it is found as well-developed crystals of different orientation. It polishes extremely well, in most cases better than pyrite which has similar hardness. Since it is the earliest mineral to fill the vein fracture, the crystals projected towards the core of the vein exhibit well-preserved idiomorphic, hexagonal-shaped crystals. Usually they are enclosed in xenomorphic sulphide minerals

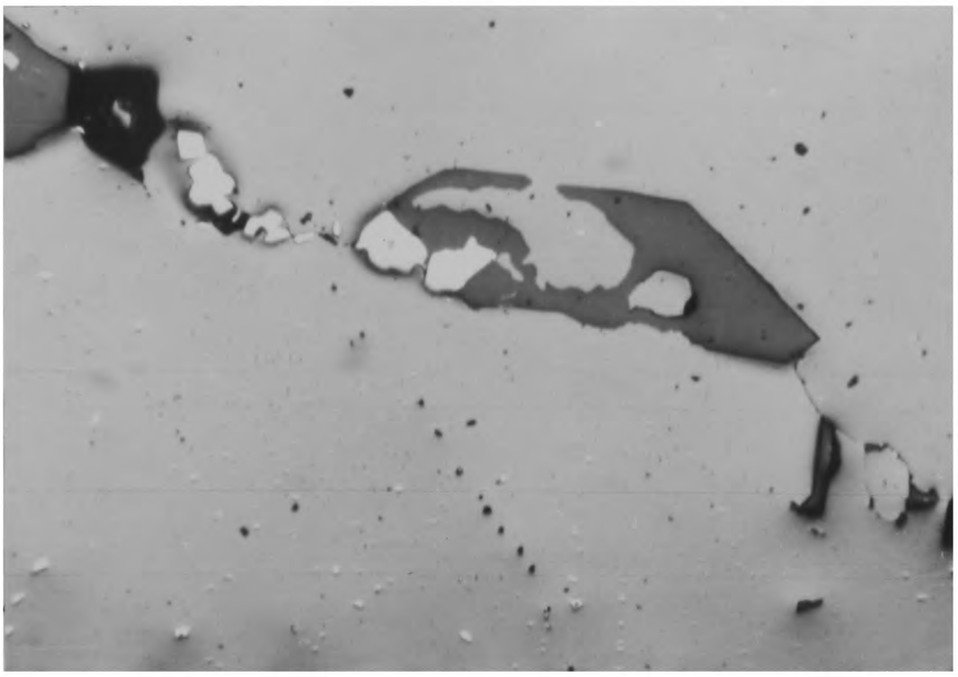

Plate 5.3.1a Sphalerite replacing euhedral quartz. x 150
(White is pyrite)

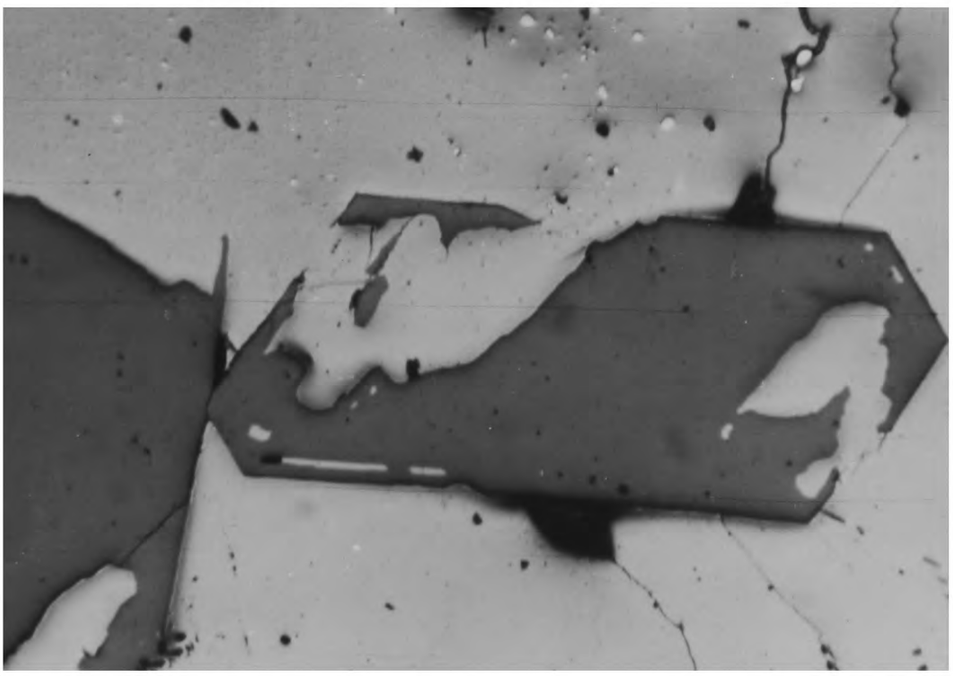

Plate 5.3.1b Sphalerite replacing euhedral quartz with pyrite. x 150

such as sphalerite and galena, which show allotriomorphic filling relations and are softer than pyrite.

Skeletal forms due to replacing sphalerite and galena and well-preserved, unreplaced idiomorphic crystals are abundant, (plates 5.3.1a and 5.3.1b). Ring and atoll textures produced by galena are also very common. Prismatic crystals showing corroded outlines due to carbonate replacement were seen in several specimens as well as carbonate veins cutting through quartz matrix. In general, it is replaced by late stage sulphides, especially by fahlerz minerals (see plate 5.7.1b).

5.3.2 Hematite: In several specimens it has been identified in insignificant amounts in a quartz matrix but at 815m. altitude at the Camideresi locality of Küçükdere Village, a limestone lens is almost completely replaced by hematite, but the deposit was not found to be economically viable (map 2,3/4H).

The identified hematite (specular) in the Küçükdere specimens is found as a bundle of interfingering blades in different orientations (plates 5.3.2a-c) or lath-shaped crystals similar to those illustrated in Ramdohr (1969) Fig. 561. Discrete blades, or laths are found scattered throughout the quartz-carbonate matrix (plate 5.3.2d) extending in places along the quartz-carbonate boundary. Some long blades were seen broken across, with smaller segments being dragged out of their original orientation.

Some bundles show strong anisotropy with bright greenish-blue polarisation colours in places with a yellowish tint while the others

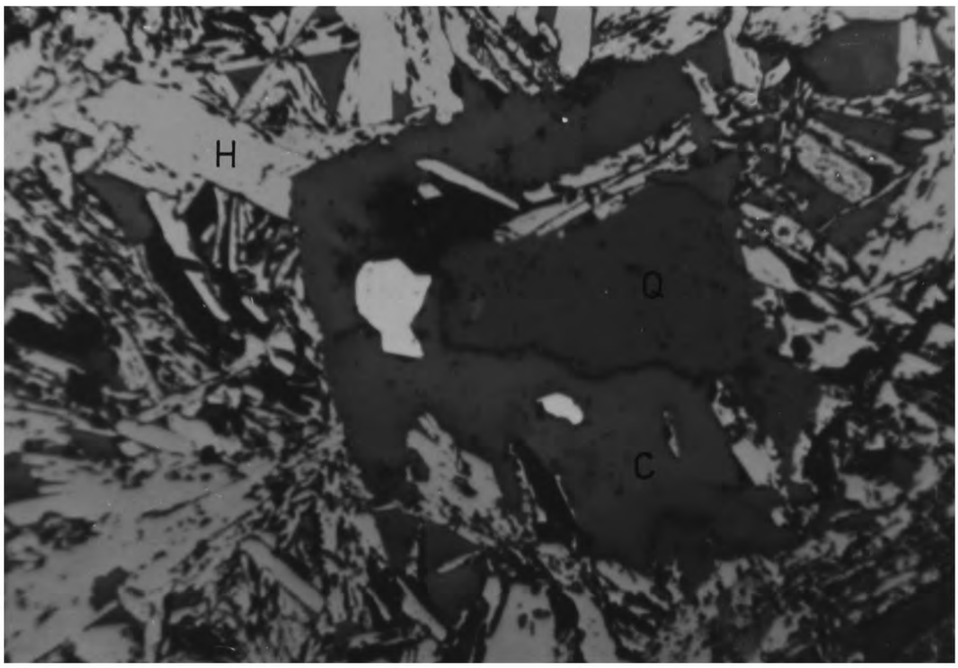

Plate 5.3.2 Quartz (Q), carbonate (C) and hematite(H) relationship. P = pyrite. x 150

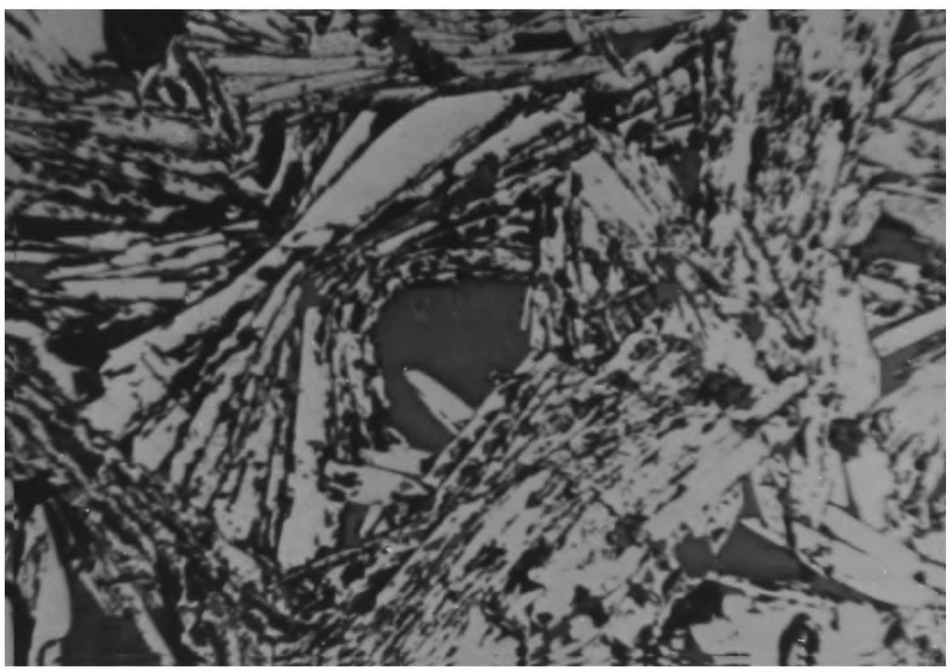

Plate 5.3.2b Bladed specular hematite crystals. x 150

Plate 5.3.2c Bladed specular hematite crystals. x 150

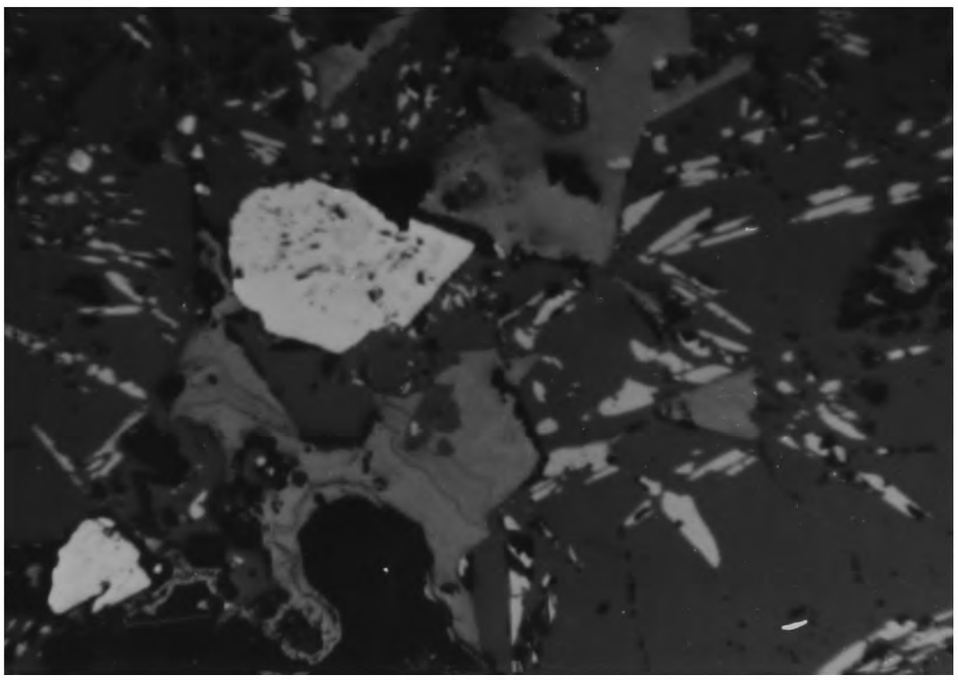

Plate 5.3.2d Bladed hematite in quartz. Colloform banding in goethite. x 150 (White is pyrite)

seem almost isotropic. Due to orientation of the crystals extinction is seen wavy. It is found altered to and veined by goethite. Pseudomorphs of goethite preserving hematite crystal outlines were also seen. Some chalcopyrite grains were observed enclosed in hematite crystals.

5.3.3 Ilmenite was recognized as exsolution lamellae in the Küçükdere hematite occurrence (specimen 22a) and in magnetites of the basaltic rocks. Its distinct reflection pleochroism and pronounced anisotropy is characteristic.

5.3.4 Goethite this alteration product was identified with its greyish-blue colour and distinct reddish and orange brown internal reflections. It is found associated mainly with altered pyrite and chalcopyrite and to a lesser extent with marcasite, hematite and sphalerite. Replacement develops in cataclastic pyrite along fractures or grain boundaries. Sometimes it is found rimming idiomorphic pyrite crystals or developing along cleavage planes. In altered hematite specimens infiltration was recognized along quartz grain boundaries as an intergranular film. Cellular-filliform or colloidal banding and rhythmic encrustations around pyrite crystals are the most common colloidal textures (plate 5.3.4). A mottled covellite-goethite intergrowth develops after alteration of chalcopyrite while pyrite always gives goethite and less commonly lepidocrocite.

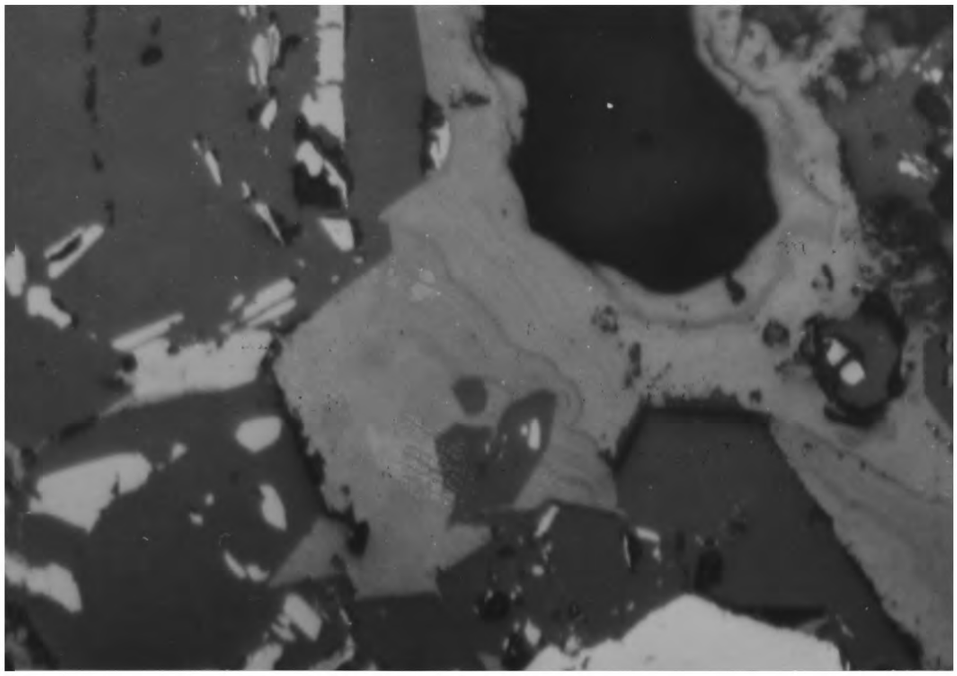

Plate 5.3.4 Bladed hematite in quartz. Colloform banding in goethite. x 300

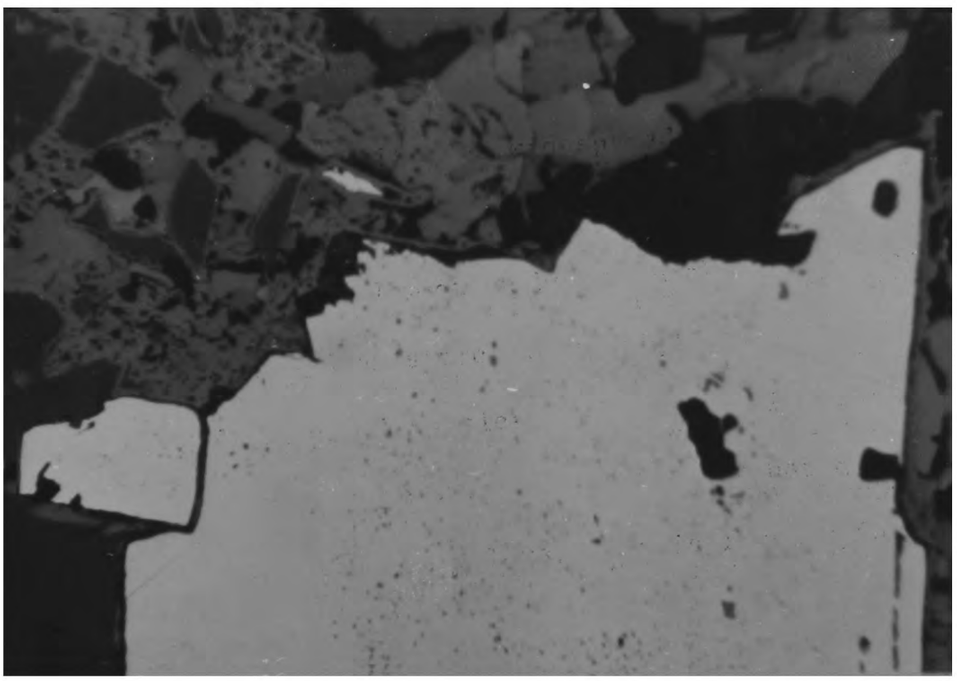

Plate 5.3.5 Lepidocrocite (light grey) adjacent to pyrite (white). x 150.

5.3.5 Lepidocrocite. In several specimens this mineral has been identified along goethite zones as discrete grains or granular aggregates. In plane polarized light its colour changes from bluish grey to dull brownish grey with rotation with a distinct bireflection. Polarization colours vary from bright emerald green to faint brownish grey. A granular lepidocrocite aggregate replacing pyrite is seen in plate 5.3.5 in which the former cubic pyrite crystal outline is rimmed by goethite with flame-like projections towards the enclosing quartz.

5.4 Sulphates

5.4.1 Baryte. Was not recognized with certainty in polished specimens but baryte crystals separated from hand specimens (21, 42,54,85,119) were X-rayed for confirmation. Specimens 21 and 119 were collected from baryte-rich veins along the Camideresi watercourse at 860m. altitude (5H) and Büyükgüre Dere at 225m. altitude (6D) respectively. Barytes in other specimens is found as a gangue mineral of polymetallic veins.

5.4.2 Anglesite. Despite the widespread alteration of galena in the studied area anglesite is less common than cerussite. It is identified in polished section by its dark brown-black colours, lack of bireflection and anisotropy, and rhythmic encrustation on galena. Usually it develops along cleavage planes and grain boundaries of galena together with cerussite and covellite. It has a transparent cloudy appearance under crossed polars. It is found veining and replacing sphalerite and fahlerz grains enclosed in sphalerite and infiltrates along quartz grain boundaries.

5.5. Carbonates

5.5.1 Cerussite Is found extensively as a weathering product of galena. The cleavage of galena is often preserved in early stages of development but in later advanced stages only relicts or kernels of galena can be seen. In the beginning of galena replacement a straight line of cerussite film along the cleavage plane or grain boundary of galena develops. Later replacement extends as spherulitic flower-like forms branching on both sides of a cleavage direction.

A secondary alteration mineral similar to cerussite was found to show excellent filliform textures (plates 5.5.1a,b).

Strong bireflection is easily observed in large granular areas. Anisotropy usually was obscured due to its transparency and it can be confused with carbonates but cerussite is always seen in grey colours with a slight greenish tint and has no striking cleavage contrary to calcite, dolomite, and siderite which tend to show idiomorphic forms.

5.5.2 Calcite, Dolomite, Ankerite and Siderite. Although dolomite is found as the common carbonate gangue in large amounts, calcite and siderite were recognised in single specimens, each from separate veins. Existence of these gangue carbonates was confirmed by XRD (see Fig. 5.5).

Although calcite shows dull-grey colours and has a low reflectivity, its strong bireflectance, fine-laminated twinning and rhombic cleavage (plate 5.5.2a) distinguish it from the other carbonates which tend to form as idiomorphic rhombohedral crystals. In specimen 133(6E) coarse granular calcite was found replaced by bornite grains which cut across a twin lamella of calcite.

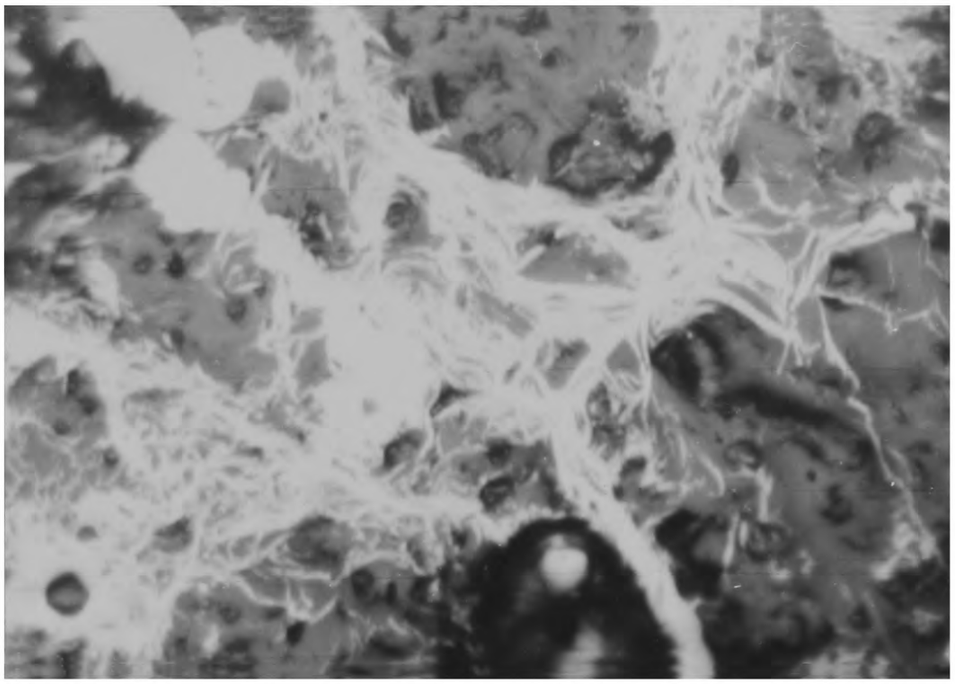

Plate 5.5.1a Galena (white) showing filliform texture. x 300

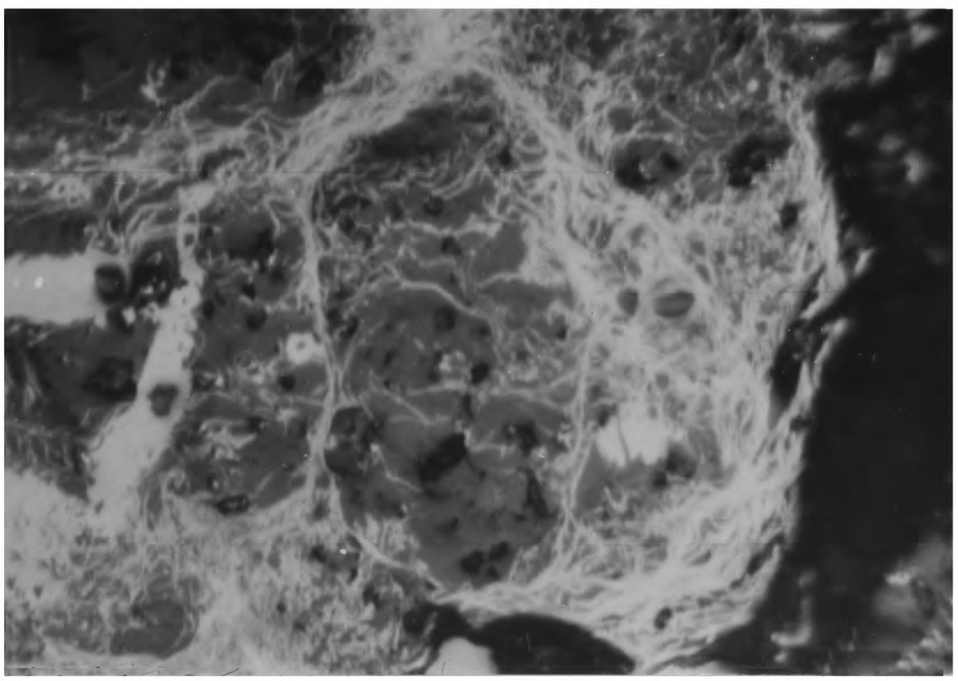

Plate 5.5.1b Galena (white) showing filliform texture. x 300

Siderite is seen as very well-preserved, zoned idiomorphic crystals (plates 5.5.2b-d) in specimen 50 (2A) and x-rayed for confirmation. Development of goethite along these crystals was also observed and in places they are seen as if being replaced by sphalerite and late-quartz cutting across the crystal outlines. The relationship with sphalerite is less decisive, i.e. sphalerite is veined and replaced by carbonates in the same specimen but this time the carbonate may be dolomite which has been confirmed by XRD. Siderite areas in this occurrence can be easily located due to reddish-brown colours in hand and polished specimens.

Ankerite has not been identified in the polished specimens but X-ray diffraction of reddish brown carbonate separated from specimen 47 and 127 has given ferroan dolomite (see Fig. 5.5).

5.5.3 Malachite and Azurite. These are not commonly found in polished specimens. Despite its low reflectivity, malachite is recognised with distinct bireflectance, light to dark brownish-grey-beige rotation colours in plane polarized light and purplish grey polarization colours if not masked by characteristic green internal reflections. In specimen 1 (2F) it was found in fibreous, radiating aggregates after chalcopyrite alteration.

Azurite is recognized occasionally with bluish internal reflections of a cloudy appearance.

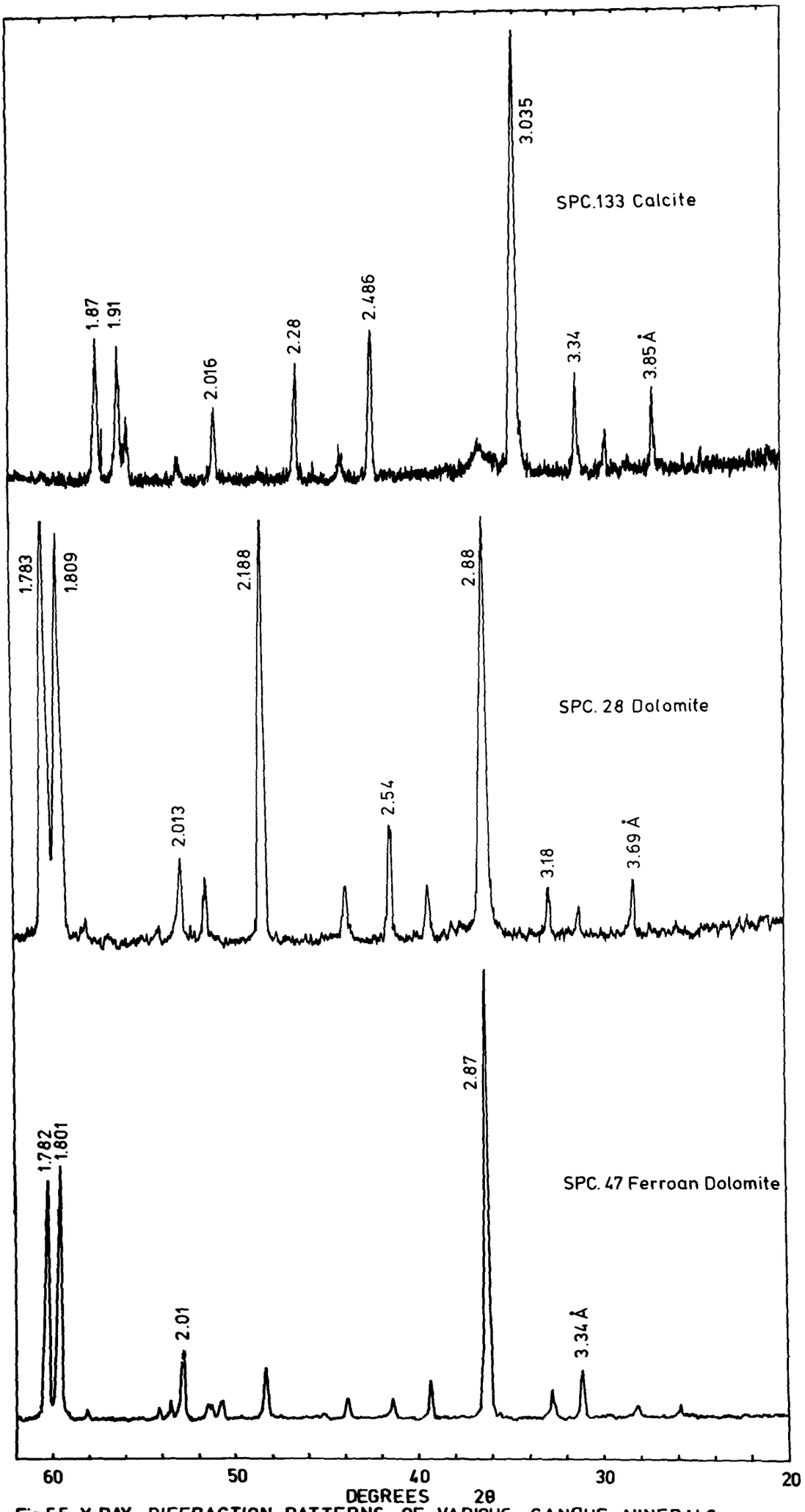

Fig 5.5 X-RAY DIFFRACTION PATTERNS OF VARIOUS GANGUE MINERALS

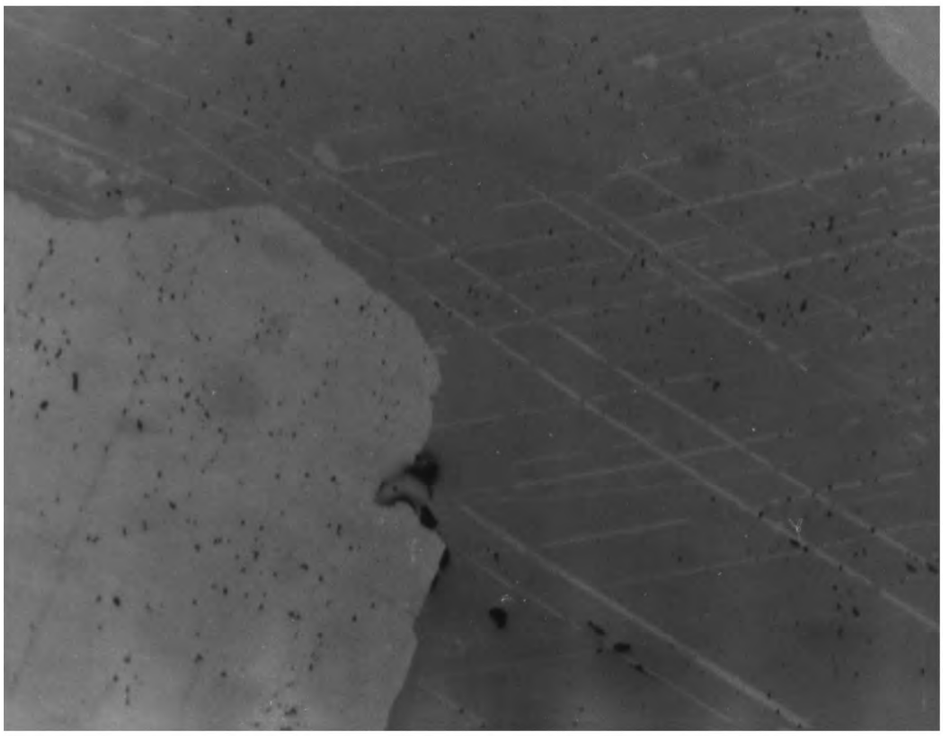

Plate 5.5.2a Calcite showing bireflection and lamellar twinning.

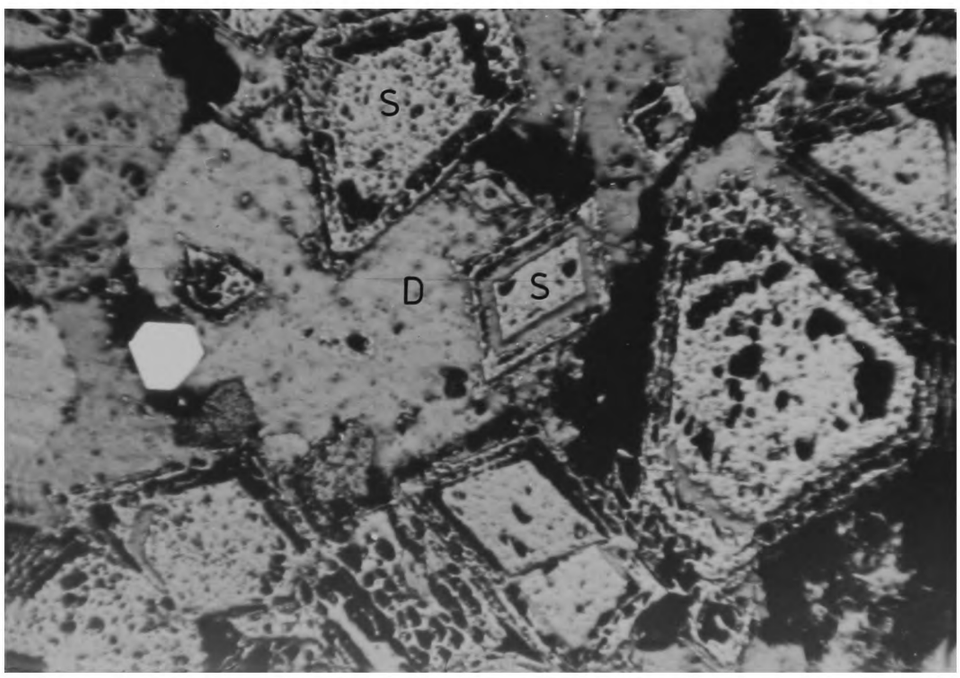

Plate 5.5.2b Siderite (S) replacing dolomite (D). Euhedral pyrite crystal. x 50

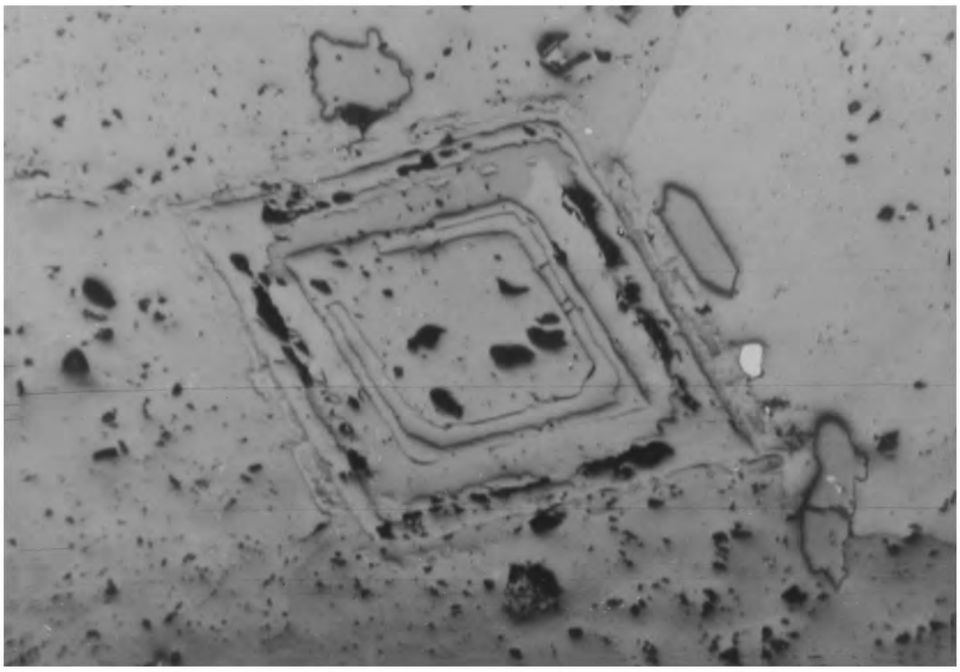

Plate 5.5.2c Detail from plate 5.52b. x 150

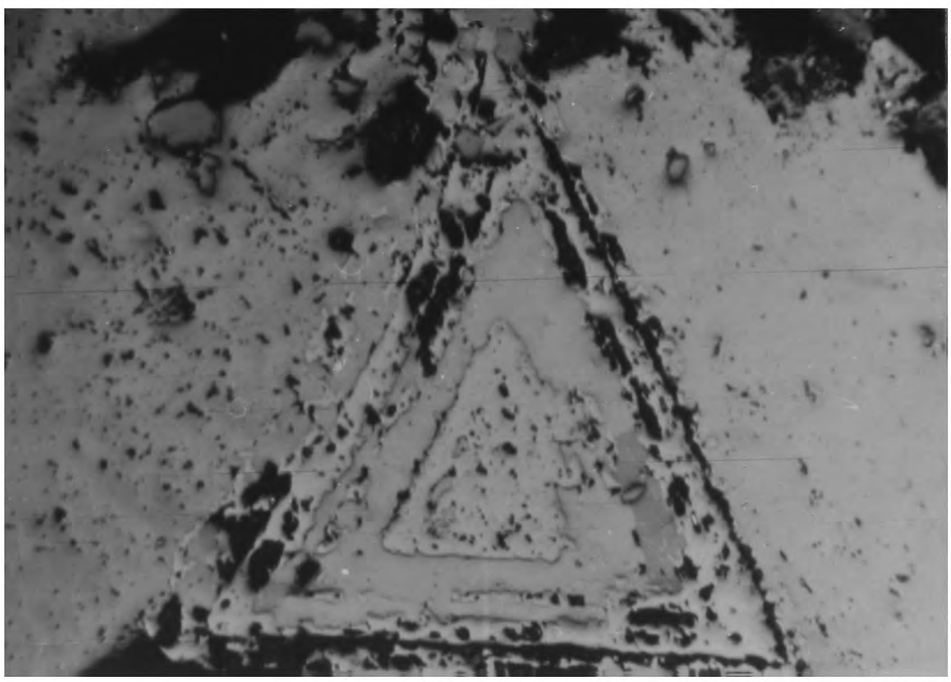

Plate 5.5.2d Detail from plate 5.5.2b. x 150

5.6 Sulphides:

5.6.1 Pyrite. By and large this is the most common and earliest formed sulphide mineral. It has been in almost every specimen studied. Three forms of pyrite can be identified in the mineralised area

1. Pyrite produced as a result of pyritization of country rock. This tends to form cubic crystals as small as 50 microns or less, disseminated in the altered rocks. Pyrite has been found, in some cases, embedded across crystal outlines.

2. Pyrite formed in the later stages of the vein mineralisation is found in small, euhedral to subhedral cubic crystals or triangular crystallites, forming stringers in sphalerite and tending to show slightly higher reflectivity and no relief, contrary to earlier ones. In places these crystallites smaller than 100 microns are seen stuck to a large, possibly early formed pyrite crystal. They develop along fractures in sphalerites in places marked by veining quartz, or healed fractures.

3. Early formed pyrites of the vein mineralisation shows hypautomorphic granular textures and is found as aggregates of interlocked crystals or grains as well as with individual cubic, octahedral and pentagonal crystal faces. Aggregates formed by three large grains about 700 by 1400 microns in size may consist of individual crystals as small as 50 microns on the triple junction or enclosed in large grains (plate 5.6.1a). Aggregates formed by 600 by 700 microns sized grains are the most common. On the other hand cubic, single or interlocked

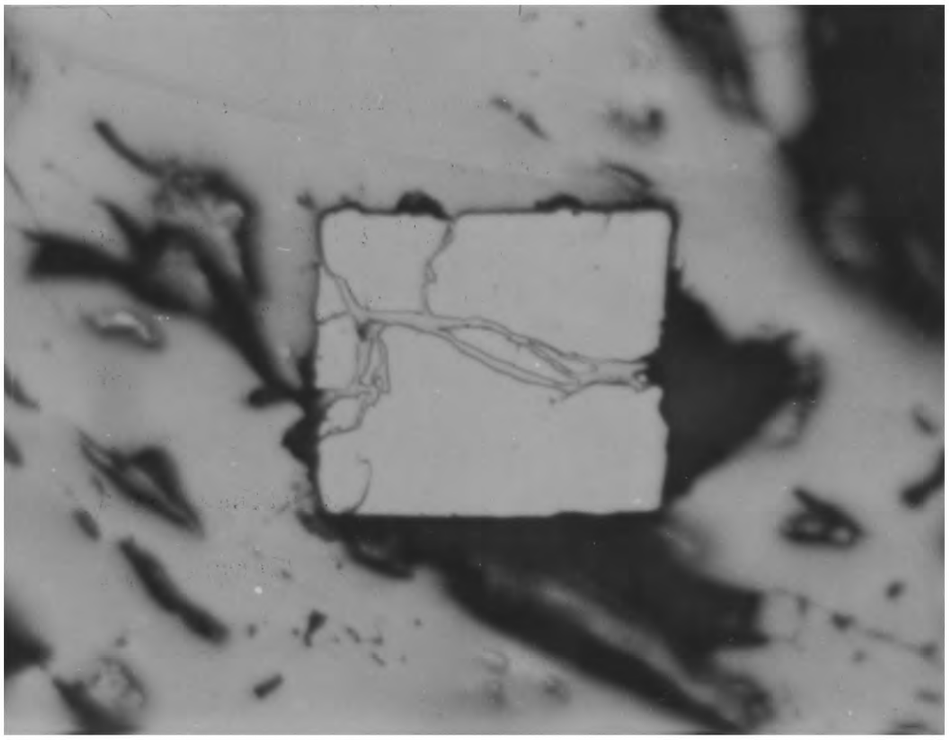

Plate 5.6.1a Fractured euhedral pyrite with chalcopyrite veinlets. x 300

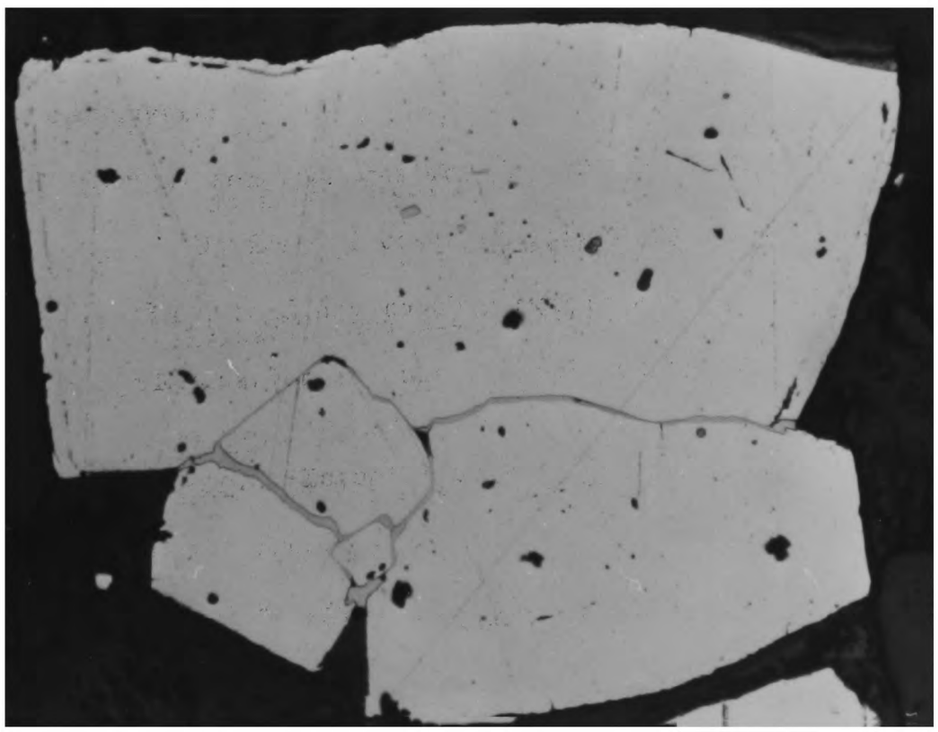

Plate 5.6.1b Chalcopyrite veinlets between pyrite grains. x 150

crystals showing striations parallel to 010 and 001 faces and varying in size from 0.5 to 2.5cm were collected from the vein wall of specimen 41. Tugal (1969) reported the grain sizes of Lahanos pyrites varying from 1 to 125 microns with an average of 100 microns.

Zoning of the idiomorphic cubic or pentagonal crystals is quite common and is usually brought out by gangue minerals, minute chalcopyrite inclusions or limonite alterations. Individual crystals are found in cubic, skeletal and polygonal subrounded forms which are usually enclosed in chalcopyrite and show good examples of cataclasis with matching walls (plate 5.6.1b). These fractures and grain boundaries of aggregates are usually filled and replaced by chalcopyrite which in turn may be replaced by galena, digenite and fahlerz selectively. Sphalerites tend to replace early euhedral crystals making embayments.

Parting and replacement along cleavage planes are not uncommon. Poikilitic, sieve-like grains or porphyroblasts may form due to quartz and chalcopyrite replacement. Either tarnishing in air or etching with $KMnO_3$+HCl solution was found to be sufficient to bring out grain boundaries. No form of colloidal pyrite was seen.

There is a tendency to show strong anisotropy with greenish blue - brownish polarisation colours in striated crystals.

5.6.2 Marcasite. Is not a very common constituent of the veins. It occurs in insignificant amounts and is found only in several grains enclosed in chalcopyrite, as blade-like, cubic and lath-shaped 50 by 250

microns size crystals. Average size of the grains varies from 45 to 90 microns although several 100 microns size cubic, twinned crystals were observed. Lamellar areas of marcasite in cubic pyrite crystals or partially replaced areas of pyrite aggregates indicates the transformation after pyrite. It is easily distinguished from pyrite with bright emerald green, strong polarisation colours and its whitish yellow colour with a greenish tint. Reflection pleochroism is also noticeable. In most of the aikinite-bearing specimens marcasite was found associated and close to these sulphosalt areas (see plate 5.7.2b).

5.6.3 Sphalerite. Is the dominant ore mineral of the polymetallic veins and is found in subhedral to xenomorphic grains or corroded, replaced forms with a coarse granular texture. Its grain size averages about 300 to 500 microns, with a range from less than 50 microns to 800 microns. Cleavage and lamellar twinning were brought out by etching with HNO_3 or $KMnO_3$+HCl solution (plates 5.6.3a). The width of lamellae varies from 30 microns or less to over 700 microns. Displacements were observed across the twin lamellae. Usually it was transparent in disc wafers prepared for fluid inclusion study but several specimens were found to be completely opaque even in disc wafers as thin as 0.5mm. In these disc wafers colours vary from whitish yellow, to honey, dark brown and black. It shows faint reddish brown internal reflections in reflected light.

Brecciation is common and brecciated grains are seen healed by late stage quartz (plate 5.6.3b). Almost all of the sphalerites

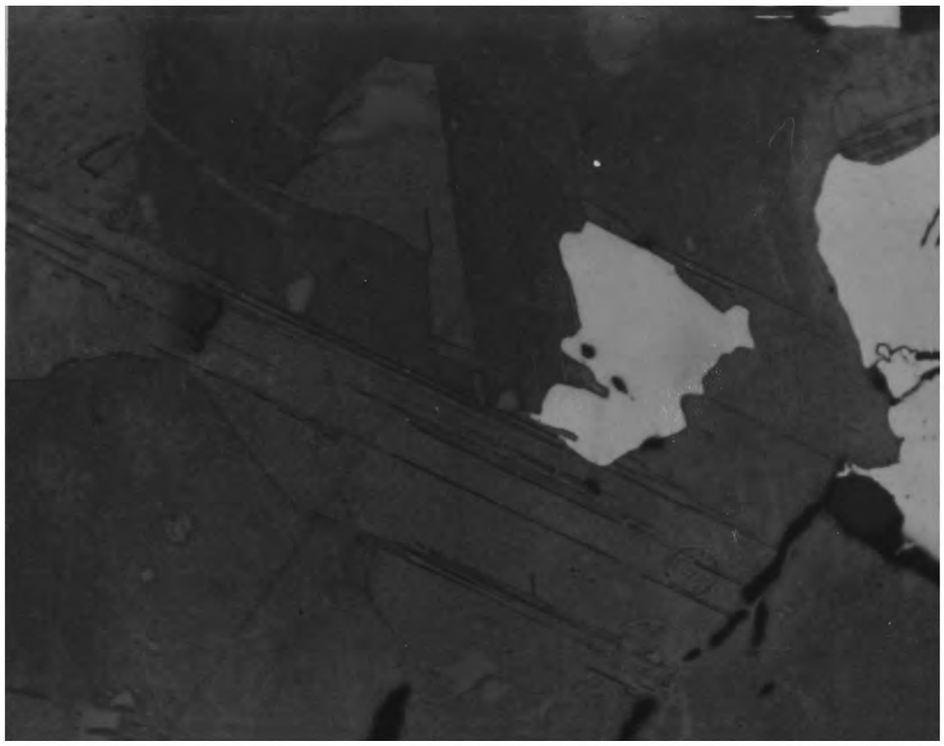

Plate 5.6.3a Lamellar twinning in sphalerite revealed by etching (HNO_3). Unetched galena (white) and pyrite. x 150

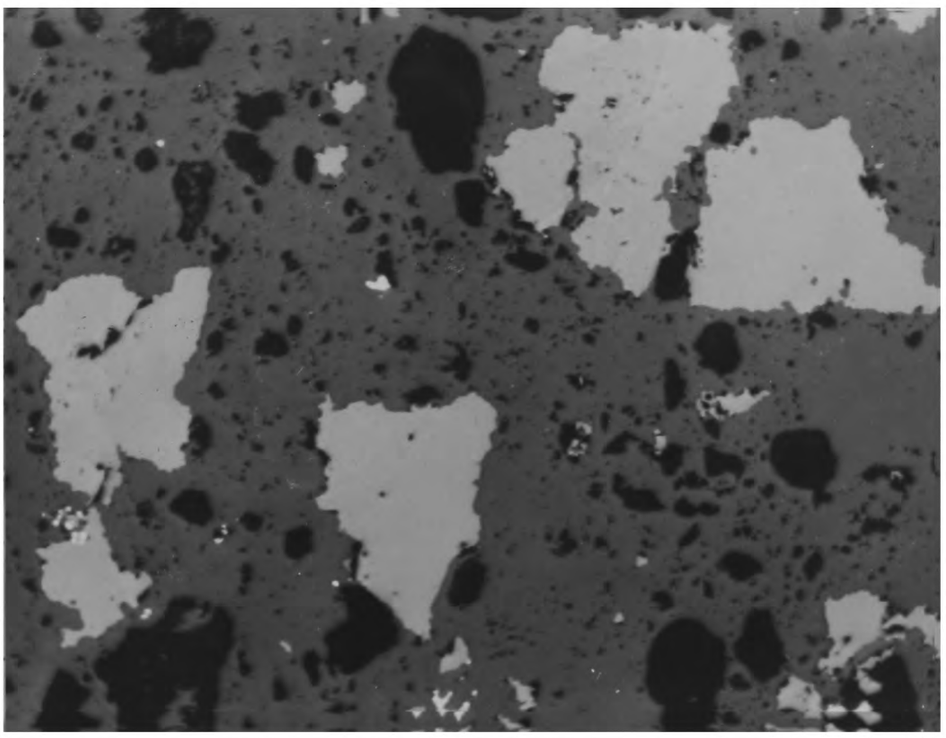

Plate 5.6.3b Late stage quartz replacing sphalerite (light grey) x 85

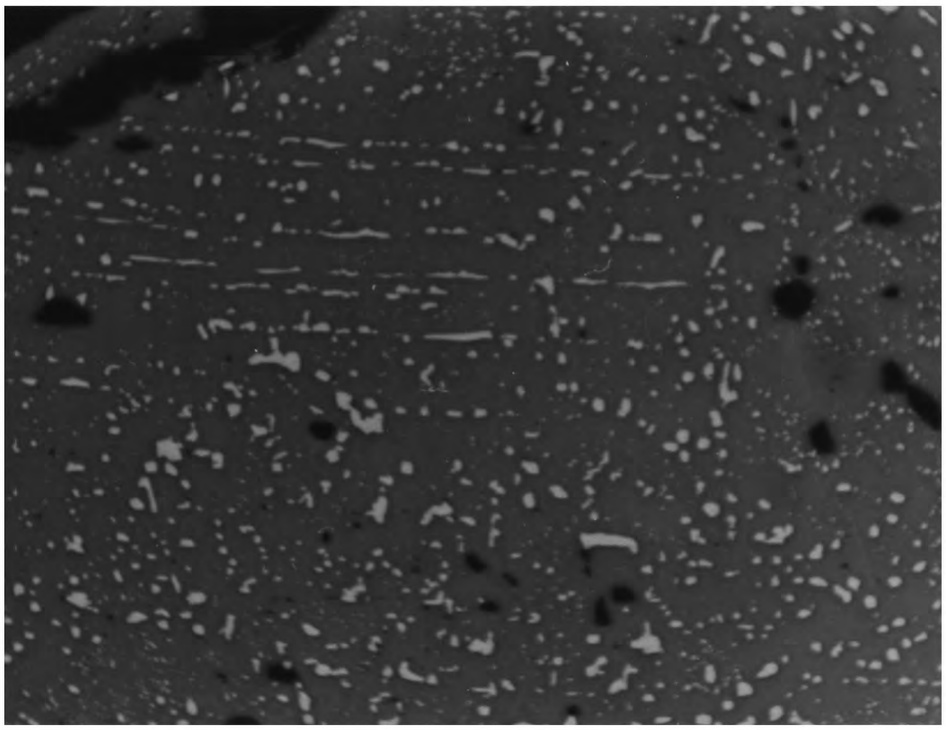

Plate 5.6.3c Chalcopyrite exsolution in sphalerite . 150

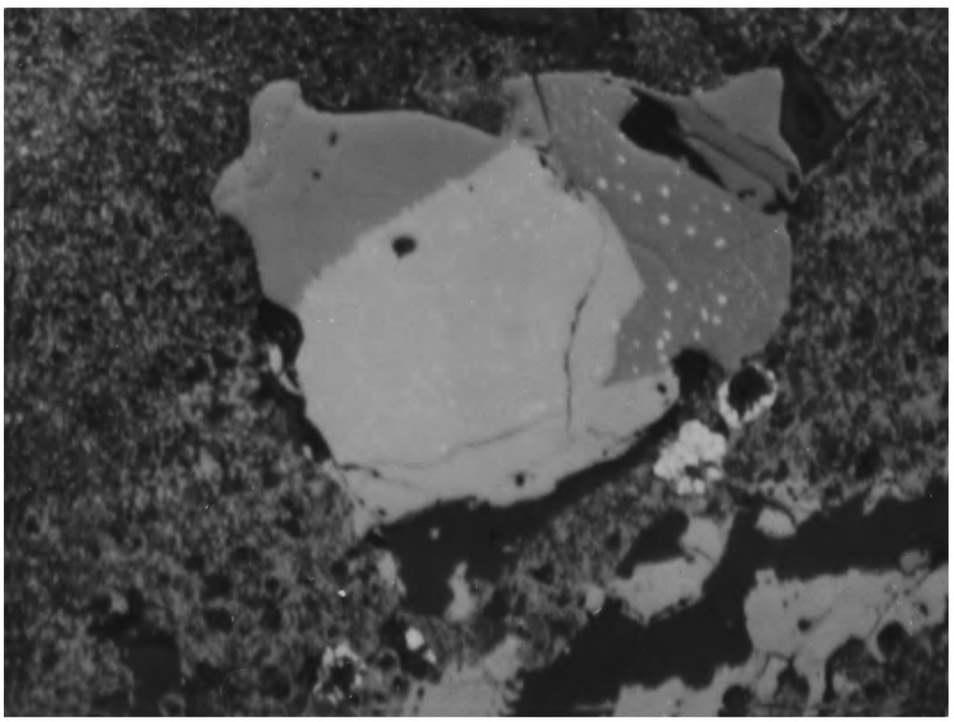

Plate 5.6.3d Sphalerite with exsolution chalcopyrite has been replaced by fahlerz in which the chalcopyrite exsolution bodies remained unaltered. x 300

Plate 5.6.3e Sphalerite(dark grey)-galena (light grey) relationship. x 1200

Plate 5.6.3f Chalcopyrite replacing sphalerite along twin boundaries revealed by etching. x 150

studied in polished sections have ovoid chalcopyrite exsolution blebs, emulsion type inclusions, exsolution lamellae, stringers and segregation veins, and several specimens show coarse unmixing (plate 5.6.3c). Sometimes the inclusions are found lined along grain boundaries or oriented along crystallographic directions. Coarse chalcopyrite inclusions are selectively replaced by either galena or fahlerz (plate 5.6.3d) or they can unite to form a ragged structure similar to that illustrated by Ramdohr (1969, Fig. 365, p.507). In some cases chalcopyrite penetrates along the cleavage and twin planes of sphalerite, in places forming islands (plate 5.6.3f). It is extensively replaced by galena and contains abundant idiomorphic or skeletal quartz crystals (plate 5.6.3e). Replacement of quartz by sphalerite may result in atoll and ring textures. It is quite often seen veined by chalcopyrite, galena, fahlerz, limonite, cerussite or dolomite, covellite and quartz. Deposition overlapping with galena was seen in some specimens.

5.6.4 Galena. Is found in allotriomorphic, poikiloblastic forms in spaces of quartz matrix or replacement forms interstitial to sphalerite. Usually it replaces cataclastic pyrite, chalcopyrite and quartz. It is seen also as ovoid inclusions in chalcopyrite. Ring and atoll textures form when quartz crystals enclosed in galena are replaced centrally. It selectively replaces pyrite crystals enclosed in chalcopyrite. Tiny patches of fahlerz are also common. In specimen 53 which has betekhtinite in large amounts digenite, decomposed from betekhtinite, replaces galena extensively forming atoll textures (plate 5.6.9a). In places

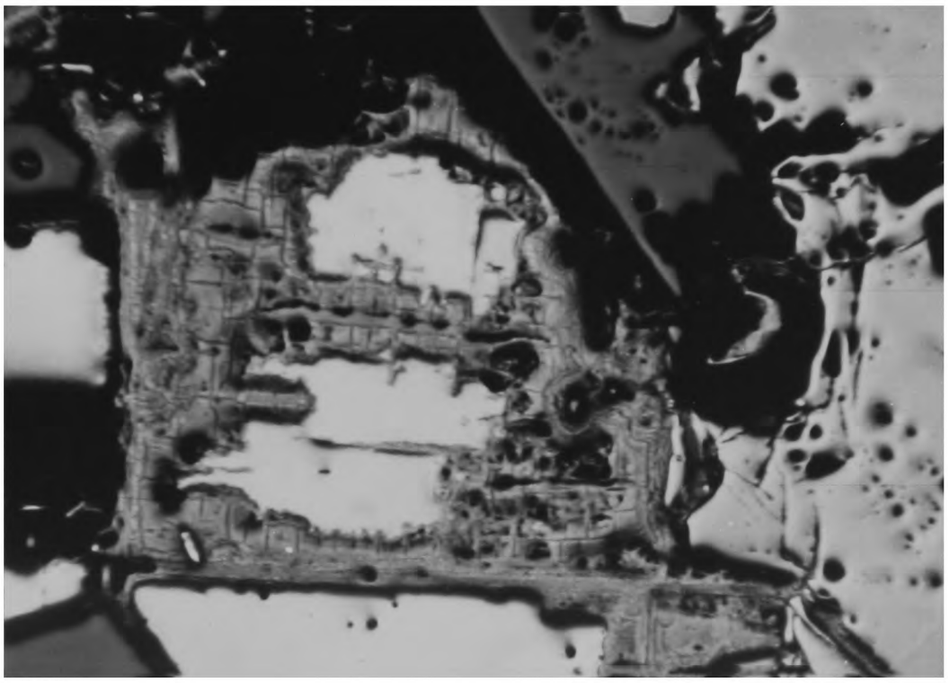

Plate 5.6.4a Galena (white) residuals in cerussite-covellite intergrowth. x 50

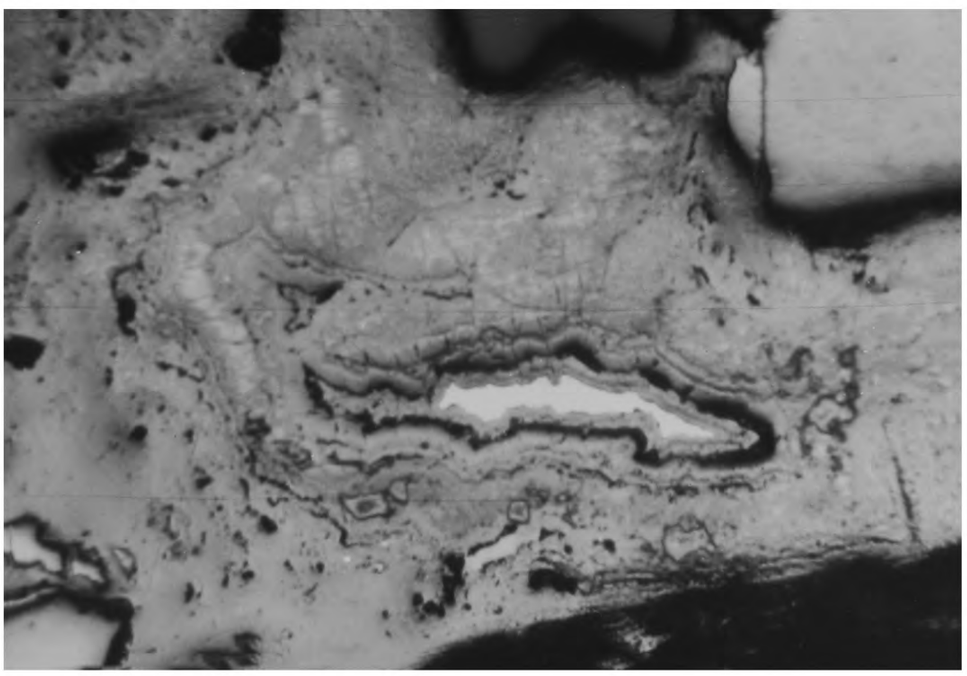

Plate 5.6.4b Similar to 5.6.4a. x 150

bornite and betekhtinite were found replacing allotriomorphic galena along cleavage planes and grain boundaries. Myrmekitic intergrowths with digenite and bornite are seen in specimen 53 as well (plate 5.6.10d).

In many specimens cerussite and covellite develop extensively at the expense of galena finally leaving a galena kernel in the centre (plates 5.6.4a,b).

5.6.5 Chalcopyrite. In pyrite-rich veins forms the major constituent after pyrite. Narrow, 1 to 10cm thick, massive chalcopyrite veins were also seen during mapping work. Throughout the studied specimens it replaces early formed pyrites extensively. Etching with HNO_3 has revealed its lamellar and coarse, granular nature (plate 5.6.5a), although allotriomorphic forms filling the open spaces between quartz crystals are not uncommon.

It shows reddish, orange, brown-greenish blue polarisation colours.

Chalcopyrite replacement develops along grain boundaries of pyrite aggregates with triple junctions (plate 5.6.5b), or along the fractures of cataclastic pyrite crystals, finally leaving tiny pyrite relics, of micron size, hardly visible (plate 5.6.5c). This replacement may result in atoll textures as well (plates 5.6.5d,e).* Chalcopyrite, replacing cataclastic pyrite along fractures, may be replaced by digenite or fahlerz. Its inclusions in pyrite or second generation sphalerite inclusions may form poikilitic textures. It is selectively replaced by galena and fahlerz.

* These plates have been omitted.

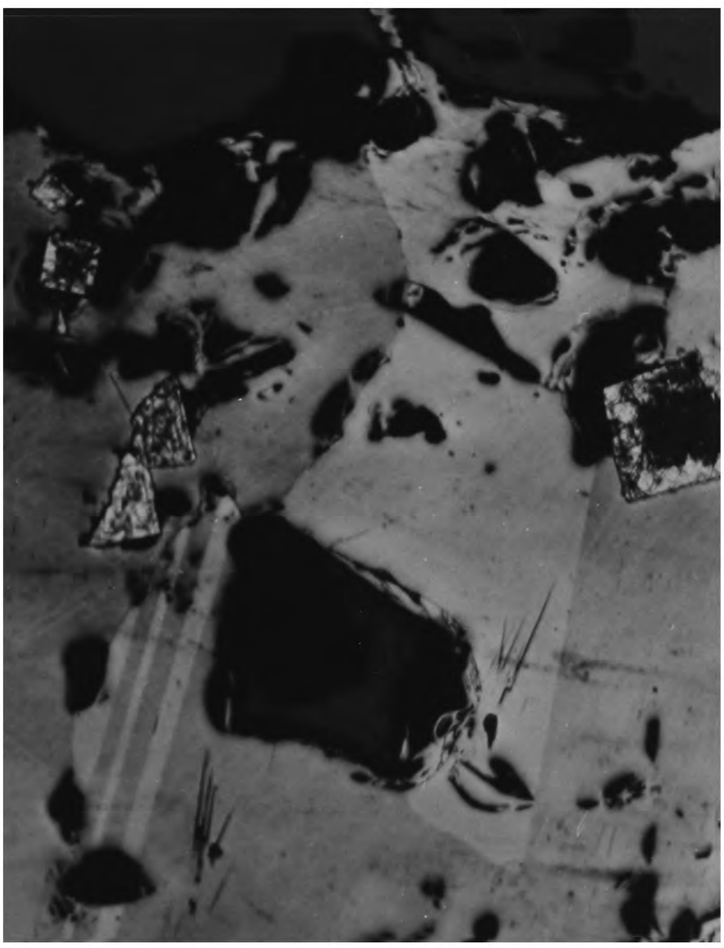

Plate 5.6.5a Twinning in chalcopyrite revealed by etching.
Euhedral pyrite. x 85

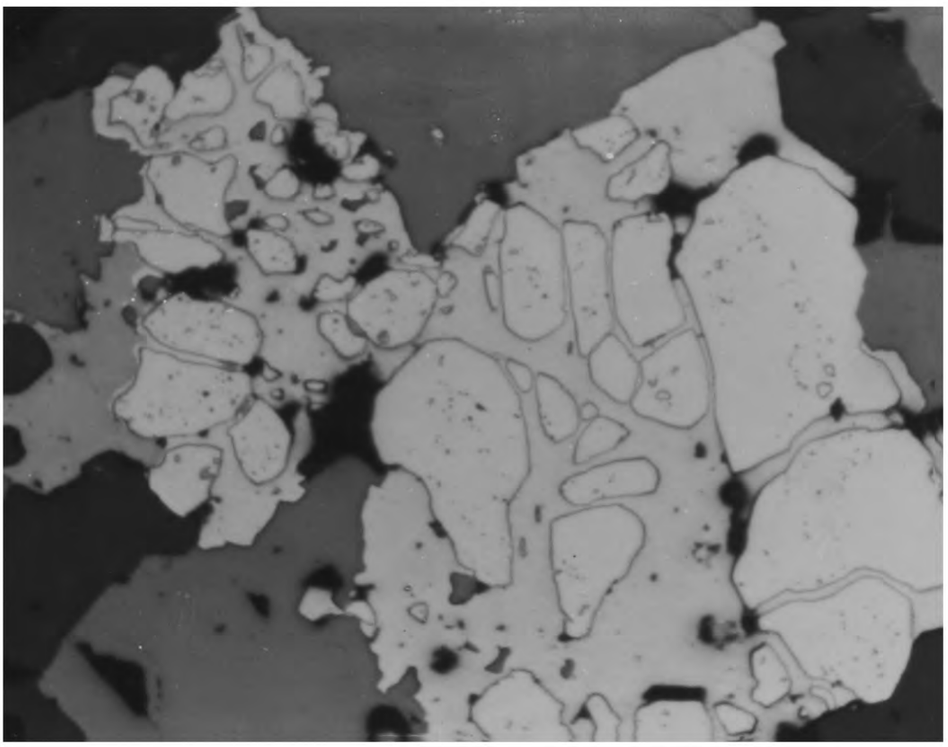

Plate 5.6.5b Chalcopyrite replacing pyrite. x 150

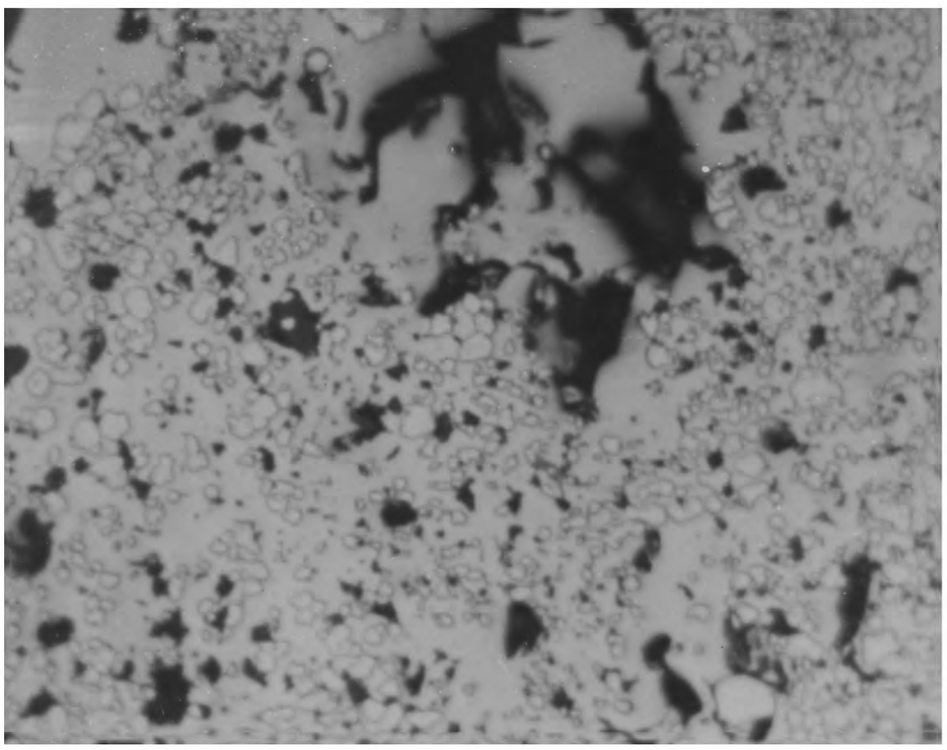

Plate 5.6.5c More advanced stage of replacement, cf. 5.6.5b. x 300

Alteration produces goethite and covellite which is commonly found veining and replacing chalcopyrite.

Paragenetically most of the chalcopyrite grains appear to be formed later than sphalerite but some embayments and large grains of chalcopyrite are found intergrown with sphalerite in mutual boundary textures which may indicate contemporaneity.

5.6.6. Bornite. Was found in only 3 specimens as a major constituent although in several specimens it was seen replacing chalcopyrite inclusions in sphalerite and pyrite.

The first specimen (133) contains pure bornite grains replaced by digenite with xenormorphic forms. Etching with $KMNO_3$+HCl solution produced excellent mosaic texture similar to that illustrated in "Bild Kartei Der Erzmikroskopi", 1960, sheet No. 0152) in which oriented lines continue in digenite areas as well (plate 5.6.6a).

It replaces some galena grains centrally. Grains containing bornite in a dolomite matrix in specimen 133 average in size 150 microns within a range 50 to 300 microns. The second specimen (104) was collected from a vein with unknown attitude (4F). Bornite is extensively replaced by chalcopyrite, in which bornite is seen as irregular patches or replacement relics. Chalcopyrite shows rim replacement with exsolution flames in places along the margins of bornite grains (plate 5.6.6b) or is seen exsolving from bornite with spindle-like Lamellae along the crystallographic planes of bornite.

In the third specimen (53), in which bornite and especially betekhtinite are found in significant amounts, bornite is found rimming,

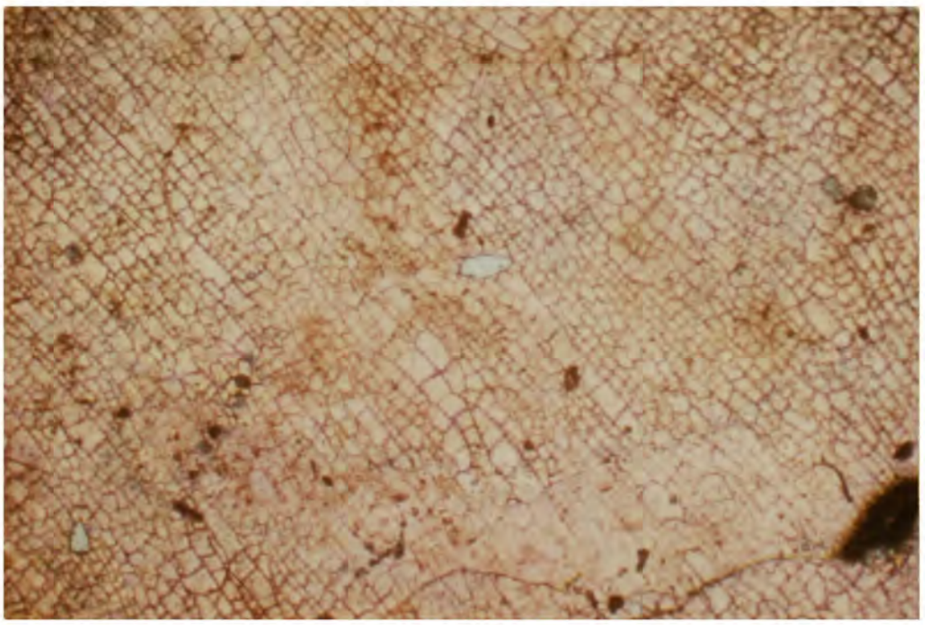

Plate 5.6.6a Mosaic texture in bornite revealed by etching. x 150
Light blue is digenite.

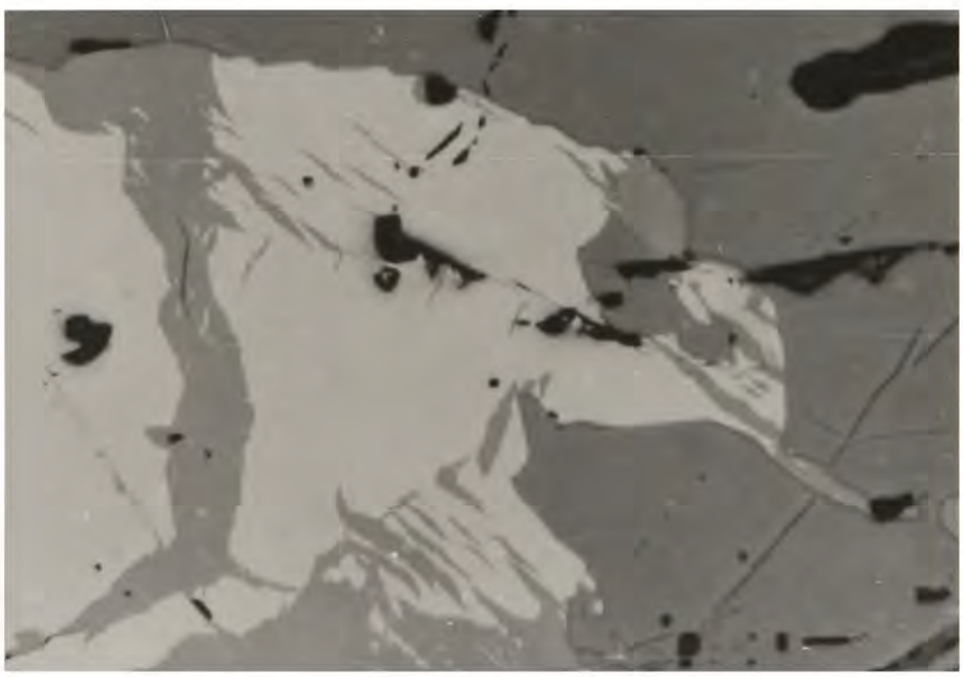

Plate 5.6.6b Chalcopyrite-bornite intergrowth. 150

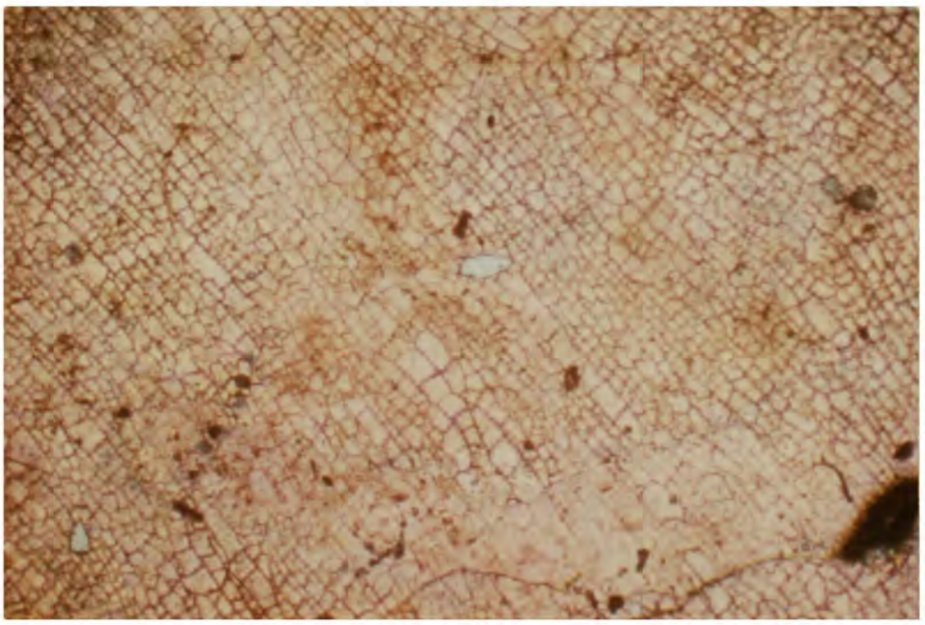

Plate 5.6.6a Mosaic texture in bornite revealed by etching. x 150
Light blue is digenite.

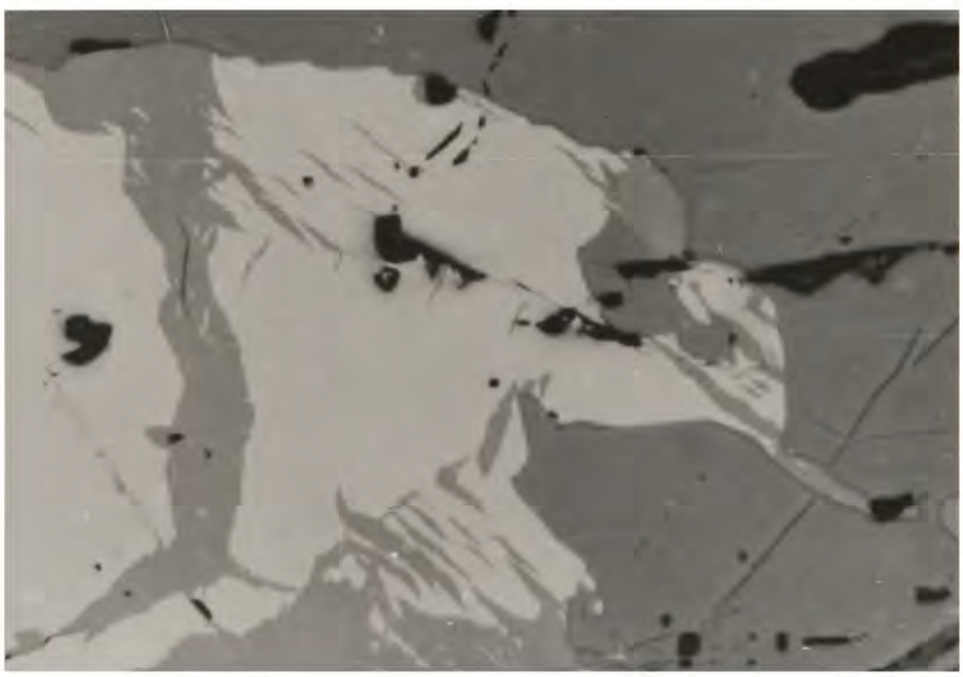

Plate 5.6.6b Chalcopyrite-bornite intergrowth. 150

veining and replacing betekhtinite producing rim or atoll textures or exsolution flames in chalcopyrite grains.

5.6.7 Idaite. Has been recognized in specimens from two different localities. The first specimen was collected from a vein in the Kuloglu locality (6A) and the second was found in the Akköy Mine specimens. Due to exsolving chalcopyrite and covellite replacement, X-ray runs were not made but probe analysis confirmed the idaite composition. The existence of idaite in these sulphide occurrences was first described by the writer although idaite has been recognised by other workers in several occurrences along the Eastern Black Sea Ore Province.

Idaite is identified by its strong reflection pleochroism and vivid, greenish polarisation colours by which it is easily distinguished from bornite. The colour changes from reddish orange to purplish grey under plane polarized light due to strong reflection pleochroism. Chalcopyrite exsolution lamellae are arranged along crystallographic planes showing a lattice texture in idaite grains (plates 5.6.7a,b). Idaite areas, in between the lamellae, may originally have been bornite. It shows mutual boundary relationship with chalcopyrite in places although idaite segregation veinlets with no exsolution lamellae were observed cutting through chalcopyrite. It also tends to replace chalcopyrite, e.g., chalcopyrite veins in sphalerite or along the chalcopyrite-sphalerite boundary.

The second form of idaite is different from the first described above. This pinkish-purple coloured form shows distinct reflection pleochroism with bright polarisation colour and is often replaced by

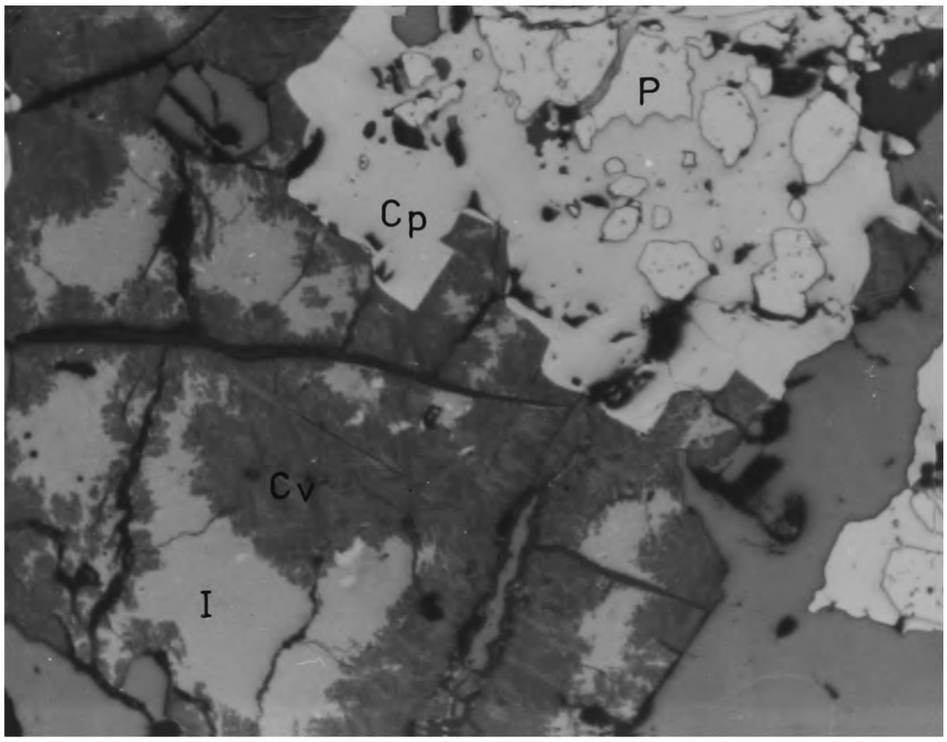

Plate 5.6.7a Idaite(I), covellite(Cv), chalcopyrite(Cp) and pyrite (P) relationship. x 300

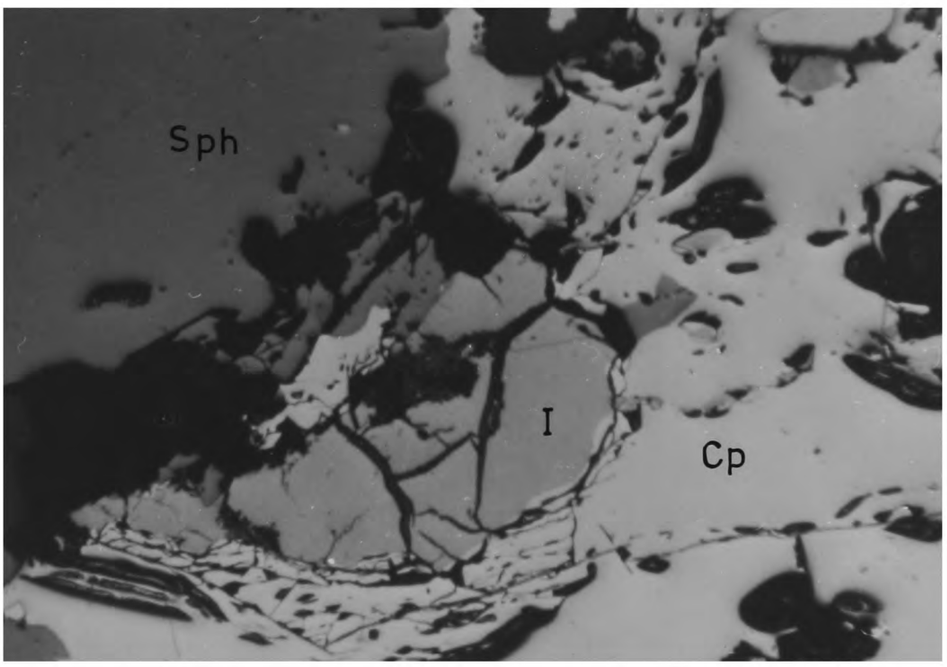

Plate 5.6.7b Idaite (I), chalcopyrite(Cp) and sphalerite(Sph) relationship. x 150

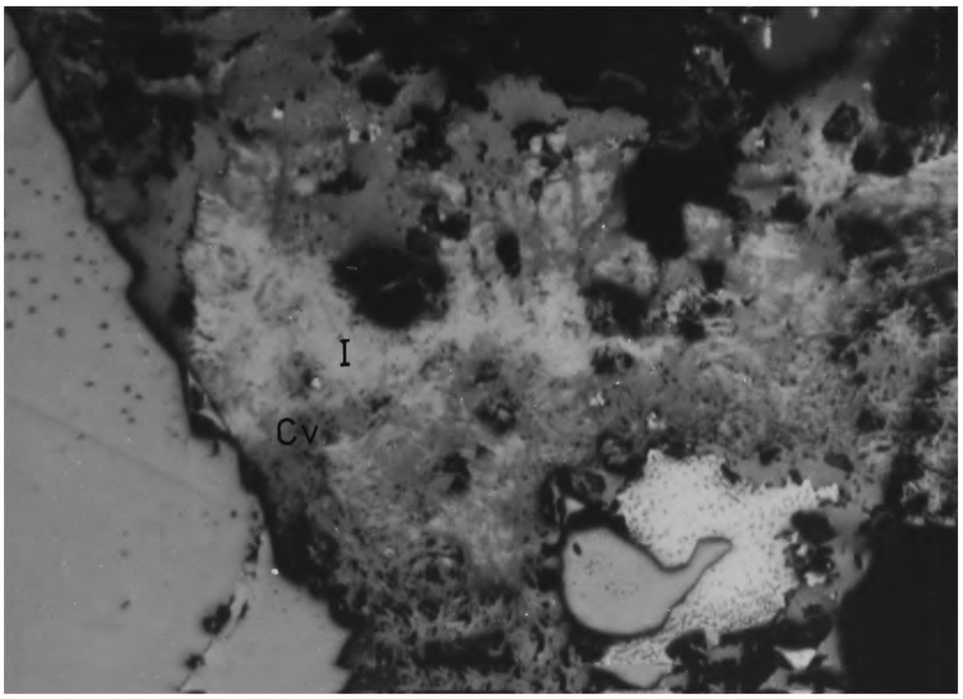

Plate 5.6.7c Idaite (I)-covellite(Cv) relation. x 150

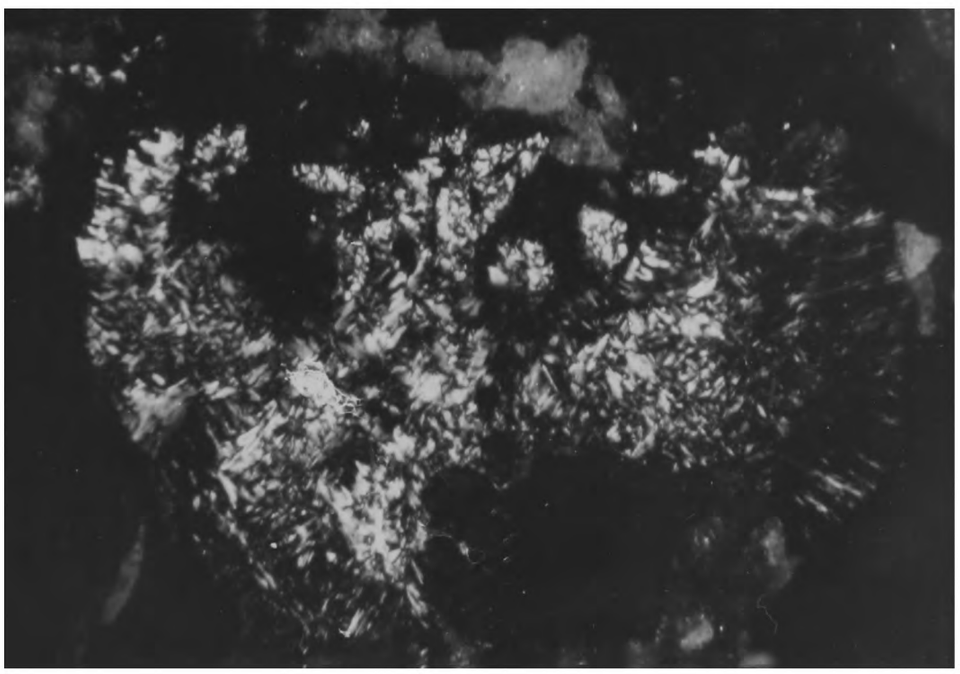

Plate 5.6.7d Same as 5.6.7c, x-polars. x 150

covellite keeping its lamellae orientation. Usually it occurs as islands in covellite (plates 5.6.7c,d). Microprobe analysis of the specimen 81 from Kuloglu locality (6A) near Darikoy gave the following result:

Cu	56.07
Fe	9.87
S	33.08
Total	99.04

formula derived from this composition is $Cu_{4.96}\ Fe_{1.0}\ S_{5.80}$ which is similar to the original formula given by Frenzel (1959a,b). On the other hand Levy (1967) gave the formula Cu_3FeS_4 based on microprobe analyses.

5.6.8 Covellite. Two common forms develop either with cerussite and anglesite from dissolving galena (see plates 5.6.5a,b) or with goethite showing intergrowth-like mottled texture due to weathering of chalcopyrite and pyrite. Several examples were seen veining and replacing sphalerite grains, in some cases leaving chalcopyrite inclusions behind. It may replace chalcopyrite along grain boundaries forming colloidal bands, or extensively with characteristic lattice structure (plates 5.6.8a,b) and it develops together with veining digenite showing cellular cementation textures in chalcopyrite. Sometimes a covellite band occurs developing outwards around fahlerz grains enclosed in sphalerite.

Covellite with its deep blue colours, distinct pleochroism and pronounced anisotropy was found to be one of the easiest minerals to recognise.

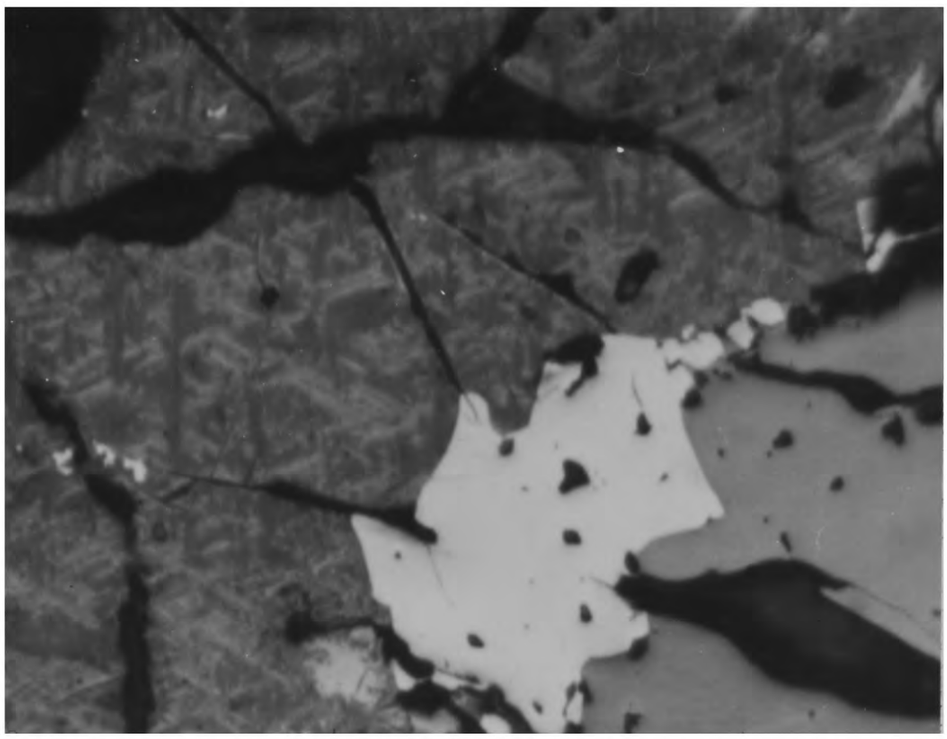

Plate 5.6.8a Lattice texture covellite with chalcopyrite and sphalerite. x 300

Plate 5.6.8b Lattice texture covellite with chalcopyrite and sphalerite, x-polars. x 300

5.6.9 Digenite is not common as a major constituent of the vein minerals. It shows sky-blue colours and is isotropic. In several specimens it is seen veining chalcopyrite irregularly, showing a cementation structure similar to Ramdohr's Fig. 199 (1969). In specimen 133 it replaces bornite as xenomorphic patches resulting in small grain pseudomorphs. Its association with small amounts of covellite when bornite grains are being replaced leaves some suspicion that digenite may also be "permanent blue" covellite. (Ramdohr, 1969 p.668) states that "... small content of Cu_2S lowers the dispersion and causes anomaly. This is also indicated by the fact that "permanent blue" covellite is often produced, e.g., through the unmixing decomposition of neodigenite". Digenite has only been found in large quantities coarsely intergrown with galena as the decomposition product of betekhtinite in specimen 53 showing atoll textures mutual boundaries and lamellar development (plates 5.6.9a,b). It is also found selectively replacing galena cores of quartz crystals.

5.6.10 Betekhtinite has not previously, to the writer's knowledge, been reported, either from this area or anywhere else in Turkey. It has been found only in one location as a major constituent, but several veins contain very small amounts.

In polished section betekhtinite has a grey to creamy colour, with a pinkish tint, and appears creamy brown against bornite. Its colours appear relatively bright when associated with bornite and digenite and dull when associated with digenite exsolution lamellae. It has a weak reflection pleochroism which varies with the orientation

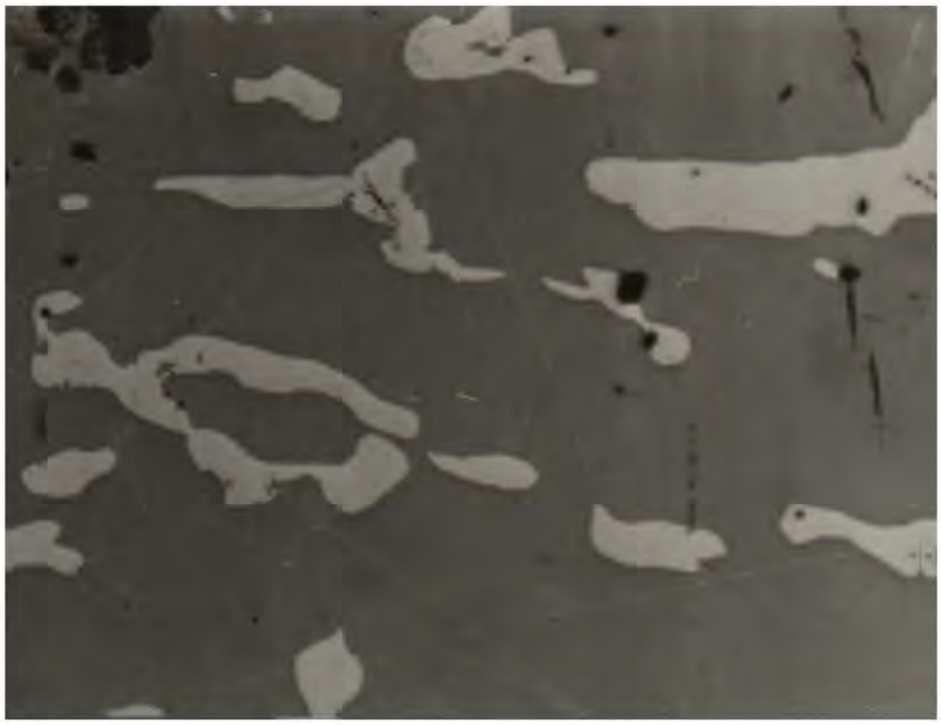

Plate 5.6.9a Galena (white) residuals in digenite. x 150

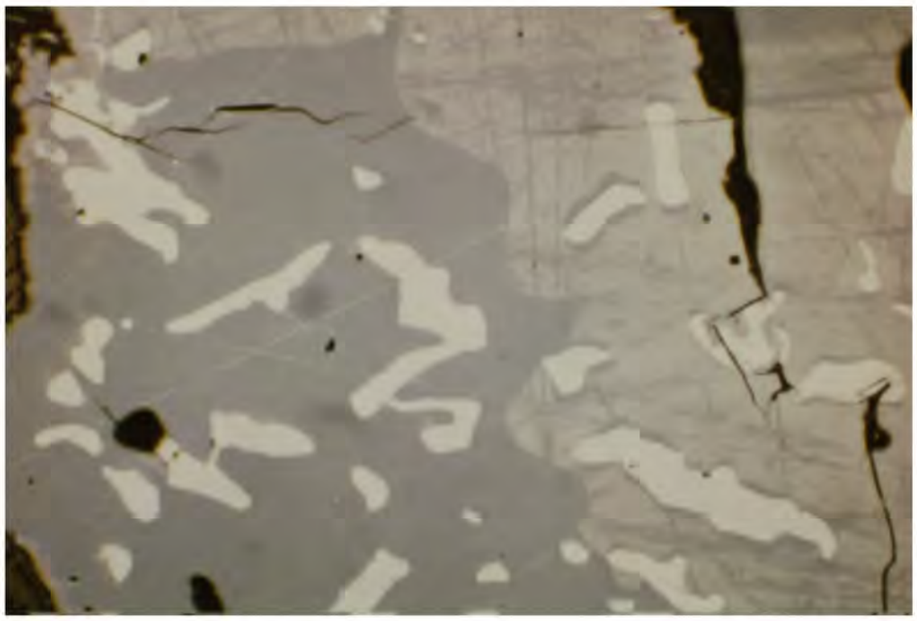

Plate 5.6.9b Mutual boundary texture between betekhtinite (grey) and digenite (blue) with galena residuals.

of the grains (plate 5.6.10a). With exactly crossed polars, polarisation colours are dull red or blue depending on the orientation whereas with slightly uncrossed polars orange, blue, yellow-green and purple colours may be seen.

Cleavage is seen only when the mineral contains digenite exsolution lamellae and is oriented in three directions in the betekhtinite.

It is found associated with galena, bornite, digenite, fahlerz, pyrite, quartz, dolomite and cerussite. Bornite was seen either forming rings around a quartz enclosure (plate 5.6.10b) or in cracks or, in many cases, rimming betekhtinite (plate 5.6.10c). Myrmekitic intergrowths of galena-bornite are also enclosed in betekhtinite as well as rare galena-digenite intergrowths (plate 5.6.10d). This myrmekitic texture, which is almost identical to that described by Schüller and Wohlman (1955) and Matsukama (1971), has been suggested as representing decomposition or breakdown of betekhtinite. Bornite and digenite were also seen veining betekhtinite.

Betekhtinite replaces galena along quartz-galena boundaries or cleavage planes of galena and is itself replaced by digenite along fractures or the crystal outlines of quartz inclusions. Some galena patches with irregular outlines were observed cutting across the digenite exsolution lamellae in betekhtinite. In places betekhtinite replaces quartz and is seen intergrown with cerussite possibly altered from pre-existing galena before betekhtinite deposition.

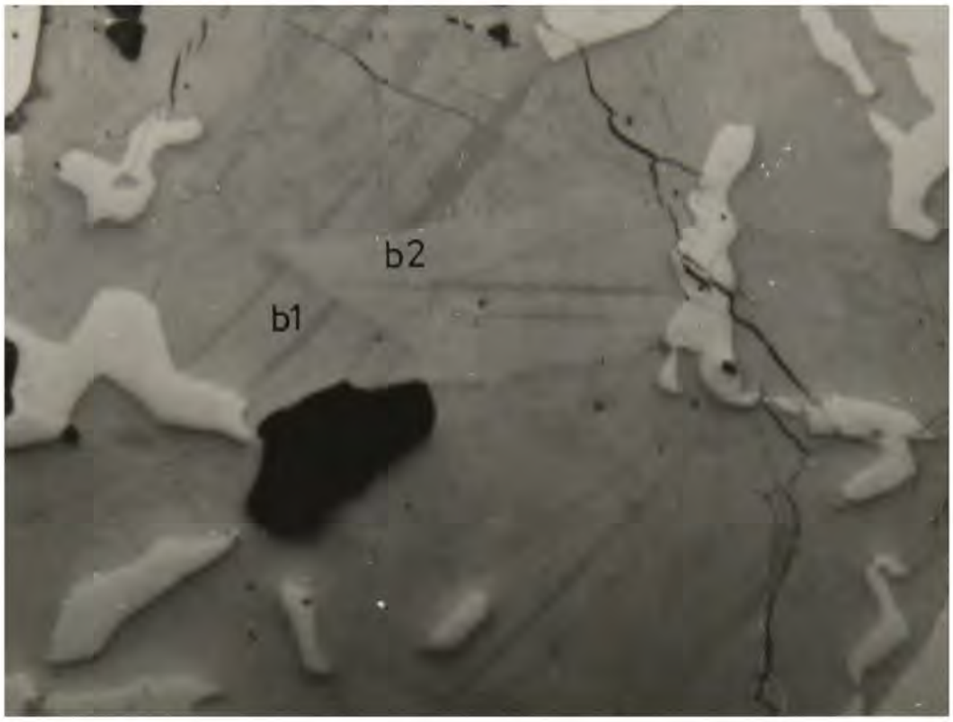

Plate 5.6.10a Reflection pleochroism revealed by betekhtinite grains (b1,b2) in different orientation. x 150

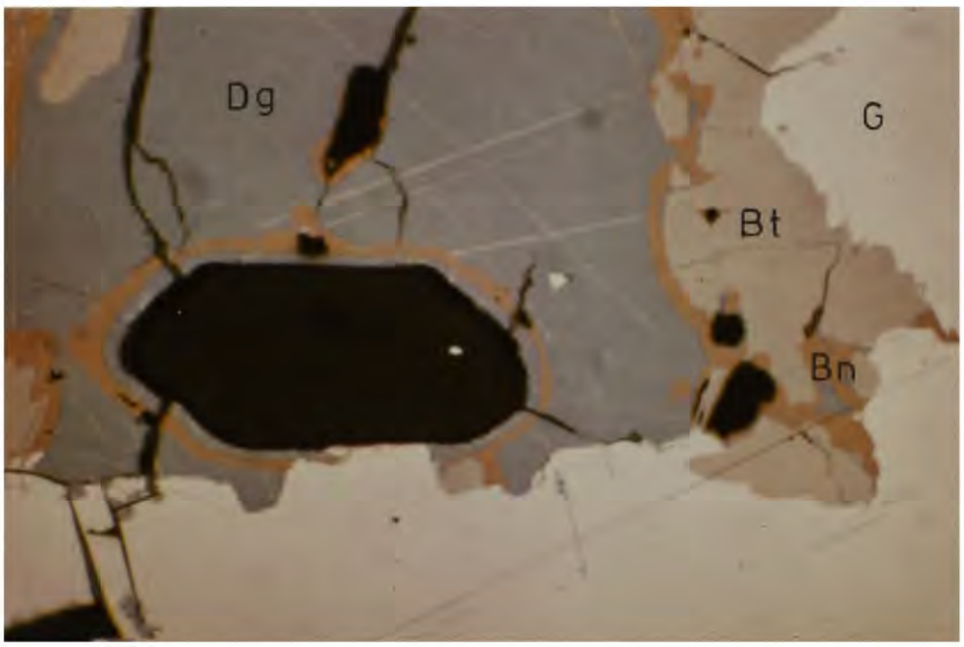

Plate 5.6.10b Galena (G), betekhtinite (Bt), bornite (Bn) digenite(Dg) and euhedral quartz (black) relationship. x 150

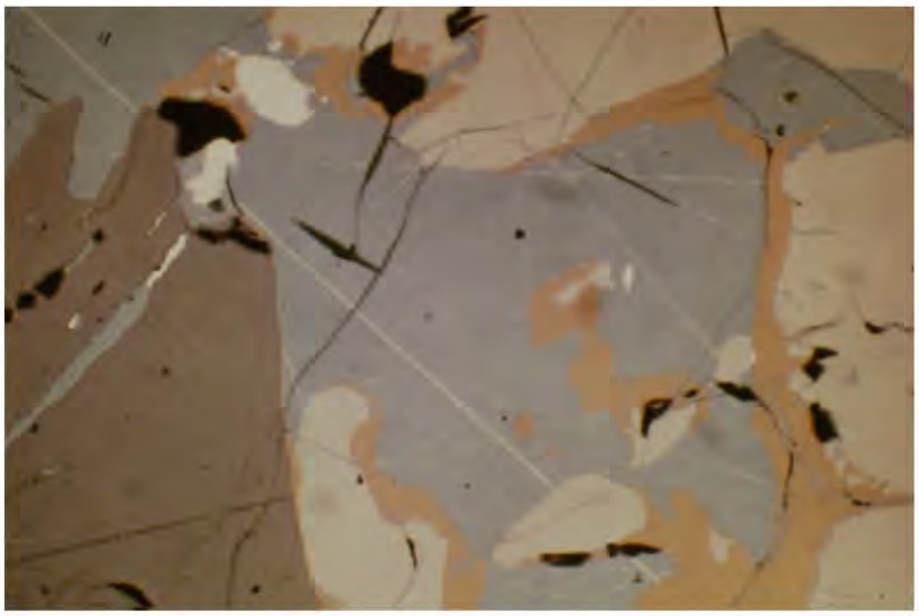

Plate 5.6.10c Similar to 5.6.10b. Sphalerite at the left of picture. x 150

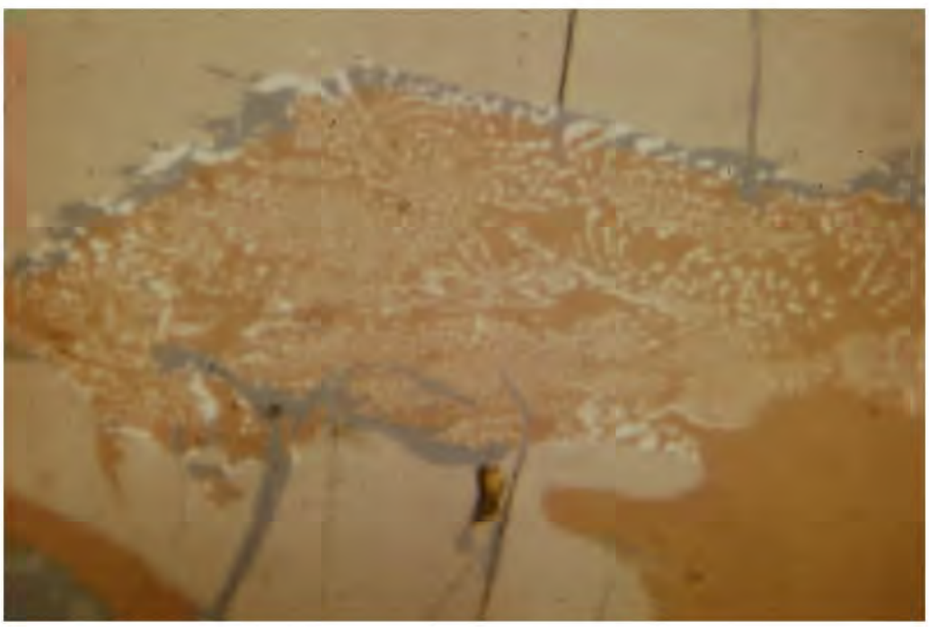

Plate 5.6.10d Myrmekitic texture between galena-bornite and galena-digenite in betekhtinite. x 675

Polishing hardness checks were made against tennantite and bornite, when in contact with these minerals, and it was found to be harder than bornite. The Vickers microhardness was found to vary from 148.9 to 182 Kg/mm^2 with a standard load of 100 p (= 100gm). Most of the measurements fall within the range of 150 Kg/mm^2. Tsonev et al (1970) have found the microhardness of betekhtinite as 210-230 Kg/mm^2 with a Hohneman type microhardness meter at a loading of 5gm.

The optical properties of the Bulancak Betekhtinite are similar to those of betekhtinite from Mansfeld and Dzhezkazgan but the intensity of anisotropy varies. It has rather smooth and rounded outlines in contrast to the prismatic, acicular habit reported from the Mansfeld and Dzhezkazgan deposits. The dominant minerals assemblages show almost similar characteristics to the Mt. Lyell occurrences (Markham and Otteman, 1968). Previously reported occurrences were confused with chalcocite and wittichenite and it has similar colour and reflectivity characteristics to enargite.

A hand specimen supplied to the writer by Ethem Acar from Harköy Mine, Tirebolu was found to contain betekhtinite which is confirmed by probe analysis given in table 5.10.2. Previously only enargite has been

described from Harköy Mine (Acar, 1974), possibly due to misidentification of betekhtinite.

5.7 Sulphosalts:

5.7.1 Fahlerz. This name was adopted from Ramdohr's original book "Die Erzmineralien und Ihre Verwachsungen" to describe Tetrahedrite-Tennantite minerals. Ramdohr (1969) describes "the commonest fahlore (CuSb-fahlore, often with Zn)" as olive brown with dirty colour tone and the pure CuAs-fahlore as greenish with a light blue tone, which becomes more distinct with greater silver contents". It is now well documented in the literature that there is almost no pure tetrahedrite and tennantite (Springer, 1969) and even in a single fahlerz crystal or grain there is often compositional zoning and heterogeneity (Smirnov et al, 1972; Yui, 1972; and plate 5.7.1a of this study) and positive correlation of Ag content with Sb (Hall, 1971; Yui, op. cit.).

For these reasons, colour is not a dependable property to differentiate tetrahedrite from tennantite. Also, colour appreciation in plane polarized light can vary appreciably depending on the enclosing or neighbouring minerals. Htein's study (1973, Fig. 1b) demonstrates that the dominant wavelength for the tetrahedrite-tennantite minerals (together with several other sulphosalts, such as boulangerite) changes within a 50nm. range whereas for the rest of the known ore minerals this range is less than 20nm. As will be explained later, previously reported tetrahedrite from the area was As-rich which is confirmed by probe analaysis. Therefore the writer abandoned any attempt at differentiation based on the colours of these minerals during the ore microscopy study.

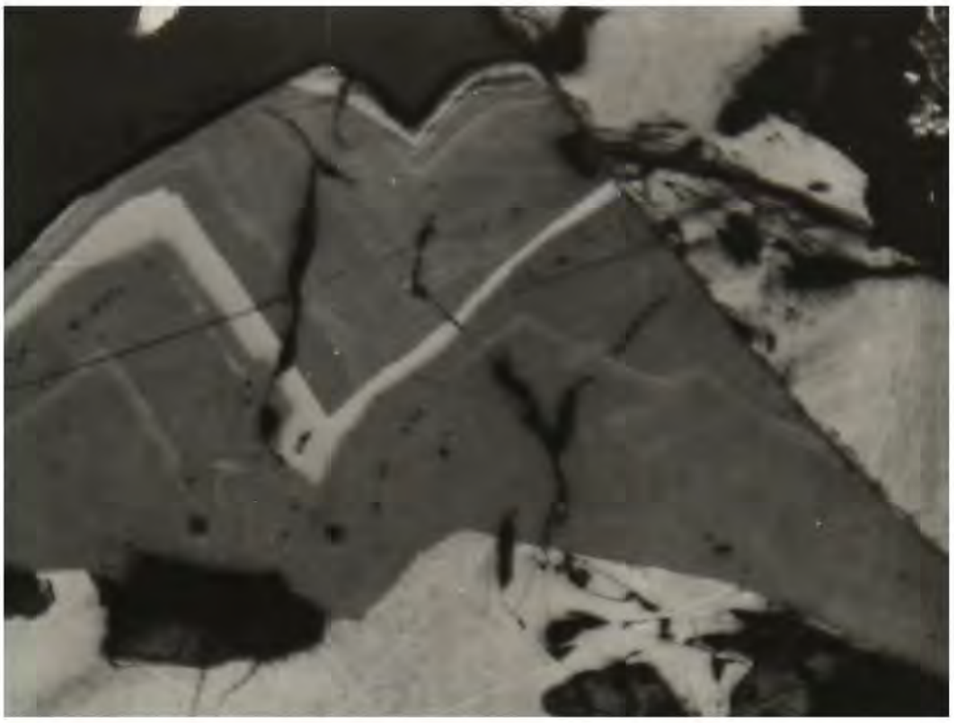

Plate 5.7.1a Zoning in fahlerz revealed by etching. x 150

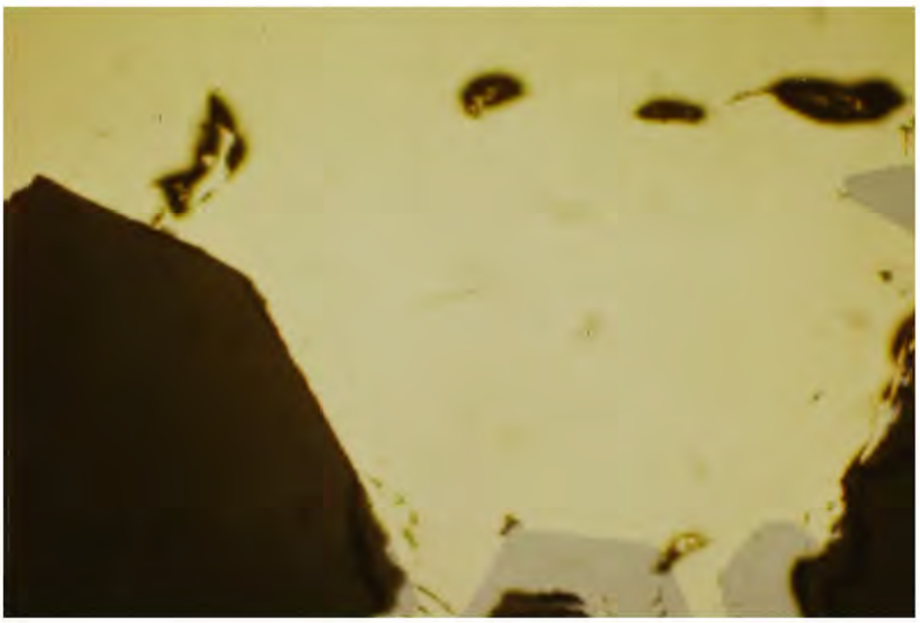

Plate 5.7.1b Fahlerz (bluish grey) replacing euhedral quartz in chalcopyrite. x 150

In the studied specimens fahlerz minerals show two distinct replacement examples. In the first instance it replaces chalcopyrite extensively especially coarse chalcopyrite inclusions and enclosures in sphalerite or idiomorphic quartz crystals enclosed in or projecting into the chalcopyrite areas (plate 5.7.1b). In one sphalerite specimen with chalcopyrite inclusions fahlerz was found replacing sphalerite but leaving chalcopyrite inclusions behind (see plate 5.6.3d). Sometimes replacement develops along the grain boundaries of allotriomorphic chalcopyrite with quartz. Pseudomorphs of hexagonal sections or prismatic projection of quartz crystals are also common. They sometimes replace chalcopyrite veins cutting across sphalerite or pyrite grains or occur as tiny replacement patches in galena.

Etching with HNO_3 was not found to be effective in many specimens but in specimen 98b has revealed excellent zoning believed to be due to heterogeneity of the grain but it was too late to do probe analysis of these zones (plate 5.7.1a). Displacement was also seen along a fracture across a zonation band in the same grain.

Tennantites were found to be more common than tetrahedrites since the probe analysis of 8 fahlerz specimens have given only 2 Sb-rich tetrahedrite compositions. Previously only tetrahedrite was reported from the area.

5.7.2 Aikinite. During the examination of the polished specimens, a greyish white coloured, anisotropic sulphosalt mineral was observed in several specimens collected from 5 different veins. This was later identified as aikinite by means of probe analysis (table 5.10.4) and confirmed by the X-ray Diffraction method (Table 5.9.4).

Minerals identified as aikinite have compositions which are not in agreement with the theoretical aikinite composition. They are suggested to be members of the aikinite-bismuthinite solid solution series and are close to the aikinite end-member.

The colour of aikinite is hardly distinguishable from that of galena. When enclosed in sphalerite and pyrite, aikinite shows greyish or dull white colours and weak anisotropy. In contrast, when associated with chalcopyrite and digenite, it appears pinkish and much brighter with a strong anisotropy. Reflection pleochroism is distinct (plate 5.7.2a). Cleavage is in one direction and is distinctive when digenite and covellite replace the mineral along cleavage planes. Elongated, lath-like,prismatic forms and xenomorphic grains are common.

Under crossed polars polarisation colours change from deep bright blue to bright yellowish-green or yellowish-brown depending on the orientation of the grains and possibly on the bismuth content.

It shows a coarse polycrystalline texture with grains oriented parallel to the prismatic direction and was seen cutting across a twin lamellae of chalcopyrite.

Aikinite grains are commonly found enclosed in chalcopyrite as rounded or elongated forms or as an island in digenite which is enclosed in chalcopyrite (plate 5.7.2b). Digenite always replaces aikinite along cleavage planes or occurs as patches throughout the aikinite grains. Tennantite (confirmed with probe analysis) was found replacing, veining or surrounding aikinite (plates 5.7.2a). It is usually found in association with pyrite and marcasite. It replaces pyrite along grain boundaries and cleavage planes or the replacement may develop from

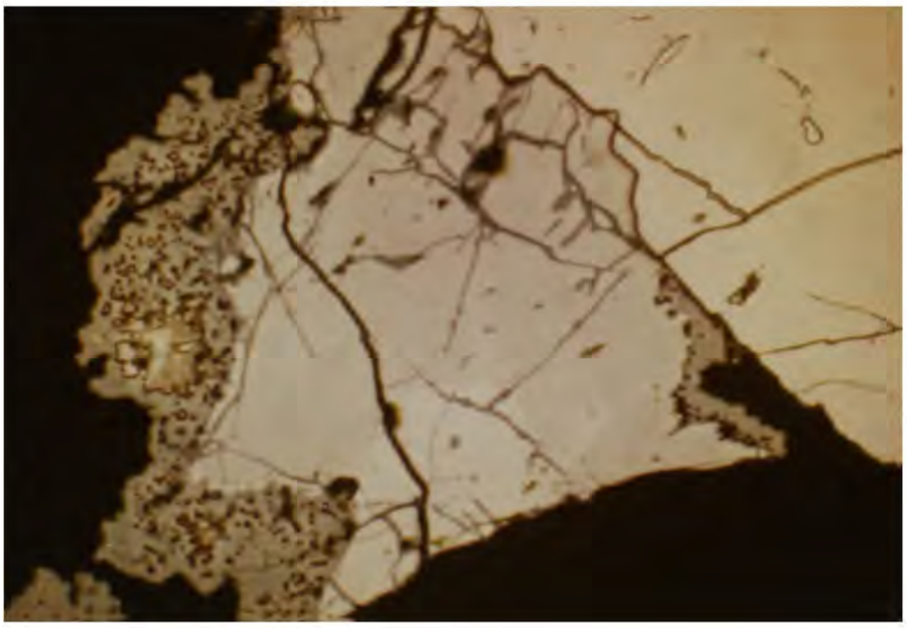

Plate 5.7.2a Reflection pleochroism in aikinite (white and grey white). Fahlerz (greenish grey) and pyrite. x 150

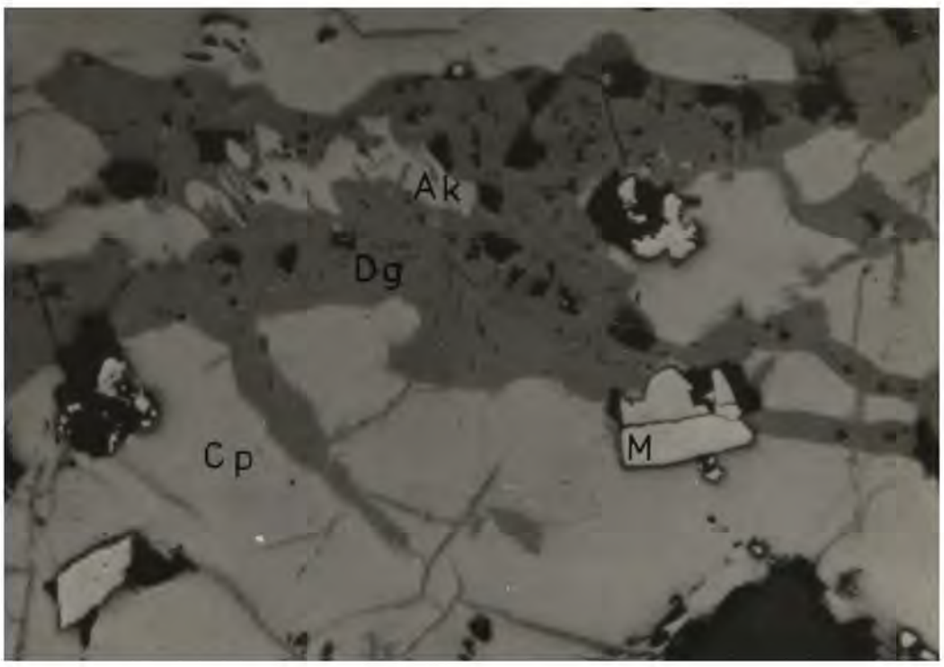

Plate 5.7.2b Aikinite (Ak), digenite(Dg), Chalcopyrite (Cp) and maracasite (M) relationship.

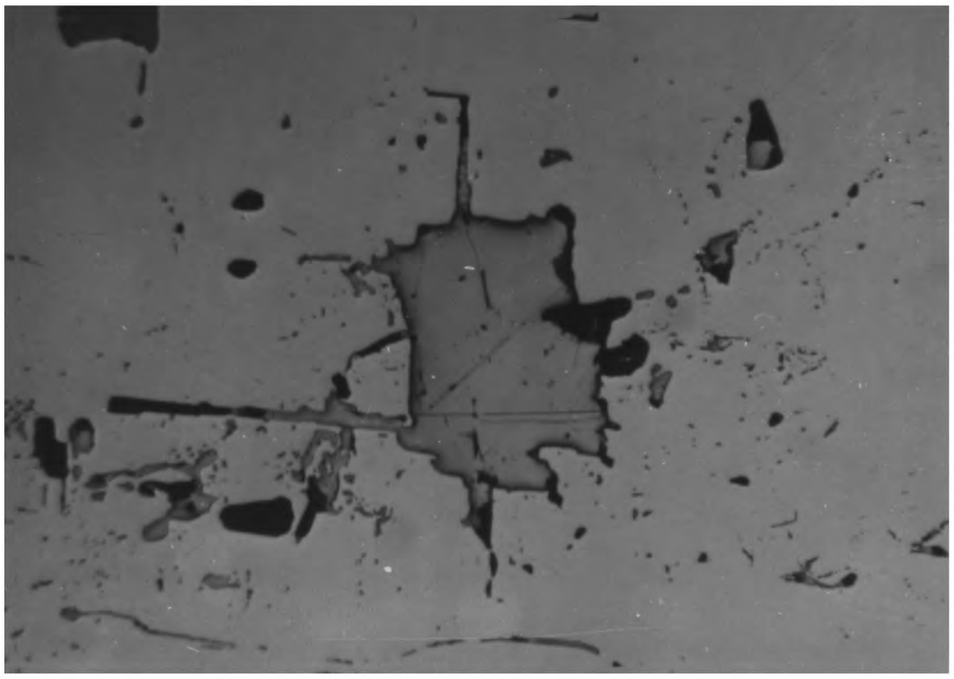

Plate 5.7.2c Aikinite (darker grey) replacing pyrite (lighter grey). x 300

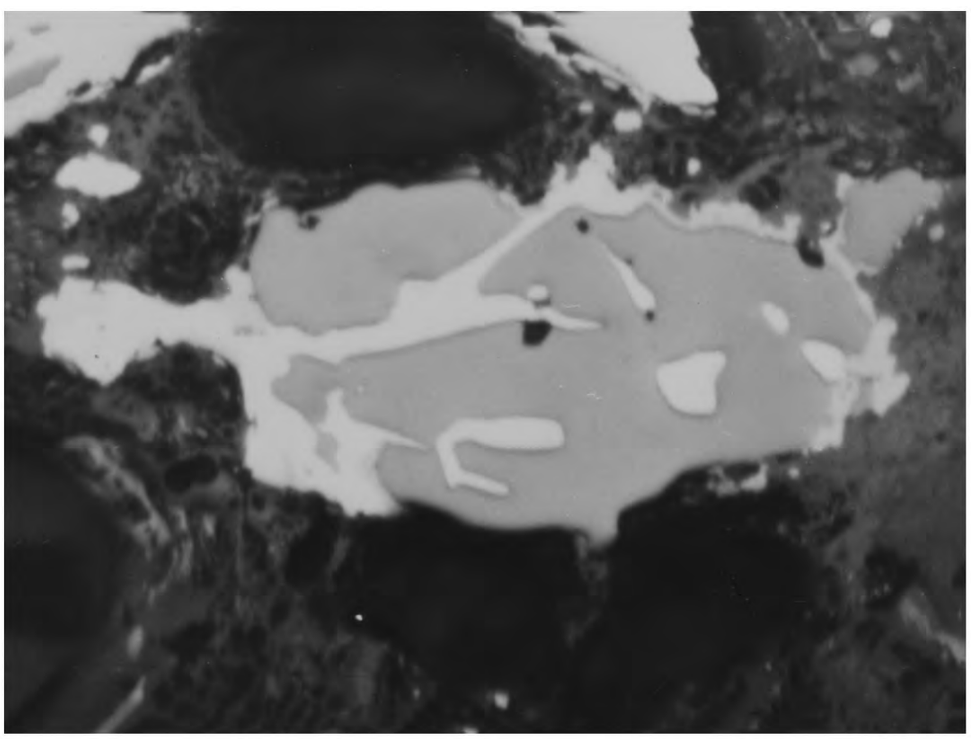

Plate 5.7.2d Aikinite (white) replacing sphalerite (light grey). x 300

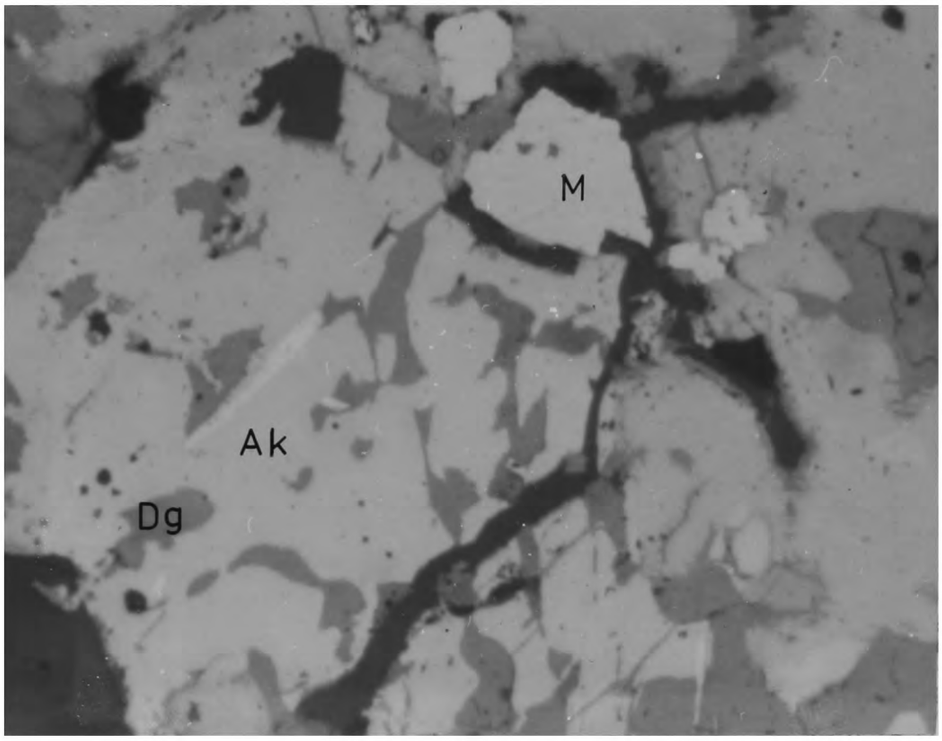

Plate 5.7.2e Unknown lamellae of bismuth sulphosalt(?) in aikinite(Ak). Digenite (Dg) and Marcasite (M). x 150

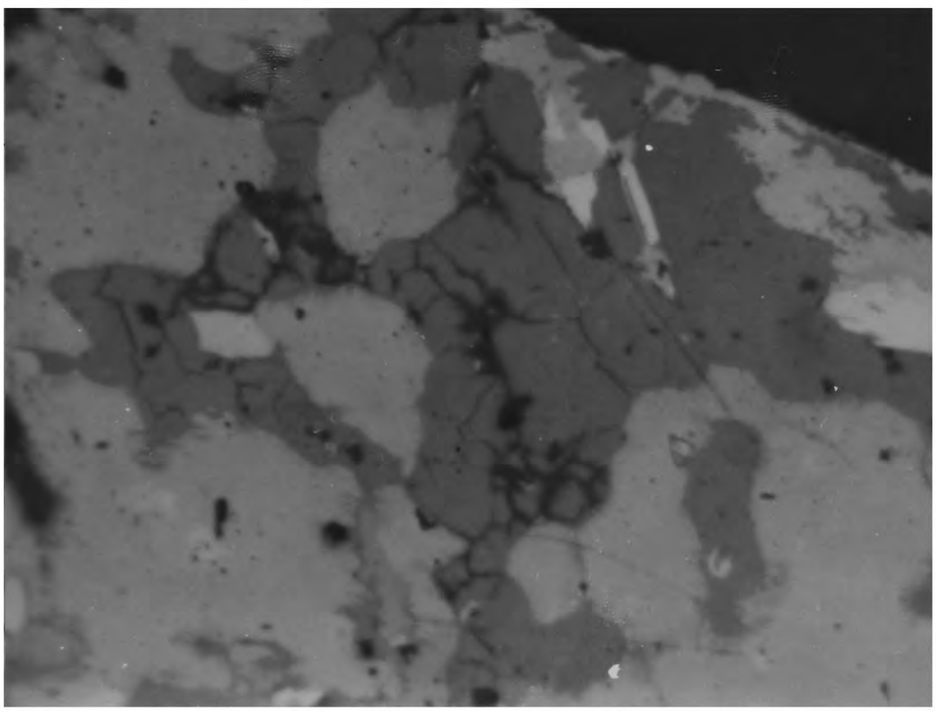

Plate 5.7.2f Similar to 5.7.2e.

the central part of a pyrite crystal along cleavage directions (plate 5.7.2c).

Replacement of sphalerite was observed in specimen 50, in which aikinite is in turn replaced by fahlerz (plate 5.7.2d). Sometimes aikinite was seen cutting across a quartz-fahlerz boundary in a limonite-digenite intergrowth resulting from the alteration of chalcopyrite which is seen as relics in this limonitic groundmass.

Finally, a white lamellae of possibly Bi-sulphosalt was observed in aikinite areas but it was not identified yet completely (plates 5.7.2e, f).

5.8 Paragenetic Sequence

The paragenesis of the ore and gangue minerals, given in Table 5.8, although based on the textural relationships, mineral stabilities and fluid inclusion study results, is somewhat speculative because the textural evidence for several ore and gangue minerals is not complete.

The lamellar form of hematite, from which ilmenite is being exsolved, and its textural relationship with quartz, suggest a formation at the beginning of the early vein stage (see plate 5.3.2d). During this stage the temperatures rise about 100°C with the formation of quartz followed by pyrite.

Fracturing occurs at the end of the early vein stage after the crystallisation of the pyrite. This is indicated by cataclasis in pyrite, and veining in sphalerite.

Most of the ore minerals form in the Base Metal stage, in the order given in table 5.8. At the end of the base metal stage a second

TABLE 5.8 Paragenetic Sequence

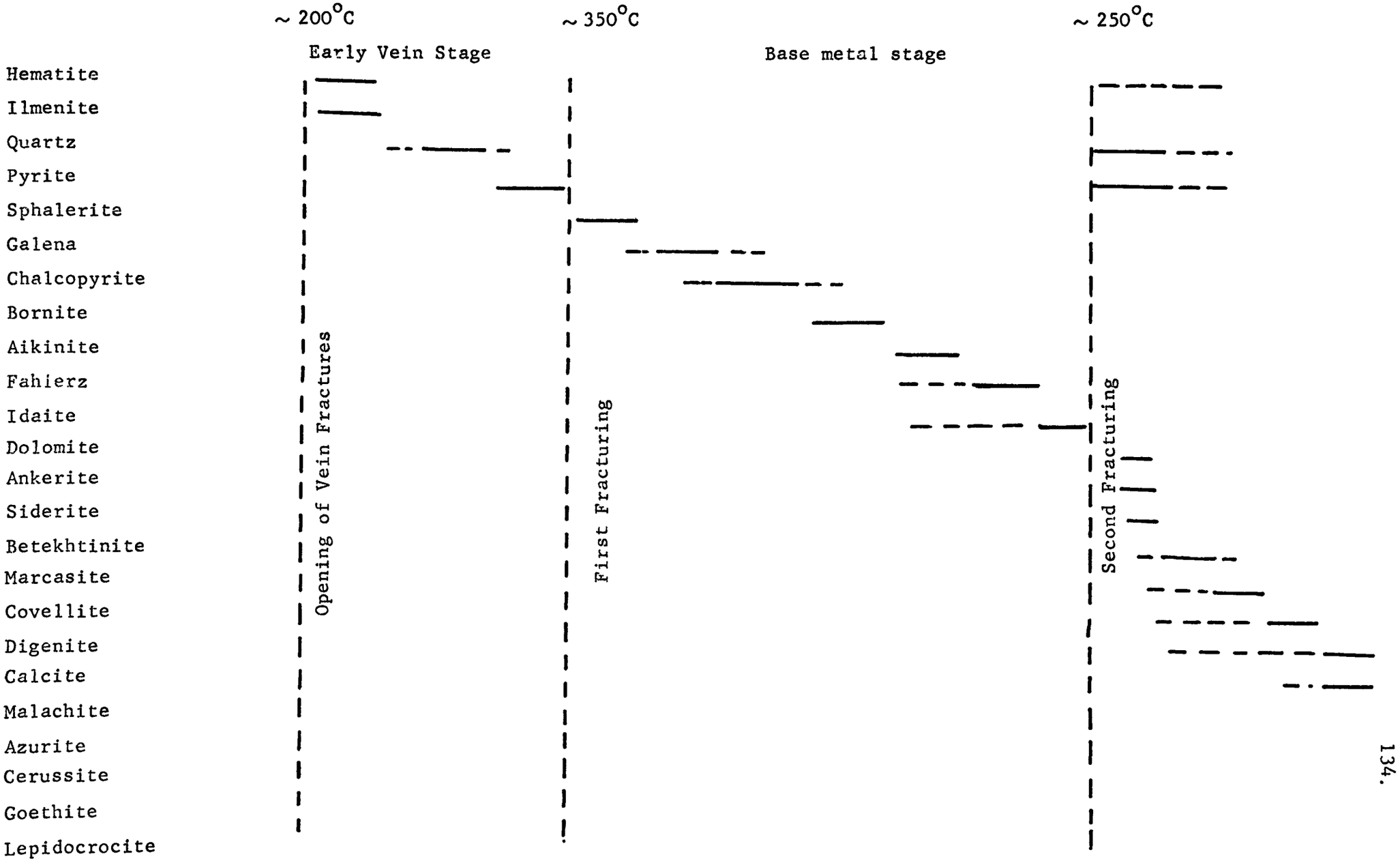

fracturing occurs which is mostly marked by large scale vein filling by gangue carbonates.

Decomposition and alteration of early formed ore minerals occur in the last stage of mineralization. These include decomposition of betekhtinite to digenite and galena, covellite and cerussite formation, and limonitization.

5B. QUANTITATIVE PHYSICAL MEASUREMENTS ON VEIN MINERALS

5.9 X-ray Diffraction

X-ray diffraction studies of various sulphides and sulphosalts as well as ganque minerals were undertaken using fibre and smear mounts for identification, d-spacing and cell-size measurements and indexing purposes. It was also intended to check the effect of the trace element content of sphalerites by measuring cell-sizes. The method and correction procedures are described in Appendix 4.

5.9.1 Pyrite. The cellsizes of 6 pyrites vary within the range 5.4172 to 5.4182 and are shown in Appendix table 4.1 with details of the diffraction pattern.

5.9.2 Sphalerite. Cell-sizes of 42 sphalerites were measured accurately using powder photographs. These cell-size values are included in table 5.10.1 and a frequency diagram is shown in Fig. 5.9.2. As seen from the figure, the cell-sizes vary from 5.4108Å to 5.4143Å with a mean 5.4124Å. The cell-size of several light and dark coloured grains of the same specimen were measured but no significant difference between the two values was observed. Examples of the various diffraction lines are given in Appendix table 4.2.

An independent check was made using the formula given by Barton and Skinner (1967, p.250) to calculate the cell-size of sphalerites. For this purpose 10 specimens having cell-sizes in the 5.4108 to 5.4143Å range were selected and using the following formula-

$$a = 5.4093 + 0.000456\ U + 0.00424\ V + 0.00202\ W$$

TABLE 5.9.2. Sphalerite cell-sizes calculated on the basis of Mole % metal contents.

Specimen No	Wt. % Fe S	Mole % FeS	Wt. % MnS	Mole % MnS	Wt. % CdS	Mole % CdS	Cell-size Calculated	Cell-size Measured
42	0.08	0.08	0.14	0.155	0.26	0.17	5.4103	5.4108
87	1.10	1.20	0.17	0.193	0.46	0.31	5.4115	5.4113
6B	0.80	0.88	0.13	0.135	0.49	0.33	5.414	5.4119
47A	1.07	1.18	0.095	0.10	0.58	0.39	5.4117	5.4121
7	3.16	2.53	0.35	0.39	0.51	0.34	5.4127	5.4123
17	1.80	1.77	0.190	0.20	0.62	0.41	5.4122	5.4125
79	0.61	0.60	--	--	0.87	0.58	5.4120	5.4128
115	2.65	2.91	0.19	0.20	0.42	0.28	5.4122	5.4131
97	1.05	1.16	--	--	0.68	0.45	5.4117	5.4136
95	1.04	1.14	--	--	1.51	1.01	5.4141	5.4143

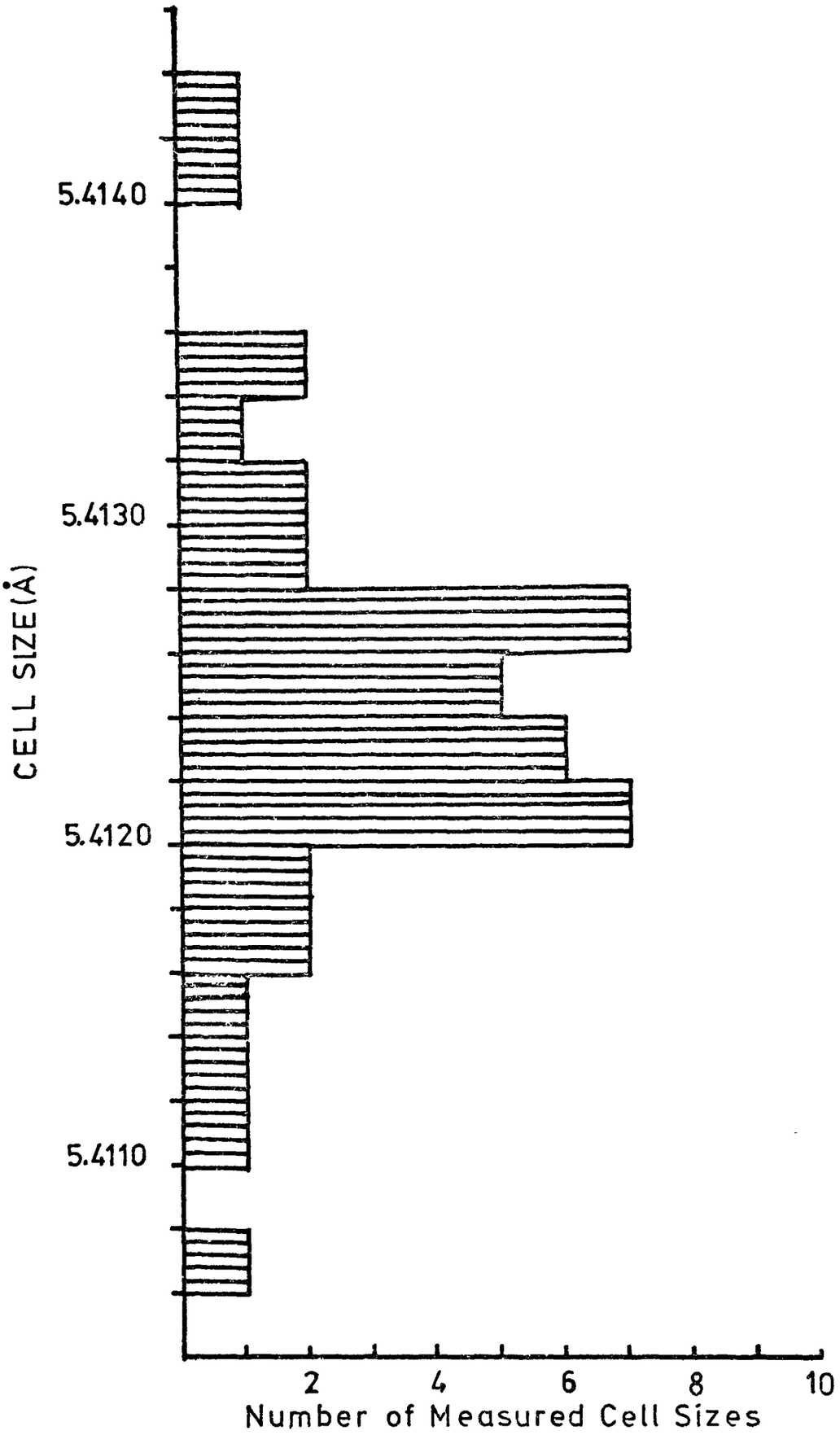

Fig 5.9.2 Frequency Diagram of Cell Sizes Measured on Sphalerite from the Bulancak Area

where U, V, and W are respectively the FeS, CdS, and MnS contents in mole percent- cellsizes were calculated. The results compared with the measured values are in good agreement and are given in table 5.9.2.

5.9.3 Betekhtinite. Only betekhtinite in specimen 53 was found large enough to obtain material for powder photography using a hand drill. Details of the various diffraction patterns are given in table 5.9.3 in comparison with other published data. The cell parameters are in agreement with those given by Dornberger-Schiff und Höhne (1959).

	Bulancak, Turkey	Mansfeld, Germany
a =	14.693 $\pm$ 0.006	14.67
b =	22.720 $\pm$ 0.003	22.80
c =	3.861 $\pm$ 0.005	3.86

Volume = 1288.9Å^3

for Z=4 the density (ρ) of betekhtinite was found to be 5.68 which is slightly lower than the measured value 6.13 by Mukanov et al (1961). However, it was calculated as 5.73 by Dornberger-Schiff un Höhne (op. cit) which is in agreement with the value given above.

5.9.4 Aikinite. Cell parameters of one aikinite specimen (20) were measured from a powder photograph. The following cell parameters are in agreement with those of the Berezovsk aikinite given by Pecock (1942)

Bulancak, Turkey	Berezovsk, Russia
a = 11.297	11.30
b = 11.654	11.64
c = 4.061	4.00
Volume = 534.65Å^3	ρ calculated (Berezovsk) = 7.22
	ρ measured " = 7.08
ρ = 7.66	

The details of the various diffraction patterns were given in Table 5.9.4.

Peacock (1942) noted that "the aikinite from Berezovsk had a spacing at d = 2.36Å which does not correspond with any possible set of planes in the mineral although it does agree with the strongest reflection in the diffraction pattern of gold which is reported to exist together with aikinite". This spacing, however, was found to occur in all aikinites shown in table 5.9.4. It therefore seems unlikely to be due to gold.

Welin (1966) has demonstrated a linear relationship between d_{220} of aikinite-bismuthinite minerals and their Pb content. The Pb and Bi contents of these minerals from Gladhammar (Sweden) and Russia (Borodaev et al, 1970) were plotted against d_{220} values together with that of Bulancak aikinite in Fig. 5.9.4. A better correlation was obtained, for both elements, from the data given by Borodaev et al (op. cit) in comparison to Welin's (1966) data. The only data given for Tari-Erkan and Newyanskya Seredovina aikinites are scattered. Curves obtained from Russian and Swedish aikinites intersect at 4.07Å for an equivalent of 33.5%Pb, both curves diverging into the bismuthinite field (Fig. 5.9.4) The d_{220} of bismuthinite given by Borodaev et al (op. cit) is 3.89Å

TABLE 5.9.3 X-Ray Diffraction data for Betekhtinites.

Bulancak			Dzhezkazgan		Radka		Mansfeld	
hkl	$^{I}/_{I_o}$	d(Å)	I	d(Å)	I	d(Å)	I	d(Å)
-	-	-	-	-	2	12.3	-	-
-	-	-	-	-	1	11.3	-	-
200	20	7.37	-	-	-	-	-	-
040	50	5.65	-	-	1	5.72	-	-
310	50	4.77	3	4.77	3	4.80	4	4.77
150	20	4.32	1	4.31	2	4.36	1	4.30
330	-	-	-	-	1	4.13	-	-
060,011	-	-	-	-	1	3.82	-	-
400	-	-	-	-	1	3.67	-	-
121	20	3.56	-	-	-	-	-	-
420	20	3.49	-	-	2	3.50	-	-
350	30	3.33	-	-	2	3.34	-	-
-	-	-	-	-	-	-	1	3.27
170,141,231	-	-	-	-	2	3.13	-	-
301,440	80	3.09	7	3.08	8	3.06	8	3.08
051,321	100	2.94	8	2.94	9	2.93	9	2.93
080	-	-	-	-	1	2.83	-	-
530,251,370	30	2.74	-	-	3	2.72	-	-
341,161,280	50	2.68	4	2.67	3	2.68	4	2.67
071,431,190	50	2.52	-	-	2	2.52	-	-
550,071	50	2.48	5	2.48	3	2.47	5	2.46
620	50	2.40	1	2.40	2	2.39	2	2.39
271	70	2.35	6	2.36	5	2.36	6	2.35
451,521	30	2.30	3	2.31	2	2.30	4	2.29
640,390,480	30	2.26	3	2.26	2	2.25	4	2.25
-	-	-	-	-	-	-	1	2.15
091	20	2.11	-	-	1	2.11	-	-
660,471,611	15	2.06	-	-	2	2.06	-	-
730,291	10	2.02	4	2.02	2	2.02	6	2.01
631	10	1.995	-	-	-	-	-	-
561	-	-	-	-	1	1.987	-	-
-	-	-	6	1.952	-	-	7	1.946
4.10.0,002	60	1.934	-	-	6	1.938	-	-
0.12.0,022	10	1.899	-	-	-	-	-	-
651	15	1.888	4	1.894	2	1.892	4	1.894
721,800,042								
491	90	1.830	10	1.832	10	1.834	10	1.832
152,770	40	1.762	6	1.766	5	1.769	7	1.766
5.11.0,262	5	1.680	1	1.684	2	1.682	1	1.682
860,172	-	-	4	1.653	3	1.649	-	-
-	-	-	-	-	-	-	4	1.643
-	-	-	-	-	2	1.596	-	-
5.13.0	20	1.506	1	1.510	-	-	1	1.514

TABLE 5.9.3 continued

	Bulancak		Dzhezkazgan		Radka		Mansfeld	
hkl	$^1/I_o$	d(Å)	I	d(Å)	I	d(Å)	I	d(Å)
-	-	-	1	1.462	1	1.462	3	1.461
-	-	-	-	-	1	1.428	-	-
2.16.0	10	1.399	1	1.409	1	1.405	3	1.406
752,6.14.0	20	1.355	2	1.363	1	1.360	3	1.359
682,6.13.1	20	1.338	2	1.340	1	1.337	3	1.340
10.8. 0	20	1.305	4	1.312	2	1.307	5	1.307
103,9.11.0	10	1.283	1	1.287	1	1.285	1	1.287
213,0.18.0	20	1.265	2	1.275	2	1.268	4	1.268
862	15	1.256	1	1.250	-	-	1	1.260
053, 792	10	1.239	-	-	1	1.242	4	1.241
882,10.9.1	20	1.206	2	1.212	1	1.214	4	1.208
-	-	-	2	1.192	-	-	4	1.191
10.02	5	1.168	-	-	-	-	-	-
11.11.0	30	1.122	1	1.126	2	1.122	7	1.125
12.71	20	1.099	7	1.103	2	1.101	8	1.103
0.11.3	50	1.093	-	-	-	-	-	-
583	10	1.089	-	-	-	-	-	-
-	-	-	1	1.074	-	-	4	1.074
11.13.0	10	1.0604	1	1.065	-	-	1	1.065
-	10	-	1	1.057	-	-	4	1.056
693	10	1.038	5	1.034	-	-	5	1.034
9.13.2	10	1.0145	5	1.018	-	-	5	1.018
14.80	20	0.984	1	1.005	-	-	-	-
15.30	20	0.970	-	-	-	-	-	-
				(1)		(2)		(3)

1. Mukanov et al, 1961
2. Tsonev et al, 1970
3. Tsonev et al, 1970

TABLE 5.9.4 X-Ray Diffraction Data for aikinites.

hkl	Bulancak	Berezovsk	Dzhido	Gladhammar
120	5.16	-	5.20	-
-	-	-	-	4.862
-	-	-	4.54	-
220	4.04	4.07	4.07	4.069
101, 011	3.80	3.77	-	3.82
130	3.66	3.67	3.66	3.716
111	-	-	-	3.626
310	3.59	3.58	3.58	3.600
021,201	3.29	-	-	3.328
121	-	3.18	3.18	3.194
211,320	3.170	-	-	3.171
040	-	-	-	2.915
221	2.856	2.88	2.85	2.87
140	-	-	-	2.84
410, 301	2.745	2.74	2.73	2.764
131,330,311	2.673	2.68	2.68	2.713
240	2.585	2.580	2.590	2.594
420	-	2.56	2.55	2.553
231, 321	2.498	2.510	2.510	2.513
041	-	-	2.40	-
411,	2.356	2.36	2.36	2.366
150,340	2.301	-	2.30	2.314
	-	2.27	2.27	2.278
510	-	-	-	2.25
241	2.174	2.17	2.190	2.183
250,421	2.145	2.15	2.16	2.157
440,051	2.015	2.02	2.03	2.024
431,151	1.985	1.984	1.99	1.993
501,151	-	-	-	1.979
530,112,511	1.9456	1.947	1.952	1.959
202,600,212	1.8778	1.883	1.888	-
441	1.8041	1.805	-	-
312,351,132	1.7638	1.766	1.766	-
360	1.7231	-	1.731	-
261	1.670	-	1.680	-
621,042,170	1.6369	1.648	1.647	-
270,710	1.5919	1.593	1.598	-
720	1.5536	-	1.564	-
370,342	1.5208	1.524	1.525	-
730,461	1.4867	1.488	1.490	-
560	1.4697	1.475	1.478	-
721	1.4488	-	1.455	-
-	-	-	1.425	-

Table 5.9.4 continued

hkl	Bulancak	Berezovsk	Dzhido	Gladhammar
062	1.4017	1.406	1.417	-
-	-	-	1.395	-
651	1.3758	1.380	1.370	-
471	1.3518	1.354	1.345	-
-	-	1.330	1.323	-
632	1.300	1.302	1.295	-
840,133	1.2688	1.271	2.265	-
-	-	-	1.241	-
481	1.232	-	1.232	-
413	1.2127	1.216	1.216	-
-	-	-	1.204	-
-	-	-	1.192	-
053,472	1.1704	1.174	1.170	-
513	1.1546	1.158	1.157	-
-	-	-	1.138	-
-	-	1.123	1.125	-
-	-	-	1.120	-
603	1.0983	-	-	-
591	1.0815	1.083	1.084	-
-	-	-	1.078	-
-	-	-	1.069	-
690,902	1.0661	-	1.0640	-
4.10.1	1.0467	-	1.049	-
-	-	-	1.041	-
-	-	-	1.031	-
-	-	-	1.027	-
723,1.11.1	1.0205	1.020	1.018	-
-	-	-	1.010	-
-	-	-	1.000	-
653	0.9928	-	0.992	-
183	0.9869	0.989	0.986	-
813,971	0.9725	0.975	-	-
823,6.10.1	0.9613	-	-	-
		(1)	(2)	(3)

1. Peacock, 1942
2. Welin, 1966
3. Welin, 1966

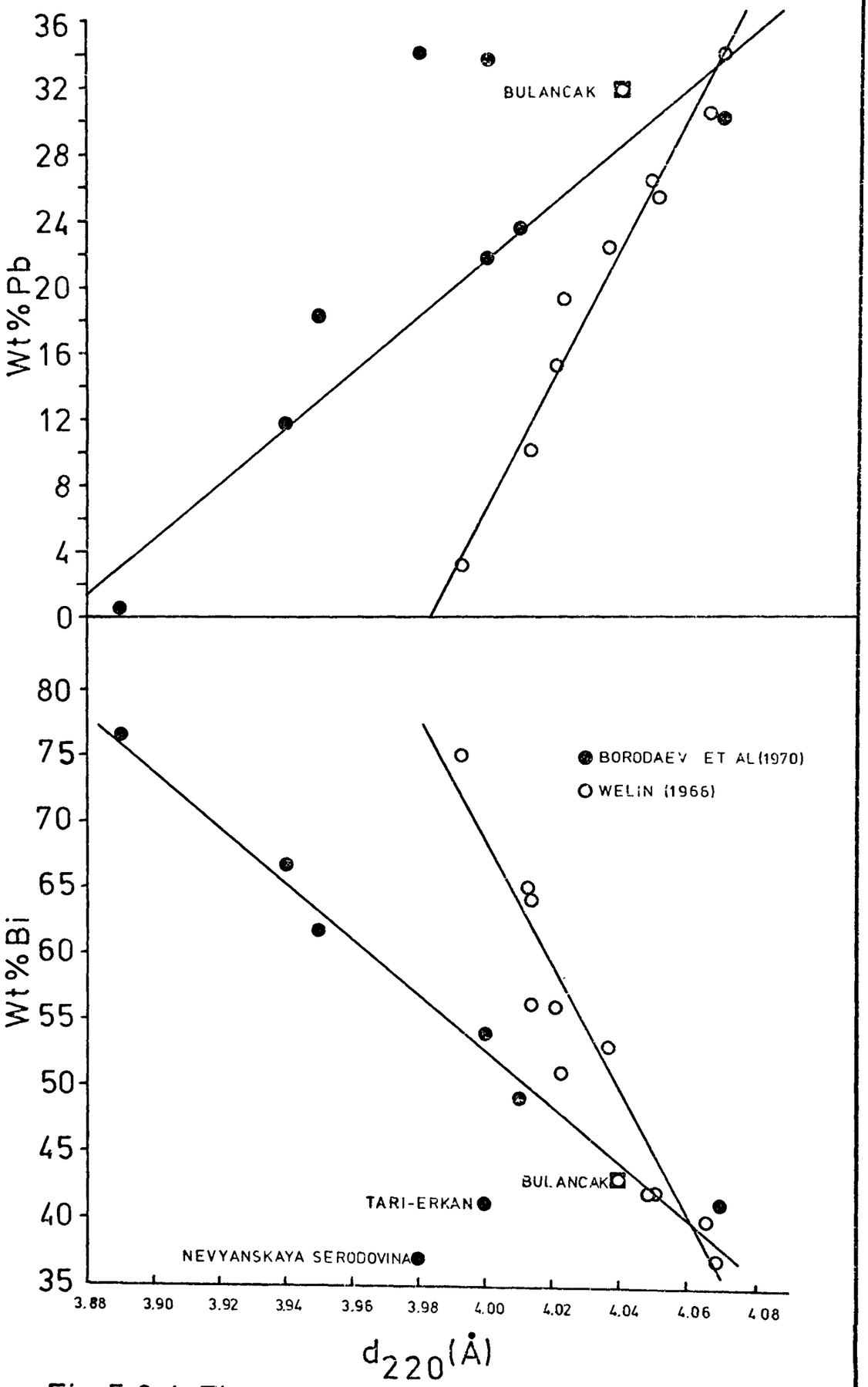

Fig 5.9.4 The relationship between d_{220} and Bi-Pb contents of aikinite-bismuthinite solid solution minerals.

whereas Welin's data given 3.993Å. For Dzhido aikinite d_{220} is 4.07Å, Gladhammar aikinite 4.069Å and that of Berezovsk aikinite 4.066, all in very good agreement.

5.10 Electron Microprobe Analysis:

5.10.1 Sphalerite. Electron microprobe analyses were largely carried out on sphalerite due to its very informative character and widespread distribution throughout the area. The Zn, Fe, Mn, Cd and S analysis of 61 sphalerites are given in table 5.10.1. Cell-size measurements and colour of the measured grains were also included in the table to show the effects of Fe, Mn, and Cd substitution on the cell-size and colour. As seen from the table Fe, Mn, and Cd contents of the sphalerites vary within the range of 0.05-2.28%, 0.04-0.92%, and 0.20-1.18%, respectively.

The wt's % of Fe, Mn, and Cd shown in table 5.10.1 were plotted in Fig. 5.10.1 to see the relationship between Fe, Mn, and Cd distribution in the area - since these are the most common elements that enter the sphalerite structure isomorphously to increase cell-size (Kullerud, 1953; Skinner et al, 1959; Barton and Toulmin, 1966; Sorokin et al, 1970).

At first sight, these Fe, Mn, Cd plots seemed to be randomly scattered but when the specimen localities, altitudes and homogenization temperatures are taken into consideration, the Mn-trend follows a distinct zone extending from NW (Kusdere) to SE (Kasyatak), almost parallel to the Kasyatak Fault, in which Mn decreases from NW to SE (specimen 126 which was collected from the exposure next to the

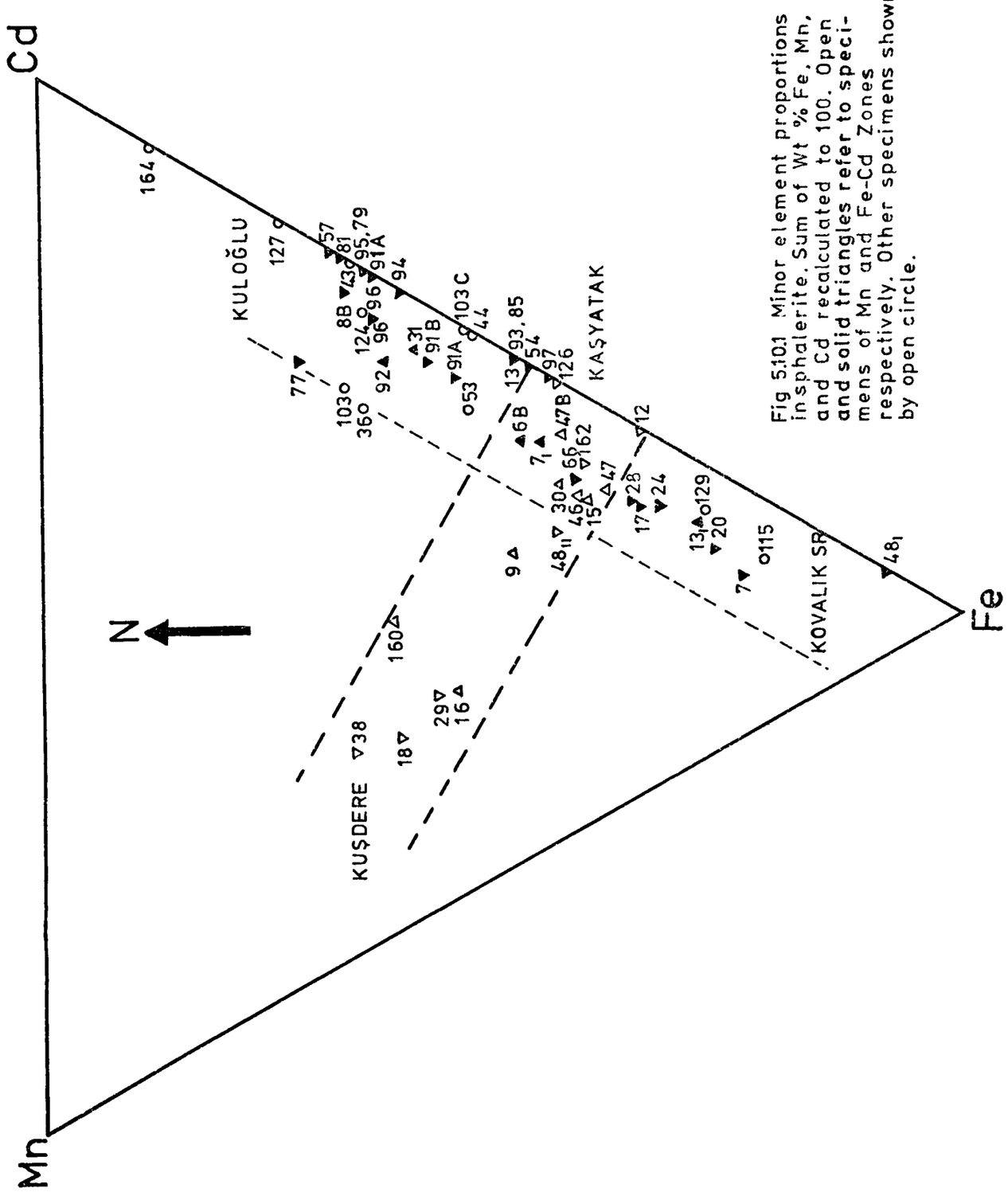

Fig 5.10.1 Minor element proportions in sphalerite. Sum of Wt % Fe, Mn, and Cd recalculated to 100. Open and solid triangles refer to specimens of Mn and Fe-Cd Zones respectively. Other specimens shown by open circle.

TABLE 5.10.1 Microprobe Analysis and cell-size measurements of Sphalerites

Sample Number	LOCALITY	ALTITUDE (MS)	ZN	S	FE	MN	CD	Cell-Size (Å)	Standard Dev.	Colour of The Sphalerite
6B	SARIDIKEN DERE	660	66.85	32.17	0.51	0.08	0.38	5.4119	0.0002	Amber-Reddish Brown
7(1)	"	595	66.18	32.80	0.72	0.09	0.50	-		Yellow-light brown
7(2)	"	595	64.51	32.75	2.01	0.22	0.40	5.4123	0.0006	"
30	"	590	66.38	32.66	0.65	0.11	0.39	5.4122	0.0005	"
31	"	580	66.00	32.70	0.41	0.05	0.54	-		
8B	KISLA CAMISI DERE	690	65.69	32.32	0.49	0.04	0.91	5.4121	0.0004	Dark Brown
8Y	"	690	66.64	32.22	0.70	0.11	0.36	5.4113	0.0004	Yellow
28	KOVALIK SR.	780	66.19	32.59	0.92	0.10	0.40	5.4123	0.0004	Dark reddish-brown
29	"	625	65.38	32.52	0.97	0.82	0.45	5.4122	0.0002	Reddish brown
24	KISLA MAH	760	65.38	32.65	1.18	0.12	0.46			
126	YAYKINLIK	570	65.83	32.70	0.74	n.d.	0.57			
9	"	705	65.58	32.71	0.72	0.26	0.41			
12	KORNALI DERE EAST BANK	565	67.11	31.81	0.93	n.d.	0.49	5.4129	0.0003	
13(1)	KORNALI DERE	585	66.21	32.75	0.64	n.d.	0.59	-		Dark reddish-brown
13(2)	"	585	65.80	32.37	1.17	0.09	0.37	5.4124	0.0005	"
160	"	540	66.22	32.59	0.57	0.46	0.44	5.4128	0.0002	
20	"	530	65.62	32.67	1.12	0.11	0.30	-		
162	"	430	64.76	32.72	1.06	0.11	0.62	-		
17	KORNALI DERE WEST BANK	625	65.98	32.57	1.14	0.12	0.48	5.4125	0.0003	Dark reddish-brown
16	"	600	65.66	32.64	0.87	0.67	0.37			
15	"	590	66.21	32.27	0.95	0.15	0.50	5.4130	0.0006	Dark reddish-brown
18	"	540	65.55	32.54	0.83	0.92	0.42	-		
46/2	SISPELIT DERE	600						5.4122	0.0004	
46/1	"	600	66.30	32.45	0.82	0.14	0.44	5.4124	0.0001	Reddish Dark-brown
48(1)	"	505	64.83	32.75	2.28	n.d.	0.20	-		Dark brown-black
48(2)	"	505	66.08	32.65	0.78	0.19	0.41	5.4122	0.0002	
47	"	540	66.96	32.23	0.52	0.06	0.26	5.4122	0.0001	Dark brown-black
47A	"	530	65.91	32.69	0.68	0.06	0.45	5.4121	0.0004	"
54	DAMYATAGI DERE	525	67.33	32.20	0.34	n.d.	0.30	5.4117	0.0003	Light brown
57	"	365	66.75	32.50	0.24	n.d.	0.52	5.4124	0.0007	Reddish dark brown
53	WEST OF GEDIK T.	470	66.69	32.37	0.54	0.09	0.53	5.4120	0.0002	Dark brown-black
36	WEST OF DONBUL T	580	67.12	32.25	0.26	0.10	0.38	5.4121	0.0002	Dark brown
37	KUSDERE	515	66.55	32.62	0.30	0.18	0.42	-		
38	"	500	66.20	32.00	0.67	0.90	0.37	5.4127	0.0007	Dark brown
44	GONURCA DERE	620	66.24	32.86	0.48	n.d.	0.53	-		
43	"	580	66.71	32.32	0.31	n.d.	0.60	5.4125	0.0005	Reddish-dark brown
42	"	550	67.19	32.15	0.05	0.09	0.20	5.4108	0.0004	Reddish brown
66(1)	TAMYANI D(INECE)	360	65.60	32.70	1.37	0.06	0.39	-		
66(2)	"	360	66.30	32.70	0.70	0.10	0.40	5.4110	0.0002	Light reddish brown
77	KUCUKGURE D.	180	67.00	32.50	0.20	0.09	0.42	5.4118	0.0003	Yellow-light brown
96	"	160	66.48	32.55	0.40	0.05	0.65	5.4123	0.0001	
81	KULOGLU (KARAYALAK)	280	66.72	32.22	0.37	n.d.	0.75	5.4140	0.0002	Amber-reddish brown
79	KULOGLU	280	66.66	32.38	0.39	n.d.	0.68	5.4128	0.0003	Yellow-light brown
85(1)	SINEKLI D. (DARIKOY)	190	66.27	32.53	1.07	n.d.	0.30	-		
85(2)	"	190	66.00	32.55	0.73	n.d.	0.68	5.4133	0.0004	Amber-Dark brown
103C		405	66.58	32.55	0.48	n.d.	0.55	5.4127	0.0003	
103		395	66.79	32.57	0.24	0.09	0.39	5.4119	0.0001	
102	DARIKOY	440	66.20	33.00	0.38	n.d.	0.58	5.4115	0.0008	
91A(1)	YK.UZUMLUK	320	66.29	32.60	0.52	0.06	0.57	-		
91A(2)	"	320	66.10	32.59	0.50	n.d.	0.84	5.4132	0.0004	Yellow-light brown
91B	"	310	66.38	32.65	0.46	0.05	0.57	5.4128	0.0002	"
93	ORTA UZUMLUK	270	65.81	32.56	0.70	n.d.	0.65	5.4127	0.0002	"
92	"	260	66.30	32.64	0.47	0.09	0.68	5.4126	0.0004	Reddish brown
94	ASAGI UZUMLUK	220	66.20	32.66	0.51	n.d.	0.76	5.4127	0.0002	Brown
95	"	170	65.79	32.56	0.66	n.d.	1.18	5.4143	0.0003	Amber-reddish brown
97	"	160	66.41	32.58	0.67	n.d.	0.53	5.4136	0.0004	Amber-dark brown
115	BUYUKGURE D.	300	65.12	32.87	1.68	0.12	0.33	5.4131	0.0005	
127	ARDAHAN DERE	260	66.37	32.58	0.27	n.d.	0.75	-		
129	"	245	65.62	32.72	1.02	0.06	0.33	-		
124	"	165	66.14	32.71	0.34	0.04	0.57	-		
164	AKKOY MINE		65.98	32.77	0.13	n.d.	0.89			

BL-5 borehole) whereas Fe and Cd variations are oriented almost perpendicular to the Mn-trend. It is interesting to note that this distinct orientation pattern reflects the dependance on two major fracture systems in the area, showing a structural control. However, the homogenization temperatures and proximity to channels of rising ore fluids seem as effective as dominant fracture systems on the distribution of Fe and Mn concentrations.

In certain specimens (7, 13, 48) the Fe-content of the sphalerite was found to vary considerably from grain to grain, even though the average of at least 5 different points on each grain was taken, and within grain variation was small. It is not known yet whether these specimens represent the area where Mn and Fe-Cd zones intersect or as demonstrated by Godovikov and Ptitsyn (1966) the dependence of FeS content of sphalerite on the composition of the original mixture. It has been suggested by these authors that at the same temperature hyrothermal recrystallization may produce sphalerite with variable amounts of FeS, even when iron sulphides crystallize out with it.

Schroll (1953) pointed out that the absolute amount of a given element, or the relative proportions of two elements that can substitute isomorphously in a given mineral are effected by (1) temperature and pressure,(2) regional factors, and (3) factors relating to the type of wall rocks and the type of igneous rocks.

The writer in a previous study (Akinci, 1969b) has summarized the following factors influencing the iron content of sphalerite:

1. The affect of solid solution between chalcopyrite and sphalerite described by Sugaki and Tashiro (1957) and Donnay and Kullerud (1958).

According to the latter authors almost 10% chalcopyrite can dissolve in ZnS at 600°C and affect the iron content. On the other hand at 500°C the solid solution of ZnS in Cu_2S is 1.5 wt.% and the solid solution of Cu_2S in ZnS is less than 0.1 wt.% (Craig and Kullerud, 1973).

2. Temperature. More iron dissolves as temperature increases.

3. Partial Pressure. With increasing P_s, pyrite rather than pyrrhotite occurs with ZnS. It is found that ZnS in equilibrium with FeS_2 contains less Fe than ZnS in equilibrium with pyrrhotite (Rose, 1961).

4. Total Pressure. Kullerud (1953) has shown experimentally that pressure decreases the solubility of FeS in ZnS.

The first and third factors as described earlier are responsible for the common textural relationship between sphalerite, pyrite, and chalcopyrite. Since highest Fe and Mn were found in specimens located along major NW-SE trending faults which served as ore-bearing channels, the temperature factor seems in close control along these fractures. In general, all these factors are common features in hyrothermal systems.

The colour bands in a sphalerite specimen were observed in a disc wafer during fluid inclusion study. In this particular specimen the colours of the bands change from whitish yellow to blood-red. The average Fe, Mn, and Cd concentrations were found to be 300 to 490ppm, 300 to 520ppm, 900 to 2500 ppm, respectively. It is interesting to note that the highest Fe and Cd concentrations were found in whitish-yellow areas (see plate 6.4.1a). The Akkőy Mine sphalerite specimen which has only 0.13% Fe was found completely opaque for fluid

inclusion study (see Table 5.10.1).

5.10.1a Comment on Colour of Sphalerites. It has been suggested that Fe is largely responsible for the colour of sphalerite and dark colours are attributed to high iron contents. Absorption studies have shown that the absorption of Fe^{+2} ions in the blue region and absorption in the red resulting from very much smaller amounts of Co^{2+} ions cause the yellow colour of natural low-iron sphalerite (Slack et al, 1966, 1967). Colour can also result from electronic transitions due to light absorption, e.g., traces of Fe^{3+} ion can absorb violet and indigo to give the complementary yellow colour.

Roedder and Dwornik (1968) analysed a colloform, thin banded sphalerite, with varying colours by electron microprobe, but it was found that iron in these bands ranged from 0.2 to 2.9%.

The present writer (1969b) has studied the effect of iron on the colour of sphalerites prepared synthetically with FeS contents varying from 0.0 to 23.48 Mole % but no significant variation of colour (calculated quantitatively using reflectivity measurements) was found with increasing iron content. Only the specimens representing extreme colour differences were distinguishable.

5.10.2 Betekhtinite. As explained earlier although betekhtinite was observed in several specimens during probe analysis study only betekhtinite in specimen 53 was known to occur to the writer - the others were identified at an advanced stage of writing the thesis and no systematic probe work could be carried out on betekhtinites.

Bulancak and Harköy betekhtinite (also identified by the writer for the first time in a specimen supplied to the writer by E.Acar, MTA Institute, Ankara) have practically the same chemical composition as the material from the six other localities previously studied (table 5.10.2). Only La Leona (Argentina) betekhtinite differs from all the other analyses listed in Table 5.10.2, since it has a very low Pb-content and somewhat higher sulphur, iron and copper contents. Silver was only reported from the Dzhezkazgan deposit specimen.

There is some doubt on the exact formula to be accepted for this mineral. Schüller and Wohlman (1955) have given $Cu_{10}(Fe,Pb)\ S_6$ although $Pb_2(Cu,Fe)_{21}S_{15}$ (Dornberger-Schiff und Höhne, 1959) is also accepted. Mukanov et al (1961) suggest $(Pb,Ag)\ (Cu,Fe)_{11}S_7$. Since the disagreement is on the number of S and Cu atoms the formulas derived were calculated on the basis of 1 Pb atom and given in the bottom part of the table 5.10.2.

5.10.2a Betekhtinite stability. The betekhtinite deposits reported from La Leona, Mansfeld and Dzhezkazgan are from similar geological environments. The betekhtinite from Bulancak, Radka (Bulgaria) and Furotobe Mine, Japan are however representatives of the Kuroko type of volcanic environment in which chalcocite developed at the expense of chalcopyrite with bornite as an intermediate stage preserved as metastable crystals.

TABLE 5.10.2 Betekhtinite Analyses from Bulancak and Harköy in Comparison with other occurrences.

	Bulancak 1a	Bulancak 1b	Harkoy 2	Mansfeld 3	Mt.Lyell 4	La Leona 5	Dzhezkazgan 6	Bulgaria 7	Japan 8
Cu	59.67	59.34	58.64	59.70	59.00	61.40	58.88	59.07	57.20
Pb	18.71	19.34	18.34	17.33	17.30	12.60	17.47	18.01	18.60
Fe	2.42	2.41	2.65	2.69	2.70	3.50	2.81	1.65	2.50
Ag	N.D.	N.D.	0.14	-	-	-	0.79	-	-
S	19.45	20.19	20.93	20.09	20.60	22.80	20.16	20.77	21.70

1a	$Cu_{10.40}\ Fe_{0.48}\ Pb_{1.0}\ Ag_{0.0}\ S_{6.72}$	(Present Study)
1b	$Cu_{10.00}\ Fe_{0.46}\ Pb_{1.0}\ Ag_{0.0}\ S_{6.75}$	"
2	$Cu_{10.43}\ Fe_{0.54}\ Pb_{1.0}\ Ag_{0.01}\ S_{7.38}$	"
3	$Cu_{11.24}\ Fe_{0.58}\ Pb_{1.0}\ Ag_{0.0}\ S_{7.50}$	(Schüller,A., 1960)
4	$Cu_{11.13}\ Fe_{0.58}\ Pb_{1.0}\ Ag_{0.0}\ S_{7.70}$	(Markham, N.L., and Otteman, J., 1968)
5	$Cu_{15.89}\ Fe_{1.03}\ Pb_{1.0}\ Ag_{0.0}\ S_{11.70}$	(Honnorez-Guerstein, B.M., 1971)
6	$Cu_{10.99}\ Fe_{0.60}\ Pb_{1.0}\ Ag_{0.09}\ S_{7.50}$	(Mukanov, K.M., et al., 1961)
7	$Cu_{10.70}\ Fe_{0.34}\ Pb_{1.0}\ Ag_{0.0}\ S_{7.45}$	(Tsonev, D., et al., 1970)
8	$Cu_{10.04}\ Fe_{0.49}\ Pb_{1.0}\ Ag_{0.0}\ S_{7.55}$	(Matsukama, T., 1971)

In experimental studies Craig and Kullerud (1967,1968) found no betekhtinite in any of their syntheses which were made at temperatures of 200°C and above. Markham and Otteman (1968) attempted to synthesize betekhtinite at 505°C but they also obtained phase assemblage as Craig and Kullerud did. Slavskaya et al (1963) heated natural betekhtinite and found it decomposed at 150°C to digenite and Galena, a mixture that also is stable at room temperature. Decomposition proceeds with decrease in volume. It seems therefore that Betekhtinite is certainly not stable above 150°C.

Matsukama (1971) suggests that as betekhtinite appears to be the last product of Kuroko deposits, it may indicate a temperature of around 100°C, the stability field being restricted within very narrow limits between those of bornite and chalcocite. The presence of betekhtinite in recrystallized galena in the Mt. Lyell deposits as described by Markham and Ottemann (1969) suggest that the temperature reached during recrystallization may have coincided with that of the betekhtinite stability field. In contrast, the Mansfeld and Dzhezkazgan betekhtinite shows breakdown to galena and copper sulphides. Textural evidence in the Bulancak specimens is not sufficient to show which direction of reaction is occurring in the assemblage betekhtinite, galena, and digenite.

5.10.3 Fahlerz. Until recently the general formula of tetrahedrite-tennantite minerals has been in dispute; mainly over the existence of a thirteenth sulphur atom, as previously two formulae, $Cu_{12}(Sb,As)_4S_{12}$ and $Cu_{12}(As,Sb)_4S_{13}$ have been quoted. With the developments in

electron microprobe analysis determination of the exact composition became possible.

Springer's study (1969) on the electron microprobe analysis of natural tetrahedrite established the general formulae $(Cu,Ag)_{10}(Zn,Fe,Cu)_2(Sb,As)_4S_{13}$. He also noted that about 11 wt.% Ag can be introduced instead of Cu and there is practically complete interchange between the pairs of Zn-Fe, and Sb-As. The reasons for accepting the 12 : 4: 13 ratio can be summarized as follows:

a. This ratio was established by Springer (1969) on natural and by Hall (1971, 1972) on synthetic minerals. Although $Cu_{12+x}Sb_{4+y}S_{13}$ is proposed by Skinner et al, (1972) in which $0 \leq x \leq 1.92$ and $-0.02 \leq y \leq 0.27$ for tetrahedrite $0 \leq x \leq 1.72$ and $0 \leq y \leq 0.08$ for tennantite is given.

b. The atomic proportions are represented as small whole numbers.

c. Wuensch (1964) determined a possible structure of tetrahedrite with the unit cell formulae 2 $(Cu_{12}\ Sb_4\ S_{13})$.

As an ore mineral and as a source of Ag, tetrahedrite (Yui, 1971) has drawn special attention. The experimental study of Maske and Skinner (1971) demonstrates that the extensive composition field of tennantite is temperature sensitive and promises significant application in the study of ore deposits.

It was hoped to conduct a systematic study on identified fahlerz minerals to see if they show any zonal distribution. Since some silver was reported after random analysis from the area and quoted to

TABLE 5.10.3 Fahlerz Analyses in Comparison with Espiye and İnköy occurrences

Specimen No.	6	1	2	7	30	9	20	Tugal 48 ESPIYE	Tugal H.A.1B INKOY
Altitude	660	690	670	595	590	705	540		
Cu	40.10	40.98	41.39	33.92	39.23	40.57	43.23	39.95	38.04
Fe	7.94	3.21	2.62	1.22	1.34	0.48	5.50	0.20	1.09
Zn	2.73	5.30	6.04	7.29	6.38	8.48	2.63	6.58	7.30
Ag	0.00	0.08	0.12	1.76	0.00	0.00	0.00		0.13
S6	0.00	0.00	0.00	24.99	23.22	0.12	0.00	15.30	21.16
As	20.15	20.47	20.11	4.60	0.00	20.06	22.35	9.53	6.10
S	28.72	28.43	27.79	25.65	30.26	28.35	25.95	27.61	26.70
TOTAL	99.64	98.47	98.07	99.43	100.43	98.06	99.66	99.17	100.52

6	$(Cu,Fe,Zn)_{12}\ AS_4\ S_{13.18}$
1	$(Cu,Ag)_{9.76}\ (Zn,Fe)_{2.10}\ AS_{4.13}\ S_{13.42}$
2	$(Cu,Ag)_{9.85}\ (Zn,Fe)_{2.18}\ AS_{4.05}\ S_{13.08}$
7	$(Cu,Ag)_{9.27}\ (Zn,Fe)_{2.25}\ (Sb,AS)_{4.49}\ S_{13.33}$
30	$(Cu,Zn,Fe)_{12.72}\ Sb_{3.28}\ S_{16.24}$
9	$(Cu,Zn,Fe)_{11.89}\ (AS,Sb)_{4.11}\ S_{13.53}$
20	$(Cu,An,Fe)_{11.73}\ AS_{4.27}\ S_{11.60}$
ESPIYE	$(Cu,Zn,Fe)_{11.89}\ AS,Sb)_{4.10}\ S_{13.98}$
INKOY	$(Cu,Ag)_{9.72}\ (Zu,Fe)_{2.13}\ (AS,Sb)_{4.14}\ S_{13.52}$

be associated with the galenas, this problem might have been solved. Several galenas were probed for silver but none was detected.

A systematic probe analysis on Fahlerz-bearing specimens along Saridiken Dere (1G) was completed and the analysis results and formulas derived are given in table 5.10.3 in comparison with an Espiye and an Inköy specimen (Tugal, 1969). Tugal's analysis were recalculated on the basis of 16 metal atoms. Specimens in table 5.10.3 are arranged from higher altitudes (No. 6) to lower altitudes (7,30). Between specimen 7 and 30 the Selmanoglu Fault is cutting across Saridiken Dere (2F). Zn and Fe contents were found antipathetic. If the isothermal anticline (see fig. 6.8) is taken into account with this analyses Zn is seen to increase towards low altitude and higher temperature area where the Selmanoglu Fault cuts across the Saridiken Dere. Ag contents also suggest an increase towards the fault.

5.10.4 Aikinite. The aikinite analyses given in table 5.10.4 do not exactly correspond to the theoretical aikinite composition but the plot is close to the aikinite end member in the PbS - Bi_2S_3 - $CuPbBiS_3$ subternary (Fig. 5.10.5).

5.10.5 Discussion on the Aikinite-Bismuthinite Solid-Solution Series. Bismuth minerals constitute approximately one-fifth of the known sulphosalts yet have received less attention than other sulphosalt groups. Aikinite was known to Mohs (1804) but has recently assumed increased importance in understanding the crystal chemistry of the bismuth sulphosalts.

TABLE 5.10.4 Electron Microprobe Analyses of Aikinites.

	1a	1b	20	25	50	Theoretical Aikinite
Cu	11.80	10.55	10.22	10.20	10.70	11.00
Pb	35.76	34.40	31.39	32.18	34.45	36.00
Bi	36.00	39.85	42.94	41.95	39.64	36.30
Ag	0 .00	0.0	0.0	0.0	0.0	-
Sb	16.20	15.40	15.75	15.83	16.27	16.70
TOTAL	99.76	100.20	100.30	100.21	101.06	100.00

1a $Pb_{1.02}\ Cu_{1.10}\ Bi_{1.02}\ S_3$

1b $Pb_{1.03}\ Cu_{1.19}\ Bi_{1.03}\ S_3$

20 $Pb_{0.98}\ Cu_{1.25}\ Bi_{0.93}\ S_3$

25 $Pb_{0.97}\ Cu_{1.22}\ Bi_{0.96}\ S_3$

50 $Pb_{1.0}\ Cu_{1.10}\ Bi_{0.98}\ S_3$

Theoretical $PbCuBiS_3$

Its structure has been studied by many workers (e.g., Peacock, 1942; Wickman, 1953) and the metal atoms were readily located. Accurate coordinates for the sulphur atoms have, however, only recently been determined by Kohatsu and Wuenesch (1971) using a single crystal from Berezovsk, Russia. Other occurrences of aikinite have been reported from Russia (Berezovsk, Dzhido), Sweeden (Gladhammar), Greenland (Ivigtut cryolite deposite, by Karup-Møller, 1973), Greece (Nicolaou and Häkli, 1970) and England (Kingsburry and Hartley, 1953).

Due to the similarity between both the space groups and cell dimensions for aikinite and bismuthinite (Peacock, 1942) Padera (1955) suggested the use of a common name Rezbanyite for intermediate aikinite-bismuthinite solid-solution minerals. These include such compositions as Gladite, $PbCuBi_5S_9$; Hammarite, $Pb_2Cu_2Bi_4S_9$ and Lindstromite, $PbCuBi_3S_6$. Another intermediate $Pb_3Cu_3Bi_7S_{15}$ was recently described by Welin (1966) who demonstrated the development of superstructures after single crystal X-ray work on these intermediate members from the Gladhammar deposits. He concluded that solid-solution between bismuthinite and aikinite is not continuous but that only discrete compositions are possible. He also suggested a structural classification for this solid-solution series.

A classification was established by Moore (1967). As aikinite is considered to be the compositional limit of Pb : Bi substitution there are no extra cavities remaining to accommodate copper. Retaining aikinite as the limit of the series, Moore (op. cit) referred to the intermediate members as Z^n aikinites, hence Gladite= 3^1 aikinite,

Hammarite= 3^2 aikinite. "Z" is defined as the integral multiple of the a-translation in aikinite for the superstructure with 4Z x in the general structural cell formula for the aikinite derivatives:

$$Cu_x\ Pb_x\ Bi_{8Z-x}S_{12Z}$$

The aikinite analyses of the present study indicate at least complete solubility between Dzhido aikinite, which is practically the nearest composition together with Berezovsk aikinite to the ideal aikinite and the 6^5 aikinite composition calculated by Moore (1967). Specimen No. 20 has an almost identical composition to 6^5 aikinite (see table 5.10.5).

Springer (1971) studied the members of the solid solution series Bi_2S_3 (Bismuthinite) - $CuPbBiS_3$(Aikinite) on the synthetically prepared specimens. His X-ray and optical study has demonstrated complete solid solution between bismuthinite and aikinite in the temperature range from 300°C upwards to the melting and breakdown points. The temperature of formation may control the derivation of superstructures. Springer (op. cit) could not, however, detect the superstructures which had been observed by Welin (1966) in natural specimens.

Recently discovered aikinite-bismuthinite solid solution series in Greece (Nicolaou and Hakli, 1970) range between 6^1 aikinite (analysis No. 1) and 5^3 aikinite (analysis No. 6). Their galenobismuthitite analysis falls within the range Hammarite and Cannizzarite on the Bi_2S_3 - PbS - $CuPbBiS_3$ subternary (Fig. 5.10.5). The aikinite compsotions vary in a random manner rather than as suggested by Moore (1967) and Welin (1966).

TABLE 5.10.5 Compositions of aikinite derivatives

Z^n	Bi_2S_3	PbS	Cu_2S	Mineral	Locality
	90.16	76.80	3.25	Bismuthinite	
6^1	89.90	9.15	3.00	-	Theoretical
5^1	87.85	9.15	3.75	-	Theoretical
4^1	85.15	12.95	4.65	Gladite	Russia
	80.10	14.90	5.00	"	Theoretical
	79.33	14.32	5.76	"	Greece
2^1	73.82	19.50	7.00	Lindstromite	Russia
	70.80	21.95	7.25	"	Theoretical
5^3	66.42	24.83	8.25	Rezbanyite	Dobsina
	65.35	26.00	8.65	"	Gladhammar
3^2	61.75	28.75	9.50	Hammarite	Russia
	60.27	25.79	9.61	"	Theoretical
4^3	57.35	32.00	10.65	-	Theoretical
5^4	54.75	34.00	11.25	-	Theoretical
6^5	53.00	35.25	11.75	-	Theoretical
	52.82	35.00	12.77	-	Present Study No. 20
	51.60	35.88	12.75	Aikinite	" No. 25
	49.00	38.80	13.20	"	" No. 1b
	48.76	38.41	13.37	"	" No. 50
	44.28	39.87	14.75	"	" No. 1a
	46.13	38.02	15.25	"	Dzhido
	41.62	41.58	13.62	"	Berezovsk

In Fig. 5.10.5 compositions of aikinite derivatives given by Moore (1967) were recalculated and plotted as Bi_2S_3, PbS and Cu_2S to compare with other known sulphosalts in the Bi_2S_3-PbS-Cu_2S ternary system. It is interesting to note that most of the known Bi-sulphosalt minerals are seen in the Bi_2S_3-$CuPbBiS_3$-PbS subternary of the ternary system. Only Wittichenite, Emplectite (and Cuprobismuthite) fall on the Bi_2S_3-Cu_2S join of the system. Although this join was studied by Buhlman (1971), and Van Hook (1960), and the Cu_2S-PbS and PbS-Bi_2S_3 join by Craig and Kullerud (1967) and the latter by Van Hook (1960) and Salanci (1965) the phase relations are not clear between bismuthinite and aikinite solid solution series and other phases of the ternary system.

No naturally occurring binary phase in the PbS-Cu_2S join is known. Phase A (7 Cu_2S.2PbS), experimentally found by Craig and Kullerud (1967), is not stable below 486°C. The validity of some of the minerals occurring on the PbS-Bi_2S_3 join is still under debate, especially Cosalite, Lillianite (Klyakhin and Dimitreva, 1968), Bursaite (Klominsky et al, 1971) and Cannizzarite (Nechelyustov and Lebedev, 1967) although Heyrovskyite (Klominsky et al, 1971), Galenobismuthitite, Bonchevite (Kostov, 1958) and Ustrarassite (Sakharova, 1955) are accepted as mineral species. X-ray data for Bonchevite and Ustrarassite are, however, very similar to that of Bismuthinite. Several minerals of the PbS-Bi_2S_3 binary series such as Beegerite, Goongarrite (Warthaite) Bismutoplagianite, Chiviatite, and Cannizzarite have, now been discredited.

Data on Aikinite, Bismuthinite, Galenobismuthitite, Nuffieldite

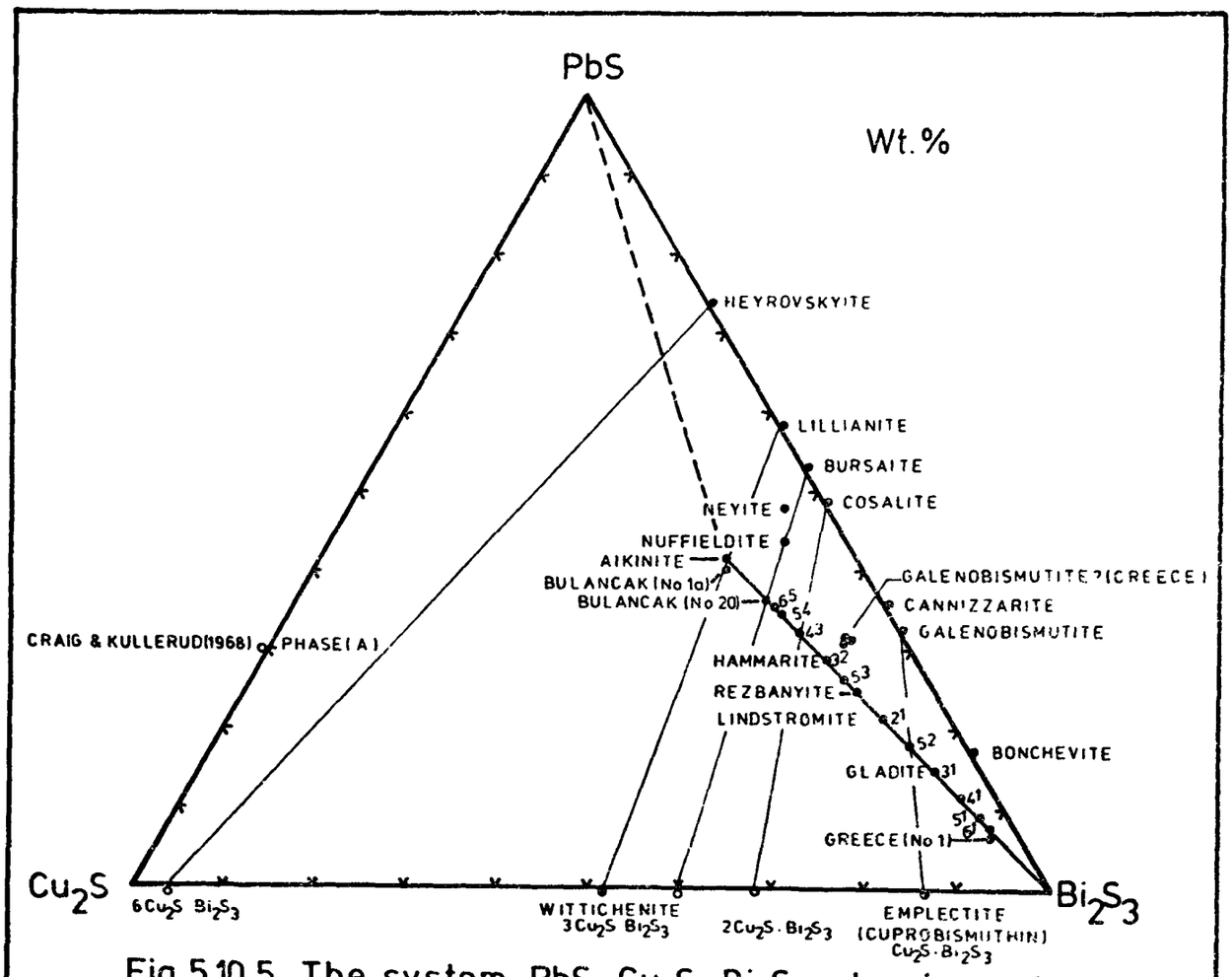

Fig 5.10.5 The system PbS-Cu_2S-Bi_2S_3 showing naturally occurring compositions (solid circles) including minerals from the Bulancak area. Stochiometric compositions are indicated with superimposed grid lines. Numbers represent Z^n aikinites according to Moore (1967).

(Kingston, 1968) and Neyite (Drummond et al, 1969) are now almost complete. The occurrence of Lillianite and intermediate members of the aikinite-bismuthinite solid-solution series from Sweden and Russia was described by Welin (1966), Borodaev et al (1970) and Borodaev and Mozgava (1971). Several Bi-Sulphosalts from Greenland were also reported by Karup-Møller (1973).

5C. DESCRIPTION OF INDIVIDUAL OCCURRENCES

5.11 Exploration activities and General Geology of Akköy Mine

This is the only deposit in the area that has been thoroughly explored by diamond drilling and it is believed that the mine reserves are accurately known.

The mine is situated 14 Km south along the Giresun to Inisdibi Village road which leaves Highway 20 some 2.5 Km west of Giresun City and follows Batlama Dere. The orebody is seen along Domuzdere which joints Batlama Dere approximately 150 m. SE of Adit No. 1.

Three exploration adits were opened by the owners in 1967-68. Each adit is approximately 15 m. long (Fig. 5.11). There is about 11 m. level difference between the lowermost Adit No. 1 and the uppermost Adit No. 3. Adit No. 2 and 3 were driven along the orebody at the overlying tuff contact where the roof of the adit is formed by tuffs. In Adit No. 1 only a 5cm. thick chalcopyrite vein was measured trending N30E and dipping about 10^{o}SE. Adit No. 2 and No. 3 were stopped when brecciated orebody replaced by strongly silicified dacite turned into quartzite-like rock. This is the exposed part of a 1 Km. long, 50 m. wide SW-NE trending silicification zone which follows biotite-andesite contacts to the SW of the mine and extends to the north cutting across Domuzdere Fault. This may suggest that surface outcrop of the orebody does not extend beyond the length of the adits to the south. A conical shape for the gently dipping orebody and brecciated dacite was suggested by the writer (MTA Rp. No. 982).

In 1971 a drilling program was carried out by EIE under the direction of METAG Ltd. for the Government Planning Organization to establish the reserve and extension of the orebody. 25 boreholes

FIG 5.11

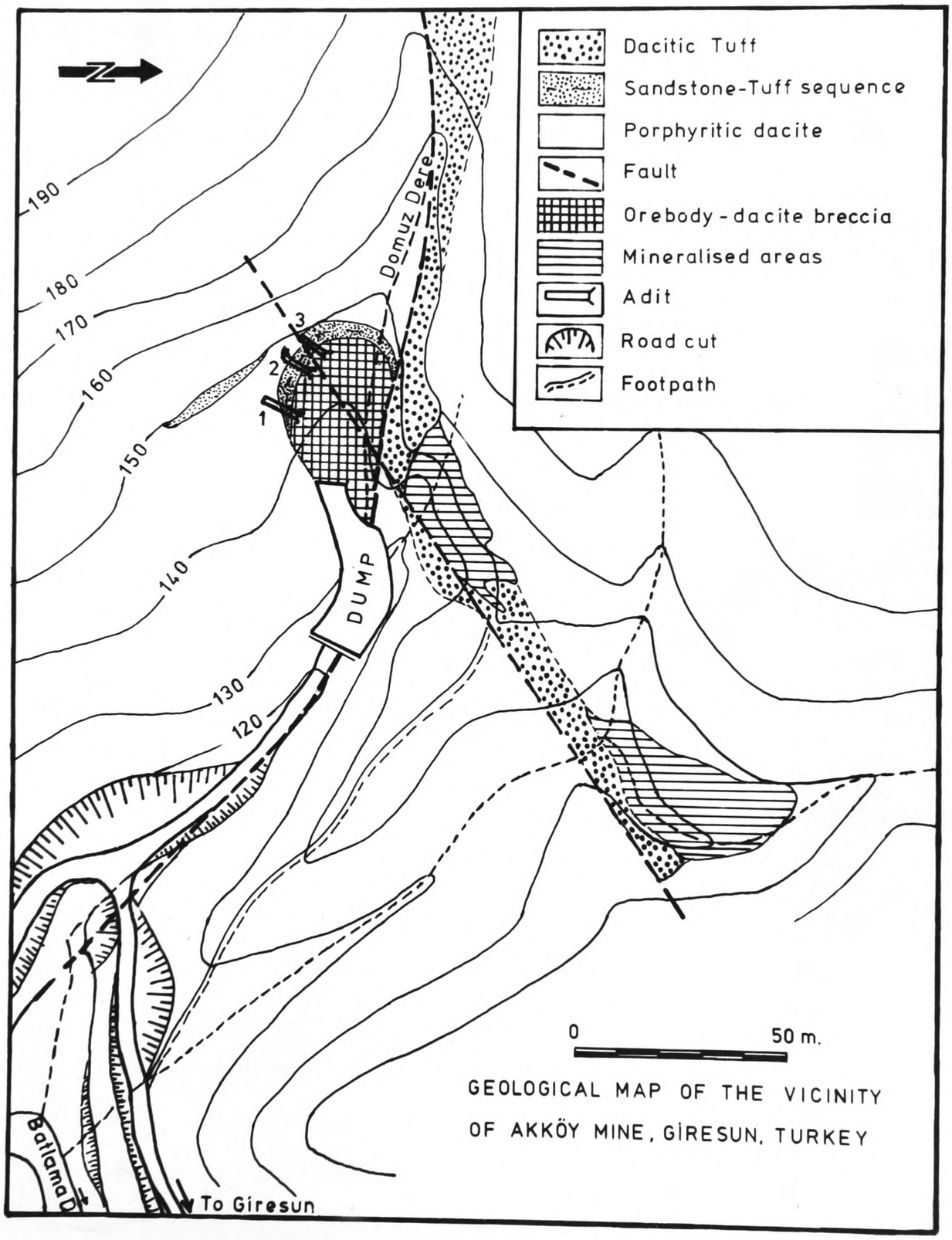
N
190
180
170
160
150
140
130
120
Domuz Dere
1
2
3
DUMP
Dacitic Tuff
Sandstone-Tuff sequence
Porphyritic dacite
Fault
Orebody - dacite breccia
Mineralised areas
Adit
Road cut
Footpath
0
50 m.
GEOLOGICAL MAP OF THE VICINITY
OF AKKÖY MINE, GİRESUN, TURKEY
To Giresun

totalling 2898.26m. were completed and 1,220,000 tons of ore with a 0.58% Cu and 3.36% Zn grade or 1,880,000 tons of ore with a 0.47% Cu and 2.86% Zn grade were estimated (METAG Rp. 1972). Unfortunately the writer was not able to see the borehole cores in 1971 when the area visited for sampling. The vicinity of the orebody was mapped by the writer in 1968 while the mine was active. Later the mine was abandoned and all the adits collapsed as stated in the METAG Report (1972).

The mineralization is located at the contact of the brecciated porphyritic dacite (Ore-bearing dacite) and dacitic tuff-sandstone layers which are best exposed between Adit No. 2 and No. 3(Plates 5.11.1 and 5.11.2). Between Adit No. 1 and No. 3 the overlying crescent shaped tuff outcrop forms a truncated anticlinal (cut by Domuzdere Fault) structure dipping 15°NE at the top of Adit No. 2 and 15°NW at the top of Adit No. 3 and almost horizontal in between. At the base, these layers start with a silicified, purple coloured, fine to medium grained tuffaceous sandstone layer showing graded-bedding, 1 to 5 cm thick (Fig. 5.11, plate 5.11.1). The sandstone passes upwards gradually into the fine-grained, kaolinized dacitic tuffs interstratified with some sandstone layers. This crescent shaped tuff outcrop is about 40 m across and between Adit No. 2 and No. 3 is displaced by another fault (Plate 5.11.2).

A zonal arrangement of the alteration around the orebody is recognized. Brecciated dull grey orebody forms the core of the strongly silicified central part of the whitish-yellow coloured silicified zone. This central silicification zone is enclosed in the second kaolinized,

Plate 5.11.1 No. 2 Adit Akköy Mine.

Plate 5.11.2 No. 3 Adit Akköy Mine.

sericitized and carbonitized alteration zone. At the outer marginal zone the dominant alteration processes are mainly albitization and chloritization.

The main mineralization occurs in the brecciated upper parts of the porphyritic dacite and there is a 1 to 5m. thick enriched zone from the dacitic tuff contact downward. The lower limit of ore deposition in the dacite corresponds with the lower limit of brecciation. Thus, ore grade is highest in the most brecciated upper region, tailing off gradually downwards into the unbrecciated dacite. This breccia may reach a thickness of 100m. (vicinity of A5 borehole). In the central parts of the breccia orebody copper is more abundant than zinc; at the margins the reverse is the case (METAG Rp., 1972). A dacitic (saddle ?) reef shape has been suggested by Pejatovic and Tesrekli (1970).

The ore has a massive, zinc-rich character at the top of the orebody along the breccia-tuff contact. Analyses (8,9) given by Pejatovic and Tesrekli indicate a Zn/Cu ratio of 8 to 11. Borehole results confirmed that a similar ratio was obtained at the bottom of the surface outcrop of the orebody while central parts are copper-rich. It can be suggested that the overall Zn/Cu ratio is approximately 6 as indicated by grade-reserve estimates.

According to Acar (1974) AAS analysis of borehole cores of Akköy Mine shows a Cd-enrichment with increasing Zn-contents over 1%.

Although the writer has not identified any significant limonite or chalcocite in the studied polished specimens, a 35-40m. oxidation zone has been found in boreholes A5 and A7 and a 5 to 8m. thick secondary enrichment zone (cementation) in boreholes A5 and A18 is reported in

METAG Rp. (1972) with chalcocite and covellite occurrence. At the contact zones between oxidation and cementation secondary malachite and azurite were formed as alteration products after chalcopyrite and possibly bornite. These alteration products can be seen between the orebody and the Domuzdere-Batlama Dere junction along Domuzdere water-course which form a fault line terminating the 35X45 surface outcrop of the orebody to the north.

5.12 Mineralogy of Akköy Orebody.

Pyrite, sphalerite, chalcopyrite, idaite, covellite and subordinate tetrahedrite and galena were identified as ore minerals and quartz, dolomite and baryte were identified as gangue minerals.

Pyrite is the earliest sulphide mineral in the paragenetic sequence if idiomorphic quartz crystals replaced by pyrite and sphalerite are excluded. It is found as cubic or skeletal and polygonal subrounded grains enclosed in and being replaced by chalcopyrite. Most of the cubic crystals show cataclasis with matching walls, fractures filled by chalcopyrite or sometimes replacement advanced along fractures. Some small cubic crystals enclosed in sphalerite show no sign of replacement in spite of advanced chalcopyrite replacement from pyrite crystal outlines towards sphalerite. These crystals may indicate a second generation as well as crystals protected from fracturing. In the six stages of the Akköy mineralization described in the METAG Report (1972) pyrite is found to form from the first to the fourth stages. The fifth and sixth stages consist only of quartz mineralization although it is found in all stages.

There are also pyrite crystals enclosed in sphalerite being replaced by chalcopyrite. Rounded pyrite grains arranged to form an atoll texture are also observed in chalcopyrite. In places pyrite crystals are sieve-like due to minute inclusions.

Sphalerite is the dominant sulphide mineral, occurring in xenomorphic, subangular grains and brecciated forms with corroded grain boundaries due to quartz invasion after brecciation. It is seen in bluish grey colours in plane polarized light and has faint brownish internal reflections. Etching with $KMnO_3$ + HCl has revealed lamellar twinning, cleavage and coarse granular character. The grains are also characterised by the absence of exsolution type chalcopyrite, although inclusions of varying sizes and veins are present. Only a few blebs were observed at very high magnification. On the other hand segregation veins of chalcopyrite may indicate that fracturing occurred during or before the unmixing of the chalcopyrite solid solution and thus chalcopyrite, segregated in the fracture or line of potential fractures forming a segregation vein (Edwards, 1965). These chalcopyrite veins and inclusions in sphalerite are selectively replaced, in addition to galena, by tetrahedrite in preference to sphalerite. On the other hand a sphalerite wedge projecting into chalcopyrite was left unreplaced by tetrahedrite which replacing chalcopyrite across the sphalerite wedge. This is believed to indicate the younger nature of sphalerite if relations are considered in three dimensions: Some tetrahedrite inclusions in sphalerite were believed to be pseudomorphs after chalcopyrite. The total amount of tetrahedrite does not exceed 1% in the polished specimens.

Sphalerite is replaced by chalcopyrite along quartz boundaries and in places replaces pyrite. In places sphalerite seems to replace chalcopyrite along quartz-chalcopyrite boundaries possibly indicating a second generation which has been reported to form in the first and third stages of mineralization (METAG Rp., 1972). Some darker, inclusion-free small grains may belong to this younger generation sphalerite.

Chalcopyrite is seldom sufficiently abundant to be visible in hand specimens. Paragenetically most of the chalcopyrite grains appear to be formed later than and replacing sphalerite but some embayments and large grains of chalcopyrite are found intergrown with sphalerite in mutual boundary texture which may indicate contemporaneity. However as explained earlier, many segregation veins or veinlets intersecting sphalerite grains are very common.

In polished specimens almost every pyrite granular aggregate, or cubic crystals enclosed in chalcopyrite, show cataclastic textures and varying degrees of replacement by chalcopyrite. Polygonal, rounded pyrite grains showing atoll textures suggest a partial replacement by chalcopyrite. Due to, possibly, second generation sphalerite replacement a sieve-like poikilitic texture develops. Sphalerite-chalcopyrite replacement textures are less decisive than pyrite. Because it could be interpreted in both ways in terms of age relations.

Irregular replacement bodies or rounded blebs of galena are seen enclosed in chalcopyrite in insignificant amounts. In addition to tetrahedrite galena replaces chalcopyrite selectively.

Idaite. This mineral has not previously been reported from Akköy Mine. Bornite was mentioned in the METAG Report (1972) but it was not described in detail and it was not stated where it exists. In specimens collected from the adits and surface outcrop of the orebody the writer has not observed any bornite. Due to the absence of any convincing evidence the writer is inclined to believe that idaite has been misidentified as bornite which seems to show exsolution lamellae of chalcopyrite but exact examination shows that the reddish-orange coloured grains are actually idaite. It's vidid greenish polarization colours are characteristic. Chalcopyrite exsolution lamellae are arranged along crystallographic directions showing a lattice texture in idaite grains. Idaite areas in between the lamellae may originally have been bornite. This possibility cannot be ruled out completely. Idaite grains with smooth curved boundaries in chalcopyrite show mutual boundary relationship and usually develop along the chalcopyrite-sphalerite boundary. Although some grains extend on both side there is a tendency to develop towards chalcopyrite. In places idaite segregation veinlets with no exsolution lamellae were observed in chalcopyrite as well. Some grains tend to replace chalcopyrite veinlets cutting across sphalerite.

A second idaite form is different from the idaite with exsolving chalcopyrite lamellae. This pinkish-purple coloured form shows distinct reflection pleochroism with bright greenish polarization colours and often is found to be replaced by covellite.

5.13 Dariköy, Üzümlük Occurrences.

The fissure veins are exposed for about 800m. along the Uzümlük Dere Obuzu (watercourse) running from Dariköy Village cemetary northwesterly, joining Kucukgure Dere at 160m. altitude (Map 2, 6B). Dariköy is situated by 8-9 Kilometers south along the Giresun-Yaykinlik Village road which leaves the main Highway 20 4 Km. west of Giresun City after the Batlama River Bridge crossing.

Underground mining was carried out at 3 places along the watercourse named as Yukarı (Upper) Uzümlük at 315m. altitude, Orta (Middle) Uzümlük at 280 m. altitude, and Asagı (Lower) Uzümlük at 220 m. altitude. The Asagi Uzümlük occurrence was mined actively until 1968 mainly for lead. The veins at these localities were either opened using explosives, by pit mining or by adits but all the works have been carried out considering the veins individually. There is no work known to the writer which considers that the N(30-50)W trending vein exposures might belong to the same single vein. This is first time has been suggested by the writer and is shown on map 2 (2B).

There are at least 3 intersecting vein systems between the Yukari and Asagi Uzümlük localities trending E-W, N-S, and N(30-50)W. Another vein follows a SW-NE trending fault cutting through the altered Lower basic series and overlying rhyodacitic rocks between Orta and Asagi Uzümlük. This vein was not explored although partly opened. During mining activities in this area attention and priority have been given to the lead-rich pockets along the exposed parts of the veins.

5.13.1 Yukarı Uzümlük. Exploration activities started in here opening small prospects along the intersecting vein system. Later two adits were driven to follow S75E and S40E trending veins at approximately 315 m. altitude. The writer was able to study a 40 cm. wide S75E trending vein extending along the left hand side wall of a 12 m. long adit in intensely altered rhyodacitic rock (Fig. 5.13.1). The adit was timbered along its entire length and accessible in 1968 but when the area was revisited in 1971 all the adits were found to be caved or collapsed.

A second adit was driven about 9 m. along the 10-15cm. wide S40E trending vein but the adit entrance is reached by a rather narrow 7 m. long U-shaped trench. There was no timbering by the time the adit was mapped by the writer in 1968. 4m. above this level a small pit, several meters wide, was opened to expose the vein before this adit was driven.

15 meters to the northwest, just below these adits, a third adit was driven at the 305m. level., similar to the 215m. level adits but no mineralisation was found in this adit which extends 3 meters in the N60E direction then turns E-W for another 3 meters. At the entrance of the adit mineralisation was observed in a breccia zone. Again the adit entrance is reached after crossing a 15m. long, narrow trench opened in the S68E direction.

5.13.2 Orta Uzümlük. Surface outcrops of the two N-S and E-W trending veins were opened and the N-S trending vein was explored by an 8m. long adit at the 270m. level in the easterly dip direction

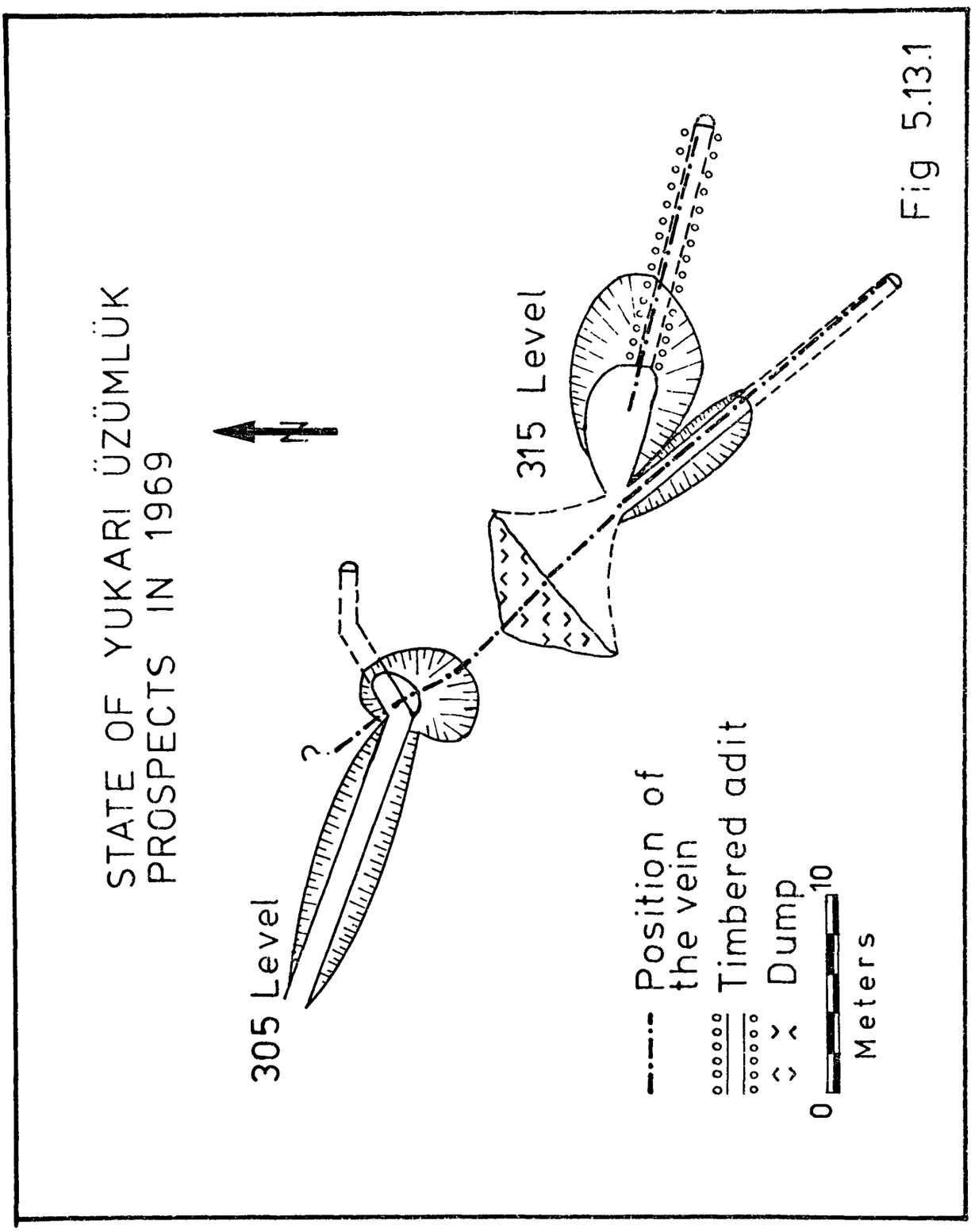
STATE OF YUKARI ÜZÜMLÜK
PROSPECTS IN 1969
N
305 Level
315 Level
?
Position of the vein
Timbered adit
Dump
0
10
Meters

Fig 5.131

after 1968. The vein is said to be cut at the 6th meter of the adit. Due to the dangerous situation of the adit in 1971 it was not possible to study the vein underground, so specimens were collected only from the surface outcrop exposed about 6-8m. above the adit where the thickness is 5-20cm.

The E-W trending vein, assumed by the writer to be the extension of the N70W trending vein at Yukar Uzümlük, is seen in a 1 meter wide andesitic rock. On both contacts of the breccia with the altered rock, 2 to 10cm. thick massive vein occurs. In the central parts of the vein zone coarse-grained, angular to subangular, altered andesitic rock fragments cemented by reddish jasper and finer rock fragments form the breccia (Plate 5.13.2). The breccia is extensively pyritized and cut by quartz which in turn seems to be replaced by reddish jasper in places. Similar breccia was observed along the N40W trending vein in the Asagi Uzümlük pits at about 220m. and 160m. altitudes where Uzümlük Dere and Küçükgüre Dere joins, but the rock fragments in this breccia are less coarse than those described above. It is possible that the N40W trending vein follows a fault zone along Uzümlük Dere. The isotherms obtained from fluid inclusion study of the Uzümlük vein minerals indicate an ore-channel for the solutions in the direction of the Uzümlük Dere watercourse (Fig. 6.8).

5.13.3 Asagı Uzümlük. Large scale underground mining activity was carried out in 1967-68 by Sevki Sayar who owned the concession and developed and exploited the vein mainly for lead. The prospect,

as mapped by the writer with the aid of Brunton compass and tape measure, is shown in Fig. 5.13.3. The vein is exposed along the "Üzümlük Dere watercourse and was first mined along the surface exposure. When the pit face became too steep an adit was driven from the 215m. level about 5m. below the pit level. The surface outcrop of the vein and the 215m. level were joined by a gentle downward incline which served as an ore-pass following the vein. Extension of the vein beyond this is not seen along the 215m. level adit (Fig. 5.13.3).

Approximately 330m. horizontal distance was measured between the surface outcrop of the vein on the pit face and the entrance of the 305m. level of the Yukari Üzümlük prospect in the direction of N18W(S18E). There is only limited information about the Üzümlük occurrences but Ryan's (1960) description "... the deposit is lead-zinc-copper in veins fractured andesite, the veins meeting at a stream bed and branching off with strike N47W and dip 45°W; strike N70W and dip 40°W. Vein widths are not given. Mineralisation is galena, sphalerite, pyrite and chalcopyrite. The fractured andesites have a gouge-like mud of exceptional specific gravity. Assays across the width of the vein showed 28.12% Pb, 6.45%Zn, 3.57%Ag, 0.02 oz Au/ton. Assay of the geuge showed 0.72% Pb, Zn, 0.39 oz Ag, 0.05 oz Au/ton. Random sample 2.20% Pb, 1.60% Zn, 0.53 oz Ag, 0.08 oz Au/ton ...." suggests that the specimens were collected from the Yukari Üzümlük locality. The information about the occurrences was given originally in Akol and Alpay's Report (MTA Rp. No. 2216).

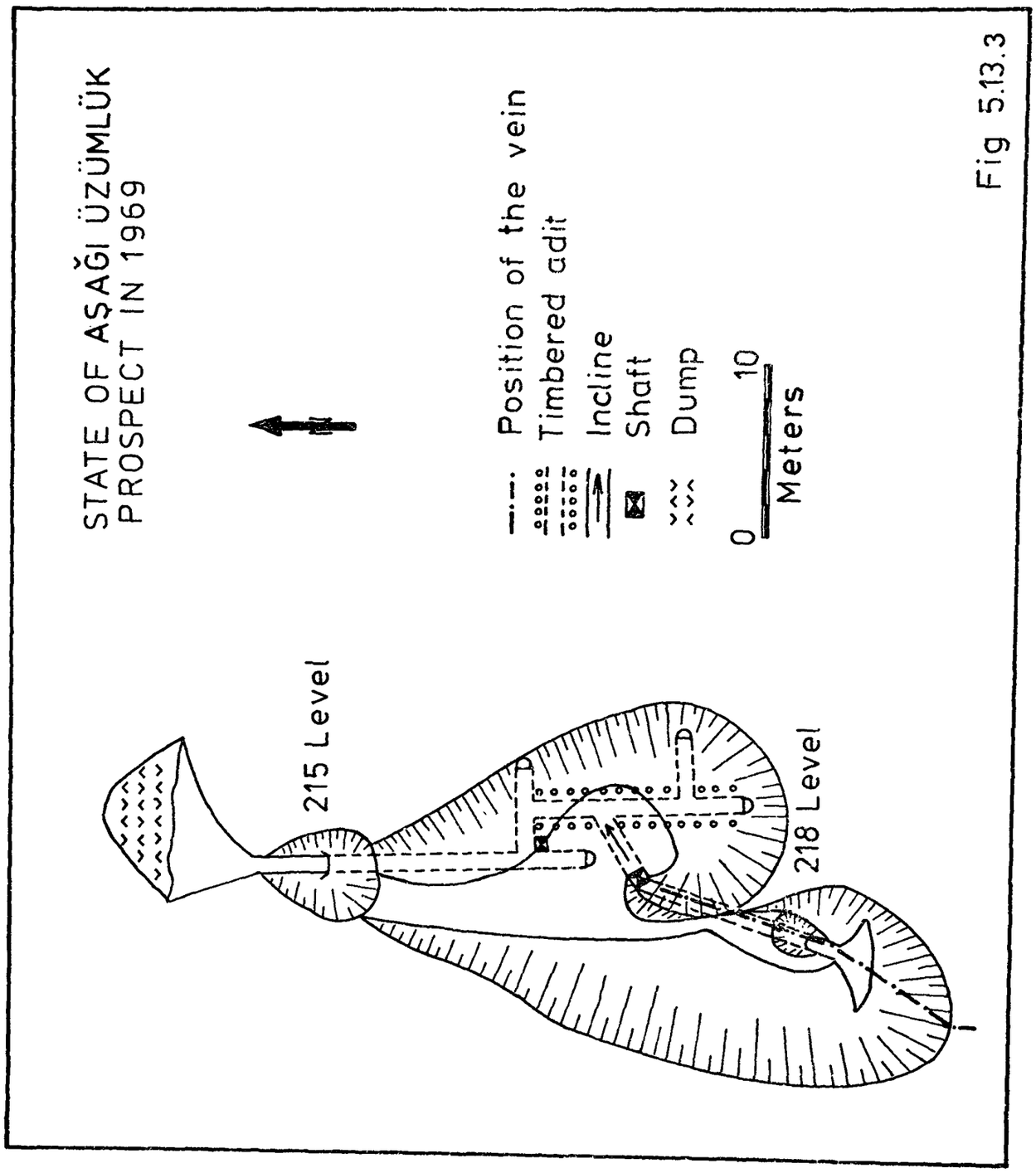
STATE OF AŞAĞI ÜZÜMLÜK
PROSPECT IN 1969
Position of the vein
Timbered adit
Incline
Shaft
Dump
0
10
Meters
215 Level
218 Level

Fig 5.13.3

In table 5.13 Electron Probe analysis and homogenization temperatures of the sphalerites were given. Cadmium shows a tendency to increase with depth, iron remaining fairly constant in the range 0.46 to 0.70 %. Isotherms indicate the highest homogenization temperatures found along the NW-SE trending Uzümlük Dere fracture zone (see Fig. 6.8).

5.14 Mineralogy of the Üzümlük Veins. Several polished specimens were studied from each vein sample collected from Uzümlük Dere occurrences. Replacement textures are dominant, secondary cerussite and covellite being seen mostly at deeper levels of the veins as alteration products after galena and chalcopyrite. The following minerals were identified during ore microscopy study and a paragenetic sequence can be given as follows:

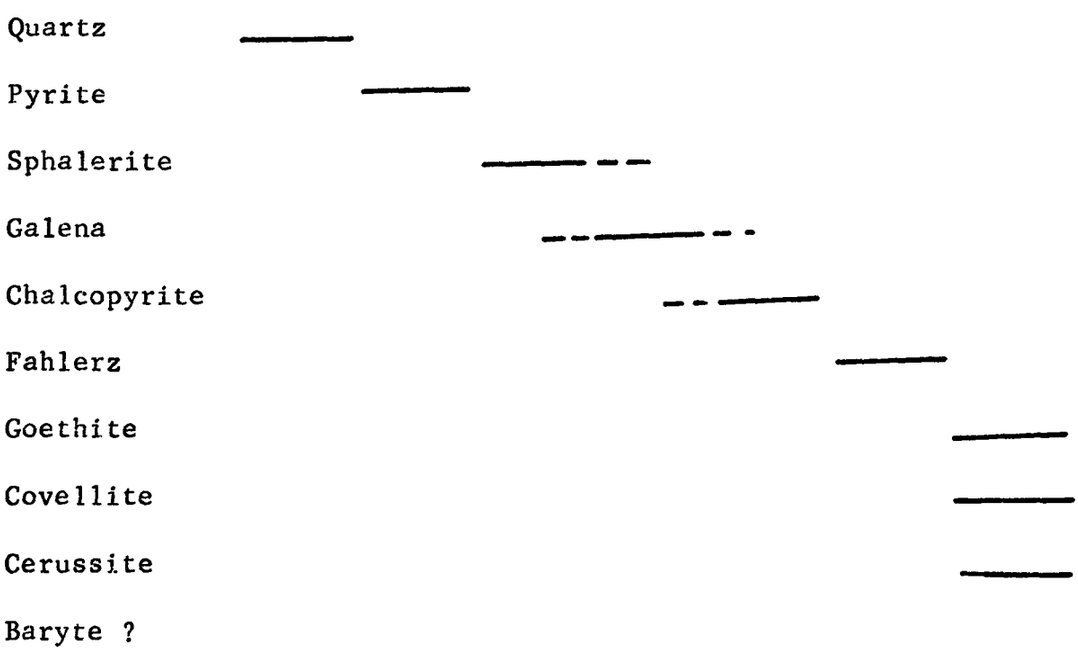

TABLE 5.13 Microprobe Analyses and Homogenization Temperatures of the Üzümlük Veins.

Locality	Altitude	Specimen No.	Zn	Fe	Mn	Cd	S	Homogenization Temperatures (°C)
Yukari Üzümlük	320	91A *	66.29	0.52	0.06	0.57	32.60	230
	310	91B **	66.38	0.46	0.05	0.57	32.65	165
Orta Üzümlük	270	93 **	65.81	0.70	n.d	0.65	32.56	250
	260	92	66.30	0.47	0.09	0.68	32.64	240
Asagi Üzümlük	220	94 *	66.20	0.51	n.d	0.76	32.66	225
	170	95 *	65.79	0.66	n.d	1.18	32.56	220
	160	97 *?	66.41	0.67	n.d	0.53	32.58	185

* (**) On the same vein system

n.d = Not detected

Quartz: Early formed idiomorphic quartz crystals were replaced by sphalerite, galena and selectively by fahlerz minerals forming atoll, ring textures and skeletal forms. There are also abundant unreplaced idiomorphic quartz crystals enclosed in sphalerite and galena. Veinlets of late stage quartz are found cutting through sphalerite grains.

Pyrite: Late stage pyrite is found as small cubic crystals or crystallites forming stringers while early formed pyrite forms cubic crystals or crystal aggregates of interlocked pyrite grains or crystals showing triple junctions. These early crystals are mostly replaced by sphalerite and galena and contain chalcopyrite inclusions. Cataclasis can be seen to some extent being replaced along fractures. Late stage pyrites tend to show slightly higher reflectivity and no relief contrary to early ones.

Sphalerite: Is seen yellowish, honey-coloured, and transparent in the disc wafers prepared for fluid inclusion studies and is the second oldest sulphide mineral in the paragenetic sequence after pyrite. It is found as xenomorphic forms with corroded grain outlines due to late stage quartz invasion. Brecciated grains are healed by these late stage quartz veins. It contains emulsion type fine chalcopyrite inclusions and large enclosed grains. Stringers of euhedral to subhedral second generation pyrite crystallites develop along fractures or healed fractures. Sometimes at the end of stringers a large grain of pyrite may be seen. Sphalerite usually replaces early formed pyrite crystals and crystal aggregates as well as early quartz crystals. Chalcopyrite penetrates along the cleavage planes of sphalerite in places forming

islands in specimen 97 (Asagı Uzümlük). Cleavage and displacement along twin lamellae of sphalerite were observed after etching. The majority of the veins are sphalerite-rich.

Galena: Although in places this is interstitial to sphalerite and replaces it together with pyrite, it is usually found in allotriomorphic forms filling the spaces between quartz crystals with polygonal straight outlines. It forms with atoll textures when it replaces hexagonal-shaped quartz crystals centrally or pyrite crystal aggregates. It fills the fractures of cataclastic pyrite in the Orta Uzümlük N-S trending vein but also replaces it to some extent. There are also segregation veinlets of galena cutting through sphalerites. In this locality it is found extensively altered to cerussite, along cleavage planes and grain boundaries, together with lesser amounts of covellite. Corroded grain boundaries are also amongst the common features. When it replaces quartz along crystal boundaries galena is also seen being replaced by fahlerz.

Chalcopyrite: The amount of chalcopyrite increases relatively in the Orta and Asagı Uzümlük veins. It shows different forms of replacement with pyrite and sphalerite, usually replacing these minerals. Although it seems to be replacing galena, its contacts with galena are less decisive - possibly deposition is overlapping with galena. It is found as allotriomorphic forms or interstitial to sphalerite and pyrite, and forms sieve-like poikilitic textures with sphalerite in specimen 97. Alteration to goethite was observed in the Orta Uzümlük

E-W trending vein. In specimen 97 it is extensively replaced by covellite.

Fahlerz: Although it is common to some extent in all specimens more Fahlerz is found in the Asagı Uzümlük vein. It has olive-green or greenish-grey colours showing no internal reflections. It shows different replacement forms such as veins along cleavage planes of sphalerite, selectively replacing quartz crystals projecting into chalcopyrite or chalcopyrite veinlets in sphalerite. It also replaces grain boundaries of allotriomorphic chalcopyrite along quartz contacts, or along enclosures of pyrite crystal aggregates. Veins and veinlets or patchy replacement forms are also not uncommon.

5.15 Kornalı Dere Occurrences.

500 meters to the northeast of Dönbül Tepe, between the 590 level adit of Etibank along the Şişpelit Dere - BL-5 borehole (Kas[illegible]atak Mh., 4E) line and Yomasapagi (3E) along the eastern and western flanks of Kornalı Dere at least 18 vein exposures were mapped in about 1 Km^2 area. The veins along Şişpelit Dere (which is found half way between Dönbül Tepe and Dinekkaya Tepe, running southeasterly, joining to Kornalı Dere at about 500m. altitude) are largely developed by Etibank and mined by the Demir Export Company (plates 5.15a, b). At 505m. altitude along Şişpelit Dere about 600 tons of polymetallic ore was recovered from the Demir Export Company pit at the entrance of a 27m. long adit driven N35W parallel to the Şişpelit Dere, but no ore was found along the adit except some malachite alterations (K. Grad Field Observations No. 266, MTA Rp. No. 982, 1970, plate 5.15b)

Plate 5.15a View of Etibank waste tip below 571 Adit near Dönbül Tepe (Sispelit Dere).

Plate 5.15b The state of Demir Export Company Şispelit Dere prospect in 1969.

Most of data about the Şişpelit Dere veins were obtained from Etibank's exploration activities which started at 592 altitude in 1968. A 40m. long adit was driven N60W but vein was not cut along the adit. At 600m. altitude just above this adit the polymetallic vein was measured as N75E (Plate 5.15a). The second N50W trending fracture parallel to the watercourse, consist of pyritic quartz vein. The chemical analysis of the polymetallic ore at this exposure gave

11.12% Pb

8.16% Zn

2.10% Cu (MTA Rp. No. 982, 1970)

An IP survey was carried out around this exposure along the profiles across Sispelit Dere by Etibank (Kaynak, 1972). According to the survey Kaynak describes the following results:

1. The (Pyrite) Vein No. 1 which is parallel to the fault line (Şişpelit Dere watercourse) extends about 175m. northwesterly. Due to topographically thickening overburden (rhyodacitic rocks, 3D) it reaches to the point beyond the depth of penetration of the IP method.

2. Vein-2 (trending N75E) follows the tuff contact (3D). This is the longest and most continuous vein of the area and extends in E-W below the tuff formation. Geophysical anomalies suggest that this is the main lode. A third vein beginning from the entrance of the adit extending about 225m., parallel to the main lode was also described.

   Assuming a 75cm. average thickness and 50m. depth, for the veins

to the head of Şişpelit Dere, Kaynak (1972) estimates about 200,000 tons of polymetallic ore.

After the geophysical survey, a second 100m. long adit was driven at 571 level approximately N50W (Fig. 5.15). The underground work was continuing when the area was visited in autumn, 1973. About 750 tons of polymetallic, breccia ore (see plate 3.4.4b) was exploited along with stoping work. The specimens collected from 600m. level outcrop, 571 level adits and Demir Export Company prospect at 505 level were studied by the writer along with Electron Microprobe analysis and fluid inclusion measurements. The following table shows the electron probe analysis and homogenization temperatures together with cell-sizes of sphalerites:

Specimen Number	Altitude	Zn	Fe	Mn	Cd	S	Cell Size	Homo-genization Temp.
46/1	600	66.30	0.82	0.14	0.44	32.45	5.4124	272°C
48	505	66.08	0.78	0.19	0.41	32.65	5.4122	252°C

The unexpected higher homogenization temperature at the higher levels of this vein may be explained with the horizontal temperature zoning to the west of these occurrences (see fluid inclusion studies chapter 6 and Fig. 6.8).

The relationship of the veins along Şişpelit Dere is less decisive. It seems that the 570-600 level vein is branching off southeasterly on both sides of the Kasyatak Fault. One branch extends downstream to join exposures at the Demir Export Company prospect (see Fig. 5.15).

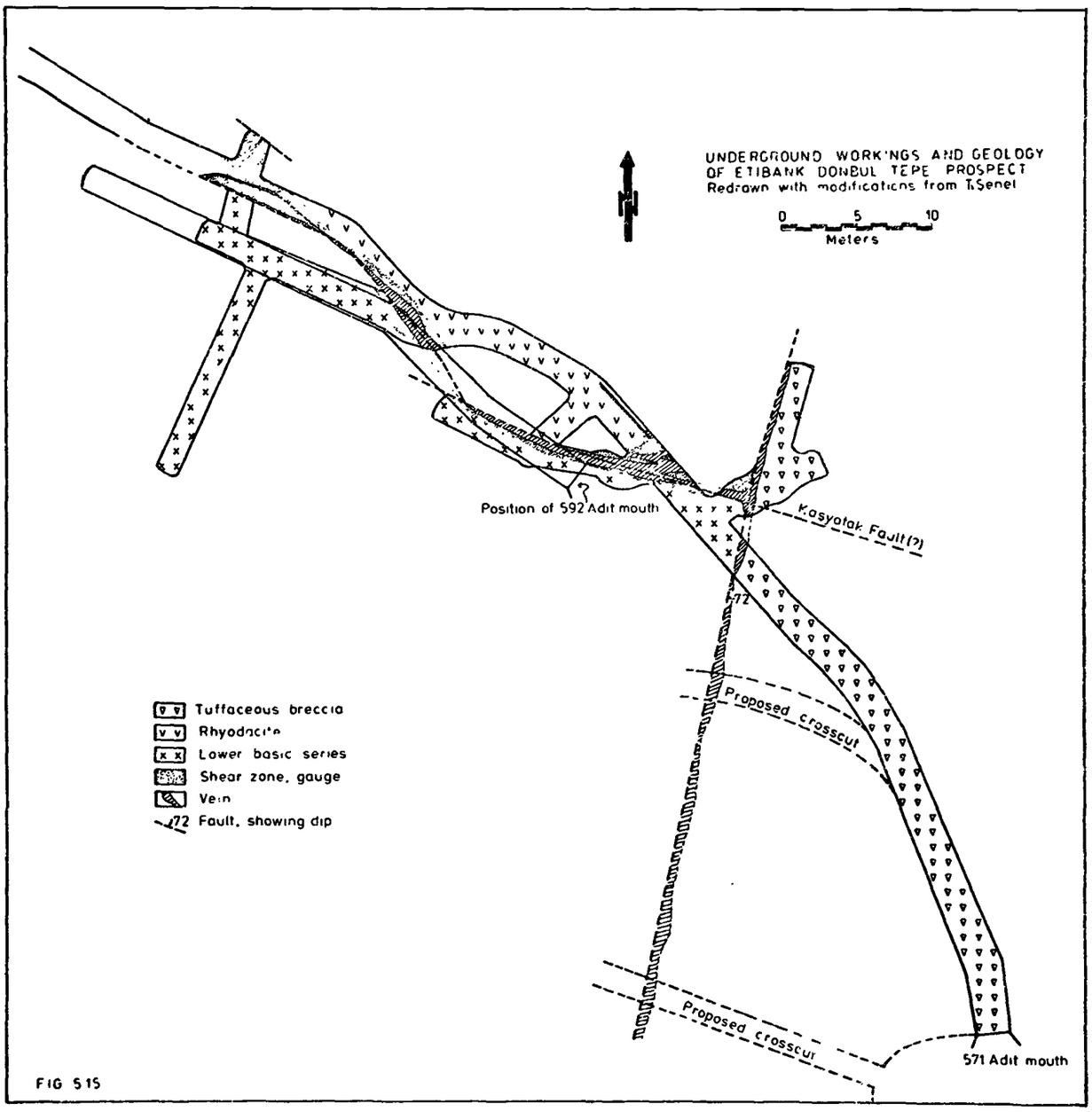
UNDERGROUND WORKINGS AND GEOLOGY
OF ETIBANK DONBUL TEPE PROSPECT
Redrawn with modifications from T.Senel
0 5 10
Meters
Position of 592 Adit mouth
Kasyotak Fault(?)
72
Proposed crosscut
Proposed crosscut
571 Adit mouth
Tuffaceous breccia
Rhyodacite
Lower basic series
Shear zone, gauge
Vein
72 Fault, showing dip

FIG 5.15

It can be inferred that the other branch extends southeasterly almost parallel to the Kasyatak Fault more than 2Km. towards the BL-5 borehole (4E) at Kasyatak and possibly extending on beyond Büyükküre Dere towards Hamidiye Village (5F).

The mineralogy of the veins is fairly simple. The dominant textural relationship is produced by extensive replacement of pyrites and sphalerites by chalcopyrite and galena. All these minerals are also replaced by Carbonate ganque. At deeper levels cerussite and possibly anglesite develop by replacing galena along cleavage planes and grain boundaries, showing concentric bands of colloidal deposition along with covellite and limonite (mainly goethite) after chalcopyrite.

Pyrite: This shows zoning, cataclasis, parting along cleavage planes, and poikilitic texture due to sieve-like chalcopyrite inclusions and replacements. There are characteristic forms of an advanced stage of pyrite replacement by chalcopyrite, i.e., in many specimens collected from the Kornali Dere area large chalcopyrite grains are seen to be spotty due to minute replacement relics of pyrite similar to intergrowth appearance (Plate 5.6.5c). In places pyrite is seen weakly anisotropic.

Sphalerite: Always contains oriented inclusions, stringers and emulsion type exsolution blebs of chalcopyrite. It replaces early formed pyrite crystals and has enclosures of skeletal and idiomorphic quartz crystals. It is usually found to be replaced by galena and veined by covellite in deeper levels.

Chalcopyrite: Is usually veined by digenite and altered to covellite + limonite giving a mottled appearance.

Galena: Is found interstitial to sphalerite and replaces it extensively. It replaces chalcopyrite in places. Itsometimes fills the fracture along cataclastic pyrite crystals and replaces it to some extent.

Fahlerz: Usually replaces galena, giving a patchy appearance, and in places chalcopyrite as well. The amount of fahlerz tends to increase at deeper levels.

Marcasite: Was identified in places as individual crystals and grains. It seems to be more common along the vein in the 571 level adit of Etibank along Şişpelit Dere.

An E-W trending vertical vein at 530m. altitude along the Kornali Dere watercourse (3E) has not drawn attention so far for any exploration work but the writer has found for the first time in Turkey a rare bismuth-sulphosalt, an aikinite-bismuthinite solid-solution in association with chalcopyrite, maracasite, digenite and pyrite. It has been studied in detail and described in Chapter 5.7.2. In this locality another N60W trending vein is found intersecting with this vein and can be inferred to extend in the direction of the Etibank BL-10 borehole in Büyükküre Dere to the south of Kasyatak Mh. (4E).

The veins in the vicinity of Kornali Dere are listed in the Table 5.10.

CHAPTER SIX
GEOTHERMOMETRY

6A. SPHALERITE GEOTHERMOMETRY

6.1 Trace Element Partition Coefficients.

Partition of trace elements between coexisting sulphides was proposed by Friedman (1949) as an applicable geothermometer and the thermodynamic principles involved in the distribution of trace elements and factors affecting the partition coefficients between coexisting minerals have been discussed extensively by McIntire (1963) and Ghosh-Dastidar et al (1970).

Barton and Skinner (1967) have suggested the use of trace element partition as opposed to the trace element content of a single mineral to establish the environmental conditions of ore deposition. Bethke and Barton (1971) have demonstrated experimentally that "The distribution coefficients are independent of composition and vary sufficiently with temperature to permit reasonably precise temperature estimates" and illustrated their application in the temperature range 200-600^{o}C combined with fluid inclusion data (Fig. 11,12). The fractionation of Cadmium, manganese, and selenium between coexisting sphalerite and galena pairs was applied to the Darwin Mine by Hall et al (1971). The temperatures obtained in this study from four different pairs, varied considerably. As pointed out by Ghosh-Dastidar et al (1970) the data resulting from distribution patterns are linear, curvilinear or scattered depending on several factors such as equilibrium between coexisting minerals, variations in pressure, temperature and change in the ratio of activity coefficients. Some limitations on the applicability of the method described by Bethke and Barton (1971) are as follows:

a. the method must be applied within 200-500^{o}C temperature range.

b. Polytyping of natural sphalerites may lead to under estimation of temperature of formation.

c. Re-equilibration after deposition in Galena is quite common especially in high-temperature deposits.

d. Partition of selenium between Chalcopyrite and sphalerite, in general, is not applicable, i.e. insensitive to temperature and pressure changes.

One of the most important limiting factors on the applicability of this method is that the concentration of Cadmium, Manganese and selenium in the impoverished phase of the coexisting sulphides is very low and extremely pure concentrates are needed before the analyses are made. As can be seen from the table given by Ivanov (1971), the overall trace element contents of most of the common sulphides are below the detection limit of the Electron Microprobe.

In several polished specimens unzoned galena and sphalerite parts were analysed for Mn, Cd, and Se but these elements were undetectable in the galenas. As will be explained and seen in plates 6.4.5.a,b,c the solid particles entrapped in fluid inclusions in sphalerites indicate that trace elements may not be sufficiently dilute before the deposition has occurred and this may effect the partition coefficients considerably. Due to the limiting factors explained, fluid inclusions have largely been employed for geothermometric measurements.

6.2 FeS Content of Sphalerite

No attempt was made to apply the sphalerite geothermometer (Kullerud, 1953) to the Bulancak Sulphide deposits because electron microprobe analysis of samples gave only a maximum of 2.28 % Fe in solid solution with sphalerite. Examination of about 300 polished ore specimens

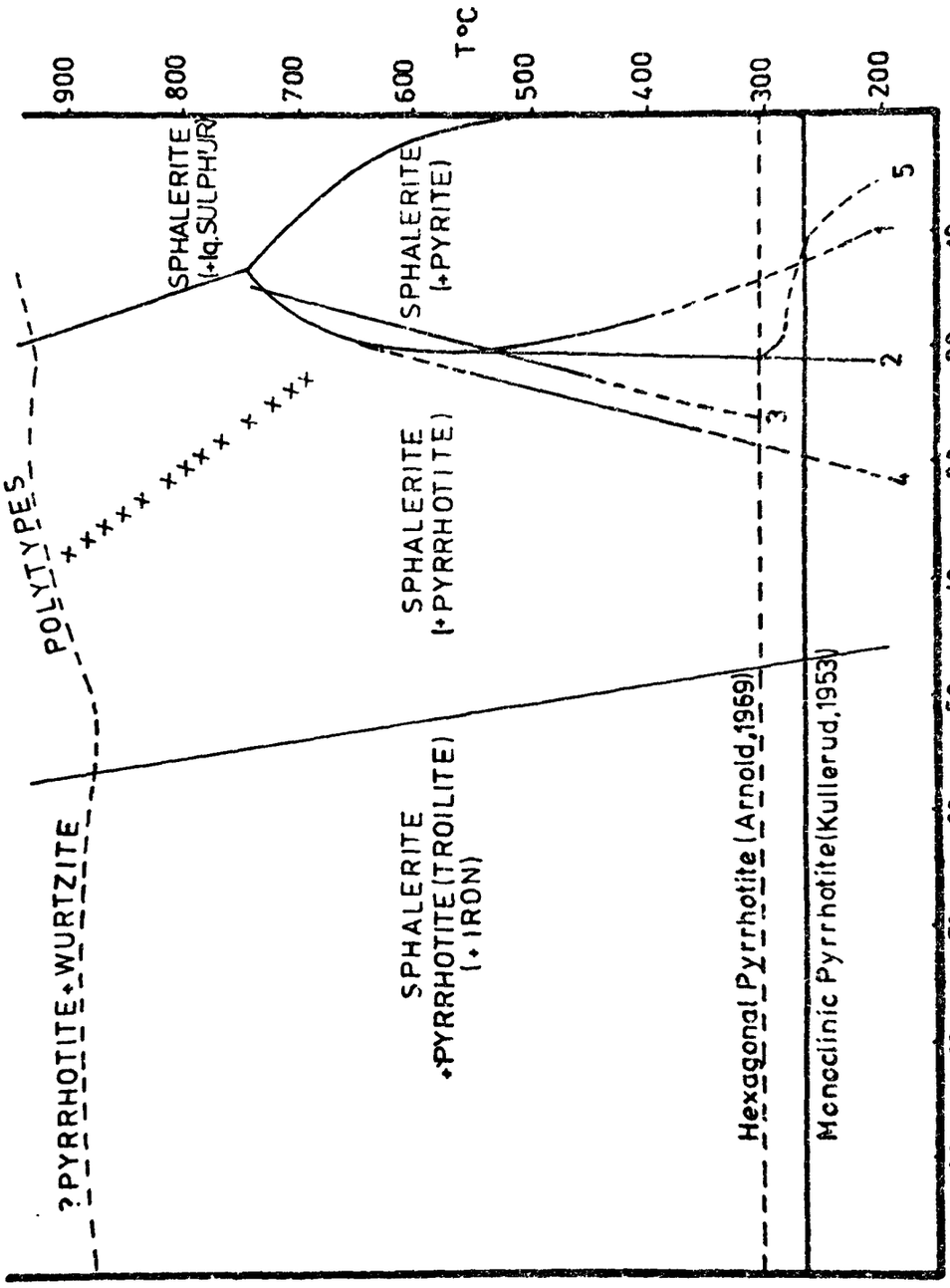

Fig 6.2 Composition of sphalerite in equilibrium with various other phases in the Fe-Zn-S system. Phase relations projected on the FeS-ZnS binary. The experimental points of Kullerud (1953) are shown by crosses. Curve (1) Barton & Toulmin (1966), (2) Boorman (1967), (3) Einaudi (1968), (4) Chernyshev & Antilogov (1967), (5) Brownie & Lowering (1973). Modified after Barton & Toulmin (1966).

from the area also indicated that no pyrrhotite but only pyrite, exists in equilibrium with sphalerite. Recent work of Barton and Toulmin (1966) has shown that for the equilibrium assemblage pyrite-sphalerite, the iron content of the sphalerite may vary widely as a function of the fugacity of the sulphur, and that the "sphalerite thermometer" for such assemblages is not yet calibrated. At present, there are several conflicting published versions of phase relations in the system Zn-Fe-S in the temperature range of greatest geological interest below 550°C. Scott and Barnes (1971) who have confirmed Boorman's (1967) results of constant composition of 20.7 $\pm$ 0.6 mole % FeS in sphalerite in equilibrium with pyrite and pyrrhotite in the temperature range between 550 and 300°C (Fig. 6.2) suggest the use of sphalerite as a geobarometer rather than geothermometer.

More recently Browne and Lovering (1973) have found sphalerite with 7.1 mole % FeS at 219°C is in equilibrium with pyrite and pyrrhotite and suggest the sharp decrease in the FeS content of sphalerite between 280 and 240°C may result from the phase change from hexagonal to monoclinic pyrrhotite, supporting the prediction of Scott and Barnes (1971). This evidence confirms that the FeS content of sphalerite is not a reliable indication of formation temperature for low temperature deposits, leaving the fluid inclusion measurement as the most reliable method.

6B. FLUID INCLUSION GEOTHERMOMETRY

6.3 Introduction

In view of the recent serious questioning of the applicability of the pyrrhotite and sphalerite geothermometer (Arnold, 1969; Barton and Toulmin, 1966) and among the numerous techniques that have been used

for geothermometry in recent years, fluid inclusion geothermometry seems to have emerged as the most informative and dependable method with which to study ore deposition and its physico-chemical environment. There is, furthermore, a possibility that homogenization temperatures and densities obtained from fluid inclusions can be used to find or pinpoint new ore occurrences when combined with other complementary data. Although there are many discussions both favourable and unfavourable about the validity of the data obtained from fluid inclusions, during the last decade, several detailed studies have shown that the data obtained from inclusions in the minerals of epithermal ore deposits exhibit high consistency (Sawkins, 1966). The minerals of the Bulancak sulphide veins were formed at relatively low temperatures and pressures and there can be little doubt that the data obtained from fluid inclusions in these minerals relatesto the physico-chemical conditions under which they were deposited.

At the time of sampling the ore zone and the surrounding country rocks, the writer was not aware of the existence of fluid inclusions in the sphalerite and gangue minerals such as quartz, dolomite, calcite and barytes. Consequently only a small number of gangue minerals were available for fluid inclusion study despite the fact that quartz was found along with sphalerite in almost every specimen studied.

6.3.1 Previous Research: There has been no previous study of fluid inclusions in the ore and gangue minerals of the mineralisation of the area South of Bulancak. Temperatures given by Tugal (1969) in the range 240-400^{o}C for the similar Karadere vein deposits (Ünye, Ordu) near to the investigated area were based on Kullerud's (1953) sphalerite

geothermometry. This is the first fluid inclusion study in Turkey to the writer's knowledge.

6.3.2 Materials Studied: Samples of both ore and gangue minerals were prepared for fluid inclusion study. For this purpose several disc wafers (doubly-polished, 0.5 to 1.0 mm. thick plates) were prepared from sphalerite, quartz, barytes, calcite and dolomite. Much of the material examined proved to be relatively unsuitable for inclusion studies for one reason or another. The most common was the opaqueness of some sphalerite specimens and too small and single-phase inclusions in gangue minerals.

Sphalerite is a difficult mineral to work with because its very high index of refraction (2.37) makes viewing difficult.

The temperatures reported for inclusion in sphalerite would be expected to be erroneously low, as the heavy black borders, a result of total reflection at the edges of the inclusion due to the extremely high index of refraction (compared with the water solution = 1.36 and liquid CO_2 = 1.18), provide abundant hiding places for tiny bubbles remaining at temperatures not below the true homogenization temperatures. Thus some inclusions in sphalerite, in which the very tiny bubble hiding along the inclusion wall showed rapid Brownian movement at 180°C, homogenized finally at 235°C. Some cases of nucleation to a larger bubble above the homogenization temperature were observed in sphalerites and barytes, but these results were discarded.

In addition to the natural imperfections, sawing, grinding and polishing of samples can produce surface disturbances that may penetrate to surprising depths even in hard minerals such as quartz. Thus, during the sawing of a clear quartz crystal with a diamond saw one may

frequently see fractures form just wide enough to be visible owing to total reflection at their margins. Even polysynthetic twinning is thought to be obtained due to the preparation procedures. These imperfections may cause the fluid to leak artificially.

Most of the quartz samples are translucent, rather than transparent because they contain large number of minute inclusions that disperse the light. This milky appearance may be due to exsolution of impurities on cooling, or minute solid inclusions trapped during growth of the crystal. Where inclusions are particularly abundant the crystal appears to be milky. Inclusions in calcite might be expected to leak more readily than those in quartz because the inclusions generally fall near cleaved surfaces. Attempts failed to study fluid inclusions in calcite from more than one locality.

Barytes in particular was difficult to work with. Although many of the baryte specimens were very rich in fluid inclusions most of them were apparently secondary and single phase, or grains shattered during freezing and after reaching temperatures over 200^{o}C during heating as a result of a series of explosions. Movement of pigmenting fluids along fractures and cleavage planes or funnel shaped linked imperfections in some specimens studied resulted in the formation of a cover of dark colour in the inclusion under investigation and spoiled it.

Dolomites, apart from their milky appearance, show similar characteristics to barytes during heating and freezing experiments.

It was hoped to conduct fluid inclusion studies on all available gangue minerals but many of these minerals were found to be either remarkably uniform and free from inclusions or else the inclusions were below the limit of resolution of the microscope currently used.

The most time-consuming activity of this entire investigation was microscopic study and classification of inclusions prior to any experiment. Photographs of the inclusions were taken before the experiments and these were used to calculate bubble to fluid ratio using a planimeter on the enlarged equivalents. Rough sketches were drawn of each inclusion before heating and freezing experiment to avoid confusing conclusions measured for freezing and intended for later use in heating experiments.

Many dark coloured sphalerite wafers did not appear promising before microscopic study to locate fluid inclusions but the writer found rather good primary inclusions in the end.

6.4 Classification and Problems of Inclusions:

6.4.1 Primary Inclusions: As noted by Roedder (1962b) inclusions can be created in several different ways. One of the most common is by dendritic or branching growth of a crystal. When this is followed by a solid perfect growth that covers the imperfect region, portions of the ore-bearing fluid from which the crystal was growing are trapped in the open spaces. Anything that temporarily halts or slows the growth of a small part of the crystal, such as another mineral grain, a globule of an immiscible liquid or gas bubble, may also cause trapping of fluid (Roedder, 1962b, 1967). When crystal growth is complete, imperfect regions, or voids, are completely sealed from the external environment. Continued cooling results in contraction of the fluid causing the appearance of a vapor bubble, which is essentially a vacuum, if a gaseous phase is not present. Inclusions formed in this way are called primary because they form simultaneously with the enclosing crystal and constitute a sample of the fluid in which the crystal grew (Plates 6.4.1 a-f).

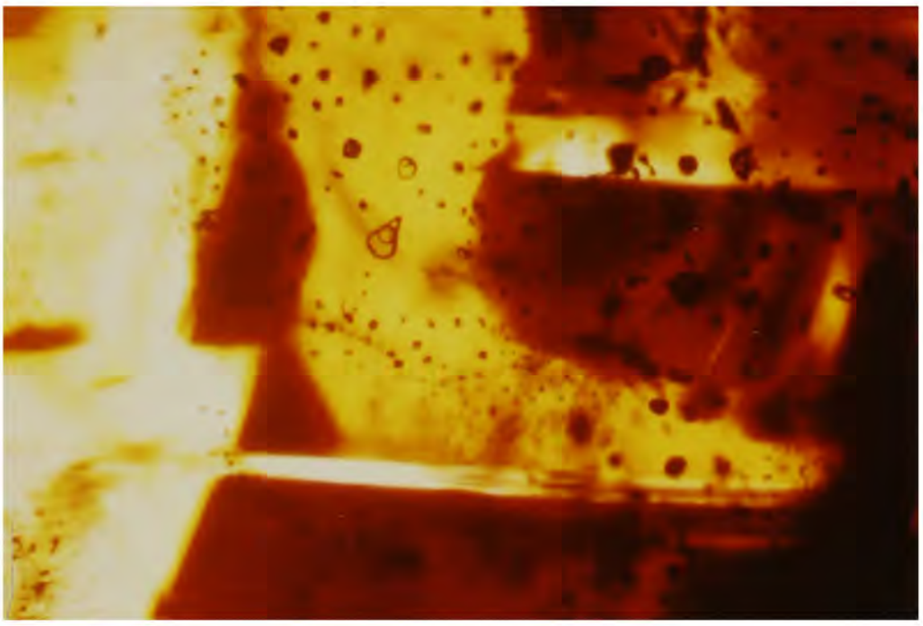

Plate 6.4.1a Primary fluid inclusions (in sphalerite).

Plate 6.4.1b Similar to 6.4.1a.

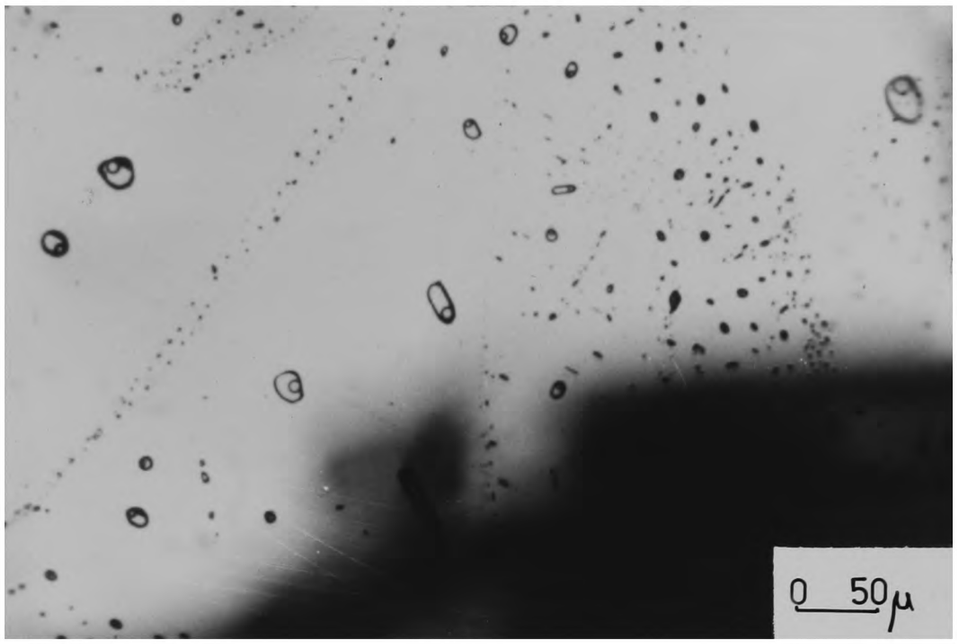

Plate 6.4.1c Isolated primary inclusions with planes of secondary inclusions (in sphalerite)

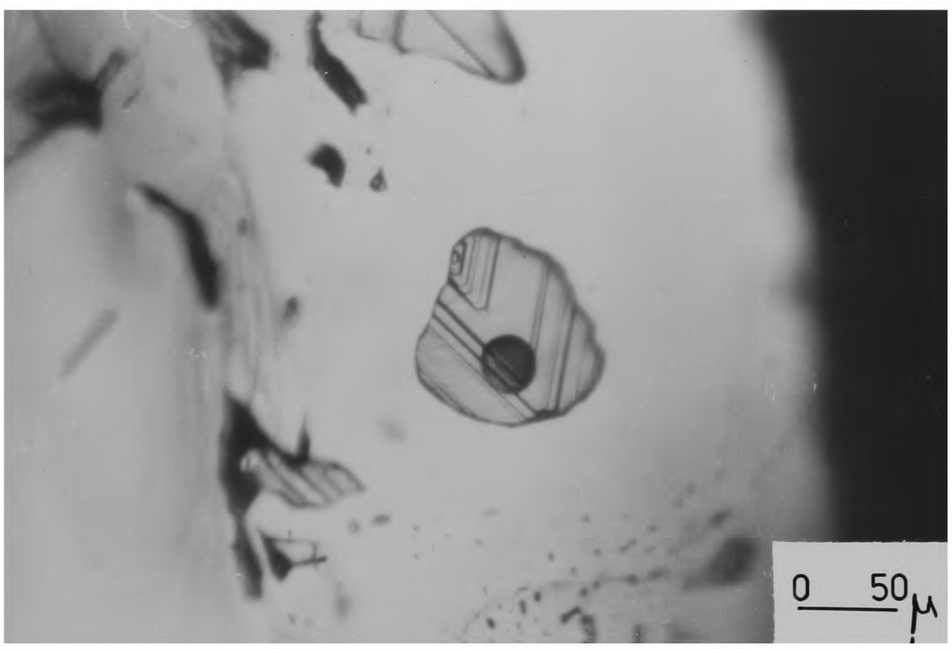

Plate 6.4.1d Primary fluid inclusion showing faceted negative crystal form (in sphalerite)

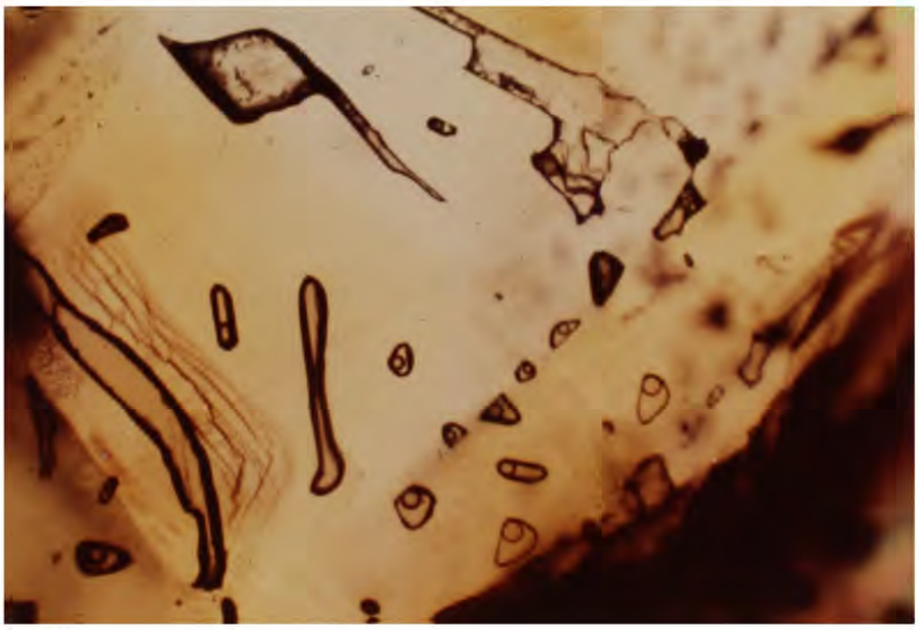

Plate 6.4.1e Fluid inclusions showing a relationship with primary colour banding (in sphalerite).

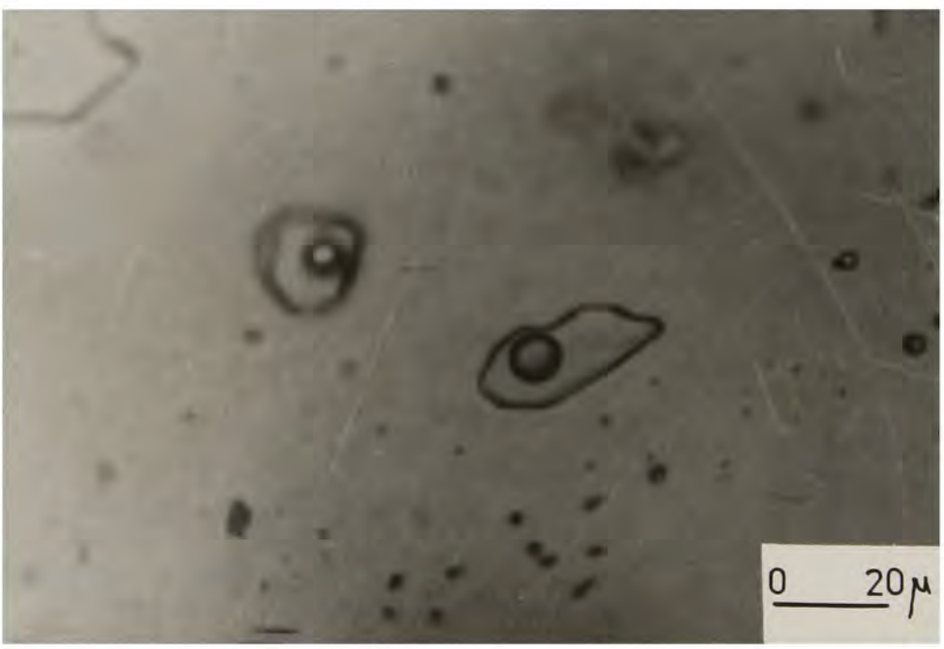

Plate 6.4.1f Isolated primary fluid inclusions in quartz.

6.4.2 Secondary inclusions originate in the rehealing of cracks in a crystal and indicate that the mineral has undergone post-crystal fracturing and has then been bathed with fluids of probably different composition and temperature. These are easily identified as those occurring along healed fractures that completely crosscut the host crystal or at least reach one exterior face.

There is a problem of distinguishing between primary and secondary inclusions. Criteria for this distinction have been given in several places in the literature (Bailey and Cameron 1951; Ermakov and others, 1965; Roedder, 1967) and will not be repeated here.

6.4.3 The term pseudo-secondary has been introduced by Ermakov and others (1965) to indicate inclusions of both primary and secondary origin (Plates 6.4.3a-d). This type is common especially in small fissures cutting across some of the inner zones of the crystal that do not reach the outer zones. The distinction between the pseudo-secondary and secondary inclusions often proved difficult. Clear-cut examples of pseudo-secondary inclusions initiating from an interior growth surface and extending towards the core of the crystals are rare, but when they cross crystal growth boundaries without offset, and form networks of whispy trains of minute inclusions along these fractures they are easily identified.

Most of the inclusions examined in sphalerites are relatively large and scattered and seem totally unrelated to fractures and yet cannot be clearly correlated with the primary features of the host. These were accepted as primary because of the difficulty in visualizing any reasonable secondary mechanism to explain them

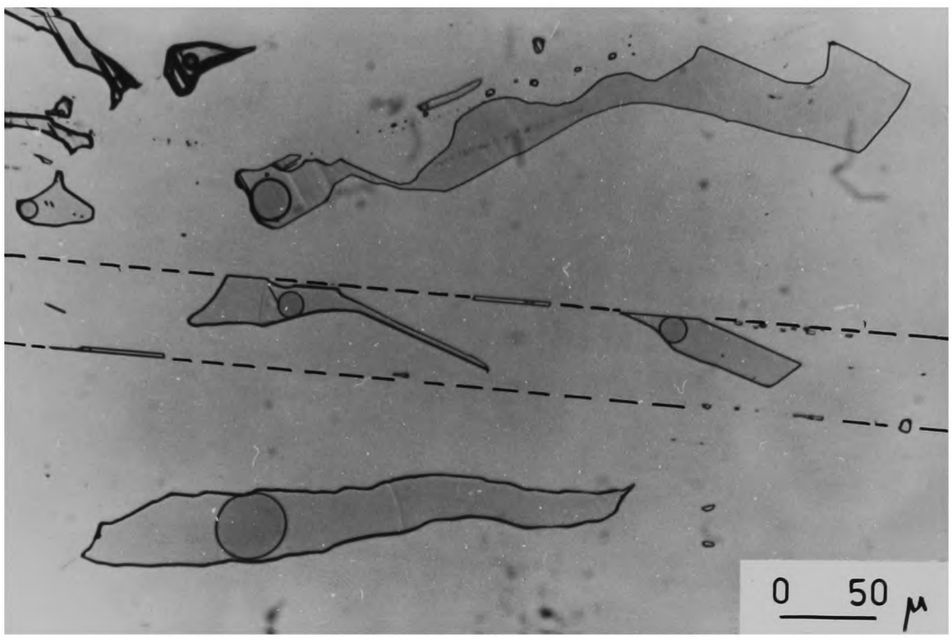

Pláte 6.4.3a Planar pseudosecondary inclusions showing some orientation with crystallographic directions (in sphalerite)

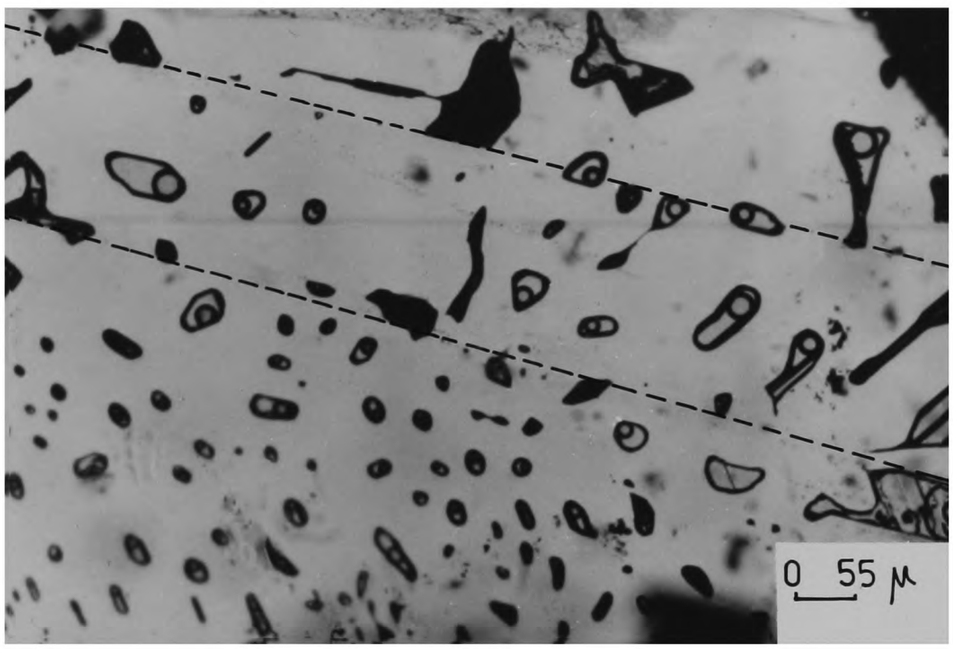

Plate 6.4.3b Faceted pseudosecondary inclusions (in sphalerite)

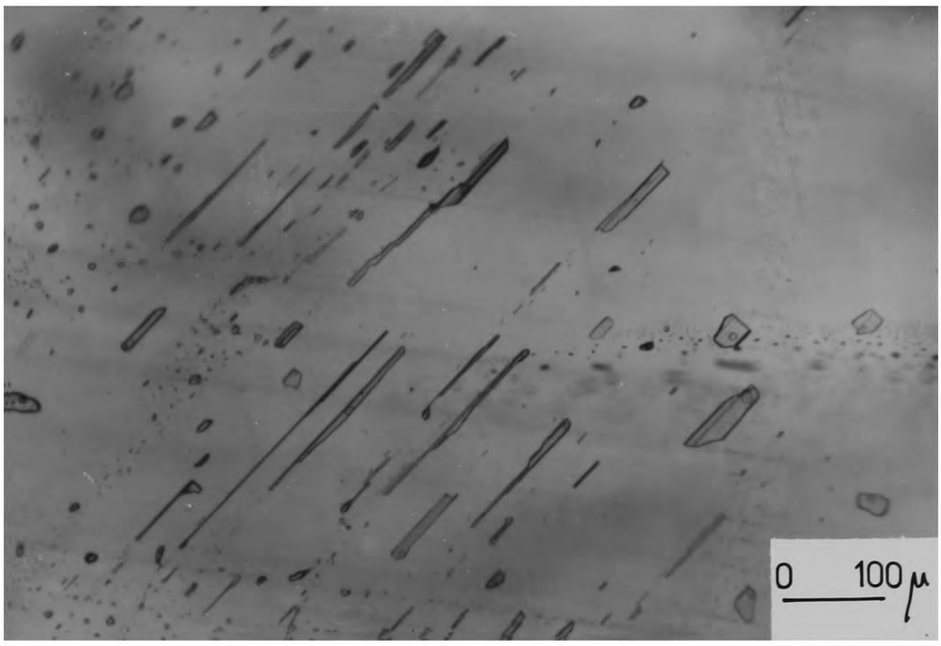

Plate 6.4.3c Planes of similarly orientated pseudosecondary inclusions showing stages of necking down (in sphalerite).

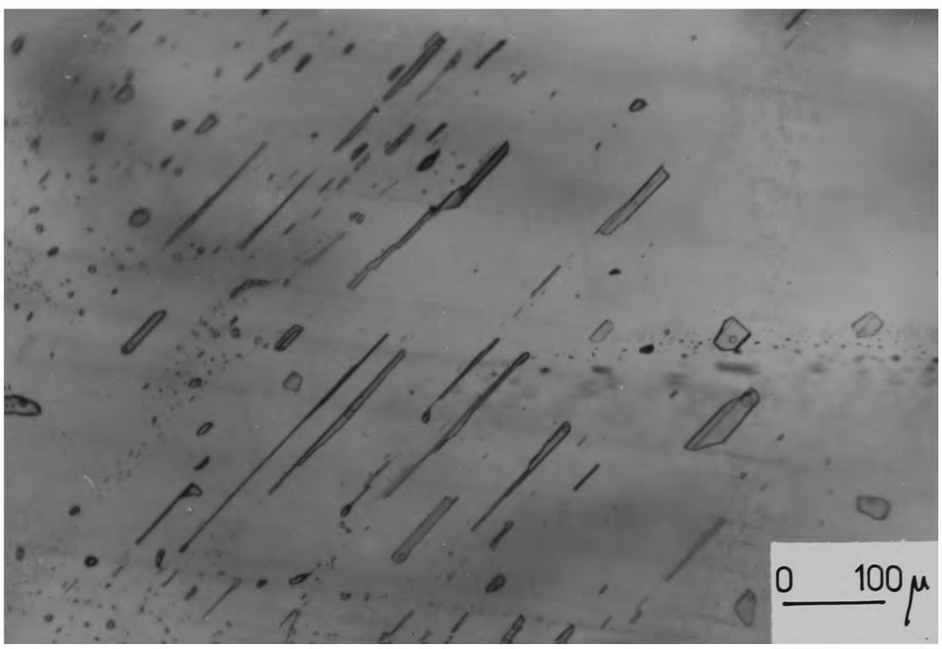

Plate 6.4.3d Secondary (pseudosecondary?) fluid inclusions in quartz.

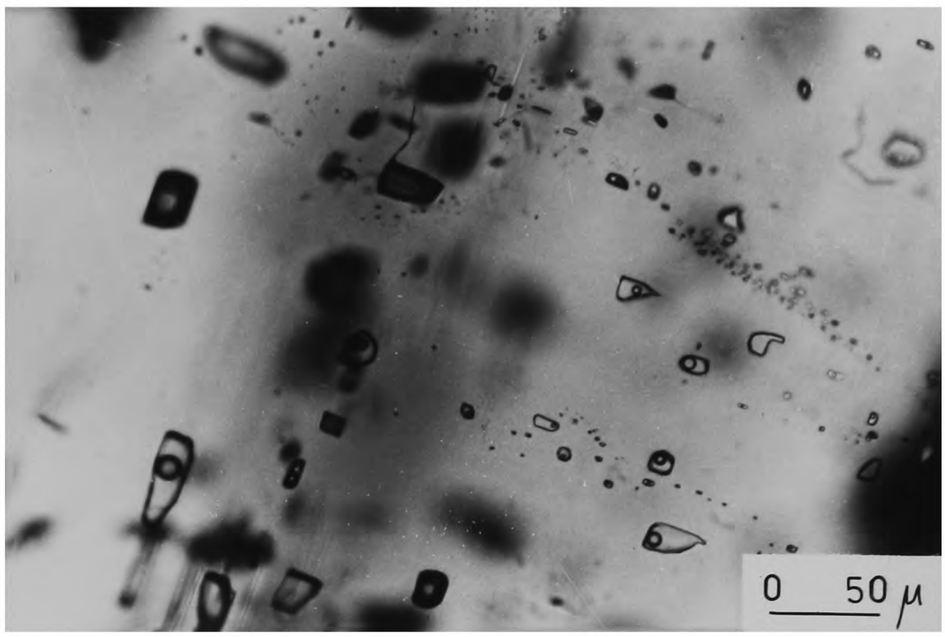

Plate 6.4.4a Gas-rich, Liquid-rich and one phase inclusions in baryte.

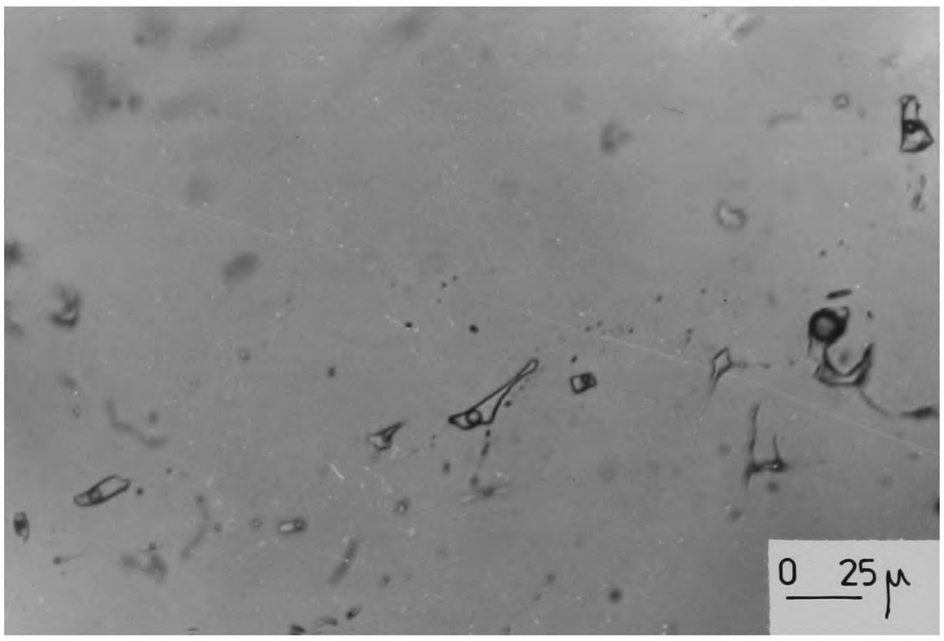

Plate 6.4.4b Secondary inclusions in quartz.

besides, several samples of sphalerite show colour banding and growth zoning (Plates 6.4.1a,b). These colour bands were later analysed for Fe, Mn and Cd distribution by electron microprobe. Primary inclusions showing the "staircase effect", thought to be due to pinching and swelling during crystal growth, were also observed along with tabular, needle-like, bullet-like, triangular, spheroidal and irregular forms.

In quartz, barytes and dolomites single phase inclusions and inclusions with linear structures were avoided and only scattered fairly large inclusions were accepted as primary.

6.4.4 Types of inclusions: Although several types of inclusion were distinguished, the great majority were of the liquid-rich type. These are characterized by high degrees of filling with the vapor content ranging from a few percent to 36%. All liquid-rich inclusions homogenized at temperatures ranging from 90 to 340°C. Salinities varied from 14% down to 4% (equivalent weight percent NaCl) in sphalerites, 10 to 1% (almost fresh water) in barytes and 8 to 3.5% in quartz. The range of salinity of the inclusions tends to decrease from sphalerite to quartz.

All-liquid inclusions were frequently seen in barytes as well as sphalerite. Those in sphalerite were thin, flattened, film-like inclusions. They may be dilute liquids trapped below 70°C (Roedder, 1967). Nucleation of a small bubble in some of these inclusions was observed during freezing experiments. Failure to nucleate the gas phase in liquid-rich inclusions may result in one phase, all liquid, low temperature inclusions. In one sphalerite specimen (plate 6.4.4c-d)

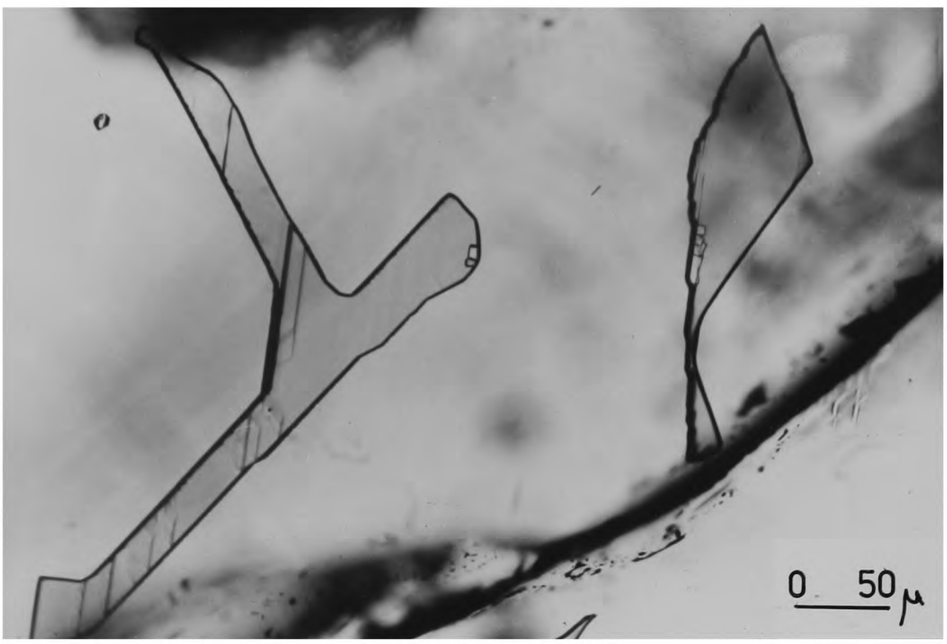

Plate 6.4.4c Gasless inclusions with isotropic daughter minerals (in sphalerite).

Plate 6.4.4d Enlargement of daughter minerals (in 6.4.4c).

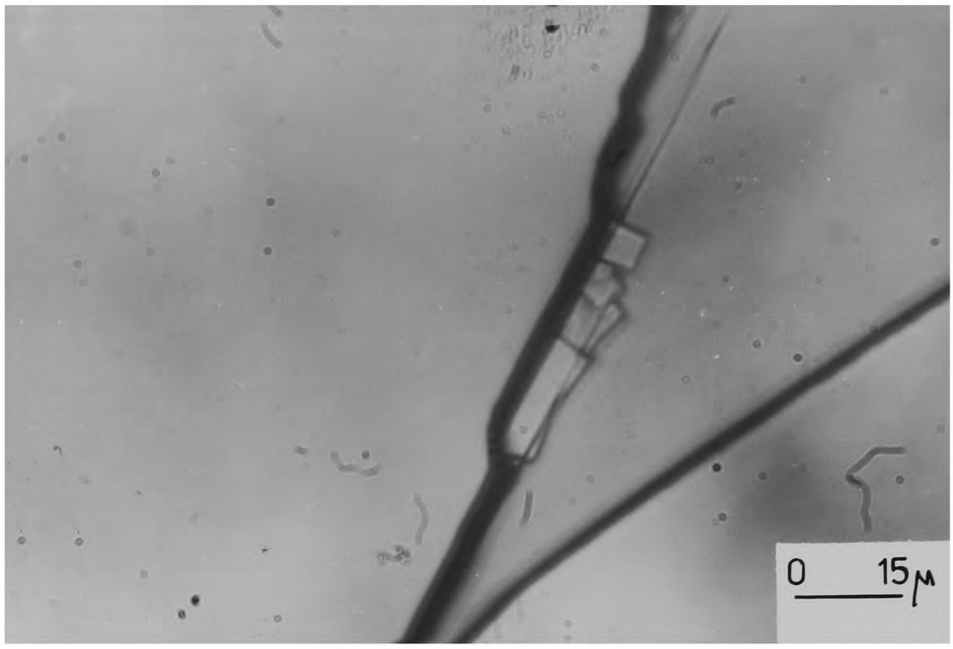

Plate 6.4.4e Enlargement of daughter minerals (in 6.4.4c).

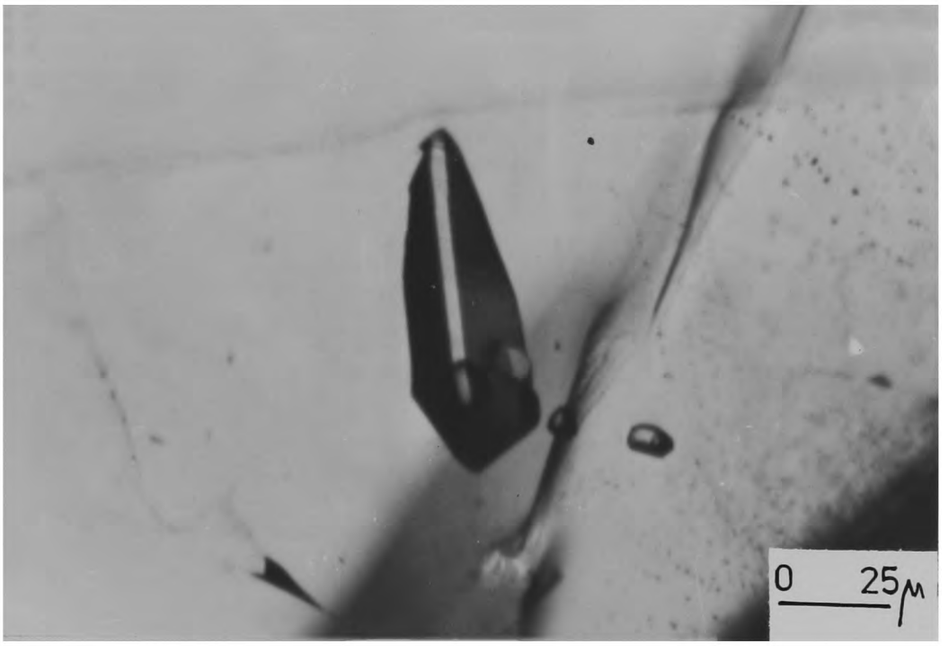

Plate 6.4.4f Sharply faceted three phase inclusion (in sphalerite).

one, possibly pseudosecondary, inclusion was found without any gas bubble but with daughter salts grown along the inclusion walls. These particular daughter minerals did not dissolve even at temperatures as high as 200°C and a liquid leakage was suspected (Plates 6.4.4c-d). In another sphalerite specimen, a halite crystal was also identified due to its isotropy and cubic shape (OTA-85, Plate 6.4.4f).

Gas-rich inclusions were also seen (OTA-21, Plate 6.4.4a) in barytes and sphalerites but these were not studied due to limitation on the heating stage and resolution of the microscope.

6.4.5 Opaque Captive Minerals: As is explained by Ermakov and others "... In such cases solutes that are similar to the substances of the host crystal may precipitate as a "film" on the walls (due to the crystal structure of the host), while other materials will come out of the solution as independent "daughter" minerals". Minerals are able to capture and to preserve particles of the medium in which their formation takes place. At the same time they may also take up some solid substances crystallizing concurrently with the minerals. Good examples of opaque captive minerals in sphalerite (OTA-29, OTA-38, Plate 6.4.5a,b) were seen. Two bubbles separated by a captive mineral were (OTA-38, Plate 6.5c) also observed. These opaque captive minerals are usually cubic or rectangular in shape. They were checked by a hand magnet but no sign of magnetism was observed. As hematite is not very common in the area and since pyrite is the only mineral formed earlier than sphalerite, so captive minerals are thought to be pyrite particles in cubic crystals but the possibility of chalcopyrite can not be discarded when the widespread existence of chalcopyrite inclusions in sphalerite is taken into account. Roedder

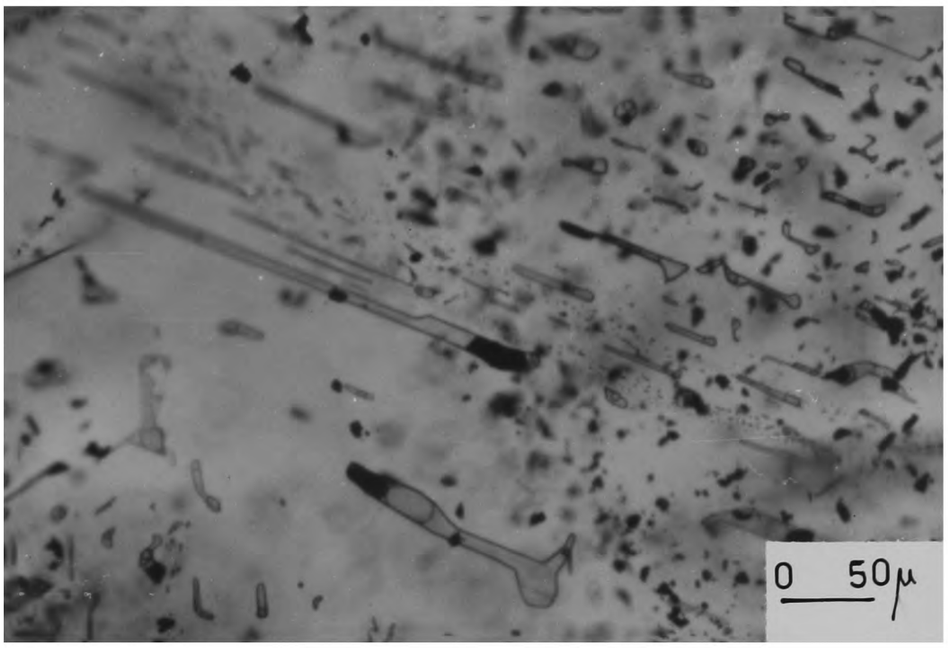

Plate 6.4.5a Solid inclusions and primary fluid inclusions with opaque captive minerals (in sphalerite).

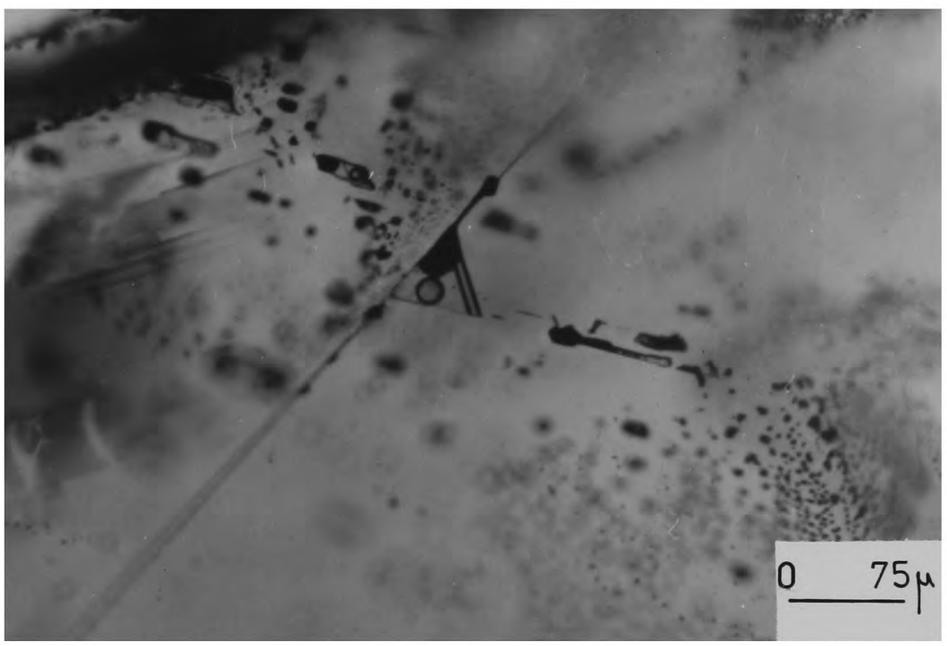

Plate 6.4.5b A primary fluid inclusion with a captive opaque mineral (in sphalerite).

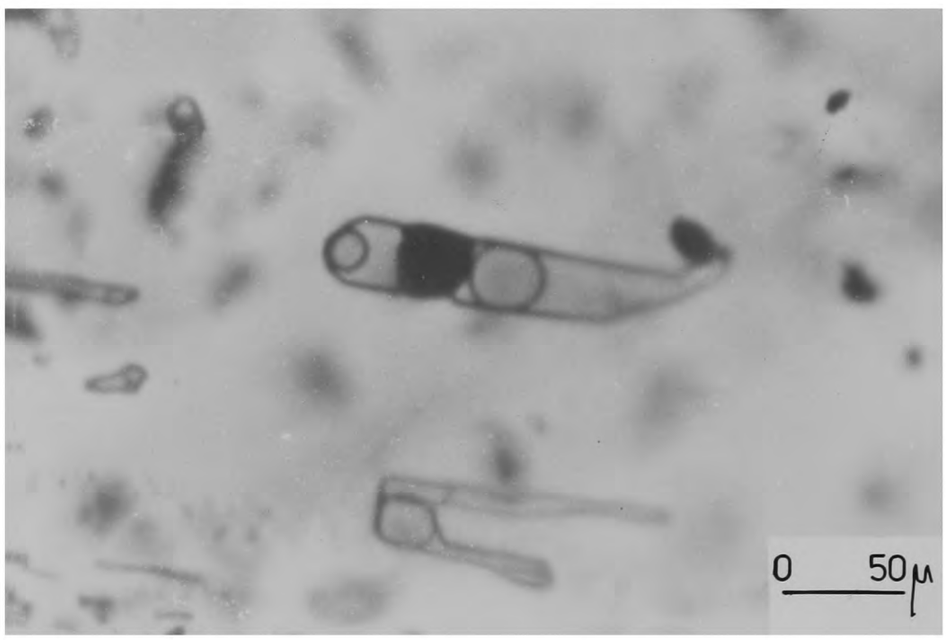

Plate 6.4.5c Primary fluid inclusion subdivided by opaque captive mineral.

(1960) assumed that, if decreasing temperature was a significant factor in causing precipitation during vein mineralization, precipitation from the fluid within the inclusion should also continue.

6.4.6 Leakage Problem of the Inclusions: The movement of the fluid into or out of inclusions after they are trapped does occur in nature, usually due to large internal and external pressure gradients. Several processes have been described by Roedder (1967). As a result of experimental evidence Roedder and Skinner (1968) concluded that fluid inclusions do not suffer a great deal of leakage.

Artificial leakage is sometimes produced during specimen preparation or heating and freezing inclusions in very cleavable minerals like barytes and dolomites. When studying these minerals either anomalous filling temperatures were obtained as an indication of leakage, or some inclusions did not homogenize within a 100°C range as compared with the bulk of the homogenization temperatures. These inclusions were either avoided or else the results were discarded after obtaining frequency diagrams (Fig. 6.4.6). The easiest check for leakage was found to be duplicated measurement and over one hundred duplicate heating runs differed only 2 to 5°C from previous measurements. The small average size ($<$ 100 microns) of most inclusions studied reduces the problem of leakage.

Inclusions showing necking down were also avoided. It has been stated by Roedder (1967) that necking down occurs very commonly in nature, and accounts for a good part of the scatter of homogenization temperature results in inclusion thermometry. However the difficulty in distinction

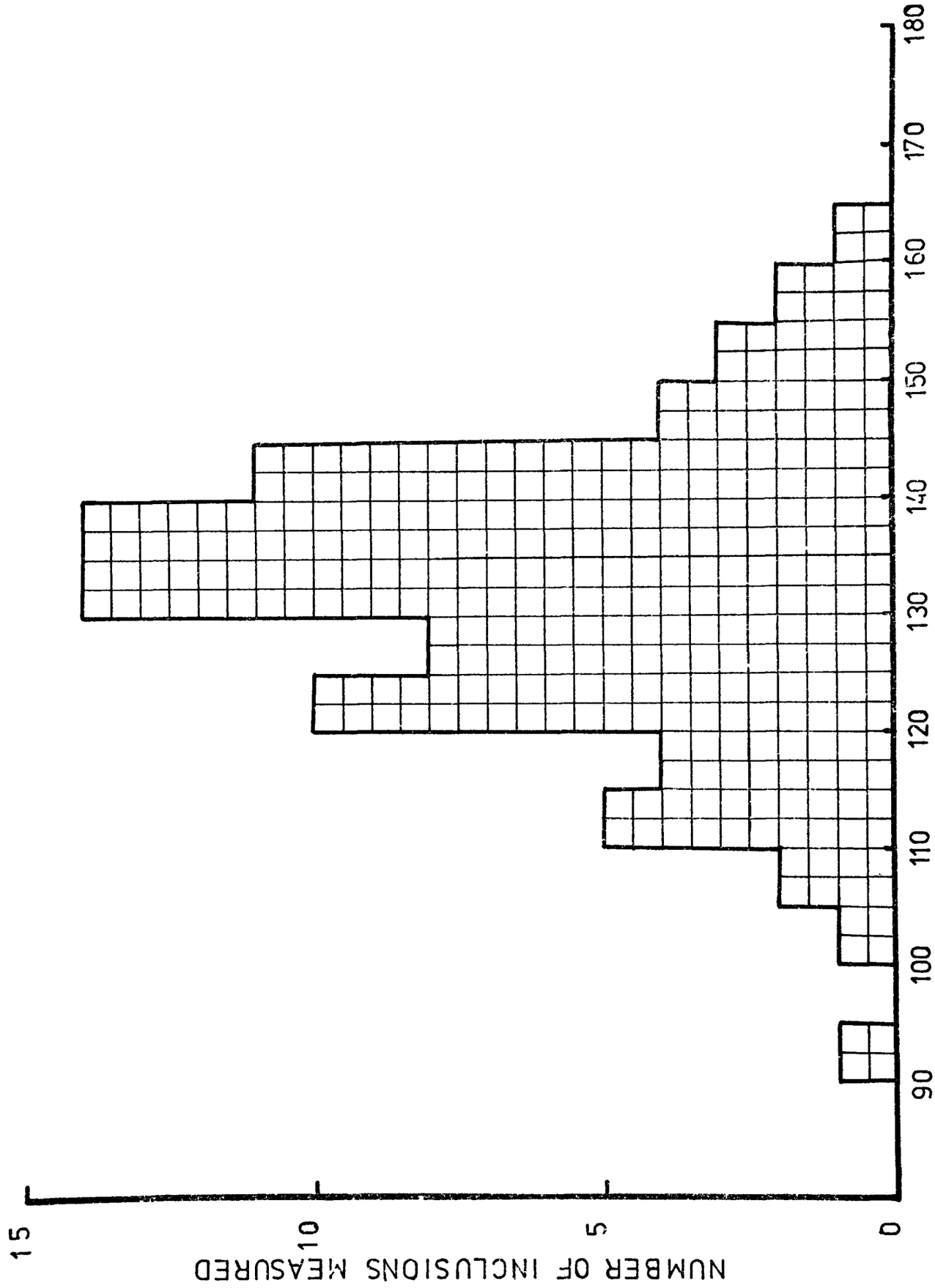

Fig 6.4.6 A plot of homogenization temperatures from sphalerite specimen 81 showing a Gaussian Distribution.

between primary and pseudosecondary inclusions must also be taken into account. The writer believes that in most published papers this has played an important role in producing widely scattered results.

6.5 Freezing Experiments

6.5.1 Salinity Measurements: As previously stated daughter salts were recognized on only two occasions. Neither measurement of volumetric proportions of daughter salts nor the temperature at which these daughter salts re-dissolved upon heating can be used to estimate the salinity of the fluids. Salinity measurements were therefore obtained from liquid-rich inclusions by the freezing method.

Although the fact that the lowering of the freezing point is proportional to the solution's concentration was stated by Ermakov and others (Translated into English 1965) the freezing method was developed by Roedder (1962, 1963) in the U.S.A. The temperature at which the last ice crystal in an inclusion remains in equilibrium with the solution is equivalent to the freezing point of the solution (Roedder 1962). Na and Cl are typically the major ions in fluid inclusions (Roedder, 1967, 1972) and in most hydrothermal solutions (Helgeson, 1964). So the freezing point determination is best expressed in terms of NaCl content and the system NaCl-H_2O is a reasonable approximation (Roedder, 1962a, Fig. 4). It is assumed that the quantity of NaCl that would produce the freezing point depression is roughly the amount of the total salt actually present. Besides the salinity, this technique helps to identify daughter salts and to study the CO_2 content of inclusions if it ever existed.

6.5.2 Freezing Stage: Present experiments were carried out on a freezing stage developed by F.W. Smith (1973, Fig. 1) in this department for studies of fluid inclusions at temperatures down to -100°C. This stage is simple and highly versatile and provides data of sufficient accuracy for present purposes. It has been reported by F.W. Smith (1973) that overall precision on calibration and duplicate runs is generally better than ± 0.5°C.

The system has great advantages over the freezing stage developed by Roedder (1962a). It has an extremely rapid cooling rate which is necessary to overcome stubborn metastability in most inclusions. It has been found by Roedder that many inclusions in sphalerite, with actual freezing temperatures of about -3°C, would not freeze even when held for an hour at -35°C. This metastable super cooling is very annoying in the experimental process.

The stage itself is made from a stronger perspex cylinder sealed off from the bottom by a clear perspex plate to transmit the light through the cylinder. This perspex cylinder, serving as a chamber for the specimen and the heat exchange medium, is encased in asbestos insulation. Three copper gauzes inserted in the chamber serve to mix the gas thoroughly as it vents upwards. The top gauze also supports the specimen which usually rests upon a small aluminium wire cage.

6.5.3 Heat Exchange Medium: Dry nitrogen, cooled by passing through a copper coil immersed in a liquid nitrogen, is introduced to the chamber through a lagged stiff polythene tube. The inserted part of the tube is coiled around the base of the chamber and perforated by a series of

upward directed pinpricks to circulate the cooled nitrogen gas. Nitrogen flow inside the chamber is controlled by a very fine needle-valve which can be adjusted to yield cooling rates up to 25°C/Min. and to raise the temperature by decreasing the cold gas flow after freezing of the inclusion is obtained. Used gas escapes around the glass lid of chamber and the lid thus forms a valve to prevent moist air from entering the chamber and causing frosting when the cold gas flow is reduced. A small jet of dry air directed on to the top of the glass lid prevents external frosting during the experiment which is sufficient to keep a clear field of view.

6.5.4 Thermocouples: A copper-constantan thermocouple attached to the specimen reads directly onto a chart recorder adapted to give maximum sensitivity in the required mV range. A second thermocouple is kept in the cell to monitor gas temperature and keep a check for possible thermal gradients.

6.5.5 Calibration: The system is calibrated regularly using standard freezing point capillaries (synthetic inclusions) containing the following substances:

Buthyric acid	-6.5
Bromine	-7.2
Methyl Benzoate	-12.3
Benzonitrile	-13.0
Quinoline	-15.9
Decane	-19.7 °C

Serious errors can be involved in obtaining freezing temperatures because there are no standards to simulate natural fluid inclusions. Various factors tending to raise the apparent freezing temperature such as large volume of sample plate, large mass of inclusion, low salinity, irregularity of inclusions, interference by the gas bubble, are described by Roedder (1962a). Any internal pressure effect, due to liquid CO_2's tendency to lower the freezing point was found to be negligible. The existence of liquid CO_2 was suspected in only a few specimens of the Bulancak Deposits. As one can expect, synthetic fluid inclusions used as standards to calibrate the stage are not as good as real standards. The present data could be as much as -2°C out, corresponding to a maximum uncertainty of 3wt.%NaCl.

6.5.6 Freezing Reactions and Products: Fluid inclusions, even thin tabular inclusions, are almost completely opaque under transmitted light when frozen. When the temperature is raised by lowering the flow of nitrogen gas using the needle valve, they become translucent rather suddenly. First melting temperatures (the approximate temperature at which an appreciable amount of fluid begins to develop in the inclusion) fall in the range -26 to -17°C. In many inclusions the first melting temperature was observed to be indistinct. Phases other than ice were not recognized. As a first indication of freezing, bubbles either distort giving a rough heart shape or contract into smaller bubbles. If freezing goes beyond this point completely opaque inclusions are obtained. During melting ice forms rounded or spheroidal grains of

high negative relief and low birefringence in the inclusion liquid. Errors may be involved in measuring the temperature at which the last ice crystal in equilibrium with the fluid disappears. This is because the crystals tend to become hidden by the opaque rims of the inclusions. However, dropping the temperature a little may induce them to reappear to confirm their presence.

Data on the freezing products and equivalent NaCl contents corresponding to the freezing points determined for each run are listed in table 6.5.6. Ice forms in undersaturated inclusions with less than 23.3 wt.% NaCl (Kelly and Turneaure, 1970). Lower first melting temperatures may indicate the presence of other salts and this has been observed on one occasion (Plate 6.4.4e). The highest salinity obtained was 13.2 equivalent wt. % NaCl (2.55 in molal concentration). Salinities are listed in Table 6.5.6. It was found that adjacent large and small inclusions of identical type in the same small growth zone had identical freezing temperatures.

6.5.7 Fluid Densities: Densities of ore-bearing fluids have been determined from the table given by Haas, Jr. (1970) and have also been listed in Table 6.5.7. These estimated densities were found to be in agreement with the ranges of estimated densities of hydrothermal brines of Roedder (1967 a, p.566) and Tugarinov and Naumov (1972). It has been stated by Roedder that "most hydrothermal ore deposits have formed from fluids in the range of 0.5 to slightly over 1.0 gm/cm^3". Densities can be calculated if the relative volumes of crystal, liquid and gas phase are known at room temperature, or by using the table given by Haas, Jr. (1970). Densities were found in the range of 0.74 to 0.98 gm/cm^3. In the early stage of

TABLE 6.5.6 Freezing Data and Equivalent NaCl content (weight % and Molal Concentration) and Densities of Fluid Inclusions.

No.	Locality	Min.	No. of Incl.	Orig.	Phases Formed	First Melt.	Final Melt.	Salinity Wt.%NaCl	Molal Conc.	Fluid D=G/CM3
6	SARIDIKEN	SPH	8	P	ICE	IND	-7	10.5	2.00	0.835
7	"	"	3	P	ICE	IND	-8	13.2	2.55	0.950
7	"	"	5	P	ICE	IND	-5	8.5	1.60	0.930
8	"	"	12	P	ICE+CO2	-20	-6.5	10.7	2.05	0.935
8	"	"	3	PS	ICE	-22	-3.0	5.2	0.90	0.880
13	KORNALI	"	4	P	ICE	IND	-8.0	13.2	2.55	0.950
17	"	"	7	P	ICE	IND	-7.0	11.8	2.30	0.900
28	KOVALIK	"	2	P	ICE	IND	-5.0	2.5	1.59	0.810
28	"	"	10	PS	ICE	IND	-1.5	2.5	0.44	0.740
30	SARIDIKEN	"	4	P	ICE	IND	-4.5	7.5	1.40	0.830
30	"	"	10	PS	ICE+CO2	IND	-1.0	1.8	0.30	-
38	KUSDERE	"	16	P	ICE+CO2	IND	-8.6	12.4	2.42	0.863
42	GONURCA	"	6	P	ICE	IND	-6.0	10.2	1.90	0.840
42	"	"	10	PS	ICE	IND	-5.0	8.5	1.60	-
43	"	"	30		ICE	-25	-5.8	9.1	1.71	0.832
48	KORNALI	"	7	P	ICE	IND	-6.0	10.2	1.90	0.845
54	DAMYATAGI	"	8	PS	ICE	IND	-3.0	5.2	0.90	0.875
57	"	"	4	P	ICE	-20	-5.5	9.1	1.70	0.830
68	B.INECE	"	12	P?	ICE	-25	-4.5	7.5	1.40	0.867
77	K.GURE D.	"	19	PS	ICE+CO2	-17	-4.0	6.8	1.25	0.920
79	KULOGLU	"	29	PS	ICE+CO2	-17	-3.0	5.2	0.90	0.810
81	"	"	14	P?	ICE	-25	-3.5	5.8	1.05	0.970
91A	UZUMLUK	"	5	PS	ICE	IND	-3.8	6.4	1.17	0.890
91B	"	"	17	P?	ICE+CO2	-21	-5.5	9.1	1.70	0.962
92	"	"	6	P?	ICE	IND	-5.9	9.8	1.84	0.950
93	"	"	18	P?	ICE	-21	-5.0	8.5	1.80	0.875
94	"	"	11	P?	ICE	-23	-4.5	7.5	1.39	0.896
95	"	"	10	P	ICE+CO2	-26	-6.5	11.0	2.11	0.925
95	"	"	17	PS	ICE	-21	-4.7	8.0	1.50	0.901
96	"	"	15	P?	ICE	-26	-5.1	8.7	1.63	0.913
97	"	"	17	P?						
97	"	"	17	P?	ICE	IND	-7.0	11.8	2.30	0.970
97	"	"	5	PS	ICE	IND	-5.0	8.5	1.60	
102	DARIKOY	"	5	PS	ICE	IND	-4.5	7.5	1.40	0.896
103	"	"	10	PS	ICE	IN	-4.7	8.0	1.50	0.915
124	B.GURE D.	"	2	PS	ICE	IND	-4.5	7.5	1.40	
49	KORNALI	QTZ	3	PS	ICE	IND	-2.2	3.8		
49	"	"	3	P?	ICE	IND	-3.5	5.8	1.05	
54	DAMYATAGI	"	24	P?	ICE+CO2	-25	-3.0	5.2	0.90	
68	B.INECE	"	6	PS	ICE	-22	-3.0	5.2	0.90	
78	K.GURE D.	"	13	PS	ICE	-25	-3.2	5.5		
91A	UZUMLUK	"	9	PS	ICE	IND	-3.8	6.5	1.19	0.888
91B	"	"	12	PS	ICE	IND	-3.5	5.8	1.105	
21	KUCUKDERE	BRT	3	P?	ICE	-24	-5.5	9.1	1.70	0.866
21	"	"	5	PS	ICE	-24	-3.8	6.5	1.20	0.900
21	"	"	2	S	ICE	-24	-3.0	5.2	0.90	
57	DAMYATAGI	"	11	P?	ICE	-26	-3.5	5.8	1.05	
85	DARIKOY	"	17	PS	ICE	-21	-4.5	7.5	1.40	0.833

P = Primary
PS = Pseudo Secondary
IND = Indistinct

SPH = Sphalerite
QTZ = Quartz
BRT = Baryte

TABLE 6.5.7 Salinities and Original Densities of Some Primary Fluids Entrapped in Sphalerites from South of Bulancak, Turkey

Sample Number	Volume Liquid /.	Percent Vapor	Density at Room Temp.	Wt. Percent H_2O	Wt. Percent NaCl	Salinity	Density Exp.	Density Calc.	Homo. Temp.
6	87.5	12.5	1.067	89.5	10.5	10.5	0.937	0.934	215
7	85	15	1.077	86.8	13.2	13.2	0.950	0.942	227
8	86	14	1.077	89.3	10.7	10.7	0.935	0.926	217
13	87.5	12.5	1.093	86.8	13.2	13.2	0.950	0.956	213
28	75	25	1.059	91.5	8.5	8.5	0.810	0.794	301
30	80	20	1.052	92.5	7.5	7.5	0.830	0.842	267
38	80.0	20.0	1.082	87.6	12.4	12.4	0.863	0.866	290
42	72.5	27.5	1.071	89.8	10.2	10.2	0.840	0.777	320
43	77.5	25.0	1.057	90.9	9.1	9.1	0.832	0.819	290
57	77.5	22.5	1.063	90.9	9.1	9.1	0.830	0.824	288
77	87.5	12.5	1.046	93.2	6.8	6.8	0.920	0.915	200
79	80	20	1.034	94.8	5.2	5.2	0.810	0.827	258
91A	85	15	1.045	93.6	6.4	6.4	0.890	0.888	230
94	85	15	1.052	92.5	7.5	7.5	0.896	0.894	225
97	90	10	1.084	88.2	11.8	11.8	0.970	0.976	185
	(1)		(2)				(3)		(4)

(1) Lemmlein and Klevstov, 1961
(2) Wolf and Brown, 1965-1966.
(3) Haas, 1970
(4) In Degrees centigrade
Exp. = Experimental
Calc. = Calculated
Wt = Weight

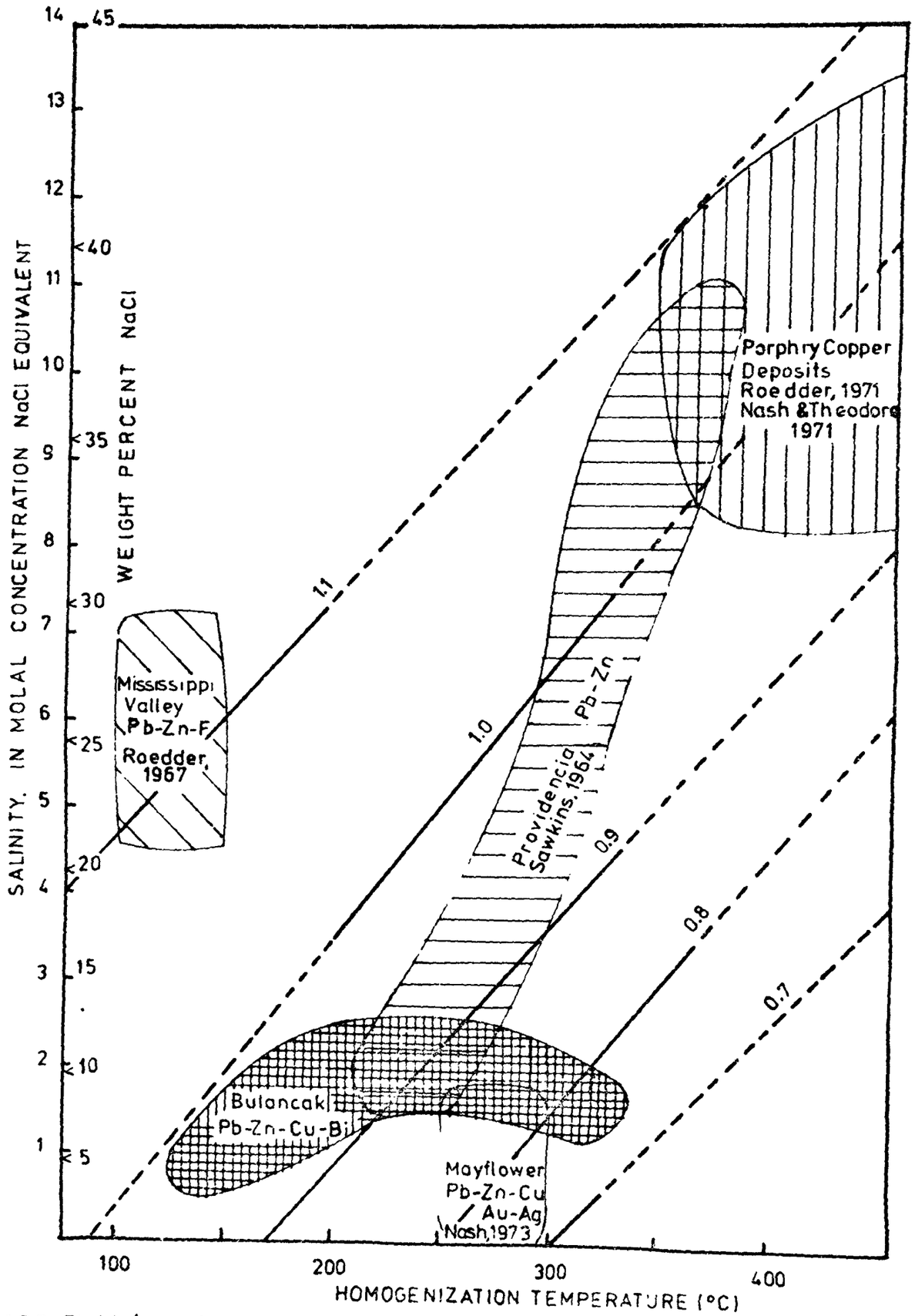

Fig 6.5.7 Fluid-inclusion homogenization temperature and salinity data for some hydrothermal deposits Diagonal grid lines show fluid densities in gm/cm^3 from the system $NaCl-H_2O$ (Hnas, 1970). Data generalized from the references given for each deposit.

sulphide mineral formation the fluid had a density of 0.74 at 300°C. In the late stages the density had risen to 0.97 at a temperature of 135°C. These density results are plotted on Fig. 6.5.7 to compare with other hydrothermal deposits.

6.5.8 CO_2 Contents: During some freezing experiments the formation of carbon dioxide hydrate was barely visible but the resolution of the microscope and the optical capability of the stage were not sufficiently good to enable detailed observations and vertification.

Assuming the formation of carbon dioxide hydrate in the inclusions at low temperatures, the hydrate dissociates completely to CO_2 gas and water in the range of about -8 to 0°C. This range indicates internal CO_2 pressure in the range of approximately 12.4 to 8.3 bars (Takenouchi and Kennedy, 1965a,Fig. 1). These low CO_2 pressures may explain the failure to form liquid CO_2 in the Bulancak inclusions. A similar case was seen in the Bolivian tin and tungsten deposits (Kelly and Turneaure, 1970). CO_2 pressures as high as 45 bars may be required insimple H_2O - CO_2 systems to form liquid CO_2 (Takenouchi and Kennedy, 1965a). Due to limiting factors in the stage design, the writer was not able to study gas-rich type inclusions. During boiling of vein fluids in early stages, CO_2 may become concentrated in the vapor phase, while dissolved salts are enriched in the coexisting liquids (Takenouchi and Kennedy, 1965b). In this way the non-existence of liquid CO_2 may be explained.

6.6 Heating Experiments.

6.6.1 Furnace: Homogenization temperatures of the inclusions were measured with a conventional home-made heating stage mounted on a leitz Model 350 heating stage microscope fitted with UM 20/0.33 and H32/0.60

objectives and a 10X ocular. The stage was originally constructed by Sawkins in 1965. Current is supplied to a nichrome coil wound around a steel cylinder (2.5 cm radius) mounted in plaster of Paris. The whole block is surrounded by an asbestos casing with upper and lower openings for viewing the specimen and for inserting the light source, and fixed by means of long screws through the asbestos casing to a mullite base (Smith, 1974b, Fig.A1). Specimens rest on a pyrex window disc which is supported by a small cylinder-shaped brass collar below and a thin disc shaped steel collar above. Brass retainers are used to fix the brass collars. There is another disc shaped brass collar in front of a steel collar above the pyrex window disc. A ceramic lid with a glass cover rest on the steel collar used to seal the specimen chamber and to change the specimen.

6.6.2 Thermocouples: Temperatures were measured with a chromel-alumel thermocouple (ice-cold-junction) pair inserted through one side of the block to the specimen chamber. A Phillips (PR 2210 U/21) chart recorder was used to measure the E.M.F. generated by the thermocouple. The slightly bent thermocouple end touches the specimen being studied approximately 2mm away from the inclusion under observation.

6.6.3 Current supplied to the nichrome coil is adjusted by a Rotary Regavolt rheostat to obtain the desired heating rates.

6.6.4 Calibration: The thermocouple was calibrated by heating organic compounds of known melting points which had been sealed into short pieces of capillary tubing. These calibration standards were placed in approximately the same position as the inclusions under investigation

so as to obtain as near identical conditions as possible. The following chemicals were used for calibration:

Chemicals	Melting Point (^{o}C)
Acetoxime	61-62
Hydroxyquinidine	75
Resorcinal	110-111
Benzoic acid	123.0
p-Nitro aniline	147.5
Succinic acid	187.0
Anthracene	215.0
Gallic acid	263.0
Benzene hexachloride	310

As a precaution against thermal gradients and overheating, the heating rate was reduced from 5^{o}C/min. to 1^{o}C/Min. approaching the homogenization temperature. A gradual heating rate is required to maintain thermal equilibrium within the inclusion being studied, to prevent anomalous low filling temperatures, decrepitation (explosion of inclusion) and leakage. Frequent checks against the melting points of standards showed that accuracy of measurement is $\pm$ 2^{o}C but uncertainties in a wider range than this can be expected at temperatures above 300^{o}C.

Many possible sources of error in the homogenization temperature measurements are present, such as the difficulty in observing the exact temperature at which the bubble disappears, i.e. at which the inclusions completely homogenize, or else the bubble hides in the black borders of the inclusion just prior to homogenization. These difficulties were

eliminated in most instances by decreasing the heating rate to a minimum and moving the light source along the inclusion. Movement of the bubble was observed in accordance with the light source after reaching a certain temperature range. This technique was used frequently for inclusions in the sphalerites. After homogenization was obtained, all inclusions were examined upon cooling for evidence of leakage. Duplicate runs were made on many of the inclusions and the homogenization temperatures were discarded if they were out of agreement with the previous measurements by more than $5^{o}C$.

One notable feature of these homogenization runs was the relatively wide variation in homogenization temperature for various inclusions even in the same sample, sometimes side by side, when considered in the light of the overall temperatures. Similar variation in homogenization temperatures can also be caused by necking down after trapping (Roedder, 1967) but this is not the case for the inclusions studied. The present results are believed to represent real variation in the formation temperatures and pressures. Another explanation for this wide variation in homogenization temperatures in specimens from the same locality is that the inclusion-bearing grains may represent different parts and different stages of the sulphide vein and sulphide mineralization under consideration.

By heating doubly polished mineral specimens (disc wafers) containing liquid and vapor bearing inclusions to a point where the bubbles disappear a minimum temperature is found at which the inclusions could have formed from a cooling ore-forming fluid. The temperature at which this filling takes place is regarded as the minimum temperature at which

TABLE 6.6 Homogenization temperatures of fluid inclusions in transparent vein and ganque minerals from South of Bulancak, Giresun, Turkey.

Sample Number	Locality	Mineral	Wall Rock	Level (MS.)	No. of Incs.	Origin	Homo. Temp (°C) Min.	Mean	Max	Strike and Dip of Vein
6B	SARIDIKEN	SPH.	Lower/Basic	660	32	P	185	215	235	N17W50NE
7	"	"	"	550	11	P	215	227	247	N40W90
7	"	"	"	"	16	PS	170	192	197	"
7	"	"	"	"	39	S	103	111	119	"
8	KIŞLA	"	"	695	79	P	183	217	265	N52W65SW
13	KORNALI	"	"	580	22	P	195	213	242	N-S90
15	"	"	"	590	19	P	252	267	282	N25W90
15	"	"	"	"	29	S	185	215	247	"
17	"	"	"	625	25	P	232	247	275	N25E49SE
17	"	"	"	"	14	S	200		227	"
28	KOVALIK	"	"	780	44	P	275	300	020	N25W55SW
29	"	"	"	625	16	P	237	247	267	N75E50NW
30	SARIDİKEN	"	"	555	25	P	242	267	284	N45W75SW
38	KUŞDERE	"	"	500	41	P	276	290	313	N35W80SW
38	"	"	"	"	42	PS	232	255	272	"
42	GONURCA D.	"	"	550	34	P	294	320	343	E-W45S
42	"	"	"	"	77	PS?	212	255	290	"
43	"	"	"	580	62	P	270	290	300	N60E60NW
43	"	"	"	"	8	S	249	251	256	"
46	DÖNBÜL T.	"	Rhyodacite	590	25	P	237	272	301	N50W70SW
46	"	"	"	"	6	S	195	200	213	"
48	KORNALI	"	Lower Basic	510	15	P	230	252	285	N40W50SW
54	DAMYATAGI	"	"	525	49	P	202	225	265	N60W35NE
57	"	"	"	365	28	PS	206	222	256	N75W90
57	"	"	"	"	7	P	272	288	304	"
62	DÖNBÜL T.	"	"	525	5	P	215	247	255	N17E30SE
66	B.INECE	"	Rhyodacite	360	24	P	240	258	270	N45W90
66	"	"	"	"	17	S	177	197	210	"
68	"	"	"	210	63	P	228	245	256	N75W90
77	KÜÇÜKKÜRE D.	"	"	180	45	P	183	200	215	N80E90
77	"	"	"	"	72	S	138	165	180	"
78	"	"	"	165	51	P?	180	205	242	N45W60NE
79	KULOGLU	"	Lower Basic	230	20	P	217	258	275	N55W60NE
79	"	"	"	"	29	S	130	155	197	"
81	"	"	"	280	80	P?	92	135	165	N-S90
85	DARIKÖY	"	"	190	55	PS	115	160	190	N60E90
85	"	"	"	"	39	P	202	217	237	"
91A	ÜZÜMLÜK	"	"	320	43	P	207	230	255	N40W70NE
91A	"	"	"	"	5	S		149		"
91B	"	"	"	310	62	P?	149	165	195	N70W90
92	"	"	"	265	67	P	207	240	290	N-S65E
92	"	"	"	"	27	PS	145	185	200	"
93	"	"	Breccia	270	53	P	215	250	265	N85W70SW
93	"	"	"	"	60	S	149	165	202	"
94	"	"	"	220	16	P	210	225	242	N30W60NE
94	"	"	"	"	54	PS	150	180	202	"
95	"	"	"	170	44	P	195	220	247	N50W65NE
96	KÜÇÜKKÜRE D.	"	Rhyodacite	265	34	P	215	230	278	N45W50SE
96	"	"	"	"	9	PS	183	195	204	"
97	"	"	Lower Basic	160	16	P	166	185	197	N70W85NE
102	DARIKÖY	"	"	440	94	P?	180	225	265	N67W90
102	"	"	C	440	16	S	135	143	149	"
103	"	"	"	410	63	P?	180	210	265	N45E65NW
126	YAYKINLIK	"	"	570	34	P	195	212	222	
28	"	DLM	"	"	24	P	222	245	265	
28	KOVALIK	QTZ	"	780	44	P	215	255	280	
46	DÖNBÜL T.	"	Rhyodacite	590	18	P	217	245	255	
57	DAMYATAGI	"	Lower Basic	365	17	P	265	275	305	
57	"	"	"	"	26	PS	208	222	237	
68	B.Inece	"	Rhyodacite	210	26	P	280	315	337	
78	KÜÇÜKKÜRE D.	"	"	165	10	P	225	240	256	
91A	ÜZÜMLÜK	"	Lower Basic	320	21	PS	191	235	255	
94	"	"	"	220	30	P	240	252	270	
103	DARIKÖY	"	"	410	63	P	195	245	265	
21	KÜÇÜKDERE D.	BRT	Dacite	855	32	P	237	265	300	N60W90
21	"	"	"	"	28	S	195	210	232	"
56	DAMYATAGI	"	Lower Basic	520	16	P	265	280	0/0	
56	"	"	"	"	22	S	207	245	260	
85	DARIKÖY	"	"	190	50	P	250	275	308	
85	"	"	"	"	43	S	183	225	247	
119	BÜYÜKKÜRE D.	"	"	225	31	P	230	250	270	
119	"	"	"	"		S	172	200	217	

SPH = Sphalerite DLM = Dolomite QTZ = Quartz BRT = Baryte P = Primary
PS = Pseudosecondary S = Secondary INCS = Inclusions

the mineral could have formed at the time of entrapment subject to a vapor pressure correction. This correction procedure will be discussed later. The results of the heating experiment were listed in Table 6.6.

6.6.5 Time-Temperature Relations: The homogenization temperatures of sulphide veins were plotted against time and paragenetic sequences to show variation of physico-chemical conditions during sulphide mineralization (Fig. 6.6.5a).

One can immediately notice the temperature zonation between the Tekmezar group veins and the Dariköy group and the rising temperature towards the end of early vein stage, reaching boiling conditions. As is discussed later, specimens 28 and 42, reached boiling conditions. As is clearly shown from the curve, homogenization temperatures first seem to rise with the formation of quartz mineralization and reach highest values in the early vein stage, then drop off continuously in the later stages of sulphide (base-metal) mineralization. In several specimens of neighbouring quartz and sphalerite (specimens, 28,46,57) inclusions were measured and the temperatures in quartz were found to be up to 50°C lower than those in sphalerite (Fig. 6.6.5b). This difference, when compared with the maximum pressure correction applied for these deposits (maximum 20°C), can be accounted for as an actual increase of depositional temperature. Unfortunately calcite was found to occur as a gangue mineral in only one locality and was not suitable for fluid inclusion study. Only one dolomite (Fig. 6.6.5b) specimen was found suitable for fluid inclusion study representing the stage of carbonate formation but not enough to complete the thermal history of the late waning stage of mineralization. In

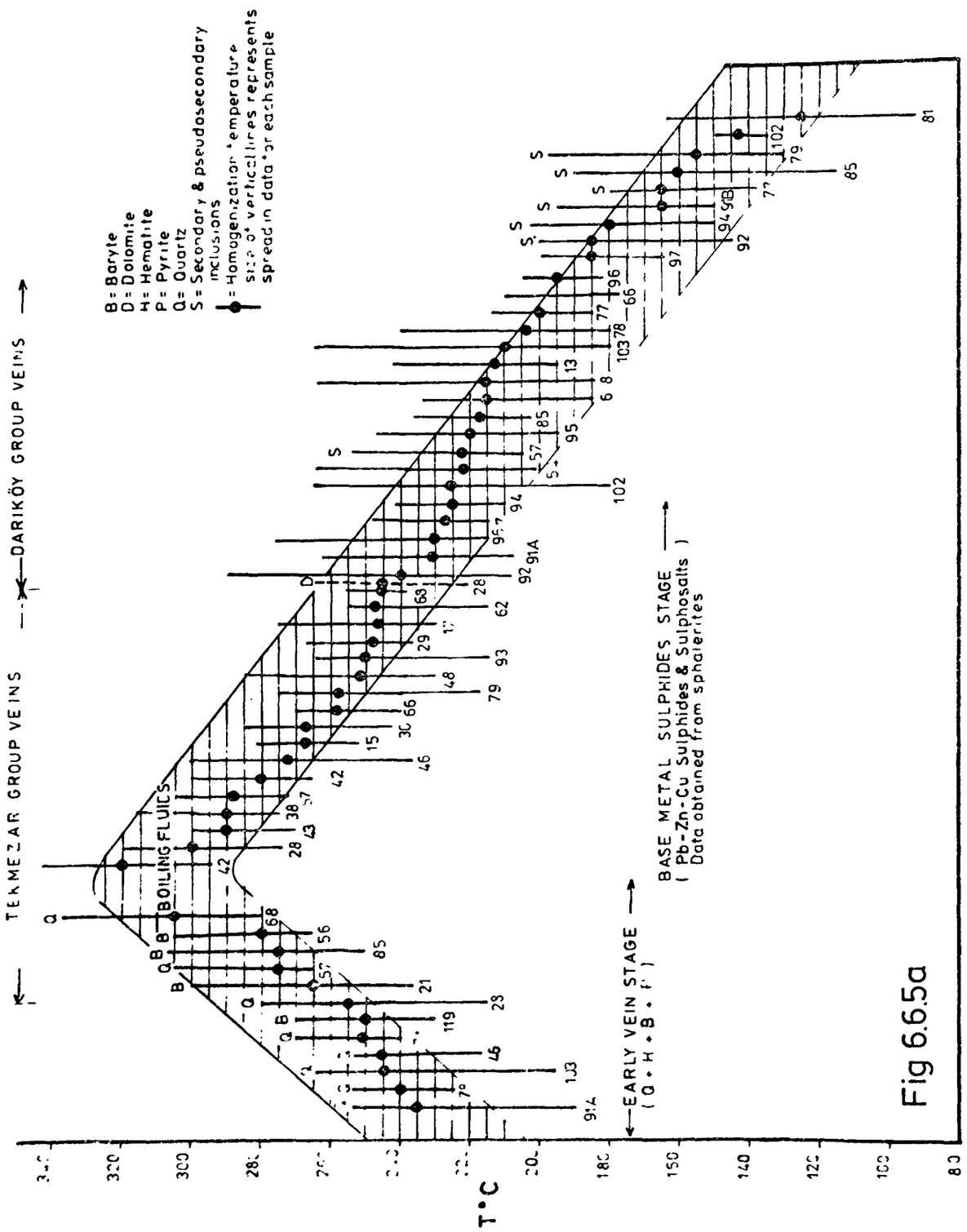
TEKMEZAR GROUP VEINS
DARIKÖY GROUP VEINS
B = Baryte
D = Dolomite
H = Hematite
P = Pyrite
Q = Quartz
S = Secondary & pseudosecondary inclusions
= Homogenization temperature
Size of vertical lines represents spread in data for each sample
BOILING FLUIDS
EARLY VEIN STAGE
(Q + H + B + P)
BASE METAL SULPHIDES STAGE
(Pb-Zn-Cu Sulphides & Sulphosalts)
Data obtained from sphalerites
T°C
TIME

Fig 6.6.5a

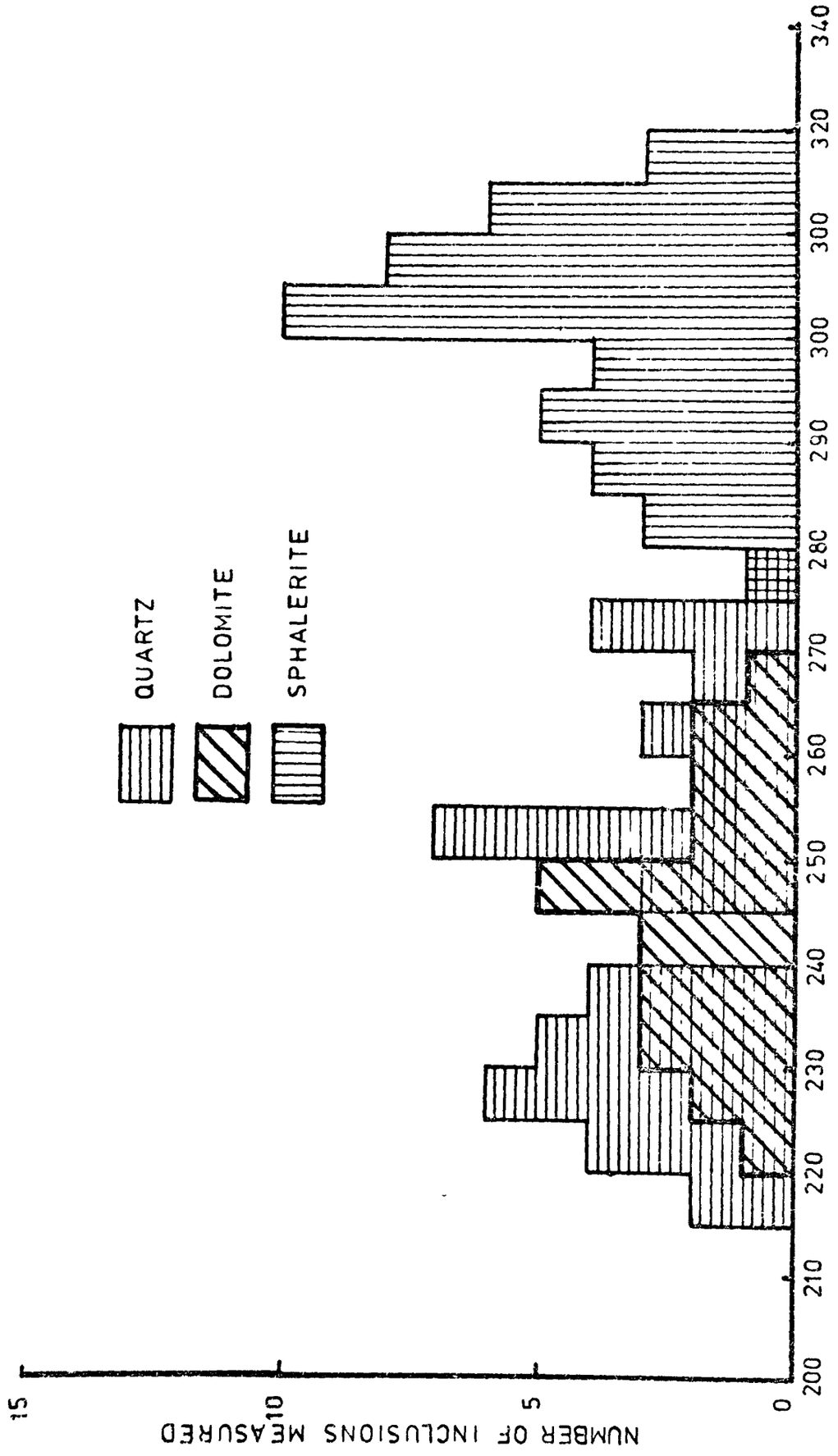

Fig 6.6.5b Frequency diagram for specimen 28. Although quartz is the early formed mineral, sphalerite formation temperature indicates an increase in temperature at the end of the early vein stage.

specimen 28, quartz, sphalerite and dolomite were found to form successively; quartz representing the early vein stage, sphalerite the end of the early vein stage or beginning of the base metal stage (Fig. 6.6.5a) and dolomite possibly representing the end of the base metal stage. In other specimens quartz homogenization temperatures either preceed those of sphalerite or else overlap them. Microscopic evidence shows that quartz is the oldest gangue mineral in paragenetic sequence in almost all these cases.

6.7 Pressure correction and interpretation of the data:

Before the application of pressure corrections the critical nature of the ore-forming fluids has to be known. As is shown earlier from the freezing data, CO_2 pressures in the Bulancak inclusions are low so that the inclusions of early vein minerals cannot be regarded as forming from immiscible CO_2 rich and H_2O rich ore fluids. These type of inclusions, discussed by Smith and Little (1959) and Roedder (1967a), give true depositional temperatures when one of them is present in the inclusions or give a maximum when a mixture of both occur. The question of the supercritical nature of the ore fluid at the time of entrapment can also be dismissed. According to the data of Sourirajan and Kennedy (1962) critical temperatures of NaCl brines with about 5 to 13 wt.% NaCl are in the range of 425 to 515°C (Fig. 6.7) - above the critical temperature for pure water and considerably above the homogenization temperatures of fluid inclusions in the Bulancak Deposits.

From the evidence and discussions above it is concluded that the early vein fluids were moderately saline and were below the critical temperature. The CO_2 content of the fluid was negligible, daughter salts other than NaCl were possibly not represented and the inclusion data is best represented and interpreted in terms of the system

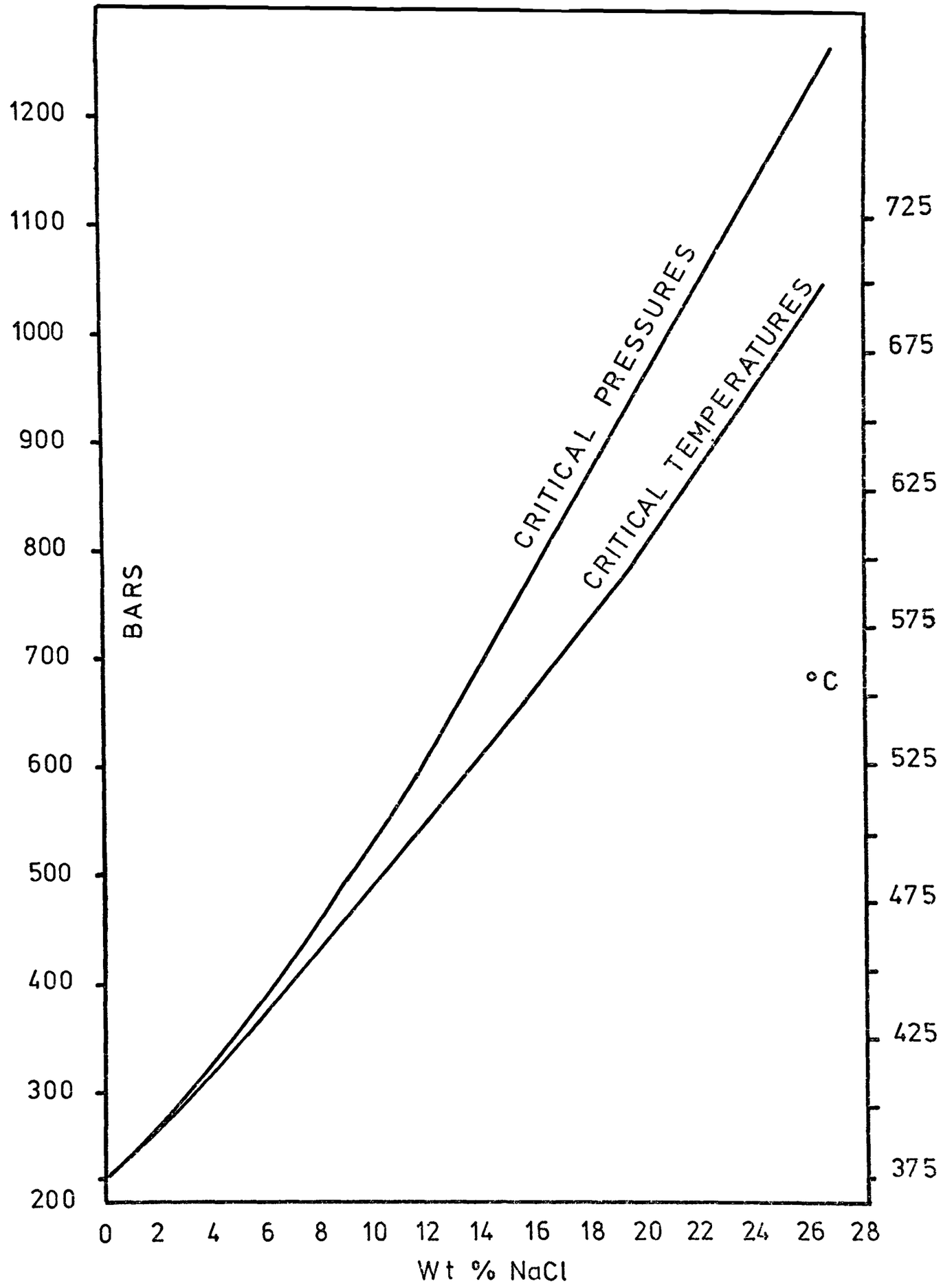

Fig 6.7 Variation of critical temperature and pressure with salinity of NaCl solutions (adapted from Kennedy,1962).

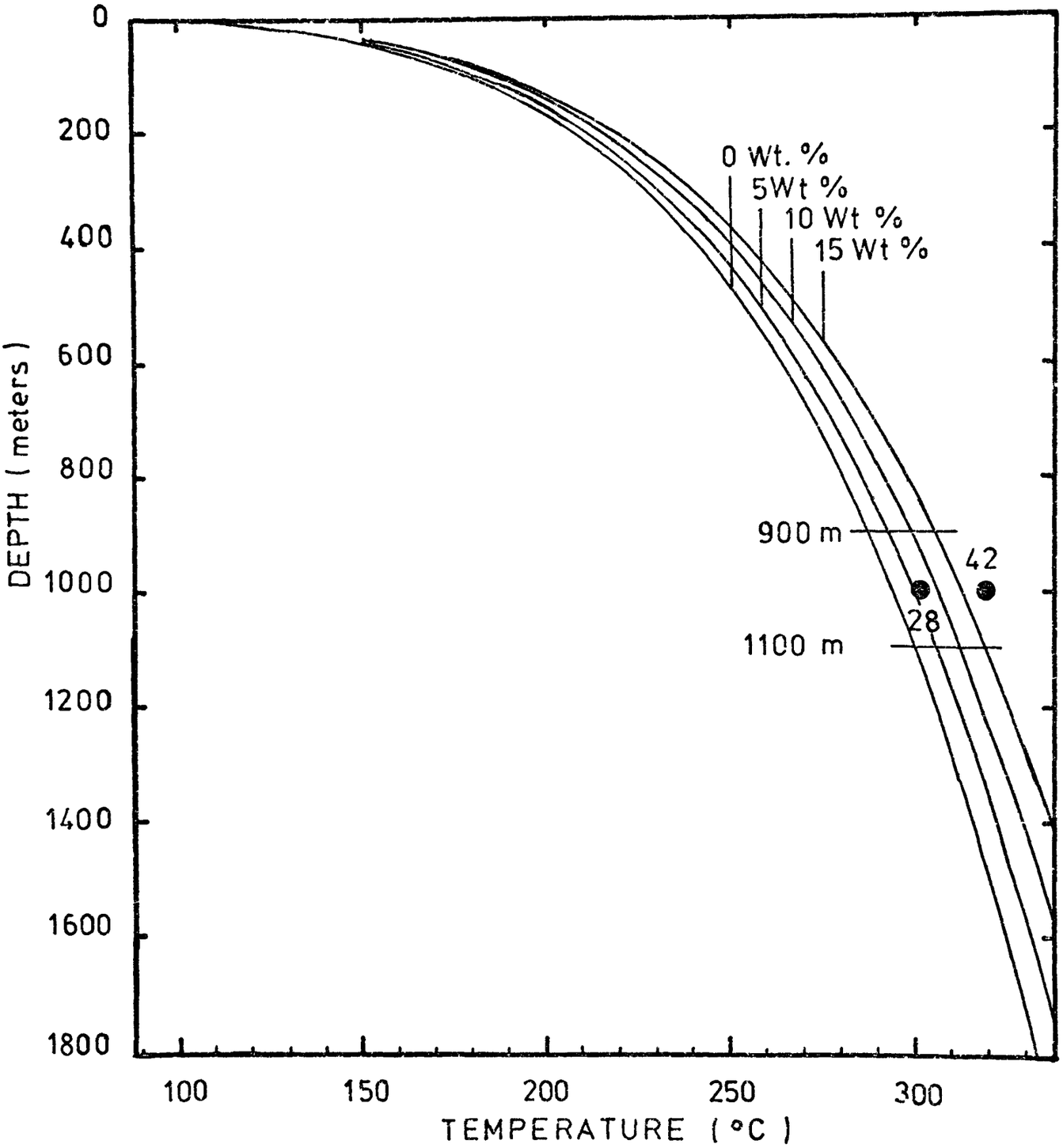

Fig 6.7.1 Boiling conditions for some inclusions from sphalerite specimens. Boiling-point curves for H_2O liquid and brine of constant composition given in Wt % NaCl are from Haas, 1971.

NaCl - H_2O. Homogenization temperatures of liquid-rich type inclusions, except several specimens which were formed under boiling conditions (require no correction), must be regarded as minimum values and require pressure correction (Fig. 6.7.1).

6.7.1 Pressure correction: Fluid inclusions of the minerals form within the depths of the earth under either a lithostatic or a hydrostatic load. A pressure correction becomes necessary when the total pressure at the time of entrapment was greater than the vapor pressure of the fluid. So the pressure correction is the amount that must be added to the homogenization temperature of an inclusion to obtain the trapping or formation temperature (Roedder, 1967a). If the pressure can be calculated from geological field data on the depth of cover, homogenization temperatures can be corrected for pressure. However, if the inclusions were formed on a liquid-vapor curve (i.e. total pressure is equal to vapor pressure Roedder, 1967a, Fig. 12.2) at the time of trapping, then no pressure correction would be added. Only a few inclusions were found to represent liquid-vapor curve conditions, all the others require some correction to raise homogenization temperatures to the temperature of formation. Most of the fluid inclusions in nature are NaCl brines so the experimental studies of the system NaCl-H_2O by Klevstov and Lemmlein (1960) and Lemmlein and Klevstov (1959) yield very close approximations for the pressure correction.

The maximum stratigraphic thickness that ever existed above the level of the lower basic series which have a very strong close relationship with the Bulancak Sulphide Veins was estimated to be 1000 meters (Gattinger et al., 1962 p.47). The pressure on the ore solutions

at this depth could not thus have been greater than the conventional 100 bars if hydrostatic, 250 bars if lithostatic. The data of Lemmlein and Klevstov (1959) relating to the correction of homogenization temperatures indicates that even at a lithostatic pressure of 250 bars the maximum correction to be applied, whatever the salinity, is $+20^{o}C$. Data obtained from the structural control of the veins, texture of the ore minerals, and the type of volcanic activity suggests pressure fluctuation during vein formation. Single phase inclusions indicate that it may drop to atmospheric pressure. The data of Klevstov and Lemmlein (1960) show that, if a sphalerite crystal were to grow from a dilute solution at a constant temperature of $300^{o}C$, but at pressures that fluctuated between about 100-1000 bars, its fluid inclusions would have filling temperatures varying from 300 to $215^{o}C$. The wide variations in homogenization temperatures due to pressure fluctuations can be explained this way.

It has been demonstrated by Kelly and Turneaure (1970) that fluid inclusions can be used as independent barometers that serve as checks on the geological estimates of depth of mineralization. But this can be achieved only under certain conditions. The method can be applied only to gas rich inclusions in minerals formed under boiling conditions. In this latter case the total pressure is equal to the vapor pressure of the boiling brine. If the salinity and homogenization temperature of the inclusions formed under boiling conditions are known total pressure can be read from the boiling curves of the system $NaCl-H_2O$ (Sourirajan and Kennedy, 1962 Haas, 1971). On the other hand Scott and Barnes (1971) have shown that sphalerite may be used as a

geobarometer if formation temperatures are above the upper stability limit of monoclinic pyrrhotite near 304°C (Arnold, 1969). This application is based on the pressure dependence of sphalerite composition in equilibrium with pyrite and hexagonal pyrrhotite between 550°C and 304°C when total pressure is about 1 Atmosphere (1,013 bars) or less. The bulk of the Bulancak sphalerites were formed below 300°C, contain a maximum of 2% Fe and are not associated with pyrrhotite. Therefore the sphalerite geobarometer can not be applied. Application of this method to Bolivian sphalerites gave results which were too high, but it was applied more successfully for other deposits (Scott and Barnes, 1971).

The following primary liquid rich inclusions formed under boiling conditions, assuming a stratigraphic load 1000 ± 100m., can be used(Fig.6.7.1) to estimate depth to the boiling curve of a 10% NaCl solution (Haas, 1971).

Spec. No.	$T_{Hom.}$ (°C)	Salinity (wt.%NaCl)	Hydrostatic Depth to the boiling curve (m).	Vapor Pressure	Lithostatic Depth.
28	300	11.8	907.3	80.0	320
42	310	8.5	1056.2	91.4	368

Freezing tests on all liquid rich inclusions in this study indicated low CO_2 pressure (~ 10 bars). The vapor pressure indicated in the table above is 85 ± 6 bars; to allow for the possible effect of low CO_2 total pressures can be accepted in the range of 90 bars. This translates to about 1000 meters hydrostatic load. This estimate is in very good agreement with depth of the load and suggests that fluid pressures were

close to the hydrostatic pressure for all vein types.

6.8 Application of the Fluid Inclusion Data to Field Problems:

As Turneaure (1960) and Kelly and Turneaure (1970) suggested, fluid inclusions can be used to pinpoint ore localization and might serve as a guide to the occurrence of high grade ore at depth if boiling conditions and temperature zoning are established. The experimental fact established by Holland (1972) "the ratio of the concentration of tin in the aqueous phase to its concentration in the silicate phase should be proportional to the forth power of chloride content of the aqueous phase", supports the Kelly and Turneaure suggestion for tin deposits: "highly saline hydrothermal solutions are excellent scavengers of the tin of granitic melts" (Holland, 1972). Nash (1972) believes fluid density is a possible tool in exploration: "if, in mapping fluid inclusion types and corresponding densities, one can demonstrate lateral and vertical zonation, these zones may suggest targets for finding ore associated with low-density (Epithermal gold?) or high-density fluids (disseminated copper or molybdenum)." Miyazawa (1967) demonstrated the use of temperature gradients obtained from the different levels of a vein to calculate the vein's lowest limit and depth of formation. He gives an average 3 to 5^{o}C/10m. temperature gradient for hydrothermal deposits, occasionally 7^{o}C/10m.

A method based on routine analysis of fluorite for yttrium has been used with success in mines of the Northern Pennine Orefield in England to predict the location of intersections in partially developed fluorite bearing orebodies (F.W. Smith, 1974a). The concentration of yttrium

increases markedly where the homogenization temperature along the vein gives maxima indicating intersecting (rich ore locations) cross vein localities.

An attempt was made to apply fluid inclusion data to the most densely studied veins of the Tekmezar and Dariköy areas. As is seen from Map 2 the zone of mineralization extends in a SW-NE direction from Kovalik Sirti in the SW, to Kuloglu in the NE. Most of the polymetallic veins are localized in three areas along this mineralization zone; when measured homogenization temperatures of the fluid inclusions representing each vein in these areas are contoured to get an isothermal map (fig. 6.8) the direction of the ore-bearing fluids was seen to follow major NW-SE trending faults. Although the faults mapped to the west of Tekmezar were not extended to the southeast when first mapped, isotherms support such an extension. So the Kovalik Sirti occurrences were fed from the Selmanoglu Fault, extending from Selmanoglu to Kişla.

The Dönbül T. occurrences were fed by the Gonurca D. Fault, extending from the Camkoza D.-Gonurca D. junction to Dönbül T. The Northeastern Dariköy occurrences were fed by a possible fault forming the Uzümlük D. line which is a mineralized breccia zone, although this area is less certainly due to intersecting N-S, NE-SW and NW-SE trending faults - but the isotherms follow a NW-SE direction.

Highest homogenization temperatures were obtained from the Tekmezar Group Veins, suggesting a horizontal zonation (see fig. 6.6.5a). These high temperatures, salinity and densities may be due either to the close proximity of the Tekmezar veins to the intrusive body to the south of the map area

ISOTHERMS IN RELATION TO SULPHIDE VEIN MINERALIZATION NEAR BULANCAK, EASTERN BLACK SEA, TURKEY.

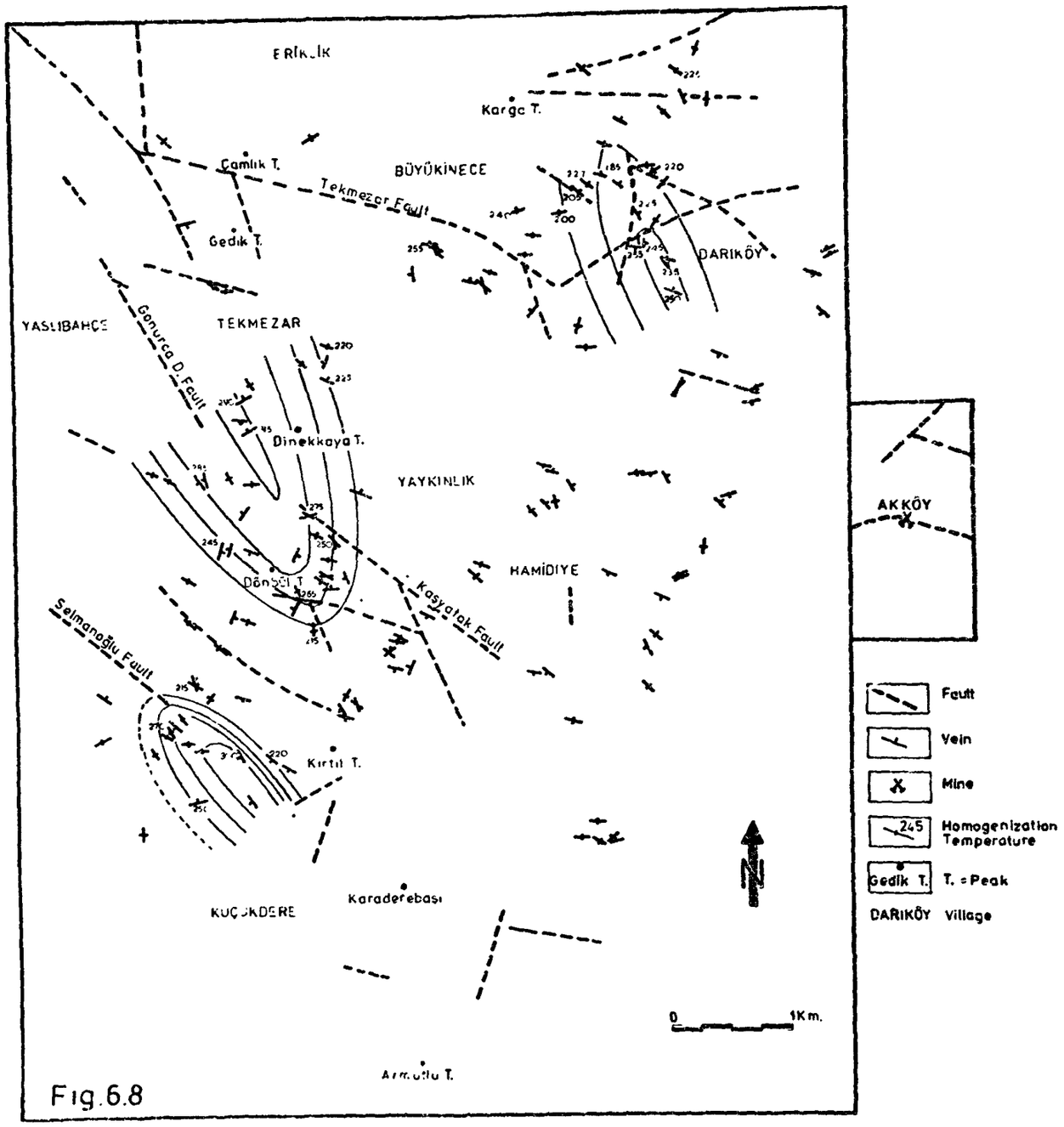

Fig.6.8

or else there is a possible deep seated intrusive body beneath the Tekmezar group veins. Isolated intrusive formations mapped occur to the northeast along Küçükgüre D. outside the map area. The most possible explanation is the extension of the main intrusive body from the southwest (outside the map area) to the northeast. These intrusives were mapped by Agar and H.H. Schultze-Westrum (1960) on the 1/25.000 scale. Data were available to calculate thermal gradients from only two veins. In the area it is difficult to follow the veins along their directions because of poor exposure, intense hydrothermal alteration of rocks and dense vegetation. Specimens 46 and 48 were collected from the 590 (in meters above the sea level) and 510 levels respectively of the first vein. This vein is situated 600 meters NE of Dönbül T. The second vein is the Uzümlük D. vein of the Darıköy area. Specimens 91 and 97 were collected from the 320 and 160 levels and the thermal gradient was found to be $3^{o}C/10m.$, but on both occasions higher homogenization temperatures were found on higher levels of the veins, due possibly to horizontal temperature zoning. So these attempts to estimate the lowest limit of depth of the veins failed.

CHAPTER SEVEN

DISCUSSIONS AND CONCLUSIONS

7.1 Environment of Ore Deposition

In relation to geotectonic development, the mineral deposits of Turkey are divided into several groups (Gümüs, 1970). One of the important events, which led to concentration of mineral deposits in particular areas, is orogeny. The mineral provinces of Turkey are, however,associated with different rock types which include deposits of varied character. It is thus not possible to combine their occurrence with plate tectonic theory by explaining them only as a result of orogenies of major tectonic units.

The regional distribution of volcanic and intrusive rocks was suggested by Seyhan (1972) as the first reason for the concentration of mineral deposits of Turkey in certain regions. As can be seen from the table below (from Seyhan, 1972) the magmatic rocks of Turkey are concentrated in three regions:

Regions	Acid to intermediate intrusives(Km^2)	Calc-alkaline rocks (in broad sense)Km^2
South Marmara (Western Pontids)	6500	11000
Eastern Black Sea (Eastern Pontids)	7500	16000
Central Anatolia (Anatolids)	3500	8000

The table clearly indicates that 80% of the intrusives and 77% of the calc-alkaline rocks are found along the Pontids. Secondly, if the insignificant basaltic rocks in the west are not taken into account,

calc-alkaline rocks cover an area of 40000 Km^2 to the west of the Antalya-Kayseri-Erzurum-Artvin line (see fig. 1b), named as "the andesite line" by Sehan, while basaltic rocks to the east of this line cover an area of 60000 Km^2. As a result of this regionally selective volcanism Kaolin deposits are concentrated in the south Marmara Region due to alteration of acid volcanic rocks and the Cu-Pb-Zn-Mn Province is also in direct relationship to the calc-alkaline volcanics of the Eastern Pontids.

The formation of the metallic provinces is largely affected by Germano and Alpine structures. A Germano-type block faulting is the dominant structural pattern throughout the Eastern Pontids.

The metallogenetic provinces of Turkey are in close relationship in terms of time and space with those of the Carpathian Mountain chain, the Transylvanian Alps, the Balkan Countries, and the Caucasus (Ramovic, 1966). The Pontid metallogenetic belt, is a part of the East European Alpine metallogenetic and volcanic belt. The similarity and relationship between the volcanic belt and the distribution of mineral deposits is striking (Dewey et al, 1973; Ramovic, op. cit.). The Alpine metallogenetic belt of eastern Europe begins in the Carpathian Mountains in Czechoslovakia (associated with Kremnica, Banska, and Matra deposits *) and extends eastward through Romania forming the Transylvanian Alps (Brad, Zlatna, Bala de Aries, Rodna and Roshia deposits *). In Yugoslavia it lies in a north-south direction through the Timok Mining District (Majdanpek, Valja Sake, and Bor deposits *) extending into Bulgaria through the Sredna Gora district and the Viskia Mountains* where the belt

* Ramovic (1966).

returns to its east-west direction. It then extends through Panagyurishte-Burgas into the Eastern Pontids (Küre, Ordu, Bulancak, Espiye, Tirebolu, Murgul, and Artvin Cu-Pb-Zn deposits). Beyond the Pontids it passes into the Minor Caucasus (Pambek-Zangezur Cu-Mo belt) and the Elburz Mountains of Iran (Fig. 7.1). Throughout the belt the mineral deposits are associated with Cretaceous-Miocene andesite, dacite, rhyolite, basaltic and spilitic lavas and tuffs and acid to intermediate intrusive rocks (Ramovic, 1966; Dewey et al, 1973).

The second Tertiary volcano-metallogenetic belt begins at Pohorje (Slovenija) passes through the Podringe and Trepca mining districts along the Vardar zone of Yugoslavia and extends through the Rhodope mountains, northeast Greece, and the Aegean islands into the south Marmara mining district. Beyond this it extends eastwards through the Anatolids into Iran with an east-west trend.

Recent detailed studies carried out by MTA along the eastern Pontids have shown the existence of Porphry Copper -type deposits (Snelgrove, 1971), Kuroko-type deposits (Tirebolu-Espiye) stockwork and vein type Cu-Pb-Zn, and skarn-type Cu-Fe deposits. There are also submarine-exhalative type nodules and vein type occurrences of manganese deposits. These deposits are all associated with Cretaceous-Plaeogene calc-alkaline volcanics, acid to intermediate intrusives and flysch sediments (Tugal, 1969; Gümüş, 1970; Hamamcıoglu and Sawa, 1971). This association suggests a subduction related mineralization (Sawkins, 1972; Dewey et al, 1973) in an island arc or destructive plate margin environment, in which the ability of ore-

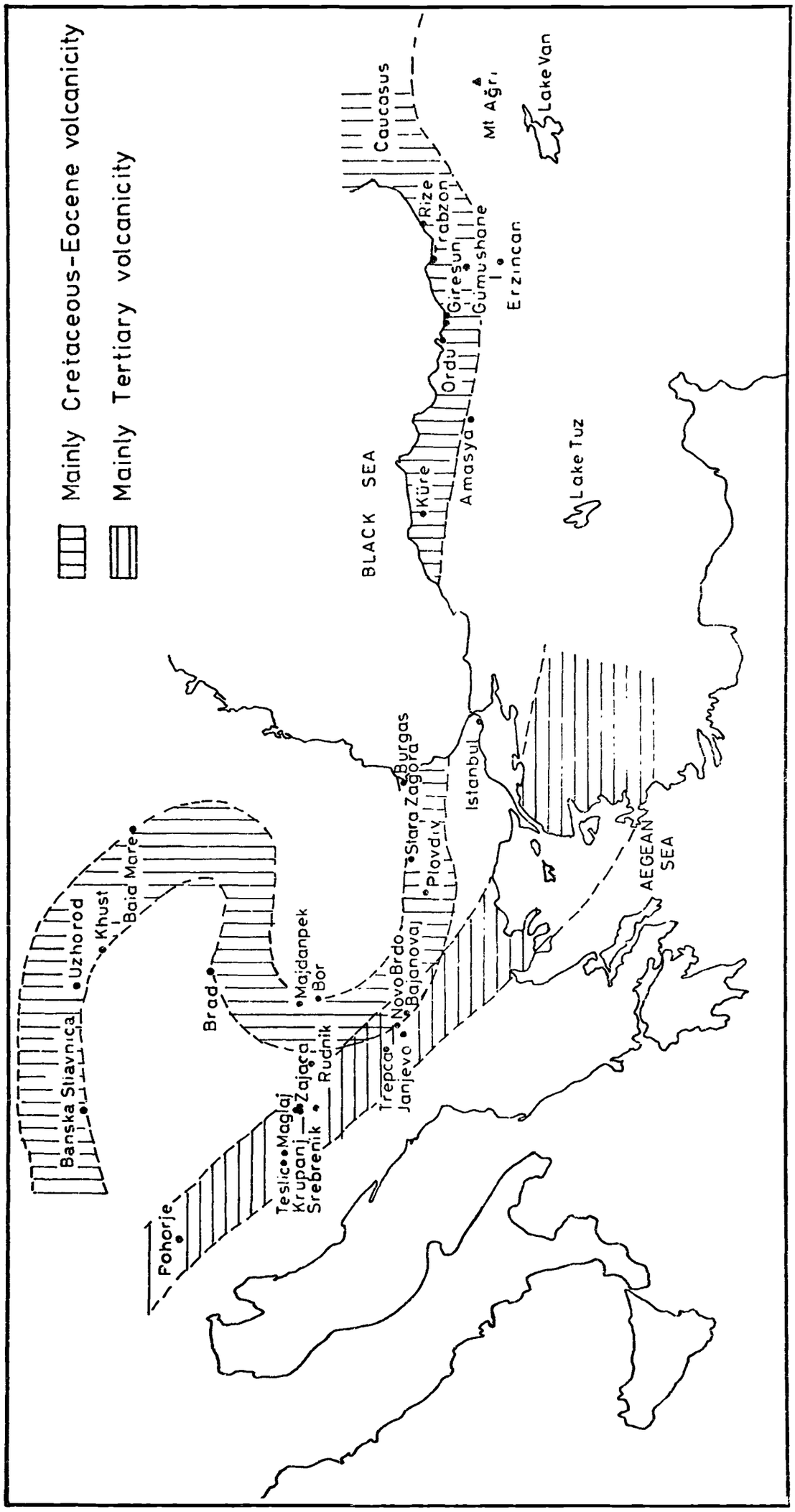

Fig 7.1 MAJOR ALPINE METALLOGENETIC BELTS IN RELATION TO THE PONTID ORE PROVINCE

bearing solutions to reach the surface was controlled by the relationship between the fracture pattern within the overlying volcanic and sedimentary rocks and the angle and speed of consumption of subducted plate.

A correlation between volcanic activity, orogeny and the peak of mineralization can be demonstrated in a similar way to that in the Western United States and Andean deposits (Sawkins, 1972; Tarling, 1973). The most important deposits of the Pontids and the other parts of Turkey are related to Alpine volcanic activity, metamorphism and tectonic events (Gümüş, 1970). If the post-Cretaceous age of the Eastern Pontid deposits is taken into consideration, a direct relationship with the Alpine plutonic rocks is also obvious.

The plate tectonic theory brought a new approach for the genesis and exploration of ore deposits as well as other subjects of geology. It is a well established fact that active oceanic ridges and ocean-floor sediments are locally enriched in metals, particularly Fe, Mn, Cu, Pb, Zn and Mo (Boström and Peterson, 1966; Corliss, 1971); these are areas which are marked by high heat flow and by volcanic exhalative processes. Trace element analyses of Mid-Atlantic ridge basalts reveals that the slowly cooled, interior portions of these submarine extrusions are depleted in several elements that are enriched in the pelagic sediments and manganese nodules especially Mn, Fe, Co and rare-earth elements (Corliss, 1971). Fresh submarine pillow basalts dredged from the ocean-floor contain vesicles in which are spherules composed primarily of Fe, Cu, Ni and S (Moore and Chalk; 1971). Although these metals concentrate around oceanic ridges, mid-oceanic

islands are poor in mineralization. This environment requires a conveyor belt system to explain the formation of sulphide deposits.

According to Tarling (1973) "differentiation to give fluids rich in metals does not take place until after new oceanic crust has been carried from the active magma injection zone. The localized high heat flows are therefore only effective in areas where hot ore fluids are making contact with sea water in the overlying sediments. This results in precipitation of copper sulphide, a mechanism suggested for the genesis of the Kuroko deposits of Japan (Horikoshi, 1969).

The metals and minerals within the oceanic lithosphere carried down at subduction zones become molten along the Benioff zone at different temperature/pressure levels and therefore the composition of the magmas (and associated metals) recycling upward from different levels, varies away from the oceanic trench in both major and trace elements (Arculus and Curran, 1970; Kuno, 1966). Great amounts of heavy metals in ocean floor sediments are potentially available for upward recycling in the island arc environments, due to the transport of the sea floor sedimentary layer down the subduction zone (Sillitoe, 1972; Wright and McCurry,1973).Compaction of the lowermost sedimentary layers will also lead to the expulsion of significant amounts of oceanic pore water. The movement of this dilute brine through the sediments may well extract associated metals and deposit them at the ocean-sediment interface region (Hirst, 1970). Recent stable isotope and fluid inclusion studies of Kuroko ores suggest that the formation of the deposits is closely related to the interaction of metal rich solutions of magmatic origin with seawater (Ohmoto, et al, 1970; Sawkins, 1972).

The orientation of metal provinces and the systematic changes of metallic elements across the island arc volcanic belts shows parallelism. Metal provinces of North and South America (Andes) are aligned parallel to the Pacific coast. Within a distance of a few hundred miles there is a systematic change across the Andean chain. Accompanying an increasing Co/Ni ratio is a change from deposits rich in Fe and Cu, to those enriched in Pb and Zn and Sn (Sillitoe, 1972). This is taken to indicate the remobilization of metals at different depths along the Benioff Zone (Peterson 1970). It has been estimated by Mero (1965) that a 10 Km thick oceanic layer of 1 Km^2 area, consisting of compacted clay-rich sediments with a specific gravity of 2.5 and an average copper content of 700 ppm and Pb content of 150 ppm, would contain 17,500 tons of copper, and 3,750 tons of lead respectively.

The calc-alkaline nature of the volcanics in the study area and along the Eastern Pontid volcapic belt was demonstrated earlier as well as in the Espiye and Gümüshane regions by Tugal (1969) and Tokel (1973). Subduction events during the Cretaceous-Eocene times in the Gümüshane region were also described by Tokel (op.cit). Bulancak Sulphide deposits were formed in an ancient island arc or destructive plate margin environment as fissure-filling Pb-Zn-Cu veins of subvolcanic hydrothermal type genetically related to post Eocene igneous activity similar to ore veins of Neogene volcanic affinity in Japan (Nakamura and Hunahashi, 1970). Their distribution is mainly confined to the Darıköy-Tekmezar area and is characterized by the presence of dominant volcanics of basalt- and andesite-dacite association.

7.2 Thermal History of the Vein Mineralization.

The structural control of the vein systems in the area has been known for a long time but some structural and mineralogical relationships were explained without scientific data. The present study of fluid inclusions demonstrates the relationship between ore-bearing solutions to certain fracture trends and may provide a guide in exploration.

As previously mentioned, minerals suitable for geothermometric measurements such as pyrrhotite, arsenopyrite and exsolved phases indicating high temperatures in sphalerite and chalcopyrite are not present. Craig and Kullerud (1973) stated that the association of hypogene idaite, marcasite and digenite is not stable at temperatures above 430°C. This temperature range possibly indicates the highest temperature at which Bulancak sulphides start to grow from the ore-bearing fluids because examination of polished specimens proved the existence of the idaite-marcasite-digenite association, but their hypogene origin is not certain.

The time-temperature curve in Fig.6.6.5a shows the variation of homogenization temperatures during vein formation. The location of the veins in the studied area was shown at the top of the curve to indicate a horizontal temperature zoning. This zoning was established by the hot spots and Bi-sulphosalts in the Tekmezar area and the observed higher temperatures at the higher levels of some previously mentioned veins. The time-temperature curve clearly indicates a temperature rise in the early vein stage from 235°C to 320°C during the crystallization of early quartz. Since the veins are narrow, the temperature of the ore-bearing solutions moving through the

fractures must have equilibrated rapidly with that of surrounding, possibly still cooling, volcanics. In other words a rapid heat exchange between the ore-bearing fluids and wall rocks may cause the temperature of the solution to increase. Most wall-rock alteration processes are suspected to be exothermic by Toulmin and Clark (1967). At the end of the early vein stage, boiling conditions for the ore fluids must have been achieved (Fig. 6.6.5a). A decrease in formation temperature appears from 350°C down to 80°C at the very late stage of mineralization. Although siderite was identified in one specimen replacing dolomite, neither siderite nor dolomite were found suitable for fluid inclusion study. Thus the range of siderite formation and the stage of carbonate formation (dolomite, calcite and siderite) is not clearly known, due to limited availability of these minerals for fluid inclusion study.

Present fluid inclusion studies support a single extended period of mineralization (in a cooling column of liquid) for the Cu-Pb-Zn sulphide deposition around the Dariköy-Tekmezar area of southern Bulancak. The rise of formation temperature in the early vein stage and progressive cooling of the later vein fluids can be explained in reference to Toulmin and Clark's (1967) discussion of the "Thermal Aspects of ore formation". Processes that tend to warm ore-bearing solutions in the early vein stage are believed to be exothermic reactions such as precipitation of solids from aqueous solution. However in the case of these sulphide veins, the process of mineralization was not simple precipitation of minerals from aqueous solution in an open fracture system, but also involved reaction of the fluid with the

wall rocks and the formation of new clay minerals and carbonates along the walls and in the host rock. Most alteration processes should be exothermic such as the simple dolomitization of calcite, alteration of potassium feldspar to muscovite and quartz. Provided the volcanic rocks of the area at the time of mineralization were still cooling, heat exchange along the fissure with this possibly still warmer environment may increase the temperature of the rising fluid, although heat exchange with the environment might at first seem more likely to be a fluid cooling process. Active boiling at the end of the early vein stage may also contribute to cooling of the fluid. Quartz is seen to form in the beginning of the early vein stage. The early precipitated quartz then became more soluble with the increasing temperature which led to boiling. This is indicated by skeletal and rounded quartz crystals (see plates 5.3.1a,b) in places completely replaced by late stage minerals.

It is clear that as the aqueous fluid rose from the depth to the surface of the earth in a fissure it underwent expansion as a result of pressure decrease. In the case of the Bulancak deposits reversible adiabatic expansion cannot be responsible for the cooling of rising fluids, because fluid inclusion studies indicates a maximum 350^{o}C formation temperature. A fluid cooling down under reversible adiabatic conditions from 350^{o}C and 1000 bars pressure to 250 bars would indicate only several degrees temperature decrease (Toulmin and Clark, 1967) for pure water, although the effect for moderately saline fluids is not known. Assuming that both reversible and irreversible adiabatic expansion have not played an important role for cooling the vein fluids below 350^{o}C, other processes are needed

to explain the temperature fall along the mineralization line with time, although conductive loss of heat to the walls of the fissures seems effective at the early vein stage. Once equilibrium conditions are achieved along these narrow fissures the temperature difference between the wall of the vein and the rising fluid should be negligible after crustification. If these processes were not taken into account to explain progressive cooling during the sulphide stage the only mechanism remaining for cooling the vein fluids would be their gradual mixing with deeply circulating meteoric water (Birkeland and Bjørlykke, 1972). In the case of the Salton Sea Geothermal System, for example, White (1968) suggests that circulating water may descend to depths of 10,000 feet or more along range-front faults. These deeply circulating waters are also responsible for variation in salinities as in the case of the Providencie Pb-Zn Mine (Fig. 6.5.7). The earlier formation of quartz in the paragenetic sequence rather than pyrite and other sulphides in sulphide veins of the study area and the non-existence of pyrite and pyrrhotite in the early vein stage of the Bolivian Tin and tungsten veins (although they are known to contain appreciable amounts of iron - as high as 3000 ppm) may be explained as being due to the predominance of SO_2 over H_2S at high temperatures of up to 600°C (Meyer and Hemley, 1967; Kelly and Turneaure, 1970).

Destruction of SO_2 during cooling of hydrothermal solutions from 600°C to 200°C can lead to the production of H_2SO_4 and hence to the precipitation of sulphate minerals. Baryte is the least soluble and most common of the alkaline earth sulphates in hydrothermal systems (Holland 1967). As shown by Holland (1967, Fig. 9.35) the

solubility of baryte increases with increasing temperature of up to 150°C in water and in concentrated NaCl solutions. Simple cooling must be an important mechanism in the precipitation of barytes as well as other gangue minerals. If the solutions with which the hydrothermal compounds are mixed (e.g. connate waters rich in Ba) are highly oxidized, then the sulphate concentration can be increased at the expense of the bisulphide concentration. But in many epithermal deposits, baryte is associated, as in the Bulancak veins, with sulphide minerals which are unstable in highly oxidized environments.

As the solubility product of calcite and dolomite decreases with increasing temperature these cannot, therefore, be precipitated from hydrothermal solutions by simple cooling. However, if, during boiling, the CO_2 content of the hydrothermal solutions decreases, then the carbonates can be precipitated.

Holland (1967) suggested that the ratio Ca/Mg+Fe of unaltered silicate wall rocks is normally sufficiently low that dolomite or an ankeritic carbonate, rather than calcite, will tend to form in alteration zones around hydrothermal veins. At Bulancak dolomite is the dominant hydrothermal carbonate, unlike the Providencie Lead-Zinc deposits (Sawkins, 1964) where calcite is the dominant hydrothermal carbonate. It has been pointed out by Helgeson (1968) that pyrite becomes less soluble than pyrrhotite as the temperature drops below 300°C. With decreasing temperature conversion of one sulphide to another may occur. In the Bulancak deposits the existence of marcasite with pyrite without any trace of pyrrhotite is distinctive.

In the case of quartz neither the pH of the solution nor the amount of dissolved salts affects its solubility on a great scale (Holland, 1967). This point has to be taken into account when a cooling fluid with a changing salinity shows increasing quartz solubility. This is seen from the corrosive effect of the later, cooler fluid on the early formed quartz crystals. A drop is normally expected in the solubility of quartz during the entire path of vein mineralization. In all studied veins quartz is the early formed mineral with some well preserved crystal outlines as well as skeletal and rounded forms (Plate 5.3.1). Even later stage mineral pseudomorphs after quartz were recognized.

These processes tend to precipitate sulphides and carbonates. In addition, replacement must have played an important role, e.g., replacement of dolomite by siderite as well as that of early sulphides by late stage sulphides.

7.3 Metal Transport in the Light of Fluid Inclusion Data.

The heavy metal content of fluid inclusions is of considerable importance in understanding the mechanism of ore-metal transport, although the small size and rare occurrence of opaque minerals indicate that the amount of precipitation of ore-metals from the ore fluid must be rather low. It is usually 1 to 10 ppm (Roedder, 1960) but 100 to 10.000 ppm each of Cu, Mn, Zn on the basis of neutron activation analysis, is reported by Czamanske et al., (1963) in some high-temperature inclusions. There is also evidence, at least at certain times in the growth history of many crystals, of

solid particles present in suspension in the fluids from which they grow.(see plates 6.4.5a,b,c).

"The water content of acid and intermediate magmas is typically in excess of 2% and frequently in excess of 4%, at least during the formation of biotite and hornblende in the late period of crystallization (Holland, 1972). Hydrothermal solutions are released from these magmas. Based on the experimental evidence of partition coefficients of Mn, Zn, and Pb, suggested by Holland (1972), it is clear that these metals are enriched in the aqueous phase during the crystallization of magma. Furthermore "the transfer of zinc from a melt into an aqueous phase can be efficient, and could remove economically interesting quantities of zinc from granitic magmas into hydrothermal solutions. The same is true of manganese and apparently also lead". Maximum transfer of zinc into the aqueous phase has been shown by Holland (1972) to be very sensitive to the initial chloride content of alkali granite melts. The proportion of zinc removed increases from 78% to 97% if the amount present in the chloride content in the magma increases from 0.7 weight % to 1.05 wt.%. This may lead to a precipitation of 60,000 tons of zinc from 1 Km^3 of granitic magma with the average 50 ppm zinc content found for granitic rocks by Turakian and Wedepohl (1961) if only 50% is extracted. The presence of pyrite as a common accessory mineral in granitic rocks and the reported sulphurization of iron (i.e. pyritization) and nickel in host rocks adjacent to sulphide ore bodies (A.J. Naldrett, 1966) and direct precipitation in many hot springs, suggest that there is always enough

reduced sulphur to form base metal sulphides, even in excess amounts. Common ore minerals, principally sulphides, are known to be extremely insoluble in pure water at almost all temperatures in the hydrothermal deposition range. They also have low solubilities in saline solutions. On the other hand volatility or transport as a vapor phase, is not an acceptable mechanism because the critical point of the saline hydrothermal solutions may be elevated to 500°C to 600 °C (Sourirajan and Kennedy, 1962). The critical point of a 13 wt.% Nacl solution is about 515°C which is within the range of fluid salinity in the Bulancak inclusions.

Colloidal transport also is not probable because of the instability of colloids in electrolytic solutions such as inclusion fluids or ore-bearing solutions. The observed zoning of ore deposits (Barnes, 1962) does not correspond with the solubilities in the form of nonionized molecular species or simple metal ions (Barnes and Czamanske, 1967).

Complex ions or molecules remain the only possibility for effective transport of the sulphide minerals of the Bulancak veins. As the problems are discussed by Barnes and Czamanske (1967) they will not be repeated here. The interesting point is that the effects of temperature as a cause of deposition are not consistent for all minerals. NH_4^+ - H_2S solution is effective for pyrite solubility whilst S^{2-} solutions are effective for cinnabar, stibnite and orpiment. HS^- solutions are effective solvents, being temperature and pressure independent, for the overall conditions of the Bulancak deposits, (Barnes and Czamanske, 1967).

From considerations of mineral solubilities (Barnes and Czamanske, p.351, fig. 8.7) the Bulancak sulphide ores containing sphalerite at temperatures below 250°C are most likely deposited from solutions in which either H_2S, or more probably HS^- is dominant. Loss of pressure, decrease in pH, or oxidation of the ore solution would lower the bisulphide concentration and could cause deposition of sphalerite and the other sulphide minerals. The common sericitic alteration in the wall rock and host rocks suggests that the pH cannot have been more than 2.5 units below neutrality (weakly acid) nor could it have ranged to strongly alkaline because sericite would be converted to K-feldspar (Barnes and Czamanske, 1967).

7.4 Suggestions for possible further work.

Arising from the present work, the writer considers that undiscovered vein type and strata-bound mineralization may exist which would merit an exploration programme, particularly in the following areas:

1. The area between the Küçükdere Village - Karaderebası Tepe Line in the south and the Yomasapagı-Selmanoglu Road in the north.
2. The area between the Evliya Tepe Fault and the Dinekkaya Tepe - Hamidiye Line including the sections of Kuşdere, Küçükgüre Dere and Büyükgüre Dere.
3. The section of Küçükgüre Dere between Damyatagı junction and Kuloglu Mah. including both banks of the stream and the Üzümlük Dere occurrences.

Although the surface outcrop of the quartz vein along the Evliya Tepe Fault looks barren it should be explored at deeper levels.

Further exploration activities may also be carried out along the formation boundaries of the Senonian sedimentary sequence between Çamkoza Dere and the Gedik Tepe - Çamlık Tepe line; the only specimen containing betekhtinite in large quantities was found in this area.

To the west of the investigated area, the area covered by the Senonian sedimentary sequence between Yaslıbahce Village and Pazarsuyu is geologically promising for Kuroko type deposits. 10.000 scale detailed geological map work there would be useful in the first stages.

7.5 Conclusions.

The investigated area,although explored extensively and mined locally,was not found to have economically viable mineralization. The present study has provided a revised geological map of the area including all the known occurrences of mineralization on the 10.000 scale.

An account of detailed mineralogical study of the veins and other occurrences has been given. Idaite was identified for the first time in the area together with Betekhtinite and Aikinite which have not to the writer's knowledge been reported previously in Turkey. Bismuth mineralization may change the economic viability of the veins.

Electron Microprobe analyses have shown the zonal arrangement and structural control of Mn and Fe-Cd distribution in sphalerites.

Fluid inclusion studies have indicated a temperature zoning and fracturesthat served as channels for rising ore-fluids were located. Applicationsof the fluid inclusion study results to exploration problems have been described.

Results of the present study suggest that a new exploration programme in the area might be worthwhile, since the possibility of undiscovered economic mineralisation still exists.

ACAR, E., (1974) Dogu Karadeniz Bölgesi Giresun ili dahilindeki bazi bakir-kurşun-çinko madenlerinin iz elementler yönünden önemi MTA Bull. (in press), Ankara.

AGAR, U. and SCHULTZE-WESTRUM, H.H., (1960) Bulancak (Giresun) bölgesi Jeolojik hartasi (1:25000): MTA Archiv No. 13462.

AKINCI, O.T., (1969a) Görele güneyindeki Koyunhamza ve Çölmekçi dereleri arasinda kalan sahanin (Çanakçi Nahiyesi Civari) Jeolojisi ve maden zuhurlari: MTA Rp. No. 32

———— (1969b) The effect of iron substitution on the cell-size reflectivity and colour of sphalerite: Unpubl. M.Sc. Thesis, Univ. of Durham.

AKOL, R. and ALPAY, B., (1955) Report on the mineral deposits of Ordu and Giresun Provinces: MTA Rp., Ankara.

ALTINLI, I.E., (1946) Ordu-Giresun vilayetlerinin Jeolojisi (Geologie des Vilayets Ordu-Giresun): 1st. Univ. Fen Fak. Mecm. Se.B., C.XI, No. 3, S.135

———— (1970) ikizdere granit karmaşigi: Rev. Fac. Sci., Univ. Istanbul, Tome XXXV, Fasc. 3-4, 161-167.

ANDERMAN, G. and KEMP, J.W., (1958) Scattered x-rays as internal standards in x-ray emission spectroscopy: Analyt. Chem., 30, 1306-1309.

ARCULUS, R.J. and CURRAN, E.B., (1972) The genesis of the calc-alkaline rock suite: Earth Planet. Sci. Lett., 15, 255-262.

ARNI, P., (1939) Tektonische, grundzuge Ostanatolien und benachbarter gebiete: MTA Publ., Serie B, No. 4, Ankara.

ARNOLD, R.G., (1969) Pyrrhotite phase relations below 304 ± 6°C at 1 Atm. total pressure: Econ. Geol., 64, 405-419.

AYISKAN, Ö., (1959) Giresun ili dahilinde, Bulancak güneyi Tekmezar Köyü civari sülfürlü cevher yataklarinin tetkik ve tesbiti hakkinda rapor: MTA, Maden Etüd Şb. Arsiv No. 587, Ankara.

BAILEY, S.W. and CAMERON, E.N., (1951) Temperatures of mineral formation in bottom-run lead-zinc deposits of the Upper Mississipi Valley as indicated by liquid inclusions: Econ. Geol., 46, 626-651.

BARNES, H.L., (1962) Mechanisms of mineral zoning: Econ. Geol., 57, 30-37.

——— and CZAMANSKE, G.K., (1967) Solubilities and transport of ore minerals: p. 334-381 in Barnes, H.L., Ed., Geochemistry of Hydrothermal Ore Deposits: Holt, Reinehart and Winston, Inc., 670p.

BARTON, P.B., Jr. and TOULMIN, P., 111., (1966) Phase relations involving sphalerite in the Fe-Zn-S system: Econ. Geol., 61, 815-849.

——— and SKINNER, B.J., (1967) Sulfide mineral stabilities: p.236-333 in Barnes, H.L., Ed., Geochemistry of Hydrothermal Ore Deposits. Holt, Reinhart and Winston, Inc., 670p.

BERG, G., (1910) Geologische Beobahtungen in Kleinasien: Zeitschr. Deutch. Geol. Ges., Abh.62.

BETHKE, M.P. and BARTON, P.B. Jr., (1971) Distribution of some minor elements between coexisting sulfide minerals: Econ. Geol., 66, 140-163.

BIRKELAND, T. and BJØRLYKKE, A. (1972) Fluid inclusion studies from the Lead- and zinc-bearing veins at Trå̊k, Bumble: Norge geol. Unders., 277, 1-15.

BLUMENTHAL, M.M., (1946) Die neue geologische Karte der Türkei under einige ihrer stratigraphisch-tektonischen grundzuge: Eclogae. Geol. Helv., 39, No. 2.

BOORMAN, R.S., (1967) Subsolidus studies in the ZnS-FeS-FeS_2 system: Econ. Geol., 62, 614-631.

BORODAEV, Yu.S., et al, (1970) Isomorphous series of Bismuthinite Aikinite: West. Mosk. Univ. Ser. IV., Geol. No. 1, 18-33.

———— and MOZGOVA (1971) New group of the sulfbismuthides of Ag, Pb and Cu: Soc. Mining Geol. Japan, Spec. Issue 2, 35-41.

BOSTROM, K. and PETERSON, M.N.A., (1966) Precipitates from hydrothermal exhalations on the East Pacific Rise: Econ. Geol., 61, 1258-1265.

BRINKMAN, R., (1968) Einige geologische Leitlinen von Anatolien (Some geologic lineaments of Anatolia: Turkey): Geol. et Paleont., 2, 111-119, Marburg.

———— (1971) The geology of Western Anatolia: p. 171-190, in Campbell, A.S., Ed., Geology and History of Turkey. Petr. Expl. Soc. Libya, 511p.

BROWN, G.M. and SCHAIRER, J.F., (1971) Chemical and Melting relations of some Calc-alkaline volcanic rocks: Geol. Soc. Am. Inc., Memoir 130, 139-157.

———— et al (1970) Petrographic mineralogic and x-ray fluorescence analysis of Lunar igneous-type rocks and spherules: Science, 167, 599-601.

BUHLMAN, E. (1971) Untersuchungen im System Bi_2S_3-Cu_2S und geologische Schußfolgerungen: Neues Jahrb. Min., Mh., 137-141.

CANN, J.R., (1970) Rb, Sr, Y, Zr and Nb in some ocean floor basaltic rocks: Earth planet. Sci. Lett., 10, 7-11.

CORLISS, J.B., (1971) The origin of metal-bearing submarine hydrothermal solutions: Jour. Geophys. Res., 76, No. 33, 8128-8138.

CRAIG, J.R., (1967) Phase relations and mineral assemblages in the Ag-Bi-Pb-S system: Mineral Deposits., 1, 278-306.

———— and KULLERUD, G., (1967) The Cu-Fe-Pb-S system. Ann. Rept. Geophys. Lab. Washington, Yr. Bk. 65, 344-352.

———— (1973) The Cu-Zn-S system: Mineral. Deposita (Berl.), 8, 81-91.

———— (1968) Phase relations and mineral assemblages in the copper-lead-sulfur system: Am. Mineralogist, 53, 145-161.

CZAMANSKE, G.K., et al (1963) Neutron activation analysis of fluid inclusions for copper, manganese and zinc: Science, 140, 401-403.

ÇOGULLU, E., (1970) Gümüşhane ve Rize granitik plutonlarının mukayeseli petrolojik ve Jeokronolojik etüdü: I.T.Ü. Maden Fakültesi (Doçentlik Tezi), Istanbul.

DE SITTER, L.U. (1964) Structural Geology: McGraw-Hill Book Company, Inc. 551p.

DEER, W.A., HOWIE, R.A. and ZUSSMAN, J. (1969): An introduction to the rock forming minerals: Fifth Edit., Longmans, 528p.

DENT, D.L. (1969) The soils of the Trabzon Catena, NE Turkey: Unpubl. M.Sc. Thesis, Univ. of Durham.

DEWEY, J.F., et al (1973) Plate tectonics and the evolution of the Alpine system: Bull. Geol. Soc. Amer., 84, 3137-3180.

DICKINSON, W.R. (1968) Circum-Pacific andesite types: J. geophys. Res., 73, 2261-2269.

———— and HATHERTON, T. (1967) Andesite volcanism and seismicity around the Pacific: Science, 157, 801-803.

DONNAY, G. and KULLERUD, G. (1958) High temperature chalcopyrite. Carnegie Inst. Wash., Yearbook 57, p.246.

DORNBERGER-SCHIFF, V.K. und HÖHNE, E. (1959) Die Kristallostruktur des Betechtinit $Pb_2(Cu,Fe)_{21}S_{15}$: Acta Cryst., 12, 646-651.

DRUMMOND, A.D., et al (1969) Neyite, a new sulphsalt from Alice Arm, British Columbia: Can. Mineralogist, 10, 90-96.

DUNCUMB, P and JONES, E.M. (1970) Electron probe micro analysis. An easy to use computer program for correcting quantitative data: Report No. 260 Tube Investment Research Labs., Hinxton Hall, Saffron Walden, Cambridge, England.

———— and REED, S.J.B. (1968) The calculation of stopping power and backscatter effects in electron probe microanalysis: N.B.S. Sp. Publ. No. 298, 133-154.

———— and SHIELDS, P.K. (1966) Effect of critical potential on the absorption correction in x-ray microanalysis, in McKinley, T.D., Heinrich, K.F.J., and Wittry, D.B., Ed., The Electron Microprobe: John Wiley and Sons, 1035p.

EDWARDS, A.B. (1965) Textures of the ore minerals and their significance fourth printing: Australasian Institute of Mining and Metallurgy, 242p.

EGERAN, E.N. (1947) Tectonique de la Turquie et relations etc.: G. Thomas, Nancy.

ERMAKOV, N.P., et al (1965) Research on the nature of mineral of mineral forming solutions, with special reference to data from fluid inclusions: Volume 22 of Internat. Ser. of Monographs in Earth Sciences, Pergamon Press, New York, 743 p.

FITTON, J.G. (1971) The petrogenesis of the calc-alkaline Borrowdale volcanic group, Northern England: Unpubl. Ph.D. Thesis, Univ. of Durham.

———— and GILL, R.C.O. (1970) The oxidation of ferrous iron in rocks during mechanical grinding: Geochim. Cosmochim. Acta, 34, 518-524.

FLANAGAN, F.J. (1969) U.S. Geological Survey Standards - II First compilation of data for the new USGS rocks: Geochim. Cosmochim. Acta, 33, 81-120.

———— (1973) 1972 values for international geochemical reference samples: Ibid., 37, 1189-1200.

FRECH, F. (1914) Der vulkanismus Kleinasiens und sein verhaeltnis zum Gebirgsbau: Peterm. Mittl. Gotha.

FRIEDMAN, I. (1949) A proposed method for the measurement of geologic temperatures: J. Geol., 57, 618-619.

FRENZEL, G. (1959a) Idait und "blaubleinder Covellin": Neues Jahrb. Mineral., Abhandl., 93, 87-132.

———— (1959b) Ein neues mineral: Idait: Neues Jahrb. Mineral., Monatsh., 142.

GABRELIAN, A.H. (1964) The tectonic structure of Anticaucasus and its position in the Mediterranean Orogenic belt: Report of the 22 Int. Geol. Congr. New Delhi.

GATTINGER, T.E., et al (1962) Explanatory text of the Geological Map of Turkey, Trabzon Sheet (1:500,000), MTA Publ., Ankara.

GEOFFROY, J. de (1960) Çayeli, Pazar ve Ardeşen Bölgelerinin Jeolojisi ve maden yataklari: MTA Rp., Ankara.

GHOSH-DASTIDAR, P., et al (1970) Factors affecting the trace element partition coefficients between co-existing sulfides: Econ. Geol., 65, 815-837.

GILL, R.C.O. (1972) The geochemistry of the Gronnedal-Ika alkaline complex, South Greenland: Unpubl. Ph.D. Thesis, Univ. of Durham.

GODOVIKOV, A.A. and PTITSYN, A.B. (1966) Entry of iron into sphalerite during hydrothermal recrystallization: Doklady Akad. Nauk SSSR, 166, 102-105.

GÖKSU, E. (1974) Explanatory text of the geological map of Turkey, Samsun Sheet (1:500,000): MTA Publ., Ankara (In pre.).

GÜMÜŞ, A. (1970) Türkiye Metalojenisi, 1:25000 ölçekli Türkiye metalojenik haritasinin izahi: MTA Publ., No. 144.

HAAS, J.L.,·Jr. (1970) An equation for the density of vapor-saturated NaCl-H_2O solutions from 75° to 325°C: Am. Jour. Sci. 269, 489-493.

———— (1971) The effect of salinity on the maximum thermal gradient of a hydrothermal system at hydrostatic pressure: Econ. Geol., 66, 940-946.

HALL, A.J.(1971) The mineralogy of some synthetic sulphosalts: Unpubl. Ph.D. Thesis, Univ. of Durham.

———— (1972) Substitution of Cu by Zn, Fe and Ag in synthetic tetrahedrite, Cu_{12} Sb_4 S_{13}: Bull. Soc. Fr. Mineral. Cristallogr., 95, 583-594.

HALL, W.E., et al (1971) Fractionation of minor elements between galena and sphalerite, Darwin Lead-Silver-Zinc mine, Inyo County, California and its significance in geothermometry: Econ. Geol., 66, 602-606.

HAMAMCIOGLU, and SAWA, T. (1971) Gelişen yeni görüşlerin ışıgı attinda Karadeniz bölgesi bakir-kurşun-çinko yataklari: Türkiye Madencilik Bilimsel ve Teknik II. Kongresi, tebligler kitabi ayri baskisi, Maden Mühendisleri Odasi yayini, 64-73, Ankara.

HAMILTON, W. (1849) Observations on the geology of Asia Minor ... etc.: Quart. Jour. Geol. Soc. London.

HELGESON, H.C. (1964) Complexing and hydrothermal Ore deposition: The Macmillan Co., 128p.

———— (1968) Geologic and Thermodynamic characters of the Salton Sea Geothermal system: Am. Jour. Sci., 266, 129-166.

HATCH, F.H., WELLS, A.K. and WELLS, M.K. (1972) Petrology of the Igneous rocks: 13th Edit., Thomas Murby and Co., 551p.

HIRST, D.M. (1971) Consideration of a sedimentary source for the heavy metal content of ore-forming fluids: Trans. Inst. Min. Met. (B), 80, B1-3.

HOLLAND, H.D. (1965) Some applications of thermochemical data to problems of ore deposits II. Mineral Assemblages and the composition of ore-forming fluids: Econ. Geol., 60, 1101-1166.

———— (1967) Ganque minerals in hydrothermal deposits: p.383-436 in Barnes, H.L., Ed., Geochemistry of Hydrothermal Ore Deposits: Holt, Reinehart and Winston, Inc., 670p.

———— (1972) Granites, solutions and base metal deposits: Econ. Geol., 67, 281-301.

HONNOREZ-GUERSTEIN, B.M. (1971) Betekhtinite and Bi-Sulphosalts from the Copper Mine of "La Leona" (Argentina): Mineral Deposita (Berl.), 6, 111-121.

HORIKOSHI, E. (1969) Volcanic activity related to the formation of the Kuroko-type deposits in the Kosaka District, Japan: Mineral. Deposita (Berl).

HORSTINK, J., (1971) The late Cretaceous and Tertiary geological evolution of Eastern Turkey: Ass. Turkish Petr. Geol., First Petroleum Congress, Ankara.

HTEIN, W. (1973) The quantitative measurement of colour in minerals: Unpubl. Ph.D. Thesis, Univ. of Durham.

ILHAN, E. (1971) The structural features of Turkey: p.159-170 in Campbell, A.S., Ed., Geology and History of Turkey. Petr. Expl. Soc. Libya, 511p.

IVANOV, V.V. (1949) Overall estimates of the average trace-element content of principal ore minerals: Dokl. Acad. Sci. USSR., Earth Sci. Sect., 186, 210-211.

JAKES, P. and WHITE,A.J.R. (1970) K/Rb ratios of rocks from island arcs: Geochim. Cosmochim. Acta, 34, 849-856.

KAADEN, G.v.d. (1966) Türkiyedeki glokofan Kayaçlarının önemi ve dagılışı: MTA Bull., No. 67, 38-68, Ankara.

KAMEN-KAYE, M. (1971) A review of depositional history and geological structure in Turkey: p.111-137 in Campbell, A.S., Ed., Geology and History of Turkey. Petr. Expl. Soc. Libya, 511p.

KARUP-MØLLER, S. (1973) A gustavite-cosalite-galena bearing mineral suite from the cryolite deposit at Ivigtut, South Greenland: Medd. Grønland, 195, No. 5, 1-40.

KAYNAK, U. (1972) Bulancak Kornalı Dere IP Etüdü Raporu: Etibank, Ankara.

KEIL, K. (1967) The electron microprobe x-ray analyzer and its applications in mineralogy: Fortschr. Miner., 44, 4-66.

KELLY, W.M. and TURNEAURE, F.S. (1970) Mineralogy, paragenesis and geothermometry of the tin and tungsten deposits of the eastern Andes, Bolivia: Econ. Geol., 65, 609-680.

KERRICK, D.M., et al (1973) The role of carbon film thickness in electron microprobe analysis: Am. Mineralogist, 58, 920-925.

KETIN, I. (1951) Über die geologie der gegend von Bayburt in Nordost Anotolien: Rev. Fac. Sci., Univ. Istanbul. Ser. B, vol. XVI, Fasc. 2.

———— (1959) Türkiyenin orojenik gelişmesi: MTA Bull., No. 53, 78-86, Ankara.

———— (1962) Explanatory text of the geological map of Turkey, Sinop Sheet (1:500,000). MTA Publ., Ankara.

———— (1966) Tectonic Units of Anatolia: MTA Bull., No. 66, 23-34, Ankara.

KINGSBURY, A.W.G. and HARTLEY, J. (1956) Cosalite and other lead sulphosalts at Grainsgill, Carrock Fell, Caldbeck, Cumberland: Min. Mag., 31, 296-300.

KINGSTON, P.W. (1968) Studies of mineral sulphosalts: XXI - Nuffieldite, a new species: Can. Mineralogist, 9, 439-452.

KLEVSTON, P.V. and LEMMLEIN, G.G. (1960) Pressure corrections for the homogenization temperature of aqueous NaCl solution: Dakl. Acad. Sci. USSR; 128, 995-997.

KLOMINSKY, J., et al (1971) Heyrovskyite, 6 ($Pb_{0.86}$ $Bi_{0.08}$ $(Ag,Cu)_{0.04}$ S. Bi_2S_3 from Hurky, Czechoslovakia, a new mineral of genetic interest: Mineral Deposita (Berl.), 6, 133-147.

KLUG, H.P. and ALEXANDER, L.E. (1962) X-ray diffraction Procedures: John Wiley and Sons, Inc., 716p.

KLYAKHIN, V.A. and DIMITRIYEVA, M.T. (1968) More information about synthetic and natural Lillianite: Dakl. Acad. Sci. USSR, Earth Sci. Sect., 178, 106-108.

KOHATSU, I. and WUENSCH, B.J. (1971) The crystal structure of aikinite, $PbCuBiS_3$: Acta Cryst., B27, 1245-1252.

KOSTOV, I. (1958) Bonchevite, $PbBi_4S_7$, a new mineral: Min. Mag., 31, 821-828.

KRÄEFF, A. (1963a) A contribution to the geology of the region between Şirya and Ardanuç: MTA Bull., No. 60 37-43, Ankara.

———— (1963b) Geology and mineral deposits of the Hopa-Murgul region (western part of the Province of Artuin) NE Turkey: Ibid. 44-59.

KRONBERG, P. (1970) Dogu Karadeniz daglarinin (Kuzeydogu Türkiye) tectonigi hakkinda veriler: MTA Bull., No. 74, 57-65, Ankara.

KULLERUD, G. (1953) The FeS-ZnS system, a geological thermometer: Norsk. Geol. Tidsskr., 32, 61-147.

KUNO, H. (1966) Lateral variation of basalt magma type across continental margins and island arcs: Bull. Volcan. Ser. 11, 29, 195-222.

LEMMLEIN, G.G. and KLEVSTOV, P.V. (1961) Relations among the principal thermodynamic parameters in a part of the system H_2O-NaCl: Geochemistry, No. 2, 148-158.

LEVY, C. (1967) Contribution a La mineralogie des sulfures de cuivre du type Cu_3XFe_4: Mem. Bur. Rech. Geol. Minieres, 54, 178.

LONG, J.V.P. (1967) Electron Probe microanalysis: p.215-260 in Zussman, J. Ed. Physical Methods in Determinative Mineralogy, Academic Press, 514p.

LOWDER, G.G. (1970) The volcanics and caldera of Talasea, New Britain: Mineralogy. Contr. Miner. Petrol., 26, 324-340.

MARKHAM, N.L. and OTTEMAN, J. (1968) Betekhtinite from Mt. Lyell, Tasmania: Mineral Deposita (Berl.), 3, 171-173.

MARPLES, J.A.C. and SHAW, J.L. (1966) Two crystallographic computer programs for Lattice parameter refinement and for calculating expected line position: UKAEA Research Group Report AERE-R5210.

MASKE, S. and SKINNER, B.J. (1971) Studies of the sulfosalts of copper I. Phases and phase relations in the system Cu-As-S: Econ. Geol. 66, 901-918.

MATSUKAMA, T. (1971) Betechtinite from the Kuroko deposits of the Furotobe Mine, Akita Prefecture, Japan: Mineral. Soc. Japan. Spec. Paper 1, 191-195.

MAUCHER, A. et al (1962) Geologisch-Lagerstättenkundliche Untersuchungen im Ostpontischen Gebirge: Bay. Akad. d.wiss.math.-nat. Kl; Abh. N.F., 109, München.

McINTIRE, W.L. (1963) Trace element partition coefficients - a review of theory and applications to geology: Geochim. Cosmochim. Acta., 27, 1209-1264.

McKENZIE, D.P. (1970) Plate tectonics of the Mediterranean region: Nature, 226, No. 5442, 239-243.

McKINSTERY, H.E. (1949) Mining Geology: Prentice-Hall, Inc., 680p.

MEISTER, E. (1913) Über den Lias in Nordanatolien: Neues Jahrb. f. Min. Bd. 35.

MERO, J.L. (1965) The mineral resources of the sea: Elsevier, Amsterdam.

METAG Report (1972) Giresun Akköy ve civari arama raporu: METAG Mühendislik Ltd. Şti., Ankara.

MEYER, C. and HEMLEY, J. (1967) Wall-Rock alteration: p.167-235, in Barnes, H.L., Ed., Geochemistry of Hydrothermal Ore Deposits. Holt, Reinehart and Winston, Inc. 670p.

MIDDLEMOST, E.A.K. (1973) A simple classification of volcanic rocks: Bull. Volcanol., 36, 382-397.

MIYASHIRO, A. (1974) Volcanic rock series in island arcs and active continental margins: Am. Jour. Sci., 274, 321-355.

MIYAZAWA, T. (1967) Lowest Limit and depth of formation of hydrothermal veins: Sci. Rept., Rokyo Kyoiku Daigaku, 9, 257-261.

MOHS, F. (1804) Des Herrn J.F. Null Mineralien-Kabinet, nach einem, durchaus auf aussere kennzeichnem gegründeten systeme geordnet: 3 abthl., 8 vo, Vienna.

MOOR, J.G. (1962) K/Na ratio of Cenozoic igneous rocks of the Western United States: Geochim. Cosmochim. Acta, 26, 101-130.

———— and CALK. L. (1971) Sulfide spherules in vesicles of dredged pillow basalt: Am. Mineralogist, 56, 476-488.

MOORE, P.B. (1967) A classification of sulfosalt structures derived from the structure of aikinite: Am. Mineralogist, 52, 1874-1876.

MTA Report No. 982 (1970) Report on the geological mapping in 1:10,000 scale of the Espiye and Bulancak district (Giresun): MTA, Ankara.

MUKANOV, K.M., et al (1961) On the occurrence of betekhtinite in the Dzhezkazgan ore deposit: Dokl. Acad. Sci. USSR, Earth Sci. Sect., 130, 133-135.

NALDRETT, A.J. (1966) The role of sulphurization in the genesis of iron-nickel sulphide deposits of the Porcupine District, Ontario CIMM Trans., 69, 147-155.

NAKAMURA, T. and HUNAHASHI, M. (1970) Ore veins of Neogene volcanic affinity in Japan: p.215-230, in Tatsumi, T., Ed., Volcanism and Ore Genesis, University of Tokyo Press, 448p.

NASH, J.T. (1972) Fluid inclusion studies of some gold deposits in Nevada: U.S. Geol. Survey, Prof. Paper 800-C, C15-19.

NASH, J.T. and THEODORE, T.G. (1971) Ore fluids in a porphyry copper deposit at Copper Canyon Nevada: Econ. Geol., 66, 385-399.

NECHELYUSTOV, G.N. and LEBEDEV, V.S. (1967) The first discovery of bonchevite in the USSR: Dokl. Acad. Sci. USSR, Earth Sci. Sect., 174, 131-134.

NELSON, J.B. and RILEY, D.P. (1945) An experimental investigation of extrapolation methods in the determination of accurate unit cell dimension of crystals: Phys. Soc. London Proc., 57, 160-177.

NICHOLLS, I.A. (1971) Santorini volcano, Greece-tectonic and petrochemical relationships with volcanics of the Aegean Region: Tectonophysics. 11, 377-385.

NICOLAOU, M. and HÄKLI, T.A. (1970) The presence of aikinite in the Aberdeen area of the Kirki Mine, Western Greece: Bull. Geol. Soc. Finland, 42, 53-55.

NOWACK, E. (1928) Eine Veise von Angora zum Schwarzen Meer: Zeitschr. d. D. Geol., Ges. für Erdkunde zu Berlin, No. 1-2.

———— (1932) Kreide-Entwicklung und Grosstektonik in Nord-Anatolien: Zentralblatt f. Min. etc., B. Stuttgart.

OHMOTO, et al (1970) The Kuroko ore of Japan: Products of seawater? (Abs.): Geol. Soc. America Ann. Mtg., Milwaukee, 640-641.

OSWALD, F. (1912) Armenian Handbuch d. regional: Geologie, Bd. V/3, H.10, Heidelberg.

PADERA, K. (1955) Beltrag zur revision der mineralien aus der gruppe von wismutglanz und aikinit: Chemie der Erde, Band 18, 14-18.

PARASKEVOPOULOS, G.M. (1956) Über den chemismus und die provinzialen verhältnisse der Tertiären und Quatären ergussgesteine des Ägäischen raumes und der benachbarten gebieten: Tschm. Mineral. Petrol. Mitt., Ser. 3, 6, 1-72.

PEACOCK, M.A. (1942) Studies of mineral sulphosalts: VI-Aikinite: Univ. Toronto Studies, Geol. Ser., No. 47, 63-69.

PEARCE, J.A. and CANN, J.R. (1971) Ophiolite Origin investigated by discriminant analysis using Ti, Zr and Y: Earth Planet. Sci. Lett., 12, 339-349.

PEJATOVIC, S. and TEŞREKLI, M. (1970) Türkiye Karadeniz Sahil metalojenik zonu, piritik ve skarn cevher zuhurlarinin kiymetlendirilmesi: MTA, Maden Etud Şb. Arşivi, Rp. No. 952, Ankara.

PETERSON, U. (1970) Metallogenic provinces in South America: Geol. Rundschau, 59, 834-897.

PHILIPPSON, A. (1919) Kleinasien: Handbuch d. regional geologie, 22, Bd. v/2, Heidelberg.

PINAR, N. and LAHN, E. (1954) Nouvelles considerations sur la tectonique de L'Anatolie: Soc. Geol. France, Bull., ser. 6, 5, 11-34.

POLLAK, A. (1961) Karadeniz sahilinde, Giresun vilayeti dahilinde Lahanos cevher yataklan MTA Bull. No. 56, Ankara.

PRICE, N.J. (1966) Fault and Joint Development in Brittle and semi-Brittle Rock: Pergamon Press Ltd., 176p.

RAMDOHR, P. (1969) Ore Minerals and Their intergrowth: Pergamon Press Ltd., 1174p.

RAMOVIC, M. (1966) Metalojeni ve Petrolojide Jeolojik Zaman faktörünün önemi: MTA Bull. No. 67, 25-37, Ankara.

REEVES, M.J. (1971) Geochemistry and mineralogy of British Carboniferous Seate earths from northern Coalfields: Unpubl. Ph.D. Thesis, Univ. of Durham.

ROEDDER, E. (1960) Fluid inclusions as samples of the ore-forming fluids: XXI Internat. Geol. Congr. Proc. Sec. 16, 218-229.

———— (1962a) studies of fluid inclusions I: Low temperature application of a dual-purpose freezing and heating stage: Econ. Geol., 57, 1045-1061.

———— (1962b) Ancient fluids in crystals: Sci. American, 207, 38-47.

———— (1963) Studies of fluid inclusions II: Freezing data and their interpretation: Econ. Geol., 58, 167-211.

———— (1967a) Fluid inclusion as samples of ore fluids: p.515-574, in Barnes, H.L., Ed., Geochemistry of Hydrothermal Ore Deposits. Holt, Reinehart and Winston, Inc., 670p.

———— (1967b) Environment of deposition of stratiform (Mississipi Valley type) ore deposits, from studies of fluid inclusions: p.349-361, in Brown, J.S., Ed., Genesis of Stratiform Lead-zinc-barite-fluorite deposits in carbonate rocks: Econ. Geol., Mon. 3.

———— (1971) Fluid inclusion studies on the porphyry-type ore deposits at Bingham, Utah, Butte, Montana and Climax, Colorado; Econ. Geol., 66, 98-120.

———— (1972) Composition of fluid inclusions: in Data of Geochemistry, Chapter JJ, U.S. Geol. Survey Prof. Paper 440-JJ, 164p.

———— and DWORNIK, E.J. (1968) Sphalerite color banding: Lack of correlation with iron content: Am. Mineralogist, 53, 1523-1529.

———— and SKINNER (1968) Experimental evidence that fluid inclusions do not leak: Econ. Geol., 63, 715-730.

ROSE, W.A. (1961) The iron content of sphalerite from the Central District, New Mexico and Bingham District, Utah: Econ. Geol., 56, 1163-1384.

RYAN, C.W. (1960) A guide to the known mineral of Turkey: MTA Publ., Ankara.

SAKHAROVA, M.S. (1955) On bismuth sulfosalts of Ustarasaisk deposit: Trans. Miner. Mos. Acad. Sci. USSR, 7, 112-126.

SALANCI, B. (1965) Untersuchungen am System Bi_2S_3 - PbS:N. Jb. Miner. Monatshefte, 384-388.

SAWKINS, F.J. (1964) Lead-Zinc ore deposition in the light of fluid inclusion studies, Providencie Mine, Zacatecas, Mexico: Econ. Geol., 59, 883-919.

———— (1966) Ore genesis in the North Pennine Orefield; in the light of fluid inclusion studies: Econ. Geol., 61, 385-401.

———— (1972) Sulfide ore deposits in relation to plate tectonics: Jour. Geol. 80, No. 4, 377-397.

SCHERMERHORN, L.J.G. (1973) What is Keratophyre: Lithos 6, 1-11.

SCHROLL, E. (1953) Uber minerale und spurenelemente vererzung, und enstehung der blei-zink-lager statte Bleiberg-Kreuth, Kartens in Osterreich: Mittl. der Osterr. Mineral. Gellschaft, Sonder heft, Nr. 2, 1-60.

SCHUILING, R.D. (1962) On petrology, age and structure of Menderes migmatile complex (SW Turkey): MTA Bull., No. 58, 71-84, Ankara.

SCHULTZE-WESTRUM, H.H. (1960) Giresun-Trabzon vilayetlerinde yapilan harita calişmalari hakkinda rapor: MTA Rp., Ankara.

_____ (1961) Das geologische profil des Aksudere bei Giresun ein beitrag zur geologie und Lagerstattenkunde der Ostpontischen erz und mineral provinz, NE Anatolien: MTA Bull., No. 57, Ankara.

SCHÜLLER, A. (1960/61) Zur Kenntnis des Betechtinit $(Cu, Fe)_{10}PbS_6$: Neues Jahrb. Mineral. Monatsh, 121-131.

———— und WOHLMANN (1955) Betechtinit, ein neues blei-Kupfer-sulfid aus den Mansfelder Rücken: Geologie, 4, 535-555.

SCOTT, S.D. and BARNES, H.L. (1971) Sphalerite geothermometry and geobarometry: Econ. Geol., 66 653-669.

SEYHAN, I. (1972) Türkiye maden provensterinen oluşuma: MTA Bull., No. 78, 51-57, Ankara.

SHAW, D.M. (1968) A review of K-Rb fractionation trends by covariance analysis: Geochim Cosmochim. Acta, 32, 573-601.

SILLITOE, R.H. (1972) Relations of metal provinces in Western America to subduction of oceanic Litosphere: Bull. Geol. Soc. Amer., 88, 813-818.

SKINNER, B.J., et al (1959) Effects of FeS on the unit-cell edge of sphalerite, a Revision: Econ. Geol., 54, 1040-1046.

SKINNER, B.J., et al (1972) Studies of the sulfosalts of Copper III. Phases and phase relations in the system Cu-Sb-S: Econ., 67, 924-938.

SLACK, G.A., et al (1966) Optical absorption of tetrahedral Fe^{+2} ($3d^6$) in cubic ZnS, CdTe, and $MgAl_2O_4$: Phys. Rev., 152, 376.

———— (1967) Far infrared optical absorption of Fe^{2+} in ZnS: Ibid, 155, 170-177.

SLAVSKAYA, A.I., et al (1963) O razlozhenii betekhtinita pri nagrevanii (Journal for Geology of ore deposit, in Russian): 3, 97-100.

SMIRNOV, V.I., et al (1972) The study of Internal chemical Heterogeneity of monocrystals with JXA-5: Geol. News. 11e, No. 1, 1973.

SMITH, F.W. (1973) A simple microscope freezing stage: Min. Mag., 39, 366-367.

———— (1974a) Factors governing the development of fluorspar orebodies in the North Pennine Orefield: Unpubl. Ph.D. Thesis, Univ. of Durham.

———— (1974b) The identification and assessment on new fluorspar orebodies in the North Pennines: An unpubl. Report to the British Steel Corporation.

SMITH, F.G. and LITTLE, W.M. (1959) Filling temperatures of H_2O - CO_2 fluid inclusions and their significance in geothermometry: Can. Mineralogist, 6, 380-388.

SNELGROVE, A.K. (1971) Metalojeni ve yeni Küresel tektonik: MTA Bull, No. 76, 135-153, Ankara.

SOROKIN, V.I., et al (1970) Variation of the a_o parameter with the content of iron in sphalerite obtained under hydrothermal conditions: Geochem. Int., 361-363.

SOURIRAJAN, S. and KENNEDY, G.C. (1962) The system H_2O-NaCl at elevated temperatures and pressures: Am. Jour. Sci., 260 115-141.

SPRINGER, G. (1969) Electron probe analyses of tetrahedrite: Neues Jahrb. Mineral. Monatsh., HFl., 24-33.

———— (1971) The synthetic solid-solution series Bi_2S_3 - $BiCuPbS_3$ (Bismuthinite-Aikinite): Ibid., 1, 19-24.

STAUB, R. (1924) Der Bau der Alpen: Bern.

STCHEPINSKY, V. (1945) Rapport sur la geologie et les resources minerals des bassin superior de Kelkit Çayi: MTA Rp. No. 2687, Ankara.

SUGAKI, A. and TASHIRO, C. (1957) Thermal studies on the skeletal crystals of chalcopyrite in sphalerite: Sci. Repts. Tohoku Univ. Ser 111, 5, 293-304.

SWEATMAN, T.R. and LONG, J.V.P. (1967) Quantitative electron-probe microanalysis of rock-forming minerals: Jour. Petrology, 10, 332-379.

TAKENOUCHI, S. and KENNEDY, G.C. (1965a) Dissociation of pressures of the phase $CO_2.5\ ^3/4\ H_2O$: Jour. Geol., 73, 383-390.

———— (1965b) The solubility of carbon dioxide in NaCl solutions at high temperatures and pressures: Am. Jour. Sci., 263, 445-454.

TARLING, D.H. (1973) Metallic Ore Deposits and Continental Drift: Nature, 243, 193-196.

TAYLOR, C.M. and RADTKE, A.S. (1965) Preparation and polishing of ores and mill products for microscopic examinations and electron microprobe analysis: Econ. Geol., 60, 1306-1319.

TCHIHATCHEFF, P.de (1867) Asie Mineure: Geologie, Paris.

TOKEL, S. (1973) The stratigraphical and volcanic history of the Gümüşhane area, North-East Anatolia: Unpubl. Ph.D. Thesis, University College London, Dept. of Geology.

TOULMIN, P. III., and CLARK, S.P., Jr. (1967) Thermal aspects of ore formation: p. 437-464, in Barnes, H L., Geochemistry of Hydrothermal Ore Deposits. Holt, Rinehart and Winston Inc., 670p.

TSONEV, D., et al (1970) Betekhtinite from the Radka deposit: Bull. Geol. Inst. Bulgar Acad. Sci. Ser. Geochem. Min. Petrogr., 19, 167-177.

TUGAL, H.T. (1969) The pyritic sulphide deposits of the Lahanos Mine area, Eastern Black Sea region, Turkey: Unpubl. Ph.D. Thesis, Univ. of Durham.

TUGARINOV, A.I. and NAUMOV, V.B. (1972) Physicochemical parameters of hydrothermal mineral formation: Geochemistry Int., 161-167.

TUREKIAN, K.K. and WEDEPOHL, K.H (1961) Distribution of the elements in some major units of the Earth's Crust: Bull. Geol. Soc. Amer., 72, 175-192.

TURNEAURE, F.S. (1960) A comparative study of major ore deposits of Central Bolivia: Econ. Geol., 55, 217-254; 575-606.

VAN HOOK, H.J. (1960) The ternary system Ag_2S-Bi_2S_3-PbS: Econ. Geol., 55, 774-776.

WELIN, E. (1966) Notes on the mineralogy of Sweeden 5. Bismuth-bearing sulphosalts from Gladhammar, a revision: Arkiv Mineral. Geol., 4, No. 13, 377-386.

WHITE, D.E. (1968) Environments of generation of some base-metal deposits: Econ. Geol., 63, 301-335.

WICKMAN, F.E. (1953) The crystal structure of aikinite, $CuPbBiS_3$: Arkiv Mineral. Geol., 1, 501-507.

WILSON, A.D. (1955) A new method for the determination of ferrous iron in rocks and minerals: Bull. Geol. Surv. G.B., 9, 56-58.

WOLF, A.W. and BROWN, M.G. (1966) Concentrative properties of aqueous solutions: p. D127-166, Conversion tables in Handbook of Chemistry and Physics, 46th Edit., Cleveland Chemical Rubber Co.

WRIGHT, J.B. and McCURRY, P. (1973) Magmas, mineralization and sea-floor spreading: Geol. Rundschau, 62, No. 1, 116-125.

WUENSCH, B.J. (1964) The crystal structure of tetrahedrite, $Cu_{12}Sb_4S_{13}$: Zeits. Kristallog., 119, 437-453.

YILMAZ, Y. (1973) The petrology and structure of the Gümüşhane granite and the surrounding rocks, North-East Anatolia: Unpubl. Ph.D. Thesis, University College London, Dept. of Geology.

YUI, S. (1971) Heterogeneity within a single grain of minerals of the Tennantik-Tetrahedrite series: Soc. Mining Geol. Japan, Spec. Issue 2, 22-29.

ZANKL, H. (1961) Magmatismus and bauplan des ostpontischen gebirges im querprofil des Harşit tales, NE Anatolien: Geol. Rundschau, Bd. 51.

APPENDIX ONE

DETAILS OF SPECIMEN COLLECTION

Specimen Collection

The investigated mineralized area, and its surroundings have been described in Chapter 1-3. As expected such humid conditions, dense vegetation and hydrothermal alteration are unfavourable for preservation of the original character of the rock types and finding exposures for rock specimen collection. Due to reasons explained above and the narrowness of the veins and rough topography, an evenly distributed sampling was not possible. The great majority of the veins are exposed only along water courses, and hazelnut plantations and dense vegetation cover the area and extend towards the south where reasonably fresh rock outcrops are found. Some recently opened roadcuts provide exposures for specimen collection.

The specimens were collected during the two field seasons, May-July 1971, and August-Sept. 1973. A list of the specimen is given in the accompanying table 1. Altitudes are also included in the table to facilitate finding veins in the field.

The rock and vein specimens are listed in numerical order in table 1. Plutonic, volcanic and sedimentary rock specimens are referred to as PR 138, VR 23, SR 24, etc. respectively.

Rock Type:

Due to the intensely altered character of the rocks a classification was not applied in the strict sense. As anticipated, there is considerable overlapping in SiO_2 contents of rocks collected

from the same stratigraphic unit around the mineralized areas due to hydrothermal alteration, e.g., specimen 165 and 166 were collected from a "porphyritic dacite" outcrop 50 meters apart near Akköy Mine. They show variations of 73.05% to 81.60% in SiO_2. Nearer to the mineralization, silicification becomes more intense. Fresher rocks were accepted as basaltic, or basaltic-andesite at SiO_2 subdivisions 53.5 and 58wt.%.

Grid reference:

All three maps were divided into 8 horizontal, numbered from 1 to 8 and 9 vertical grids referred to as A, B, C., etc., and in the text. The approximate rock and vein specimen localities or any location are given in two figures in parenthesis, i.e. (3H).

Locality names:

Names have been taken from the 25,000 scale Giresun G40-a2, a3 and b1, b4 sheets and from the local people.

Altitudes:

All altitudes were measured by altimeter or taken from the reports or maps prepared by ETIBANK, the state-owned Mining Company.

APPENDIX TABLE 1 LOCATION OF ROCK AND VEIN SAMPLES

Specimen Number	Locality	Altitude (MS)	Grid Reference
1	Sarıdıken Dere	690	2F
2	"	670	"
3	"	630	"
4	"	630	"
6A	"	660	"
6B	"	660	"
6C	"	655	"
7	"	595	"
8	Kısla Camisi Dere (Etibank 695 Adit)	695	3F
VR8A	"	695	"
9	761 Peak, Kasyatak	705	3E
10	Kornalı Dere East Bank	600	"
11	"	590	"
12	"	565	"
VR12A	"	565	"
13	Kornalı Dere	585	"
VR13A	"	585	"
VR14	"	580	"
15	Kornalı Dere West Bank	590	"
16	"	600	"
17	"	625	"
VR17A	"	625	"
18	"	540	"
19	Kornalı Dere	530	"
20	"	540	"
21	Camideresi, Küçükdere Village	855	414
22	"	820	415H
VR23	NW of Armutlu Tepe	700	3I
SR24	SW of Kırtıl Tepe	760	3F/G
25	Kısla Mahallesi	760	3G
SR26	SW of Kırtıl Tepe	750	3F/G
27	SE of BL-4 Borehole, Kovalık Sr.	780	3F
28	S of "	780	2F
VR28A	"	780	"
29	North bank of Kısla Camisi Dere	625	2G
30	Sarıdıken Dere	590	2F
31	"	575	"
31A	"	570	"
32	"	500	"
33	Western Tributary of Sarıdıken Dere	670	1F
VR33A	"	670	"
34	Dönbül Dere, Yomasapagı	670	2E
34A	"	650	"
35	"	610	"
36	Northern Tributary of Dönbül Dere	610	2D
37	Kusdere	515	"
37A	"	515	"
VR37B	"	515	"
38	"	500	"
39	"	435	"
39A	"	400	"
40	"	385	"
41	E of BL-2 Borehole, Gonurca Dere	570	3D
41A	"	550	2D
42	"	550	"
43	NW of BL-3 Borehole, "	580	2C
44	"	665	2/3C
VR45	Sispelit Dere	670	3D
46	" Etibank Adits	600	3D
47	"	540	3E
47A	"	540	3E
VR47B	"	530	"
48	Sispelit Dere, Demir Export Company Adit	505	"
VR48A	"	505	"
VRM48A	"	505	"
VR49A	Kornalı Dere	500	"
50	W of Camlık Tepe, Madenyanı	370	2A
VR50A,B,C	"	370	"
VR51	"	300	"
VR52	Kuruköseoglu - Tasdibek	270	1A
53	West of Gedik Tepe	470	2B
VR53A,B	"	470	"

Specimen Number	Locality	Altitude(MS)	Grid Reference
54	Damyatagı Dere, Tekmezar	525	3C
55	"	455	"
56	"	520	"
57	"	365	"
58	NW of Dönbül Tepe, Dönbül Dere	650	2/3E
SR59	"	620	2E
60	"	580	"
61	"	570	"
62	"	525	"
63	W of Dönbül Tepe, Dönbül Dere	465	"
64	Tamyanı Dere, Büyükinece	380	4B
65	"	370	"
66	"	360	"
VR67	E of Büyükinece Village	230	5B
68	"	210	"
69	Tamyanı Dere, Büyükinece	400	4B
VR69,A,B,C	"	400	"
70	"	250	"
71A	Küçükgüre Dere	215	"
71B	"	215	"
VR72	"	210	4/5B
73	"	210	5B
74	"	200	"
75	"	195	"
76	"	190	"
77	"	180	"
78	"	160	"
79	Kuloglu Mahallesi, Darıköy	230	6A
80	"	220	"
81	Kuloglu Mahallesi, Karayalak Locality	280	"
82	"	210	"
83	"	190	"
84	Alibasoglu Mahallesi, Sinekli Deresi	200	6B
85	"	190	"
86	"	180	"
87	NE of Kırtıl Tepe, Hamidiye Road	740	3F
88	"	750	"
VR88A	"	750	"
89	"	750	"
90	"	755	"
VR90A	"	755	"
91A	Üzümlük Dere, Darıköy	315	6B
91B	"	305	"
92	"	265	"
93	"	270	"
94	"	220	"
VR94A,B	"	220	"
95	"	170	"
VR95A	"	170	"
96	Küçükgüre Dere	160	5B
97	"	160	5/6B
98	Büyükgüre Dere	700	3F
99	E of Kargaoglu Mahallesi, Darıköy	250	7B
VR99A	"	250	"
100	"	270	"
101	S of "	250	"
102	Elevlioglu Mahallesi, Darıköy	440	6B/C
103	E of Cimanoglu Mahallesi, Darıköy	400	6C
VR103A,B	"	400	"
103C	"	410	"
104	Agayeri Locality, Hamidiye	700	4F
105	"	650	"
106	"	600	"
106A	Büyükgüre Dere	550	"
107	"	540	4E
108	"	530	"
109	Vicinity of BL-6, BL-7 Boreholes	520	"
109A	"	520	"
110	"	500	"
111	Etibank 475 Adit, Büyükgüre Dere	475	"
112	"	385	"
113	Büyükgüre Dere	320	5D

APPENDIX TABLE 1: continued

Specimen Number	Locality	Altitude(MS)	Grid Reference
114	Büyükgüre Dere	310	5D
115	"	300	"
116	"	290	"
117	"	280	"
118	"	235	6D
119 (Baryte Vein)	"	225	"
120	"	215	"
121	Ardahan Dere	190	"
122	Büyükgüre Dere	170	7D
123	"	165	7C
124	"	160	"
125	"	145	"
126	BL-5 Borehole, Kasyatak	570	4E
127	Ardahan Dere	260	6F
VR127A	"	260	"
VR128A	"	250	"
VR128B	"	250	"
129	"	245	"
VR130	"	240	6E
131	"	235	"
132	"	230	"
133	"	205	"
134	"	190	6D
VR135	NE of 523 peak, Hamidiye	320	"
VR130	"	340	"
VR137	Ardahan Dere	515	5I
VR138	"	460	5/6H
VR139	W of Kırtıl Tepe	850	3F
VR140	S of "	850	3G
VR141	"	850	"
VR142	S of Karaderebasi Tepe	910	4H
VR143	E of Camideresi Occurrence,Küçükdere	900	"
VR144	S of Armutlu Tepe	950	4I
VR145	N of Evliya Tepe	810	3F
VR146	E of Evliya Tepe	740	"
VR147	E of 774 peak, Hamidiye	710	4F
VR148	"	710	"
VR149	Dinekkaya Tepe, Tekmezar	680	3D
VR150	Gedik Tepe, Yukarı Tekmezar	600	2B
VR151	Tekmezar-Eriklik Road	510	2A
VR152	"	510	"
VR153	Camkoza Dere, Yaslıbahce	300	1D
VR154	"	300	1C
VR155	"	285	"
VR156	"	255	"
VR157	"	260	1B
VR158	W bank of Imam Dere, Karakoc	290	"
VR159	Imam Dere	240	1A/B
160	Kornalı Dere	540	3E
161	"	480	"
162	"	430	3D
164	Akköy Mine Orebody	140-150	8D
VR165	E of Akköy Mine, Giresun Road	125	"
VR166	"	125	"
VR167	Kovalık Sr.	650	2F
VR168	Kısla Mahallesi Road	710	3G
169	Körükyeri Dere, Tekmezar	540	2B
46/3	Sispelit Dere, 571 Adit	571	3D

APPENDIX TWO

ROCK ANALYSIS

Specimen Preparation.

Hand specimens of volcanic rock samples were cleaned of all foreign material prior to crushing then were split into coarse fragments less than 5cm. using a hydroaulic splitter. These coarse fragments were reduced to gravel size using a Sturtevant 2" x 6" Roll Jaw Crusher. The crushed sample was quartered and approximately 100 grams of it were placed in a Tema Laboratory Disc Mill, model T-100 with a tungsten-carbide widia grinding barrel. Grinding was achieved in two stages in order to avoid additional oxidation during grinding (Fitton and Gill, 1970). After 30 seconds grinding a representative sample of a few grams was withdrawn for the FeO determination. However due to the altered nature of the rocks, grinding in most cases was completed within 30 seconds, when the resultant powder began to adhere to the walls of the mill.

Neat briquettes were prepared from the rock powders. For this purpose the powders were compressed with a hydraulic press operating at 800-900 Kg/cm^3 (5-6 tons/sq. in.) after mixing the powder with 5 drops of 2% solution of Mowiol which serves as an inert organic binder. The briquettes were allowed to dry for several days prior to analyses.

XRF Analyses, Major elements.

The X-ray Fluorescence analyses were carried out on a Phillips PW1212 automatic spectrometer. Analyses were carried out by manual

Loading in 1971 but in 1973, Torrens Industries TE108 Automatic sample loader was introduced. The routine operating conditions were described by Reeves (1971).

All major elements, apart from Mn, were determined using a Cr tube in vacuum. Mn was determined separately during trace element determinations using a w tube.

In order to minimize instrumental drift due to electronic instability, the "fixed counts" method was used together with a monitor on which the time (T) to accumulate a predetermined 'N' counts is automatically recorded. The loaded next three samples are then counted over the same time interval (T) for the same element.

The international rock standards G1, G2, GA, GH, GR, GSP1, AGV-1, BCR-1, BR, S1, T1, W1 and wet chemically analysed sedimentary sulphur standards were used to cover the range of compositions. The compositions of the internal standards taken were those reviewed by Flanagan (1969, 1973).

Errors arising from absorption differences between standards and unknowns were corrected by means of a "mass absorption correction program" as described by Reeves (1971). All Fe is expressed as Fe_2O_3 in these analyses when FeO is not determined by wet chemical methods.

Wet Chemical Analyses*, Major elements.

About 23 reasonably fresh rock specimens were analysed for FeO wet chemically by the metavanadate method (Wilson, 1955). All specimens were also analysed for CO_2, H_2O and specimens with high

* Analyses by Mr R. Lambert.

sulphur contents due to disseminated sulphide minerals were also checked by wet chemical methods.

XRF Trace Element Analyses.

Trace element analyses were performed on the same briquettes used for the majors. The elements Ba, Nb, Zr, Y, Sr, Rb, Zn, Cu, and Ni were determined using a W target in evacuated X-ray path.

Calibration curves for trace element analyses were established using a series of synthetic glass standards (prepared by Pilkington Research Laboratory for use in Lunar investigations (Brown, et al, 1970)) spiked with the trace elements. These standards are in two sets in order to avoid interfering peaks. The analytical counts were converted to concentrations (ppm) by means of a computer program "TRATIO" written by R. Gill (1972). The program uses a count-rate function (P-b/b-1) to enable background scatter to be used as a variable internal standard (Anderman and Kemp, 1958). It makes corrections for blank/contamination and K_β interference to be included and calculates the Lower Limit of detection of each element analysed. Lower Limits of detection (LLD) for trace elements are given below together with the upper limits of calibration:

Elements	LLD(ppm)	Upper Limit of Standard (ppm)
Ba	9	5000
Nb	3	250
Zr	3	5000
Y	3	500
Sr	3	1100
Rb	3	1000
Zn	2	1000
Cu	2	1000
Ni	2	1000

Major and trace element analyses are given in appendix tables 2A-2D In the tables trace elements below 2 ppm are below the detection limit.

APPENDIX TABLE 2A ANALYSES OF LOWER BASIC SERIES ROCKS, MAJORS AND TRAC

	8A	28A	23	137	122	14	69C	130	128B	72
PERCENT										
SIO2	43.38	46.10	48.08	49.02	54.60	55.93	56.51	57.31	58.19	60.18
AL2O3	20.63	18.50	13.60	17.50	15.46	18.90	25.47	17.07	16.19	14.62
FE2O3	0.45	1.79	3.24	1.39	3.20	1.30	4.99	11.35	0.78	1.68
FEO	9.63	6.68	5.72	7.30	7.55	4.86	N.D.	N.D.	6.21	5.77
MGO	13.99	12.70	13.03	6.35	5.51	8.47	1.55	7.57	12.11	8.15
CAO	0.71	1.44	8.76	6.70	5.90	1.14	1.40	0.13	0.31	1.36
NA2O	0.50	0.05	2.32	0.95	1.37	2.88	0.11	4.04	3.83	3.80
K2O	2.60	2.72	0.65	2.88	1.81	1.26	2.20	0.01	0.02	0.00
TIO2	0.65	0.61	0.58	0.62	0.92	1.84	0.55	0.84	0.45	0.45
MNO	0.46	0.67	0.24	0.28	0.23	0.20	0.15	0.28	0.20	0.19
S	2.61	0.23	0.09	1.75	0.20	0.18	0.66	0.06	0.07	0.09
P2O5	0.04	0.07	0.07	0.08	0.12	0.14	0.09	0.14	0.06	0.12
CO2	1.17	6.10	1.41	3.98	3.40	1.04	3.79	0.00	0.48	2.00
H2O	2.31	2.11	1.63	1.62	0.38	3.12	1.28	0.63	0.72	1.48
TOTAL	99.13	99.97	99.44	100.42	100.65	99.26	98.75	99.43	99.62	99.89
PPM										
BA	244	151	206	308	167	164	159	45	38	26
NB	6	3	1	4	2	12	8	2	0	2
ZR	62	32	25	29	67	212	205	70	31	77
Y	13	9	14	12	25	35	23	27	17	26
SR	8	16	183	59	58	54	24	61	44	81
RB	77	76	16	106	51	33	65	4	4	0
ZN	486	0	88	126	240	209	207	390	325	213
CU	24	0	27	231	29	4	0	44	2	0
NI	12	26	172	13	3	3	19	2	20	1

APPENDIX TABLE 2A ANALYSES OF LOWER BASIC SERIES ROCKS, MAJORS AND TRAC

	99A	94A	146	50B	145	33A	109A	13A	95A	94B
PERCENT										
SIO2	62.15	62.20	63.82	64.25	65.62	66.80	69.46	69.50	70.00	70.17
AL2O3	16.82	22.86	20.84	21.44	18.54	21.62	15.52	15.10	18.02	15.19
FE2O3	7.76	4.48	2.60	0.50	2.89	1.35	2.45	2.38	3.27	4.72
FEO	N.D.	N.D.	1.74	3.17	N.D.	N.D.	N.D.	N.D.	N.D.	N.D.
MGO	3.50	0.00	3.89	1.76	1.89	0.90	1.65	7.09	0.00	0.03
CAO	0.53	0.14	0.01	0.47	1.56	0.00	1.84	0.04	0.11	0.00
NA2O	0.10	0.70	0.11	0.11	0.45	0.14	0.13	0.16	0.30	0.27
K2O	1.91	5.79	4.89	3.39	3.86	4.93	4.69	2.90	4.67	3.81
TIO2	0.69	0.94	0.60	0.85	0.43	0.42	0.37	0.40	0.73	0.51
MNO	0.22	0.00	0.02	0.11	0.07	0.00	0.13	0.09	0.00	0.01
S	1.80	2.28	0.05	1.51	0.09	1.13	1.72	2.10	1.87	5.06
P2O5	0.11	0.10	0.08	0.08	0.11	0.09	0.12	0.08	0.15	0.08
CO2	5.84	0.43	0.15	2.12	3.89	0.55	2.29	0.00	0.42	0.38
H2O	0.70	0.32	0.04	0.51	0.77	1.65	0.32	0.12	0.65	1.07
TOTAL	102.13	100.24	98.84	100.27	100.11	99.58	100.69	99.96	100.19	101.39
PPM										
BA	180	453	300	702	515	924	692	410	215	207
NB	1	2	11	1	14	12	12	8	4	0
ZR	73	73	192	23	185	185	180	157	89	97
Y	22	11	15	12	18	14	16	20	27	56
SR	9	48	15	4	55	135	347	21	16	23
RB	37	135	118	70	128	165	157	78	116	35
ZN	0	476	71	92	63	0	226	221	0	345
CU	108	0	6	145	3	0	7	3	203	0
NI	6	3	7	11	7	5	6	7	4	6

APPENDIX TABLE 2A ANALYSES OF LOWER BASIC SERIES ROCKS, MAJORS AND TRAC

	103A	103B	149	37B	47B	17
PERCENT						
SIO2	70.51	70.94	76.29	77.93	80.56	81.50
AL2O3	15.82	16.82	16.62	14.10	10.52	9.78
FE2O3	4.90	3.59	0.31	1.07	1.90	0.60
FEO	N.D.	N.D.	N.D.	N.D.	N.D.	3.52
MGO	0.04	0.65	0.46	1.01	0.73	0.36
CAO	0.07	0.06	0.00	0.00	0.11	0.22
NA2O	0.24	0.20	0.15	0.18	0.30	0.25
K2O	4.25	4.72	4.66	3.70	2.71	2.24
TIO2	0.57	0.62	0.46	0.29	0.21	0.12
MNO	0.00	0.01	0.00	0.02	0.12	0.00
S	4.88	3.07	0.05	0.62	0.10	1.56
P2O5	0.13	0.12	0.05	0.10	2.01	0.05
CO2	0.00	0.24	0.00	0.61	1.34	0.00
H2O	0.42	0.56	0.74	0.19	0.34	0.25
TOTAL	101.83	101.59	99.49	99.82	100.45	100.45
PPM						
BA	507	524	579	468	176	268
NB	0	3	15	13	1	3
ZR	66	87	196	152	138	98
Y	40	29	16	14	42	25
SR	146	18	40	12	51	34
RB	121	129	144	115	93	73
ZN	89	70	4	171	0	99
CU	13	8	1	7	0	6
NI	3	2	4	5	4	3

APPENDIX TABLE 28 ANALYSES OF PORPHYRITIC DACITE ROCKS, MAJORS AND TRACES

	138*	67	143	48A	147	M48A	136	142	12A	140
PERCENT										
SIO2	63.98	64.26	68.03	68.66	68.87	69.60	70.06	70.65	72.00	71.92
AL2O3	15.46	16.02	14.51	16.56	16.53	13.55	18.24	16.28	15.45	17.06
FE2O3	6.30	0.59	2.31	2.70	1.38	5.20	2.98	3.34	2.32	1.76
FEO	N.D.	2.55	N.D.	N.D.	0.88	N.D.	N.D.	N.D.	N.D.	N.D.
MGO	4.26	1.22	2.29	2.86	1.15	1.78	0.38	0.94	2.18	0.88
CAO	3.17	4.32	3.45	3.67	1.45	1.36	0.08	0.30	0.00	0.00
NA2O	3.05	0.39	0.06	0.08	0.52	0.14	4.66	0.17	1.00	0.17
K2O	1.59	3.77	4.56	4.25	4.20	3.79	1.80	4.03	2.75	5.00
TIO2	0.42	0.34	0.22	0.43	0.26	0.43	0.32	0.37	0.22	0.51
MNO	0.15	0.18	0.17	0.24	0.02	0.14	0.03	0.09	0.10	0.01
S	0.57	0.17	0.44	0.80	0.06	4.30	0.08	0.41	0.58	1.21
P2O5	0.11	0.08	0.07	0.10	0.08	0.11	0.05	0.08	0.06	0.04
CO2	0.75	6.89	4.02	2.77	2.70	1.00	0.16	1.92	2.73	0.10
H2O	1.00	0.35	1.50	0.07	1.65	0.31	1.28	0.40	0.79	0.69
TOTAL	100.81	100.95	101.57	100.07	100.20	100.61	100.22	98.98	100.18	99.35
PPM										
BA	225	348	829	283	448	330	142	266	309	645
NB	2	1	14	2	17	1	2	2	1	12
ZR	91	116	156	90	160	59	192	131	159	188
Y	24	26	12	39	13	45	26	26	41	15
SR	146	43	43	68	218	422	75	28	20	13
RB	41	103	194	148	114	132	34	120	82	156
ZN	98	54	44	0	35	265	34	264	300	7
CU	37	2	63	26	0	3	1	4	8	0
NI	2	2	2	3	2	5	3	3	4	4

* Quartz-Microdiorite specimen.

APPENDIX TABLE 2B ANALYSES OF PORPHYRITIC DACITE ROCKS, MAJORS AND TRACES

	9[illegible]A	165	144	141	148	88A	127A	139	135	166
PERCENT										
SIO2	72.50	73.05	73.70	74.96	75.77	75.90	76.45	77.36	79.42	81.60
AL2O3	14.66	15.21	16.37	16.56	15.06	14.13	13.92	13.36	13.05	12.64
FE2O3	2.13	1.34	1.83	1.92	1.46	2.60	2.17	1.95	[illegible].32	[illegible].10
FEO	N.D.	N.D.	N.D.	N.D.	N.D.	N.D.	N.D.	N.D.	N.D.	N.D.
MGO	1.01	4.86	2.40	[illegible].69	[illegible].55	[illegible].57	1.16	[illegible].71	[illegible].32	[illegible].58
CAO	1.47	[illegible].00	[illegible].00	[illegible].00	[illegible].07	[illegible].00	[illegible].08	[illegible].00	[illegible].00	[illegible].00
NA2O	[illegible].23	[illegible].27	[illegible].19	[illegible].21	[illegible].24	1.18	[illegible].20	[illegible].22	1.76	[illegible].30
K2O	4.19	2.92	4.11	4.32	4.94	3.90	3.74	3.78	1.83	3.63
TIO2	[illegible].23	[illegible].23	[illegible].31	[illegible].32	.12	[illegible].51	[illegible].40	[illegible].22	[illegible].29	[illegible].21
MNO	[illegible].16	[illegible].02	[illegible].05	[illegible].00	[illegible].02	[illegible].00	[illegible].03	[illegible].05	[illegible].00	[illegible].00
S	[illegible].78	[illegible].66	[illegible].11	[illegible].04	[illegible].06	1.48	[illegible].19	[illegible].95	[illegible].09	[illegible].28
P2O5	[illegible].06	[illegible].05	[illegible].06	[illegible].04	[illegible].05	[illegible].09	[illegible].08	[illegible].05	[illegible].04	[illegible].04
CO2	2.33	[illegible].54	[illegible].22	[illegible].00	[illegible].00	[illegible].45	[illegible].70	[illegible].70	[illegible].42	[illegible].00
H2O	[illegible].56	[illegible].75	[illegible].71	[illegible].91	[illegible].70	[illegible].50	[illegible].90	[illegible].39	[illegible].64	[illegible].76
TOTAL	1[illegible].30	99.90	1[illegible].26	99.93	99.04	1[illegible].31	1[illegible].02	98.99	98.18	99.54
PPM										
BA	389	311	253	4[illegible]4	165	195	342	147	1532	4429
NB	3	[illegible]	1	3	2[illegible]	1	2	3	[illegible]	2
ZR	138	138	166	147	1[illegible]5	88	147	115	13[illegible]	121
Y	33	33	25	33	1[illegible]	59	38	24	15	33
SR	22	9	1[illegible]	31	92	1[illegible]	8	73	39	142
PB	125	37	1[illegible]	131	151	131	75	129	3[illegible]	62
ZN	63	58	41	1[illegible]	17	[illegible]	345	18	21	59
CU	4	1	2	2[illegible]	[illegible]	[illegible]	29	169	1	5
NI	5	5	2	2	2	4	6	2	1	2

APPENDIX TABLE 2C ANALYSES OF RHYODACITIC ROCKS, MAJORS AND TRACES

	51	15J	53A	152	50A	45	50C	69A	53B
PERCENT									
SIO2	71.12	73.65	75.09	75.29	75.33	75.86	77.13	81.38	82.20
AL2O3	25.86	17.12	12.69	14.28	14.58	13.69	9.81	6.72	10.31
FE2O3	3.21	1.04	0.24	1.66	0.90	0.25	5.20	4.57	1.21
FEO	N.D.	N.D.	2.79	N.D.	1.03	N.D.	N.D.	N.D.	N.D.
MGO	0.49	0.81	0.83	0.57	0.81	0.66	0.21	0.85	0.69
CAO	0.29	0.00	0.00	0.00	0.00	0.00	0.00	0.47	0.00
NA2O	1.15	3.66	0.14	2.51	0.18	0.35	0.10	0.08	0.13
K2O	2.60	4.50	3.72	3.11	4.33	3.55	0.77	0.27	2.95
TIO2	0.29	0.34	0.18	0.25	0.29	0.29	0.37	0.11	0.14
MNO	0.09	0.00	0.01	0.00	0.01	0.00	0.10	0.09	0.02
S	1.37	0.05	3.40	1.42	0.83	0.07	3.50	1.88	0.95
P2O5	0.09	0.05	0.05	0.08	0.05	0.04	0.09	0.07	0.04
CO2	2.49	1.10	0.06	0.09	0.82	2.77	2.02	2.95	0.65
H2O	0.63	0.71	0.89	0.80	0.59	2.23	0.51	0.37	0.49
TOTAL	99.68	99.33	100.09	100.06	99.75	99.76	99.81	99.81	99.78
PPM									
BA	482	381	812	396	353	501	216	43	468
NB	5	3	0	5	6	1	3	0	2
ZR	142	141	129	108	141	146	48	62	100
Y	18	36	36	16	33	48	35	12	23
SR	49	24	11	42	6	60	10	111	17
RB	70	148	124	89	139	111	21	1	92
ZN	80	11	26	9	19	6	145	227	30
CU	16	3	29	5	16	6	0	10	11
NI	2	3	0	3	4	3	8	16	3

APPENDIX TABLE 2D ANALYSES OF BASALTIC DYKE ROCKS, MAJORS AND TRACES

	157	52	128A	156	155	158	159	154
PERCENT								
SIO2	45.05	48.20	49.50	49.53	50.22	52.00	52.30	53.00
AL2O3	14.43	14.20	19.50	15.63	14.64	13.50	16.28	16.00
FE2O3	3.95	2.29	3.60	1.68	0.62	1.38	2.38	2.93
FEO	5.81	6.39	3.80	4.49	5.14	6.87	4.81	3.94
MGO	4.33	5.42	3.80	8.40	8.01	4.00	9.03	3.95
CAO	12.67	11.94	6.00	11.74	11.98	10.20	6.85	7.20
NA2O	1.61	1.65	2.30	1.54	1.22	1.50	4.04	3.28
K2O	1.87	2.00	3.00	2.90	2.55	2.00	2.40	3.45
TIO2	0.97	0.85	0.73	0.79	0.73	0.66	0.56	0.69
MNO	0.18	0.19	0.28	0.15	0.15	0.15	0.14	0.13
S	0.11	0.07	0.10	0.08	0.09	0.12	0.07	0.08
P2O5	0.28	0.26	0.38	0.36	0.40	0.20	0.24	0.24
CO2	8.23	6.30	7.00	1.92	3.80	7.00	0.60	4.36
H2O	0.36	0.15	0.22	0.68	0.30	0.50	0.34	0.55
TOTAL	99.85	99.91	100.21	99.89	99.85	101.08	100.04	99.80
PPM								
BA	644	620	487	906	737	493	498	832
NB	9	3	10	3	4	5	4	7
ZR	77	69	175	79	73	73	82	169
Y	22	23	35	18	20	20	23	19
SR	519	477	79	542	531	392	313	329
RB	49	71	94	93	82	81	107	137
ZN	70	74	231	108	67	78	43	66
CU	32	53	3	70	78	44	7	58
NI	35	44	4	125	112	83	100	9

APPENDIX THREE

MINERAL ANALYSES

Electron Microprobe Analyses.

As in the case of Bi-sulphosalts and fahlerz minerals, optical properties and colours of the opaque minerals are not always sufficient to establish the composition and identification of a mineral with any certainty. Minerals several microns in size, representing solid-solution series or copper sulphide compositions between covellite ($Cu_{1.0}S$ and chalcocite ($Cu_{2.0}S$) are sometimes difficult to identify, at least, one can not be sure of the exact number of copper atoms. In these cases the Electron Microprobe can be employed to establish exact compositions or to investigate chemical zoning and exsolution intergrowths.

The problems involved in microprobe analysis and associated correction techniques have been widely discussed by Duncumb and Shields (1966), Duncumb and Reed (1967), Keil (1967), Sweatman and Long (1969). Mounting techniques and preparation of polished specimens have been described by Taylor and Radtke (1965) and Long (1967).

Specimen Preparation: Polished thin sections and polished ore specimens were prepared as described by Tugal (1969). Additional techniques used during the analyses were as follows:

Small sphalerite fragments embedded and polished in resin, were drilled as 0.5mm cylinders suitable for mounting in the microprobe standard holder which makes possible to analyse up to 25 different specimens without changing the operational setup. Standard 37 mm size polished specimens of other sulphides and sulphosalts were directly used with areas to be analysed marked with ink or being photographed. Disc wafers in some cases were employed to analyse the variation of Mn, Cd, and Fe in the colour bands in sphalerite to make viewing possible in both transmitted and reflected light, wafers are also useful for sphalerites with extremely abundant emulsion or exsolution type chalcopyrite blebs to avoid erronous iron values due to these blebs in the excited area below the specimen surface by electron beam.

Carbon Coating: Because of x-ray absorption increasing carbon film thickness causes greater reduction in x-ray intensity for lighter elements than heavier ones. Specimens and standards were carbon coated simultaneously by monitoring carbon film thickness during evaporation. The amount of carbon deposited was judged by the degree of contrast obtained on a glazed white tile on which a spot of diffusion pump silicone fluid was placed; the area covered by silicone fluid remained white during carbon deposition, while the remainder of the tile grew progressively darker until deposition stopped.

The role of carbon film thickness in Electron Microprobe analysis was discussed by Kerrick et al (1973) in detail so will not be repeated here. Samples and standards were cleaned and recoated frequently to avoid deterioration of the carbon film coating.

Analytical Conditions: The instrument employed during this investigation was a Cambridge Scientific Instruments "Goescan - Mk II" with a take-off angle of 75^{o}. Rock-forming minerals were analysed with an accelerating voltage of 15 KU and a specimen current of 0.07μA. 20 KV accelerating voltage was used for opaque ore minerals and specimen currents were changed from 0.02μA to 0.12μA depending on the elements and lines excited.

The "Geoscan" has two spectrometers and four pre-set spectrometer positions. In general, the specimen current 0.04μA was suitable for all elements with atomic numbers between 11 (Na) and 28 (Ni) for oxide minerals. Major elements of feldspars and pyroxenes were determined as pairs simultaneously with preset peaks and backgrounds for each element. In the case of sulphide and sulphosalt analyses with elements ranging from Z = 16 (S) to 83 (Bi) difficulties were encountered in count rates and analytical lines to be used due to interfering peaks, so the specimen current was changed during each analysis to keep count rates as low as possible to avoid the maximum correction to be applied to raw counts.

Analytical runs were begun by counting 5 or more often 10 seconds counts on each standard and unknown peaks and on both sides of the peak for backgrounds. This counting technique was applied to all unknowns as long as there was no interfering pulses on low or high 2θ side of peak positions, otherwise background counts were taken only on one side of the peak. Bi and Pb $M\alpha$, Pb$M\alpha$ and S$K\alpha$, Zn$K\beta$ and Cd$L\alpha$; Zn and Cu$K\alpha$ with As$L\alpha$ were amongst the interfering lines. These problems were minimized by scanning across the major peaks before the analyses were made on unknowns and then either taking background counts only on

one side of the peak or changing the analysing crystal to be used. Fahlerz analysis is a good example which contains interfering As, Cu and Zn peaks.

The standards and analytical conditions used are given in appendix tables 3.1 and 3.2.

Corrections: Raw counts were first corrected for a 4 microseconds dead time and drift with the aid of the on-line Varian 620-100 computer, by the program "TIM-3" written by Dr A. Peckett. This is an assember version of the Fortran IV TIM 1 of Duncomb and Jones (1970). The Program corrects for mass absorption, secondary fluorescence and the atomic number effect (stopping power and electron back-scatter) in the manner described by Sweatman and Long (1969) for K, L, and M lines.

Lowest Limit of Detection and Accuracy: The theoretical size of electron beam is about 1 μm but but the area excited in the sample was found greater than this - it is considered to be within the resolution range of 5-15μm.

For trace element analysis in sphalerites lowest limit of detection was calculated for each element as follows:

$$LLD = \frac{3}{M}\sqrt{Rb/Tb}$$

where M = mean peak counts/sec/%

Rb = mean background counts per second

Tb = total counting time on backgrounds.

APPENDIX TABLE 3.1 FELDSPAR AND PYROXENE

Optimum Analysing Conditions and Standards Used for Electron Microprobe Analysis

Element	Line	Analysing Crystal	Counter	2 θ (Peak)	2 θ(Background)	Standard
Na	K_{α_1}	KAP	Flow	$53^{\circ}14'$	$+1^{\circ}30'$	Jadeite
Mg	"	"	"	$43^{\circ}42'$	-2	MgO
Al	"	"	"	$36^{\circ}32'$	± 2	Al_2O_3
Si	"	"	"	$31^{\circ}02'$	$-1^{\circ} + 1^{\circ}30'$	Wollastonite
K	"	Quartz	"	$67^{\circ}58'$	-2	Orthoclase
Ca	"	LiF	"	$113^{\circ}02'$	-2	Wollastonite
Ti	"	"	"	$86^{\circ}05'$	+2	TiO_2
Cr	"	"	Sealed	$69^{\circ}16'$	+2	Cr_2O_3
Mn	"	"	"	$62^{\circ}48'$	+2	Mn metal
Fe	"	"	Flow	$57^{\circ}20'$	+2	Fe metal
Ni	"	"	Sealed	$48^{\circ}34'$	+2	Ni metal

APPENDIX TABLE 3.1 FELDSPAR AND PYROXENE

Optimum Analysing Conditions and Standards Used for Electron Microprobe Analysis

Element	Line	Analysing Crystal	Counter	2 θ (Peak)	2 θ(Background)	Standard
Na	K_{α_1}	KAP	Flow	53°14'	+1°30'	Jadeite
Mg	"	"	"	43°42'	-2	MgO
Al	"	"	"	36°32'	±2	Al_2O_3
Si	"	"	"	31°02'	-1° + 1°30'	Wollastonite
K	"	Quartz	"	67°58'	-2	Orthoclase
Ca	"	LiF	"	113°02'	-2	Wollastonite
Ti	"	"	"	86°05'	+2	TiO_2
Cr	"	"	Sealed	69°16'	+2	Cr_2O_3
Mn	"	"	"	62°48'	+2	Mn metal
Fe	"	"	Flow	57°20'	+2	Fe metal
Ni	"	"	Sealed	48°34'	+2	Ni metal

APPENDIX TABLE 3.2 SULPHIDE AND SULPHOSALT

Optimum Analysing Conditions and Standards Used for Electron Microprobe Analysis

Element	Line	Analysing Crystal	Counter	2 θ(Peak)	2 θ(Background)	Standards
S	K_{α_1}	Quartz	Flow	106°59'	$\mp$ 2*	ZnS, FeS_2
Mn	"	LIF	Sealed	62°52'	$\mp$ 1°30'	$MnSiO_3$
Fe	"	"	"	57°25'	$\mp$ 1°30'	FeS_2
Cu	"	"	"	44°24'	+ 2*	Cu metal Chalcostibite
Zn	"	"	"	41°40'	+ 1°30'*	ZnS
As	L_{α_1}	KAP	Flow	42°38'	+ 3*	As metal
Ag	L_{α_1}	Quartz	"	76°37'	+ 2	Ag metal
Cd	L_{α_1}	"	"	72°30'	+ 2*	CdS
Sb	L_{α_2}	"	"	61°40'	+ 2	Sb_2S_3
Pb	M_{α_2}	"	"	104°27'	$\mp$ 2*	PbS
Bi	M_{α_1}	"	"	99°52'	$\mp$ 2*	Bi metal

* Only for standards. Interfering peaks must be checked on unknowns.

Calculated lowest limit of detection is in the range of 200-500ppm. For manganese it was calculated about 300ppm and values below 300ppm (0.03%) was not taken into consideration.

Under the ideal conditions an accuracy of 1% of the wt.% present is possible using the electron microprobe (Long, 1976). On the other hand Springer (1969) quoted an approximate experimental error $\pm$ 2% of the wt.% present on the basis of analysis carried out on natural tetrahedrites.

The corrected probe analysis of feldspars and pyroxenes were recast into their atomic proportion and end member composition with the aid of program TABLIT developed by Mr E.B. Curran, and given in Appendix table 3A and 3B respectively. Electron microprobe analyses of sphalerites are already given in table 5.10.1.

APPENDIX TABLE 3A FELDSPAR ANALYSIS OF BULANCAK VOLCANICS

	1	2	3	4	5	6	7	8	9	10
	052.1	052.2	052.3	052.4	052.5	154.1	154.2	154.3	154.4	154.5
OXIDE WEIGHT PERCENTAGE										
SIO2	49.69	49.64	51.12	50.53	48.08	54.20	54.70	55.26	56.03	54.91
TIO2	-	-	-	-	-	-	-	-	-	-
AL2O3	29.73	29.90	28.09	28.71	30.22	27.17	28.01	27.09	26.84	27.36
FEO	1.33	1.25	2.23	1.42	1.70	0.08	0.09	0.03	0.05	0.14
MNO	-	-	-	-	-	-	-	-	-	-
MGO	-	-	-	-	-	-	-	-	-	-
CAO	15.49	15.56	15.62	14.38	16.05	11.50	11.52	10.96	10.66	10.62
K2O	0.78	0.64	1.11	1.09	0.41	0.53	0.55	0.53	0.67	0.57
NA2O	2.17	2.44	2.38	2.47	1.78	7.95	4.94	5.33	5.35	5.47
TOTAL	99.19	99.43	100.55	98.60	98.24	101.43	99.81	99.20	99.60	99.07
ATOMIC PROPORTIONS ON THE BASIS OF 6 OXYGENS										
SI	1.736	1.725	1.767	1.767	1.695	1.838	1.859	1.887	1.903	1.878
TI	0.000	0.000	0.000	0.000	0.000	0.000	0.000	0.000	0.000	0.000
AL	1.221	1.225	1.145	1.184	1.256	1.087	1.123	1.091	1.075	1.104
FE2	0.039	0.036	0.064	0.042	0.050	0.002	0.003	0.001	0.001	0.004
MN	0.000	0.000	0.000	0.000	0.000	0.000	0.000	0.000	0.000	0.000
MG	0.000	0.000	0.000	0.000	0.000	0.000	0.000	0.000	0.000	0.000
CA	0.578	0.579	0.579	0.539	0.606	0.418	0.420	0.401	0.388	0.389
K	0.035	0.028	0.049	0.049	0.018	0.023	0.024	0.023	0.029	0.025
NA	0.147	0.164	0.160	0.168	0.122	0.523	0.326	0.353	0.353	0.363
END MEMBER COMPOSITIONS										
AB	19.31	21.30	20.27	22.19	16.31	54.26	42.35	45.43	45.81	46.71
AN	76.13	75.03	73.51	71.37	81.22	43.36	54.55	51.66	51.42	50.09
OR	4.56	3.67	6.22	6.44	2.47	2.38	3.10	2.97	3.77	3.20

APPENDIX TABLE 3A FELDSPAR ANALYSIS OF BULANCAK VOLCANICS

	11	12	13	14	15	16	17	18	19	20
	155.1	155.2	155.3	156.1	156.2	156.3	156.4	156.5	157.1	157.2
OXIDE WEIGHT PERCENTAGE										
SIO2	48.98	48.33	47.97	47.85	48.21	48.40	64.75	65.28	47.91	48.37
TIO2	-	-	-	-	-	-	-	-	-	-
AL2O3	31.49	31.29	31.93	31.41	31.86	31.66	18.89	18.54	31.67	31.38
FEO	0.06	0.88	0.87	0.07	0.03	0.09	0.03	0.10	0.02	0.05
MNO	-	-	-	-	-	-	-	-	-	-
MGO	-	-	-	-	-	-	-	-	-	-
CAO	16.47	16.25	16.91	16.54	16.21	16.62	0.88	0.64	16.58	16.24
K2O	0.28	0.42	0.21	0.53	0.34	0.31	11.54	11.00	0.25	0.24
NA2O	2.31	2.57	2.22	2.35	1.95	1.73	3.02	3.01	2.46	2.22
TOTAL	99.59	99.74	100.11	98.75	98.60	98.81	99.11	98.57	98.89	98.50
ATOMIC PROPORTIONS ON THE BASIS OF 6 OXYGENS										
SI	1.691	1.677	1.658	1.672	1.679	1.683	2.230	2.250	1.673	1.687
TI	0.000	0.000	0.000	0.000	0.000	0.000	0.000	0.000	0.000	0.000
AL	1.282	1.280	1.301	1.294	1.308	1.298	0.767	0.753	1.301	1.291
FE2	0.002	0.026	0.025	0.002	0.001	0.003	0.001	0.003	0.001	0.001
MN	0.000	0.000	0.000	0.000	0.000	0.000	0.000	0.000	0.000	0.000
MG	0.000	0.000	0.000	0.000	0.000	0.000	0.000	0.000	0.000	0.000
CA	0.609	0.604	0.626	0.620	0.605	0.619	0.032	0.024	0.619	0.607
K	0.012	0.019	0.009	0.024	0.015	0.014	0.507	0.484	0.011	0.011
NA	0.155	0.173	0.149	0.159	0.132	0.117	0.202	0.201	0.166	0.150
END MEMBER COMPOSITIONS										
AB	19.93	21.74	18.97	19.85	17.52	15.56	27.21	28.40	20.88	19.56
AN	78.49	75.93	79.85	77.20	80.47	82.60	4.38	3.34	77.73	79.05
OR	1.59	2.34	1.18	2.95	2.01	1.83	68.41	68.27	1.40	1.39

APPENDIX TABLE 3A FELDSPAR ANALYSIS OF BULANCAK VOLCANICS

	21	22	23	24	25	26	27	28	29	30
	157.3	158.1	158.2	158.3	158.4	158.5	158.6	158.7	159.1	159.1
OXIDE WEIGHT PERCENTAGE										
SIO2	49.38	48.95	49.46	50.26	50.07	50.27	50.04	49.88	50.35	47.50
TIO2	-	-	-	-	-	-	-	-	-	-
AL2O3	31.39	30.85	30.23	31.03	31.09	31.05	31.21	31.27	29.11	30.63
FEO	0.05	0.77	0.79	0.73	0.77	0.84	0.83	0.74	0.69	0.54
MNO	-	-	-	-	-	-	-	-	-	-
MGO	-	-	-	-	-	-	-	-	-	-
CAO	16.51	15.35	14.70	15.45	15.73	14.77	15.73	15.88	15.76	14.65
K2O	0.23	0.33	0.49	0.25	0.33	0.39	0.24	0.31	0.25	0.15
NA2O	2.25	2.81	3.31	2.60	2.33	2.77	2.59	2.71	2.87	6.15
TOTAL	99.81	99.06	98.98	100.32	100.32	100.09	100.64	100.79	99.03	99.57
ATOMIC PROPORTIONS ON THE BASIS OF 6 OXYGENS										
SI	1.699	1.703	1.722	1.721	1.716	1.724	1.711	1.705	1.750	1.663
TI	0.000	0.000	0.000	0.000	0.000	0.000	0.000	0.000	0.000	0.000
AL	1.274	1.265	1.241	1.252	1.256	1.256	1.258	1.260	1.193	1.264
FE2	0.001	0.022	0.023	0.021	0.022	0.024	0.024	0.021	0.020	0.016
MN	0.000	0.000	0.000	0.000	0.000	0.000	0.000	0.000	0.000	0.000
MG	0.000	0.000	0.000	0.000	0.000	0.000	0.000	0.000	0.000	0.000
CA	0.609	0.572	0.548	0.567	0.578	0.543	0.576	0.582	0.587	0.550
K	0.010	0.015	0.022	0.011	0.014	0.017	0.010	0.014	0.011	0.004
NA	0.153	0.190	0.224	0.173	0.155	0.184	0.172	0.180	0.194	0.418
END MEMBER COMPOSITIONS										
AB	19.53	24.42	28.16	23.01	20.73	24.76	22.64	23.19	24.44	42.98
AN	79.16	73.69	69.10	75.54	77.33	72.94	75.98	75.07	74.16	56.56
OR	1.31	1.89	2.74	1.46	1.93	2.29	1.38	1.74	1.40	0.46

APPENDIX TABLE 3B CLINOPYROXENE ANALYSIS OF BULANCAK VOLCANICS

	1	2	3	4	5	6	7	8	9	10
	S23/1	S23/2	S23/3	S23/4	S23/5	S52/1	S52/2	S52/3	S52/4	S52/5
OXIDE WEIGHT PERCENTAGE										
SIO2	51.82	52.44	53.46	54.05	52.60	49.17	50.57	48.67	48.48	50.05
TIO2	0.05	0.02	0.21	0.12	0.12	0.35	0.33	0.59	0.50	0.53
AL2O3	1.74	1.49	2.27	1.36	1.98	4.15	2.76	5.41	5.22	4.62
CR2O3	1.02	0.72	0.48	0.85	5.36	0.10	0.16	0.11	0.11	0.11
FEO	3.00	3.54	4.74	3.12	0.24	6.10	9.98	6.91	6.08	7.07
MNO	0.01	0.03	0.03	0.02	0.04	0.05	0.19	0.05	0.04	0.06
MGO	17.58	17.69	17.17	17.60	17.58	16.39	12.70	14.82	15.00	15.16
CAO	23.49	23.63	21.97	22.64	21.00	22.96	22.73	23.24	23.45	21.97
NA2O	0.18	0.18	0.08	0.03	-	0.17	0.52	0.42	0.42	0.30
TOTAL	98.79	99.74	100.41	99.79	98.92	99.44	99.94	100.13	99.30	99.87
ATOMIC PROPORTIONS ON THE BASIS OF 6 OXYGENS										
SI	1.919	1.927	1.943	1.967	1.922	1.836	1.908	1.813	1.817	1.858
TI	0.001	0.001	0.006	0.003	0.003	0.010	0.009	0.014	0.014	0.015
AL	0.076	0.065	0.097	0.058	0.085	0.183	0.123	0.238	0.231	0.202
CR	0.030	0.021	0.014	0.024	0.155	0.003	0.005	0.003	0.003	0.003
FE2	0.093	0.109	0.144	0.095	0.007	0.190	0.315	0.215	0.191	0.220
MN	0.000	0.001	0.001	0.001	0.001	0.002	0.006	0.002	0.001	0.002
MG	0.970	0.969	0.930	0.954	0.957	0.912	0.714	0.823	0.838	0.839
CA	0.932	0.931	0.856	0.883	0.822	0.919	0.919	0.928	0.942	0.874
NA	0.006	0.013	0.006	0.002	0.000	0.012	0.038	0.030	0.031	0.022
END MEMBER COMPOSITIONS										
CA	46.71	46.32	44.32	45.68	45.98	45.42	47.03	47.16	47.77	45.19
MG	48.62	48.22	48.17	49.38	53.54	45.09	36.54	41.82	42.50	43.36
FE	4.67	5.46	7.51	4.94	0.48	9.50	16.43	11.02	9.73	11.45

APPENDIX TABLE 3B CLINOPYROXENE ANALYSIS OF BULANCAK VOLCANICS

	1	2	3	4	5	6	7	8	9	10
	S155/1	S155/2	S155/3	S155/4	S155/5	S155/6	156/1	156/2	156/3	156/4
OXIDE WEIGHT PERCENTAGE										
SIO2	50.48	51.08	50.86	49.44	50.89	49.40	50.12	50.26	53.24	52.27
TIO2	0.27	0.27	0.27	0.62	0.62	0.62	0.32	0.32	0.32	0.30
AL203	2.89	2.36	2.89	4.89	2.58	5.25	4.90	4.73	2.48	2.36
CR203	0.25	0.33	0.21	0.41	0.29	0.61	0.39	0.42	0.28	0.27
FEO	6.00	8.12	5.62	6.45	6.08	6.69	7.28	6.11	5.64	5.80
MNO	0.18	0.18	0.18	0.14	0.14	0.14	0.24	0.24	0.24	0.09
MGO	15.78	14.08	15.56	14.66	15.69	14.49	14.36	14.84	16.11	15.86
CAO	23.13	23.49	23.84	23.34	22.70	22.73	21.98	22.39	22.14	22.61
NIO	-	-	-	-	-	-	0.05	0.05	0.05	-
TOTAL	98.98	99.91	99.43	99.95	98.99	99.93	99.64	99.36	100.53	99.56
ATOMIC PROPORTIONS ON THE BASIS OF 6 OXYGENS										
SI	1.890	1.912	1.894	1.838	1.902	1.836	1.866	1.869	1.943	1.932
TI	0.008	0.008	0.008	0.017	0.017	0.017	0.009	0.009	0.009	0.008
AL	0.128	0.104	0.127	0.214	0.114	0.230	0.215	0.207	0.107	0.103
CR	0.007	0.010	0.006	0.012	0.009	0.018	0.011	0.012	0.008	0.008
FE2	0.188	0.254	0.175	0.201	0.190	0.208	0.227	0.190	0.172	0.179
MN	0.006	0.006	0.006	0.004	0.004	0.004	0.008	0.008	0.007	0.003
MG	0.880	0.786	0.864	0.812	0.874	0.803	0.797	0.822	0.876	0.874
CA	0.928	0.942	0.951	0.930	0.919	0.905	0.877	0.892	0.866	0.896
NI	0.003	0.000	0.001	0.000	0.000	0.000	0.001	0.001	0.001	0.000
END MEMBER COMPOSITIONS										
CA	46.35	47.41	47.67	47.76	45.97	47.14	45.96	46.66	45.06	45.90
MG	43.98	39.52	43.27	41.72	44.19	41.80	41.76	43.01	45.60	44.77
FE	9.67	13.08	9.06	10.53	9.83	11.06	12.28	10.33	9.34	9.33

APPENDIX TABLE 3B CLINOPYROXENE ANALYSIS OF BULANCAK VOLCANICS

	11	12	13	14	15	16	17	18	19	20
	156/5	156/6	156/7	156/7A	158/1	158/2	158/3	158/4	158/5	158/6
OXIDE WEIGHT PERCENTAGE										
SIO2	52.76	52.86	52.22	52.76	53.29	53.35	53.00	53.35	53.90	52.67
TIO2	0.35	0.35	0.34	0.36	0.23	0.23	0.26	0.26	0.26	0.26
AL2O3	2.74	2.89	2.71	2.54	2.37	2.20	2.85	2.85	3.00	2.61
CR2O3	0.22	0.23	0.27	0.28	0.45	0.32	0.21	0.22	0.18	0.18
FEO	6.16	5.96	6.00	5.83	5.25	5.16	5.24	5.41	5.25	8.63
MNO	0.09	0.09	0.09	0.09	0.21	0.21	-	-	-	-
MGO	16.13	15.65	15.98	16.03	17.94	17.99	17.40	17.71	17.30	16.35
CAO	22.43	22.44	22.02	22.32	20.89	20.91	21.80	20.38	21.13	19.70
NIO	-	-	-	-	0.14	0.13	-	0.05	-	-
TOTAL	100.58	100.47	99.63	100.15	100.77	100.51	100.76	100.23	101.02	100.39
ATOMIC PROPORTIONS ON THE BASIS OF 6 OXYGENS										
SI	1.939	1.933	1.927	1.935	1.932	1.938	1.923	1.937	1.942	1.937
TI	0.001	0.010	0.009	0.008	0.006	0.006	0.007	0.007	0.007	0.007
AL	0.118	0.125	0.118	0.110	0.101	0.094	0.122	0.122	0.127	0.113
CR	0.006	0.007	0.008	0.008	0.013	0.009	0.006	0.006	0.005	0.002
FE2	0.188	0.182	0.185	0.179	0.159	0.157	0.159	0.164	0.158	0.265
MN	0.003	0.003	0.003	0.003	0.006	0.006	0.003	0.003	0.003	0.002
MG	0.879	0.853	0.879	0.876	0.969	0.974	0.941	0.958	0.929	0.896
CA	0.879	0.879	0.871	0.877	0.812	0.814	0.847	0.793	0.816	0.776
NI	0.002	0.003	0.003	0.003	0.004	0.004	0.003	0.001	0.003	0.001
END MEMBER COMPOSITIONS										
CA	45.39	45.86	44.94	45.33	41.69	41.72	43.52	41.41	42.87	41.36
MG	45.14	44.48	45.36	45.28	49.80	49.92	48.31	50.23	48.81	46.24
FE	9.81	9.65	9.71	9.39	8.51	8.37	8.17	8.36	8.31	13.70

APPENDIX TABLE 3B CLINOPYROXENE ANALYSIS OF BULANCAK VOLCANICS

	21	22	23	24	25	26	27	28	29
	158/6A	158/7	158/8	S159/1	S159/2	S159/3	S159/4	S159/5	S159/6
OXIDE WEIGHT PERCENTAGE									
SIO2	51.36	53.49	52.84	52.64	51.63	51.28	51.93	53.13	53.12
TIO2	0.26	0.26	0.32	0.35	0.30	0.32	0.25	0.35	0.39
AL2O3	4.99	2.26	1.69	2.79	2.56	1.84	2.81	1.91	1.94
CR2O3	0.17	0.12	-	0.15	0.13	0.13	0.37	-	-
FEO	10.09	6.66	10.01	5.94	5.72	6.55	4.92	8.85	7.28
MNO	-	-	0.24	0.19	0.19	0.29	0.14	0.29	0.34
MGO	13.95	16.25	13.14	16.63	17.84	17.31	17.74	15.72	16.16
CAO	19.73	21.18	21.91	21.06	22.48	22.95	21.17	21.58	21.15
NIO	-	-	-	0.05	0.07	0.10	0.07	0.07	0.07
TOTAL	100.55	100.22	100.15	99.80	100.92	99.68	99.45	102.89	100.41
ATOMIC PROPORTIONS ON THE BASIS OF 6 OXYGENS									
SI	1.896	1.957	1.971	1.932	1.888	1.878	1.912	1.951	1.955
TI	0.007	0.007	0.009	0.010	0.008	0.009	0.007	0.010	0.011
AL	0.217	0.097	0.074	0.121	0.110	0.081	0.122	0.082	0.084
CR	0.005	0.003	0.000	0.004	0.004	0.004	0.011	0.000	0.000
FE2	0.312	0.204	0.312	0.182	0.175	0.205	0.151	0.272	0.224
MN	0.000	0.000	0.008	0.006	0.006	0.006	0.004	0.009	0.009
MG	0.767	0.886	0.731	0.912	0.972	0.964	0.973	0.864	0.884
CA	0.780	0.830	0.876	0.828	0.881	0.919	0.835	0.811	0.832
NI	0.000	0.000	0.000	0.001	0.002	0.003	0.002	0.002	0.002
END MEMBER COMPOSITIONS									
CA	41.97	43.24	45.47	43.00	43.31	43.89	42.52	41.51	42.69
MG	41.27	46.14	37.92	47.22	47.80	46.03	49.55	44.10	45.36
FE	16.75	10.61	16.61	9.77	8.89	10.08	7.93	14.39	11.95

APPENDIX FOUR

X-RAY DIFFRACTION

Powder Diffraction Method.

The material for powder diffraction photographs was normally obtained when large amounts of material was available by separating vein and gangue minerals from the hand specimens and then collecting pure grains by hand picking under the binocular. When only minerals in the polished specimen were available a needle mounted in a hand drill was used to avoid impurities. In this way material for powder photographs was obtained while the specimen was viewed under the microscope.

A Debye-Scherrer Camera (114.6 mm diameter) using the Straumanis film technique was employed with filtered cobalt radiation to obtain powder photographs as described by Klug and Alexander (1962).
The powder so obtained was mounted on a silica glass fibre using collodion solution as anadhesive to give a total diameter of 0.30 mm. These coated fibres were then mounted in the Camera and centered. Narrow collimeter and beam trap were used exclusively exposure times were in the order of 10-12 hours using the spot focus of a Philips 1130 3 kilowatt generator at a power of 60 KV./30mA.

Measurement of Powder Photographs.

The measurements were made on the photographs using the standard Hilger and Watts film measuring scale, fitted with a vernier capable of readings to 0.0125° $2\theta = 0.05$mm.

Since "d" is a function of $\sin\theta$ ($d = \lambda/2 \sin\theta$) the d - spacings can be determined more accurately at higher values of θ

$$\Delta d \text{ (precision)} = \frac{0.0125d}{\tan\theta}$$

A computer program DPOW written by A. Hall (1971) based on Cohen's least squares method, was used to get cell-sizes from both front and back reflection lines.

The program corrects for film shrinkage, and computes the values of 2θ, $\sin^2\theta$, d and $\sin^2\theta n/\sin^2\theta$, (where 1 = K$\alpha$, line n = K$\alpha_n$ th line) for the $\bar{\alpha}$, α_1 and α_2 lines and before the $\sin^2\theta_n/\sin^2\theta_1$ values are compared a correction is applied to convert all $\sin^2\theta$ values to equivalent $\sin^2\theta\,\alpha_1$ values using the factor given by Klug and Alexander (1962)

For 'Co' radiation $\sin^2\theta\,\alpha_1 = \sin^2\theta\,\alpha_2 \times 0.9970$

$\sin^2\theta\,\alpha_1 = \sin^2\theta\,\bar{\alpha} \times 0.99856$

Indexing and Calculation of Cell Parameters.

Cubic Minerals: As described by Hall (op. cit.) the $\sin^2\theta_n/\sin^2\theta_1$ value were used to obtain a factor, N_1 (the $h^2 + k^2 + L^2$ value of the first line). If the hkl value of the first line is known $N_1 = h^2 + k^2 + L^2$.

N_1 then used in DPOW to compute the approximate N values ($h^2 + k^2 + L^2$) of each line -

$$N_n \text{ (approx)} = \frac{\sin^2\theta_n}{\sin^2\theta/N_1}$$

in DPOW, N was rounded to the nearest integer and used to calculate the apparent cubic unit cell-edge of each line

$$a_n = \frac{\sqrt{N.\lambda^2}}{n\mathrm{Sin}^2\theta}$$

During this process the $\mathrm{Sin}^2\theta_1/N_1$ value was recalculated after indexing each line of relative intensity greater than 20, using the N value (integer) just established for the line.

This is necessary because precision and accuracy is low at low 2θ values as a result of line displacement due to absorption of the X-ray beam by the sample (Klug and Alexander, 1962).

According to Nelson and Riley (1945) measurements on X-ray powder photographs of cylindrical specimens (as described earlier) of different absorption and thickness, taken in a camera without eccentricity, show that the absorption error in the apparent unit-cell dimensions (a) is proportional to $\mathrm{Cos}^2\theta/\mathrm{Sin}^2\theta + \mathrm{Cos}^2\theta$. It is demonstrated by Nelson and Riley (op. cit.) that the plot of cell size against $\frac{1}{2}(\mathrm{Cos}^2\theta/\mathrm{Sin}^2\theta + \mathrm{Cos}^2\theta/\theta)$ is linear down $\theta = 30^\circ$. The extrapolated values for cell size are in good agreement with this function. The writer previously (1969a) extrapolated cell-size values of synthetic iron-bearing sphalerite samples and found that the cell-size values corresponding to back reflection lines $\theta = 45^\circ$ or higher, gave a much better relationship than those from front reflections. It is easily seen from the N.R. function formula that when θ goes to 90° deviations go to zero. The back reflection lines were also used by Skinner et al (1959) for precise cell-size measurements.

A computer program called NELRIL written by A.Hall (1971) at the writer's suggestion was employed to compute accurate cell-sizes of cubic minerals using 2θ values previously calculated by DPOW program.

The NELRIL calculates N.R. function for each 2θ value and extrapolates against cell-size value of each diffraction line where true cell-edge expressed as "Intercept of Regression" is calculated at $\theta = 90^{o}$. The procedure was repeated twice rejecting points plotted outside 1.5 x standard deviations from the best fitting line. "Standard error of the intercept" was calculated and given as the error of the extrapolated (accurate) cell edge. Various diffraction patterns of pyrites and sphalerites were given in Appendix Table 4.1 and 4.2.

Non-Cubic Minerals: DPOW was also employed to obtain the d-spacings of the diffracted lines which were fed into two programs GENSTRUK and COHEN for indexing and calculating the unit cell parameters, respectively. These programs are described by Marples and Shaw (1966) in a report published by UKAEA.

GENSTRUK produces a listing of line positions on being given non-cubic unit-cell parameters. Either film readings or observed d-values may be given as input. These lines are indexed by comparison with the generated lines. The observed line indices which do not fit the space group of the mineral must be rejected manually.

COHEN calculates the best lattice parameters and standard deviations using the given indexed set of d-values and rejects the lines not in agreement with the majority.

SPECIMEN PYRITE 7

ANALYSIS OF POWDER PHOTOGRAPH USING CO RADIATION AND 11.460 CM DIAMETER DEBYE SCHERRER CAMERA

FACTOR= 2.4974

ALPHA	LEFT	RIGHT	SUM	TWO THETA	SIN SQUARED	ANGSTROMS	REL.INT.	N	A
3	5.905	12.590	18.495	33.391	0.08253	3.1158	40	3.00	5.39665
3	5.370	13.120	18.490	38.710	0.10984	2.7908	90	4.00	5.40159
3	4.890	13.600	18.490	43.505	0.13735	2.4153	70	5.00	5.40173
3	4.455	14.040	18.495	47.876	0.16463	2.2061	70	6.00	5.40373
3	3.655	14.840	18.495	55.868	0.21945	1.9108	50	8.00	5.40448
3	2.575	15.910	18.485	66.607	0.30148	1.6392	100	11.00	5.40681
3	2.245	16.250	18.495	69.953	0.32861	1.5615	20	11.99	5.40912
3	1.920	16.570	18.490	73.175	0.35528	1.5017	30	13.00	5.41456
3	1.595	16.895	18.490	76.422	0.38261	1.4471	40	14.00	5.41450
3	0.001	18.500	9.246	92.447	0.52135	1.2397	20	19.98	5.40365
3	35.740	18.790	54.530	95.337	0.54650	1.2118	20	20.00	5.41492
3	35.425	19.105	54.530	98.484	0.57376	1.1817	20	20.99	5.41524
3	35.110	19.425	54.535	101.655	0.60101	1.1546	20	21.99	5.41557
3	34.470	20.060	54.530	108.024	0.65471	1.1062	20	23.96	5.41947
1	34.450	20.075	54.525	108.199	0.65616	1.1042	60	24.00	5.41957
2	33.405	21.120	54.525	118.638	0.73964	1.0423	30	27.00	5.41589
1	32.720	21.810	54.530	125.506	0.79039	1.0061	40	29.00	5.41799
2	32.665	21.865	54.530	126.055	0.79428	1.0058	20	29.02	5.41637
1	32.325	22.200	54.525	129.427	0.81755	0.9892	30	30.00	5.41833
2	32.270	22.255	54.525	129.976	0.82124	0.9892	20	30.01	5.41781
1	31.455	23.070	54.525	138.118	0.87226	0.9577	50	32.00	5.41767
2	31.390	23.135	54.525	138.767	0.87602	0.9577	30	32.01	5.41770
1	28.840	25.690	54.530	164.266	0.98127	0.9030	40	36.00	5.41775
2	28.645	25.890	54.535	166.239	0.98565	0.9029	20	36.01	5.41735

$a_o = 5.4182 \pm 0.0003$

SPECIMEN PYRITE 1

ANALYSIS OF POWDER PHOTOGRAPH USING CO RADIATION AND 11.460 CM DIAMETER DEBYE SCHERRER CAMERA

FACTOR= 2.4973

ALPHA	LEFT	RIGHT	SUM	TWO THETA	SIN SQUARED	ANGSTROMS	REL.INT.	N	A
3	6.215	12.89	19.105	33.339	0.08229	3.1204	40	3.00	5.40472
3	5.675	13.42	19.095	38.684	0.10978	2.7026	9	4.00	5.40516
3	5.200	13.90	19.100	43.454	0.13703	2.4180	7	5.00	5.40685
3	4.765	14.34	19.105	47.824	0.16429	2.2083	7	6.00	5.40926
3	3.970	15.14	19.110	55.790	0.21889	1.9132	5	8.00	5.41136
3	2.910	16.20	19.110	66.379	0.29966	1.6352	1	11.00	5.42321
3	2.580	16.535	19.115	69.701	0.32654	1.5664	2	11.99	5.42623
3	2.260	16.86	19.120	72.922	0.35316	1.5062	3	13.00	5.43071
3	1.940	17.185	19.125	76.144	0.38026	1.4516	4	14.00	5.43125
3	0.001	18.755	9.555	91.905	0.51662	1.2453	2	19.02	5.42832
3	36.025	19.08	55.105	95.365	0.54675	1.2105	2	20.13	5.41369
3	35.700	19.40	55.100	98.587	0.57465	1.1808	2	21.16	5.41163
3	35.390	19.71	55.100	101.684	0.60125	1.1544	2	22.14	5.41448
3	34.745	20.36	55.105	108.152	0.65577	1.1053	2	24.14	5.41508
1	33.735	21.37	55.105	118.241	0.73659	1.0422	6	27.00	5.41539
2	33.690	21.415	55.105	118.690	0.74104	1.0420	3	27.00	5.41442
1	33.005	22.105	55.110	125.558	0.79076	1.0059	4	29.00	5.41672
2	32.950	22.155	55.105	126.083	0.79447	1.0057	2	29.01	5.41572
1	32.605	22.500	55.105	129.529	0.81823	0.9888	3	30.00	5.41605
2	32.545	22.560	55.105	130.128	0.82225	0.9885	2	30.02	5.41447
1	31.745	23.360	55.105	138.128	0.87227	0.9577	5	32.00	5.41764
2	31.660	23.445	55.105	138.969	0.87718	0.9571	3	32.00	5.41413
1	29.715	25.995	55.710	161.420	0.97394	0.9063	4	36.00	5.43809
2	28.930	26.175	55.105	166.240	0.98565	0.9029	2	36.28	5.41735

$a_o = 5.4172 \pm 0.0005$

SPECIMEN PYRITE 41

ANALYSIS OF POWDER PHOTOGRAPH USING CO RADIATION AND 11.46 CM DIAMETER DEBYE SCHERRER CAMERA

FACTOR= 2.4984

ALPHA	LEFT	RIGHT	SUM	TWO THETA	SIN SQUARED	ANGSTROMS	REL.INT.	N	A
3	5.91	12.58	18.490	33.328	0.08223	3.1214	40	3.00	5.40646
3	5.375	13.115	18.490	38.675	0.11965	2.7632	90	4.00	5.40634
3	4.895	13.59	18.485	43.447	0.13699	2.4184	70	5.00	5.40765
3	4.455	14.03	18.485	47.844	0.16442	2.2075	70	6.00	5.40713
3	3.66	14.825	18.485	55.789	0.21888	1.9133	50	8.00	5.41151
3	2.585	15.9	18.49	66.557	0.30108	1.6313	100	11.00	5.41039
3	2.25	16.235	18.485	69.88	0.32830	1.5629	20	11.98	5.41409
3	1.92	16.565	18.485	73.178	0.35530	1.5017	30	13.00	5.41440
3	1.595	16.89	18.485	76.425	0.38264	1.4473	40	14.00	5.41427
3	0.061	18.475	9.243	92.257	0.51969	1.2417	20	19.01	5.41226
3	35.735	18.78	54.515	95.28	0.54671	1.2114	20	19.98	5.41737
3	35.42	19.09	54.51	98.403	0.57307	1.1824	20	20.97	5.41853
3	35.1	19.42	54.52	101.651	0.60197	1.1546	20	21.99	5.41574
3	34.46	20.05	54.51	107.997	0.65448	1.1064	20	23.95	5.42
1	33.445	21.07	54.515	118.165	0.73601	1.0426	60	27.00	5.41754
2	33.3	21.21	54.51	119.589	0.74689	1.0372	30	27.00	5.38953
1	32.705	21.81	54.515	125.56	0.79078	1.0058	40	29.00	5.41667
2	32.655	21.855	54.51	126.035	0.79414	1.0059	20	29.00	5.41686
1	32.305	22.2	54.505	129.508	0.81809	0.9889	30	30.00	5.41652
2	32.255	22.255	54.51	130.032	0.82161	0.9889	20	30.00	5.41657
1	31.445	23.06	54.505	138.102	0.87217	0.9578	50	32.00	5.41796
2	31.38	23.13	54.51	138.777	0.87607	0.9577	30	32.00	5.41753
1	28.825	25.675	54.500	164.265	0.98125	0.9039	40	36.00	5.41779
2	28.64	25.865	54.505	166.134	0.98543	0.9039	20	36.00	5.41796

$a_o = 5.4175 \pm 0.0004$

SPECIMEN PYRITE 76

ANALYSIS OF POWDER PHOTOGRAPH USING CO RADIATION AND 11.46[illegible] CM DIAMETER DEBYE SCHERRER CAMERA

FACTOR= 2.4999

ALPHA	LEFT	RIGHT	SUM	TWO THETA	SIN SQUARED	ANGSTROMS	REL.INT.	N	A
3	5.980	12.635	18.615	33.273	[illegible].08197	3.1265	40	3.00	5.41518
3	5.440	13.175	18.615	38.673	[illegible].10964	2.7033	90	4.00	5.40661
3	4.965	13.650	18.615	43.423	[illegible].13685	2.4197	70	5.00	5.41052
3	4.525	14.090	18.615	47.822	[illegible].16428	2.2084	70	6.00	5.40942
3	3.730	14.885	18.615	55.772	[illegible].21876	1.9138	50	8.00	5.41301
3	2.660	15.955	18.615	66.471	[illegible].30040	1.6332	100	11.00	5.41655
3	2.320	16.295	18.615	69.871	[illegible].32793	1.5631	20	12.01	5.41466
3	2.000	16.615	18.615	73.071	[illegible].35441	1.5036	30	13.00	5.42119
3	1.675	16.945	18.620	76.346	[illegible].38197	1.4483	40	14.00	5.41905
3	[illegible].001	18.535	9.308	92.267	[illegible].51978	1.2415	20	19.05	5.41179
3	35.680	18.940	54.620	96.305	[illegible].55491	1.2016	21	20.34	5.37377
3	35.455	19.155	54.610	98.584	[illegible].57394	1.1815	20	21.04	5.41439
3	35.145	19.470	54.615	101.629	[illegible].60079	1.1548	21	22.02	5.41657
3	34.495	20.125	54.620	108.154	[illegible].65579	1.1053	23	24.04	5.41503
1	33.495	21.125	54.620	118.153	.73592	1.0427	60	27.01	5.41787
2	33.445	21.175	54.620	118.653	[illegible].73975	1.0422	30	27.00	5.41546
1	32.755	21.860	54.615	125.528	[illegible].79155	1.0060	40	29.00	5.41745
2	32.700	21.925	54.625	126.128	[illegible].79479	1.0055	20	29.03	5.41463
1	32.365	22.250	54.615	129.428	[illegible].81755	0.9892	30	30.00	5.41831
2	32.310	22.315	54.625	130.028	[illegible].82158	0.9889	20	30.02	5.41668
1	31.465	23.125	54.590	138.302	[illegible].87333	0.9571	50	32.00	5.41435
2	31.430	23.195	54.625	138.827	[illegible].87636	0.9575	30	32.06	5.41664
1	28.880	25.740	54.620	164.301	[illegible].98135	0.9029	40	36.03	5.41752
2	28.690	25.935	54.625	166.226	[illegible].98562	0.9029	20	36.00	5.41743

$a_o = 5.4180 \pm 0.0006$

SPECIMEN PYRITE 90

ANALYSIS OF POWDER PHOTOGRAPH USING CO RADIATION AND 11.460 CM DIAMETER DEBYE SCHERRER CAMERA

FACTOR= 2.4980

ALPHA	LEFT	RIGHT	SUM	TWO THETA	SIN SQUARED	ANGSTROMS	REL.INT.	N	A
3	6.090	12.765	18.855	33.349	0.08233	3.1196	30	3.00	5.40329
3	5.545	13.305	18.850	38.769	0.11016	2.6968	90	4.00	5.39370
3	5.070	13.780	18.850	43.515	0.13741	2.4147	70	5.00	5.39954
3	4.635	14.215	18.850	47.862	0.16454	2.2067	60	6.00	5.40521
3	3.840	15.010	18.850	55.806	0.21900	1.9127	50	8.00	5.41000
3	2.760	16.085	18.845	66.572	0.30129	1.6319	100	11.00	5.40929
3	2.430	16.415	18.845	69.870	0.32792	1.5631	20	11.98	5.41477
3	2.095	16.755	18.850	73.242	0.35583	1.5005	20	13.00	5.41031
3	1.775	17.080	18.855	76.464	0.38297	1.4464	40	14.00	5.41194
3	9.761	18.655	9.425	92.227	0.51943	1.2429	20	18.99	5.41363
3	35.915	18.965	54.880	95.317	0.54633	1.2110	20	19.97	5.41576
3	35.600	19.275	54.875	98.440	0.57338	1.1821	20	20.96	5.41702
3	35.285	19.595	54.875	101.587	0.60043	1.1552	30	22.00	5.41819
3	34.630	20.250	54.880	108.157	0.65581	1.1053	20	24.03	5.41490
1	33.630	21.250	54.880	118.149	0.73588	1.0427	60	27.00	5.41799
2	33.575	21.305	54.880	118.699	0.74018	1.0423	30	27.00	5.41419
1	32.890	21.985	54.875	125.518	0.79948	1.0061	40	29.00	5.41769
2	32.835	22.045	54.880	126.093	0.79455	1.0056	20	29.02	5.41547
1	32.495	22.385	54.880	129.493	0.81797	0.9899	30	30.00	5.41692
2	32.440	22.440	54.880	130.048	0.82166	0.9889	20	30.01	5.41641
1	31.630	23.245	54.875	138.108	0.87220	0.9577	50	32.00	5.41785
2	31.565	23.315	54.880	138.783	0.87611	0.9577	30	32.00	5.41743
1	29.710	25.870	54.880	164.312	0.98138	0.9029	50	36.00	5.41745
2	28.820	26.060	54.880	166.211	0.98559	0.9029	30	36.00	5.41752

$a_o = 5.4179 \pm 0.0007$

SPECIMEN PYRITE 111

ANALYSIS OF POWDER PHOTOGRAPH USING CO RADIATION AND 11.460 CM DIAMETER DEBYE SCHERRER CAMERA

FACTOR= 2.4992

ALPHA	LEFT	RIGHT	SUM	TWO THETA	SIN SQUARED	ANGSTROMS	REL.INT.	N	A
3	5.685	12.550	18.435	33.314	0.08216	3.1228	40	3.00	5.40878
3	5.355	13.085	18.440	38.637	0.10944	2.7057	90	4.00	5.41146
3	4.870	13.570	18.440	43.485	0.13722	2.4163	70	5.00	5.40311
3	4.435	14.000	18.435	47.809	0.16420	2.2191	70	6.00	5.41088
3	3.635	14.800	18.435	55.806	0.21900	1.9127	50	8.00	5.40997
3	2.565	15.875	18.440	66.527	0.30084	1.6319	100	11.00	5.41251
3	2.235	16.210	18.445	69.851	0.32777	1.5635	20	11.98	5.41601
3	1.900	16.535	18.435	73.150	0.35507	1.5022	30	13.00	5.41614
3	1.575	16.860	18.435	76.399	0.38242	1.4474	40	14.00	5.41586
3	0.961	18.450	19.219	92.283	0.51989	1.2414	20	19.03	5.41122
3	35.690	18.760	54.450	95.379	0.54687	1.2104	20	20.02	5.41311
3	35.390	19.060	54.450	98.378	0.57285	1.1826	20	20.97	5.41955
3	35.060	19.385	54.445	101.652	0.60098	1.1546	20	22.00	5.41571
3	34.420	20.030	54.450	108.074	0.65513	1.1059	20	23.98	5.41773
1	33.415	21.030	54.445	118.096	0.73548	1.0430	60	27.00	5.41949
2	33.365	21.090	54.455	118.646	0.73970	1.0422	30	27.00	5.41567
1	32.675	21.775	54.450	125.518	0.79048	1.0060	40	29.00	5.41768
2	32.620	21.835	54.455	126.093	0.79455	1.0056	20	29.02	5.41546
1	32.275	22.175	54.450	129.517	0.81815	0.9889	30	30.00	5.41631
2	32.220	22.225	54.445	130.042	0.82167	0.9889	20	30.00	5.41636
1	31.420	23.030	54.450	138.064	0.87195	0.9579	50	32.00	5.41865
2	31.345	23.100	54.445	138.789	0.87614	0.9577	30	32.00	5.41732
1	28.795	25.660	54.455	164.333	0.98142	0.9329	40	36.00	5.41733
2	28.600	25.855	54.455	166.281	0.98573	0.9029	20	36.00	5.41712

$a_o = 5.4179 \pm 0.0005$

SPECIMEN SPHALERITE 6B

ANALYSIS OF POWDER PHOTOGRAPH USING CO RADIATION AND 11.46[illegible] CM DIAMETER DEBYE SCHERRER CAMERA

FACTOR= 2.5028

ALPHA	LEFT	RIGHT	SUM	TWO THETA	SIN SQUARED	ANGSTROMS	REL.INT.	N	A
3	6.150	12.825	18.975	33.413	[illegible].18264	3.1138	100	3.00	5.39318
3	5.620	13.355	18.975	38.719	[illegible].13989	2.7[illegible]2	30	4.00	5.40044
3	3.910	15.[illegible]65	18.975	55.838	[illegible].21924	1.9117	90	8.00	5.40709
3	2.850	16.130	18.980	66.475	[illegible].30[illegible]43	1.6331	80	11.[illegible]0	5.41626
3	2.530	16.460	18.990	69.729	[illegible].32677	1.5659	20	11.96	5.42430
3	1.250	17.750	19.[illegible]00	82.594	[illegible].43555	1.3563	30	16.[illegible]0	5.42521
1	[illegible].001	18.[illegible]95	9.491	92.242	[illegible].51956	1.24[illegible]9	40	19.11	5.40903
2	[illegible].001	18.730	9.491	92.492	[illegible].52174	1.241[illegible]	20	19.11	5.40935
1	34.635	2[illegible].290	54.925	1[illegible]8.194	[illegible].65611	1.1[illegible]43	50	24.[illegible]0	5.40975
2	34.585	20.340	54.925	1[illegible]8.694	[illegible].66[illegible]26	1.1[illegible]32	40	24.00	5.40438
1	33.625	21.315	54.940	118.38[illegible]	[illegible].73766	1.[illegible]414	40	27.[illegible]0	5.41147
2	33.580	21.360	54.940	118.831	[illegible].74111	1.[illegible]413	30	27.[illegible]0	5.41[illegible]50
1	31.630	23.320	54.950	138.4[illegible]3	[illegible].87392	[illegible].9568	30	32.[illegible]0	5.41254
2	31.560	23.390	54.950	139.1[illegible]4	[illegible].87795	[illegible].9567	20	32.[illegible]1	5.41175
1	29.890	25.[illegible]60	54.950	155.823	[illegible].95614	[illegible].9147	85	35.[illegible]0	5.41170
2	29.770	25.180	54.950	157.[illegible]24	[illegible].96133	[illegible].9147	60	35.[illegible]0	5.41153
1	28.945	26.[illegible]00	54.945	165.258	[illegible].98354	[illegible].9019	20	36.[illegible]0	5.41148

SPECIMEN SPHALERITE 7

ANALYSIS OF POWDER PHOTOGRAPH USING CO RADIATION AND 11.460 CM DIAMETER DEBYE SCHERRER CAMERA

FACTOR= 2.5000

ALPHA	LEFT	RIGHT	SUM	TWO THETA	SIN SQUARED	ANGSTROMS	REL.INT.	N	A
3	6.095	12.745	18.840	33.250	0.08186	3.1286	100	3.00	5.41889
3	5.555	13.285	18.840	38.650	0.10951	2.7049	30	4.00	5.40974
3	3.845	14.995	18.840	55.750	0.21859	1.9145	90	8.00	5.41501
3	2.775	16.065	18.840	66.449	0.30122	1.6336	80	11.00	5.41813
3	2.450	16.390	18.840	69.699	0.32653	1.5664	20	11.96	5.42631
3	1.160	17.685	18.845	82.624	0.43581	1.3559	30	16.00	5.42355
1	0.001	18.625	9.420	92.045	0.51784	1.2430	40	19.04	5.41799
2	0.001	18.650	9.420	92.295	0.52002	1.2430	30	19.04	5.41829
3	35.810	18.960	54.770	95.751	0.55019	1.2068	20	20.20	5.39720
1	34.555	20.220	54.775	108.326	0.65721	1.1033	50	24.00	5.40524
2	34.515	20.260	54.775	108.726	0.66052	1.1029	30	24.00	5.40332
1	33.550	21.235	54.785	118.425	0.73801	1.0412	40	27.00	5.41019
2	33.500	21.785	55.285	121.425	0.76069	1.0278	30	28.00	5.43840
1	31.550	23.245	54.795	138.475	0.87434	0.9566	30	32.00	5.41124
2	31.485	23.310	54.795	139.125	0.87807	0.9566	20	32.00	5.41137
1	29.820	24.975	54.795	155.775	0.95597	0.9148	60	35.00	5.41218
2	29.700	25.095	54.795	156.975	0.96017	0.9148	40	35.00	5.41290

SPECIMEN YELLOW SPHALERITE 8

ANALYSIS OF POWDER PHOTOGRAPH USING CO RADIATION AND 11.46[illegible] CM DIAMETER DEBYE SCHERRER CAMERA

FACTOR= 2.5[illegible]18

ALPHA	LEFT	RIGHT	SUM	TWO THETA	SIN SQUARED	ANGSTROMS	REL.INT.	N	A
3	5.890	12.56[illegible]	18.450	33.374	[illegible].08245	3.1173	10[illegible]	3.00	5.39933
3	5.355	13.[illegible]9[illegible]	18.445	38.702	0.10980	2.7013	3[illegible]	4.00	5.40264
3	3.645	14.81[illegible]	18.445	55.815	0.21906	1.9124	9[illegible]	8.00	5.40921
3	2.570	15.875	18.445	66.572	0.30120	1.6313	9[illegible]	11.00	5.40929
3	2.235	16.215	18.450	69.950	[illegible].32858	1.5615	2[illegible]	12.00	5.40936
3	1.955	17.50[illegible]	18.455	82.784	[illegible].43719	1.3537	4[illegible]	16.00	5.41499
1	9.001	18.435	9.224	92.174	0.51897	1.2416	5[illegible]	19.02	5.41214
2	9.001	18.466	9.224	92.424	0.52115	1.2417	3[illegible]	19.02	5.41245
3	35.635	18.775	54.41[illegible]	95.64[illegible]	[illegible].54914	1.2079	2[illegible]	20.11	5.40191
1	34.375	20.035	54.410	108.249	[illegible].65657	1.1039	6[illegible]	24.00	5.40785
2	34.340	20.[illegible]70	54.41[illegible]	108.599	[illegible].65947	1.1038	4[illegible]	24.00	5.40759
1	33.375	21.05[illegible]	54.425	118.331	0.73728	1.0417	5[illegible]	27.00	5.41284
2	33.320	21.11[illegible]	54.43[illegible]	118.9[illegible]7	[illegible].74169	1.0[illegible]8	3[illegible]	27.00	5.41838
1	31.370	23.[illegible]6[illegible]	54.43[illegible]	138.42[illegible]	1.87402	[illegible].9568	4[illegible]	32.00	5.41222
2	31.300	23.13[illegible]	54.43[illegible]	139.121	1.87805	[illegible].9566	3[illegible]	32.00	5.41144
1	29.635	24.795	54.43[illegible]	155.783	1.95[illegible]1	[illegible].9148	8[illegible]	35.[illegible]	5.41211
2	29.515	24.915	54.43[illegible]	156.984	[illegible].96[illegible]2[illegible]	[illegible].9148	6[illegible]	35.00	5.41191

SPECIMEN SPHALERITE 17

ANALYSIS OF POWDER PHOTOGRAPH USING CO RADIATION AND 11.46[illegible] CM DIAMETER DEBYE SCHERRER CAMERA

FACTOR= 2.4906

ALPHA	LEFT	RIGHT	SUM	TWO THETA	SIN SQUARED	ANGSTROMS	REL.INT.	N	A
3	5.840	12.535	18.375	33.349	[illegible]8233	3.1196	100	3.00	5.40323
3	5.300	13.[illegible]75	18.375	38.729	[illegible].10994	2.6996	2[illegible]	4.01	5.39914
3	3.585	14.79[illegible]	18.375	55.814	[illegible].21906	1.9125	9[illegible]	8.00	5.40927
3	2.510	15.865	18.375	66.523	[illegible].30181	1.6329	8[illegible]	11.00	5.41280
3	2.175	16.20[illegible]	18.375	69.861	[illegible].32785	1.5633	2[illegible]	11.99	5.41536
3	[illegible].885	17.49[illegible]	18.375	82.712	[illegible].43657	1.3547	3[illegible]	16.00	5.41882
1	[illegible].001	18.42[illegible]	9.187	91.977	[illegible].51725	1.2437	4[illegible]	18.98	5.42109
2	[illegible].001	18.45[illegible]	9.187	92.276	[illegible].51986	1.2432	3[illegible]	19.00	5.41916
3	36.650	18.75[illegible]	55.401	9[illegible].837	[illegible].51730	1.2567	2[illegible]	18.59	5.47793
1	34.380	20.[illegible]20	54.[illegible]00	1[illegible]8.473	[illegible].65841	1.1023	5[illegible]	24.00	5.40131
2	34.345	2[illegible].055	54.4[illegible]	1[illegible]8.819	[illegible].66129	1.1023	4[illegible]	24.00	5.40116
1	33.365	21.[illegible]35	54.4[illegible]	118.582	[illegible].73921	1.[illegible]403	4[illegible]	27.00	5.40579
2	33.320	21.[illegible]80	54.4[illegible]	119.[illegible]31	[illegible].74264	1.[illegible]402	3[illegible]	27.00	5.40493
1	31.355	23.[illegible]45	54.4[illegible]	138.6[illegible]7	[illegible].87509	[illegible].9562	3[illegible]	32.00	5.40890
2	31.290	23.11[illegible]	54.4[illegible]	139.254	[illegible].87881	[illegible].9562	2[illegible]	32.00	5.40911
1	29.625	24.775	54.4[illegible]	155.841	[illegible].95621	[illegible].9147	7[illegible]	35.00	5.41151
2	29.510	24.89[illegible]	54.4[illegible]	156.987	[illegible].96121	[illegible].9148	5[illegible]	35.00	5.41188

SPECIMEN SPHALERITE 42

ANALYSIS OF POWDER PHOTOGRAPH USING CO RADIATION AND 11.46[illegible] CM DIAMETER DEBYE SCHERRER CAMERA

FACTOR= 2.5049

ALPHA	LEFT	RIGHT	SUM	TWO THETA	SIN SQUARED	ANGSTROMS	REL.INT.	N	A
3	6.540	13.2[illegible]	19.740	33.366	[illegible].08241	3.1181	100	3.00	5.40057
3	6.000	13.735	19.745	38.726	[illegible].10993	2.6997	3[illegible]	4.00	5.39943
3	4.300	15.44[illegible]	19.740	55.81[illegible]	[illegible].21903	1.9126	9[illegible]	8.00	5.40961
3	3.240	16.51[illegible]	19.750	66.481	[illegible].30047	1.6329	85	11.00	5.41584
3	2.900	16.85[illegible]	19.750	69.888	[illegible].32807	1.5628	2[illegible]	12.01	5.41353
3	1.620	18.14[illegible]	19.760	82.763	[illegible].43702	1.3540	3[illegible]	16.00	5.41608
1	0.001	19.[illegible]87	9.873	92.249	[illegible].51962	1.2408	4[illegible]	19.05	5.40873
2	0.001	19.11[illegible]	9.873	92.549	[illegible].52224	1.2404	2[illegible]	19.07	5.40678
1	34.980	20.68[illegible]	55.660	108.359	[illegible].65748	1.1031	5[illegible]	24.00	5.40412
2	34.945	20.72[illegible]	55.665	108.734	[illegible].66059	1.1029	3[illegible]	24.00	5.40302
1	33.980	21.70[illegible]	55.680	118.479	[illegible].73842	1.0409	4[illegible]	27.00	5.40870
2	33.940	21.74[illegible]	55.680	118.879	[illegible].74148	1.0410	2[illegible]	27.00	5.40914
1	31.980	23.70[illegible]	55.680	138.518	[illegible].87458	0.9564	3[illegible]	32.00	5.41048
2	31.915	23.765	55.680	139.169	[illegible].87832	0.9565	2[illegible]	32.00	5.41059
1	30.240	25.44[illegible]	55.680	155.953	[illegible].95660	0.9145	6[illegible]	35.00	5.41039
2	30.125	25.555	55.680	157.195	[illegible].96161	0.9146	4[illegible]	35.00	5.41175

SPECIMEN SPHALEITE 47A

ANALYSIS OF POWDER PHOTOGRAPH USING CO RADIATION AND 11.46[illegible] CM DIAMETER DEBYE SCHERRER CAMERA

FACTOR= 2.5015

ALPHA	LEFT	RIGHT	SUM	TWO THETA	SIN SQUARED	ANGSTROMS	REL.INT.	N	A
3	6.410	13.[illegible]70	19.480	33.320	[illegible].08219	3.1222	100	3.00	5.40778
3	5.870	13.610	19.480	38.723	[illegible].10991	2.6999	30	4.00	5.39985
3	4.160	15.320	19.480	55.834	[illegible].21920	1.9118	90	8.00	5.40752
3	3.080	16.400	19.480	66.640	[illegible].30175	1.6295	85	11.00	5.40441
3	2.750	16.740	19.490	69.992	[illegible].32893	1.5607	20	11.99	5.40650
3	1.465	18.025	19.490	82.850	[illegible].43777	1.3529	30	16.00	5.41145
1	0.001	18.960	9.742	92.239	[illegible].51953	1.2416	40	19.02	5.40918
2	0.001	18.985	9.742	92.489	[illegible].52171	1.2410	30	19.01	5.40951
3	36.170	19.280	55.450	95.499	[illegible].54792	1.2093	20	20.93	5.40794
1	34.965	20.555	55.460	108.207	[illegible].65622	1.1042	50	24.00	5.40929
2	34.870	20.590	55.460	108.557	[illegible].65912	1.1041	40	24.00	5.40933
1	33.885	21.580	55.465	118.438	[illegible].73810	1.0411	40	27.09	5.40984
2	33.850	21.615	55.465	118.788	[illegible].74079	1.0415	30	27.02	5.41168
1	31.885	23.575	55.460	138.425	[illegible].87414	[illegible].9567	30	32.00	5.41214
2	31.820	23.645	55.465	139.1[illegible]	[illegible].87793	[illegible].9567	20	32.00	5.41181
1	30.150	25.315	55.465	155.81[illegible]	[illegible].95618	[illegible].9148	70	35.[illegible]0	5.41183
2	30.030	25.435	55.465	157.011	[illegible].96129	[illegible].9147	50	35.[illegible]0	5.41165

SPECIMEN SPHALERITE 79

ANALYSIS OF POWDER PHOTOGRAPH USING CU RADIATION AND 11.461 CM DIAMETER DEBYE SCHERRER CAMERA

FACTOR= 2.5006

ALPHA	LEFT	RIGHT	SUM	TWO THETA	SIN SQUARED	ANGSTROMS	REL.INT.	N	A
3	6.110	12.765	18.875	33.283	0.08202	3.1255	10[illegible]	3.[illegible]	5.41355
3	5.570	13.300	18.870	38.660	[illegible].10957	2.7042	3[illegible]	4.[illegible]	5.40837
3	3.885	15.015	18.900	55.664	0.21798	1.9172	9[illegible]	8.[illegible]	5.42265
3	2.790	16.080	18.870	66.467	0.30036	1.6332	8[illegible]	11.[illegible]	5.41687
3	2.455	16.420	18.875	69.843	0.32770	1.5636	2[illegible]	12.[illegible]	5.41658
3	1.170	17.715	18.885	82.746	0.43687	1.3543	3[illegible]	16.[illegible]	5.41761
1	0.001	18.655	9.440	92.178	0.51980	1.2416	4[illegible]	19.[illegible]4	5.41196
2	0.001	18.685	9.440	92.478	0.52162	1.2411	3[illegible]	19.[illegible]5	5.41[illegible]2
1	34.600	20.250	54.851	108.232	[illegible].65643	1.1941	5[illegible]	24.[illegible]0	5.40844
2	34.570	20.290	54.860	108.582	[illegible].65933	1.1939	4[illegible]	24.[illegible]0	5.40818
1	33.595	21.275	54.870	118.384	0.73769	1.0414	4[illegible]	27.09	5.41135
2	33.550	21.320	54.870	118.834	0.74114	1.0412	3[illegible]	27.[illegible]0	5.41039
1	31.595	23.285	54.880	138.439	0.87413	1.9567	3[illegible]	32.[illegible]8	5.41189
2	31.530	23.345	54.875	139.[illegible]65	[illegible].87772	0.9568	2[illegible]	31.99	5.41244
1	29.870	25.005	54.875	155.669	0.95559	0.9153	7[illegible]	35.[illegible]0	5.41326
2	29.745	25.130	54.875	156.919	0.95998	0.9149	5[illegible]	35.[illegible]0	5.41254
1	28.930	25.945	54.875	165.071	0.98312	0.9121	2[illegible]	36.[illegible]	5.41263

SPECIMEN SPHALERITE 95

ANALYSIS OF POWDER PHOTOGRAPH USING CO RADIATION AND 11.46[illegible] CM DIAMETER DEBYE SCHERRER CAMERA

FACTOR= 2.5004

ALPHA	LEFT	RIGHT	SUM	TWO THETA	SIN SQUARED	ANGSTROMS	REL.INT.	N	A
3	5.965	12.615	18.580	33.255	[illegible]8188	3.1281	1[illegible]	3.[illegible]	5.418[illegible]2
3	5.430	13.155	18.585	38.631	[illegible].10941	2.7061	3[illegible]	4.[illegible]	5.41225
3	3.715	14.865	18.580	55.759	[illegible].21866	1.9142	9[illegible]	8.[illegible]	5.4142[illegible]
3	2.645	15.935	18.580	66.460	[illegible].30931	1.6334	85	11.[illegible]	5.41735
3	2.305	16.275	18.580	69.861	[illegible].32785	1.5633	2[illegible]	12.01	5.41536
3	1.930	17.560	18.590	82.663	[illegible].43615	1.3554	3[illegible]	16.[illegible]	5.42148
1	0.001	18.5[illegible]	9.291	92.102	[illegible].51834	1.2424	4[illegible]	19.[illegible]4	5.41541
2	0.001	18.538	9.291	92.402	[illegible].52195	1.2419	3[illegible]	19.06	5.41345
1	34.475	20.[illegible]0[illegible]	54.575	108.114	[illegible].65545	1.1048	5[illegible]	24.[illegible]	5.41248
2	34.430	20.14[illegible]	54.570	108.539	[illegible].65897	1.1042	4[illegible]	24.[illegible]	5.4[illegible]964
1	33.460	21.115	54.575	118.265	[illegible].73678	1.0421	4[illegible]	27.0[illegible]	5.4147[illegible]
2	33.415	21.160	54.575	118.715	[illegible].74023	1.0419	3[illegible]	27.[illegible]	5.41372
1	31.460	23.12[illegible]	54.580	138.293	[illegible].87328	[illegible].9572	3[illegible]	32.[illegible]	5.41451
2	31.390	23.19[illegible]	54.585	138.994	[illegible].87732	[illegible].9570	2[illegible]	32.01	5.41369
1	29.730	24.85[illegible]	54.580	155.596	[illegible].95533	0.9151	6[illegible]	35.[illegible]	5.41401
2	29.615	24.965	54.580	156.746	[illegible].95938	[illegible].9152	4[illegible]	35.[illegible]	5.41421

SPECIMEN SPHALERITE S7

ANALYSIS OF POWDER PHOTOGRAPH USING CO RADIATION AND 11.46 CM DIAMETER DEBYE SCHERRER CAMERA

FACTOR= 2.5008

ALPHA	LEFT	RIGHT	SUM	TWO THETA	SIN SQUARED	ANGSTROMS	REL.INT.	N	A
3	6.230	12.9[illegible]	19.13[illegible]	33.361	[illegible].08239	3.1185	1[illegible]	3.[illegible]	5.4[illegible]140
3	5.705	13.425	19.130	38.612	[illegible].11931	2.7[illegible]74	3[illegible]	4.[illegible]	5.41479
3	3.985	15.145	19.130	55.818	[illegible].21909	1.9123	9[illegible]	8.[illegible]	5.41894
3	2.915	16.220	19.135	66.546	[illegible].30199	1.6315	8[illegible]	11.[illegible]	5.41117
3	2.580	16.555	19.135	69.897	[illegible].32815	1.5626	2[illegible]	11.99	5.41291
3	1.295	17.840	19.135	82.751	[illegible].43691	1.3542	3[illegible]	16.[illegible]	5.41674
1	[illegible].001	18.775	9.566	92.117	[illegible].51847	1.2422	4[illegible]	19.[illegible]1	5.41473
2	[illegible].001	18.8[illegible]	9.566	92.367	[illegible].52065	1.2423	3[illegible]	19.[illegible]1	5.41594
3	36.015	19.1[illegible]5	55.120	95.423	[illegible].54726	1.2[illegible]	2[illegible]	2[illegible].4	5.41123
1	34.755	2[illegible].365	55.121	1[illegible]8.027	[illegible].65473	1.1[illegible]54	4[illegible]	24.[illegible]	5.41544
2	34.710	2[illegible].41[illegible]	55.120	1[illegible]8.477	[illegible].65847	1.1[illegible]47	3[illegible]	24.[illegible]	5.41173
1	33.730	21.395	55.125	118.3[illegible]5	[illegible].73719	1.[illegible]418	3[illegible]	27.[illegible]	5.41357
2	33.680	21.445	55.125	118.8[illegible]6	[illegible].74[illegible]92	1.[illegible]414	2[illegible]	27.[illegible]2	5.41127
1	31.725	23.395	55.120	138.337	[illegible].87353	[illegible].9577	4[illegible]	32.[illegible]	5.41373
2	31.655	23.465	55.120	139.[illegible]37	[illegible].87757	[illegible].9569	3[illegible]	32.[illegible]	5.41292
1	31.[illegible]05	25.115	55.120	155.542	[illegible].95513	[illegible].9152	7[illegible]	35.[illegible]	5.41456
2	29.885	25.235	55.120	156.743	[illegible].95937	[illegible].9152	5[illegible]	35.[illegible]	5.41424

SPECIMEN SPHALERITE 115

ANALYSIS OF POWDER PHOTOGRAPH USING CO RADIATION AND 11.46 CM DIAMETER DEBYE SCHERRER CAMERA

FACTOR= 2.5004

ALPHA	LEFT	RIGHT	SUM	TWO THETA	SIN SQUARED	ANGSTROMS	REL.INT.	N	A
3	6.280	12.965	19.245	33.43	.08272	3.1122	13	3.00	5.39059
3	5.740	13.5	19.240	38.8	.11036	2.6944	3	4.00	5.38882
3	4.030	15.21	19.240	55.9	.21974	1.9095	9	8.00	5.40787
3	2.960	16.280	19.240	66.61	.30151	1.6341	9	11.00	5.40658
3	2.620	16.62	19.240	70.1	.32967	1.5614	2	12.01	5.40527
3	1.330	17.91	19.240	82.912	.43831	1.3529	3	16.00	5.40811
1	0.001	18.835	9.620	92.159	.51884	1.2418	4	18.97	5.41278
2	0.001	18.86	9.620	92.41	.52102	1.2419	2	18.96	5.41319
3	36.070	19.165	55.235	95.462	.54769	1.2096	2	19.99	5.41952
1	34.805	20.430	55.235	108.114	.65546	1.1048	5	24.00	5.41246
2	34.760	20.475	55.235	108.564	.65919	1.1041	3	24.01	5.40877
1	33.785	21.450	55.235	118.316	.73717	1.0418	4	27.00	5.41328
2	33.735	21.505	55.240	118.841	.74119	1.0412	3	27.00	5.41321
1	31.780	23.455	55.235	138.369	.87372	.9569	4	32.00	5.41315
2	31.705	23.530	55.235	139.119	.87803	.9566	3	32.00	5.41148
1	30.050	25.185	55.235	155.671	.95560	.9151	8	35.00	5.41324
2	29.930	25.305	55.235	156.872	.95981	.9151	6	35.00	5.41299
1	29.100	26.135	55.235	165.173	.98335	.9121	2	36.01	5.41210

MAP 1

GEOLOGICAL MAP OF THE TEKMEZ DARIKÖY AND AKKÖY' AREA OF SULPHIDE MINERALIZATION, SOUTH OF BULANCAK, EASTERN BLACK SEA, TURKEY.

ERİKLİK
BÜYÜKİNECE
DARIKÖY
AKKÖY
YAŞLIBAHÇE
TEKMEZAR
YAYKINLIK
HAMİDİYE
KÜÇÜKDERE
Çamlık T.
Gedik T.
Dolik T.
Dinekkaya T.
Dönbül T.
Evliya T.
Kirli T.
İnceali T.
Armutlu T.
Çamlıca D.
Görüveri
Gönürca D.
Damyatağı D.
Küçükgüre D.
Büyükgüre D.
Kuş D.
Savcılık D.
Kornalı D.
Karadere
Küçükdere
Ardahan D.
Batkınç D.

GİRESUN G 40 SHEET
BLACK SEA
BULANCAK
1:200.000

LEGEND

- Scree
- Basalt dyke
- Quartz - Microdiorite — Paleocene
- Agglomerate, sandstone, and limestone (Senonian)
- Biotite-andesite, lower part brecciated
- Rhyodacite and rhyodacitic pyroclastics
- Alternating tuffaceous breccia and sandstone
- Coarse, porphyritic dacite and dacitic tuff
- Pelitic limestone and tuff
- Lower basic series — Upper Cretaceous
- Fault showing dip, dashed where inferred or poorly located
- Vertical fault, arrows indicate direction of relative lateral movement
- Geological contact, dashed where poorly located
- Strike and dip of bedding
- Slag
- Mineral occurrence
- Fossil locality
- Accessible roads
- Peak altitude in ms.
- Streams and tributaries
- Landslide

0 50 meters

MAP2

MAP SHOWING THE DISTRIBUTION AND TYPE OF MINERALIZATION IN RELATION TO GEOLOGY.

Legend

- Scree
- Basalt dyke
- Quartz-Microdiorite
- Agglomerate, Sandstone, Limestone
- Biotite-andesite
- Rhyodacite and rhyodacitic pyroclastics
- Alternating tuffaceous breccia and sandstone
- Porphyritic dacite
- Pelitic limestone and tuff
- Lower basic series
- Fault showing dip, solid where known, dashed where inferred or poorly located.
- Vertical fault — U = Upthrown side, D = Downthrown side
- Geological contact, dashed where poorly located
- Strike and dip of bedding
- Strike and dip of vein
- Vertical vein
- Approximate position of vein

P = Pyrite vein
Cp = Chalcopyrite vein
Q = Quartz vein
B = Baryte vein
Bi = Bi-Sulphosalt
Bt = Betekhtinite
Hm = Hematite

- Sulphide occurrences of unknown attitude
- Mine, inactive
- Adit, open and caved
- Slag
- Streams and tributaries
- Landslide
- 934 Peak altitude, Ms.
- BL-4 Etibank borehole

0 500 Meters

MAP 3

MAP SHOWING SPECIMEN LOCALITIES

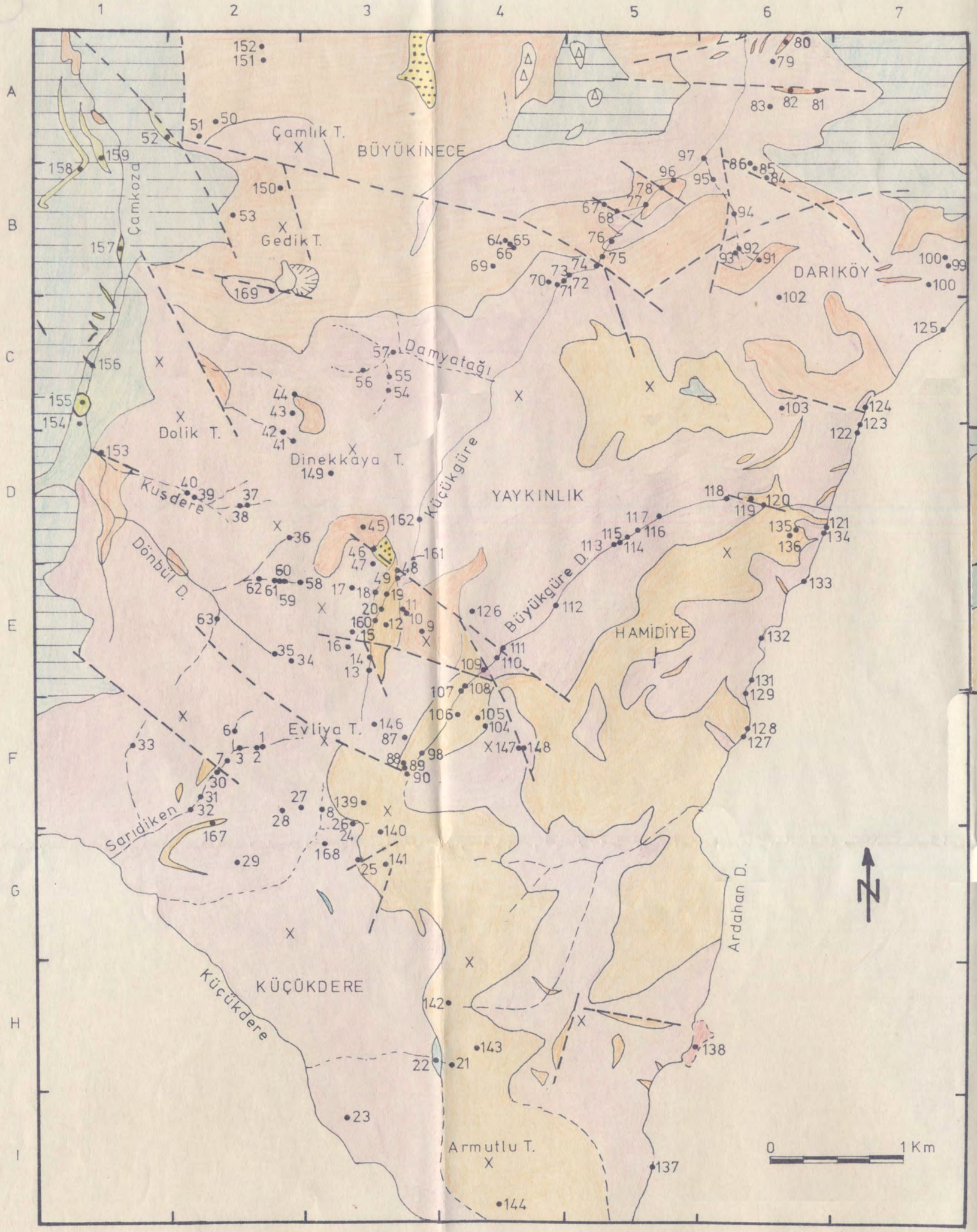

- Scree
- Basalt dyke
- Quartz-Microdiorite
- Agglomerate, sandstone, limestone
- Biotite-Andesite
- Rhyodacite & pyroclastics
- Tuffaceous breccia & sandstone
- Porphyritic dacite
- Pelitic limestone & tuff
- Lower basic series
- • 23 Specimen number